Development of a Synthetic Wrist Impact Surrogate for Sports Applications

GEMMA ELIZABETH LESLIE

PhD 2022

Development of a Synthetic Wrist Impact Surrogate for Sports Applications

GEMMA ELIZABETH LESLIE

A thesis submitted in partial fulfilment of the requirements of Manchester Metropolitan University for the degree of Doctor of Philosophy

Department of Engineering

Manchester Metropolitan University

2022

<u>Abstract</u>

Wrist injuries are common in snowboarding. Snowboarding wrist protectors are available, but there is limited research on their effectiveness. Previous research has explored tests for assessing the performance of wrist protectors, including bend tests and impact tests. BS EN ISO 20320:2020 was recently published as a standard for snowboarding wrist protectors. Performance testing of wrist protection typically use a wrist surrogate. The surrogate in BS EN ISO 20320:2020 consists of a simple representation of a hand and forearm, made from stiff materials and connected with a hinge joint. It is expected that a wrist surrogate utilising soft tissue simulants, rather than just stiff materials, would give a better prediction of human response under impact. Two styles of wrist protector, short and long, were chosen for testing with a developed compliant surrogate and an equivalent stiff one. A compliant surrogate with a 3 mm thick silicone outer layer and a stiff core was developed for use in a bend test for wrist protectors. Adding silicone to the surrogate increased the measured stiffness of both protectors. Finite element modelling and experiments were then used to inform the thickness of the soft tissue simulant on the palm of a wrist surrogate intended for impact testing. Impact tests against BS EN ISO 20320:2020 were conducted to determine the ability of the protector's palmar region to limit force, and the effect of introducing an anvil shaped like a hand, and compliance in the form of a layer of silicone. Both protectors' palmar regions were better at limiting force when impacted on an anvil shaped more like a hand, and further so, when adding a silicone layer to the anvil. A compliant surrogate with a 7 mm thick silicone layer over the palmar side of the hand, and a 3 mm thickness elsewhere, was then developed for use in a pendulum impact test, which tested the entire protector. Adding compliance to the surrogate reduced the peak force and increased the time to reach this peak. This PhD project has demonstrated that testing with a biofidelic wrist surrogate can affect the measured performance of wrist protectors. Future work could further develop the biofidelity of the surrogate, such as by including a bone simulant, instrumentation and adding stiffness to the joint, to further our knowledge of wrist injury mechanisms and the effectiveness of wrist protectors.

Outputs from this thesis

Leslie, G., Allen, T., Winwood, K., Wang, W., K. and Hamilton., 2022. Repeatability of a Bend Test For Measuring the Stiffness of Snowboarding Wrist Protectors. In *Multidisciplinary Digital Publishing Institute Proceedings.*

Leslie, G., Wang, W., Winwood, K., Liauw, C., Hamilton, N. and Allen, T., 2020. Effect of Surrogate Surface Compliance on the Measured Stiffness of Snowboarding Wrist Protectors. In *Multidisciplinary Digital Publishing Institute Proceedings* (Vol. 49, No. 1, p. 84).

Conference Presentations

25th June 2020: Oral Presentation: Effect of Surrogate Surface Compliance on the Measured Stiffness of Snowboarding Wrist Protectors. 13th conference of the International Sports Engineering Association – Tokyo, Japan.

20th February 2020: 3-Minute Lightning Talk. 4th Sport Engineering Seminar Day – Advance Wellbeing Research Centre, Sheffield.

7th April 2019: Oral Presentation: Development of a Tissue Simulant to Improve Assessment of Snowboarding Wrist Protectors. 23rd International Congress of Snow Sports Trauma and Safety – Squaw Valley, California.

6th March 2019: MMU PGR Conference –Poster and Oral Presentation.

30th January 2019: Oral Presentation: Development of a Tissue Simulant to Improve Assessment of Snowboarding Wrist Protectors. 3rd Sport Engineering Seminar Day – Loughborough University.

16th May 2018: MMU 3MT- Science and Engineering Heat.

<u>Acknowledgements</u>

Acronyms, Definitions and Terminologies used

PPE	Personal Protective Equipment
Biofidelic	Modelling the response of a human
Surrogate	Artificial representation of a living human
CAD	Computer Aided Design
FE	Finite Element
ISO	International Organisation for Standardisation
BSI	British Standards Institution
In-Vivo	Experimentation or measure done in or on tissue in an artificial environment outside the organism
SD	Standard Deviation
CV	Coefficient of Variation
GLM	General Linear Model
DIC	Digital Image Correlation
DS	Design Stage
PP	Polypropylene
HDPE	High Density Polyethylene
PU	Polyurethane
CoM	Center of Mass

Contents

Table of Figures

Table of Tables

1. <u>Introduction, Aim and Objectives</u>

1.1   Introduction

This thesis documents the development of a wrist surrogate for assessing the protective capabilities of snowboarding wrist protectors. A surrogate aims to provide an artificial representation of a living human. This chapter outlines the motivation behind the research, as well as the aims and objectives.

1.2   Motivation for research

There are about 10-15 million snowboarders worldwide, and the sport is particularly popular amongst adolescents and younger adults (Michel *et al*., 2013). The wrist is the most common injury site amongst snowboarders, accounting for approximately 35 to 45% of all snowboarding injuries (Michel *et al*., 2013). These injuries can be attributed to snowboarders instinctively placing out their hands in an attempt to cushion a fall (Maurel *et al*., 2013). The most common wrist injury amongst snowboarders is a distal radius fracture, resulting from a compressive load applied to a hyperextended wrist (Michel *et al.,* 2013). Beginners and inexperienced snowboarders have been reported to be at the greatest risk of sustaining a wrist injury (Maurel *et al.,* 2013; Idzikowski *et al.,* 2000; Kim *et al.,* 2012).

Wrist protectors are available to snowboarders, and are typically designed to limit / reduce impact forces and prevent wrist hyperextension (Michel *et al*., 2013). There are various wrist protector designs on the market, however currently there is limited research on testing such products. Therefore the question arises as to which specific design or protective component offers an adequate level of protection. Recent previous research has looked to further our understanding of the performance of snowboarding wrist protection, through the development of specific testing methods (Adams *et al*., 2016, Adams, 2018; Adams *et al*., 2021) and finite element (FE) models (Newton-Mann, 2019). Such research informed the development of the first standard for snowboarding wrist protectors, BS EN ISO 20320:2020[1], which was published in April 2020. BS EN ISO 20320:2020 includes

---

[1] Protective clothing for use in Snowboarding - Wrist protectors - Requirements and test methods

two main tests for assessing the performance of snowboarding wrist protectors, i) a quasi-static bend test for measuring their stiffness when fitted to a wrist surrogate, and hence their ability to prevent hyperextension, and ii) a simple drop tower style impact test, for measuring the impact performance of the palmar region when placed on fully constrained, rigid hemispherical anvil.

This project further develops previous published work and further tunes existing previous work on test methods for snowboarding wrist protection, by developing a more novel biofidelic wrist surrogate. Tests for assessing sports personal protective equipment (PPE), such as wrist protection, typically utilise a surrogate or anvil to represent the human limb. These surrogates often consist of simplified geometries and stiff materials that only provide a basic representation of the interaction between the human body, and prevent the PPE from deforming under impact as it would during a real life human scenario (Payne, 2015). It is proposed that improvements in sports surrogates to increase biofidelity (modelling the response of a human), coupled with instrumentation, is crucial in the development, testing and certification of sports PPE (Payne *et al*., 2014). Improved surrogates could also lead to a better understanding of the injury mechanism.

The findings of this current research will help further knowledge of the injury mechanism of the wrist and the effect of snowboarding wrist protection, alongside supporting work on the continued development and improvement of BS EN ISO 20320:2020.

1.3   Aim and Objectives

The aim of this PhD project is to develop an improved wrist surrogate for assessing the protectiveness of snowboarding wrist protectors.

This aim will be achieved via the following objectives:

1. To identify the internal and external geometry, main components and articulating joint of the wrist and forearm.
2. To identify a suitable synthetic soft tissue simulant for a wrist surrogate.
3. To determine the effect of adding a skin simulant to a wrist surrogate on the measured bending stiffness of snowboarding wrist protectors.

4. To determine the effect of a soft tissue simulant on the impact performance of the palmar region of snowboarding wrist protectors.

5. To determine the effect of adding a skin and soft tissue simulant to a wrist surrogate on the impact performance of snowboarding wrist protectors.

6. To make recommendations on tests for snowboarding wrist protectors and how to use biofidelic surrogates to further the understanding of injury risk.

1.4   Thesis structure

This project concerned the development of a wrist surrogate for assessing the effectiveness of snowboarding wrist protectors. The current state-of-the-art wrist surrogates were critiqued and an action priority matrix was used to determine the surrogate elements this project focused on, with an incremental approach and testing at each stage of development. A suitable soft tissue simulant for a wrist surrogate was identified through material characterisation tests and the agreement of this response with values of organic tissue and soft tissue simulants in the literature. A compliant wrist surrogate was then developed for the bend test that was developed by Adams *et al*. (2016), and then implemented into BS EN ISO 20320:2020, for measuring the stiffness of snowboarding wrist protectors. To determine a suitable soft tissue simulant thickness for the palm region of a wrist surrogate intended for use in impact tests, FE modelling and physical impact tests were conducted. Impact tests were conducted against BS EN ISO 20320:2020, alongside the incorporation of an anvil shaped more like a hand, and the addition of compliance to the anvil via a soft tissue simulant. A wrist surrogate was then developed for the pendulum impact test developed by Adams *et al.* (2021) for determining the performance of snowboarding wrist protectors. For each test, the effect of the developed surrogate was determined relative to a comparable 'non-developed' one, based on the current state-of-the-art. The results from all the tests (bend test, impact test from BS EN ISO 20320:2020 and pendulum impact test) were then combined to provide recommendations on certification tests for snowboarding wrist protectors and the use of biofidelic surrogates. Figure 1-1 outlines the process followed in this project and what is presented in each chapter.
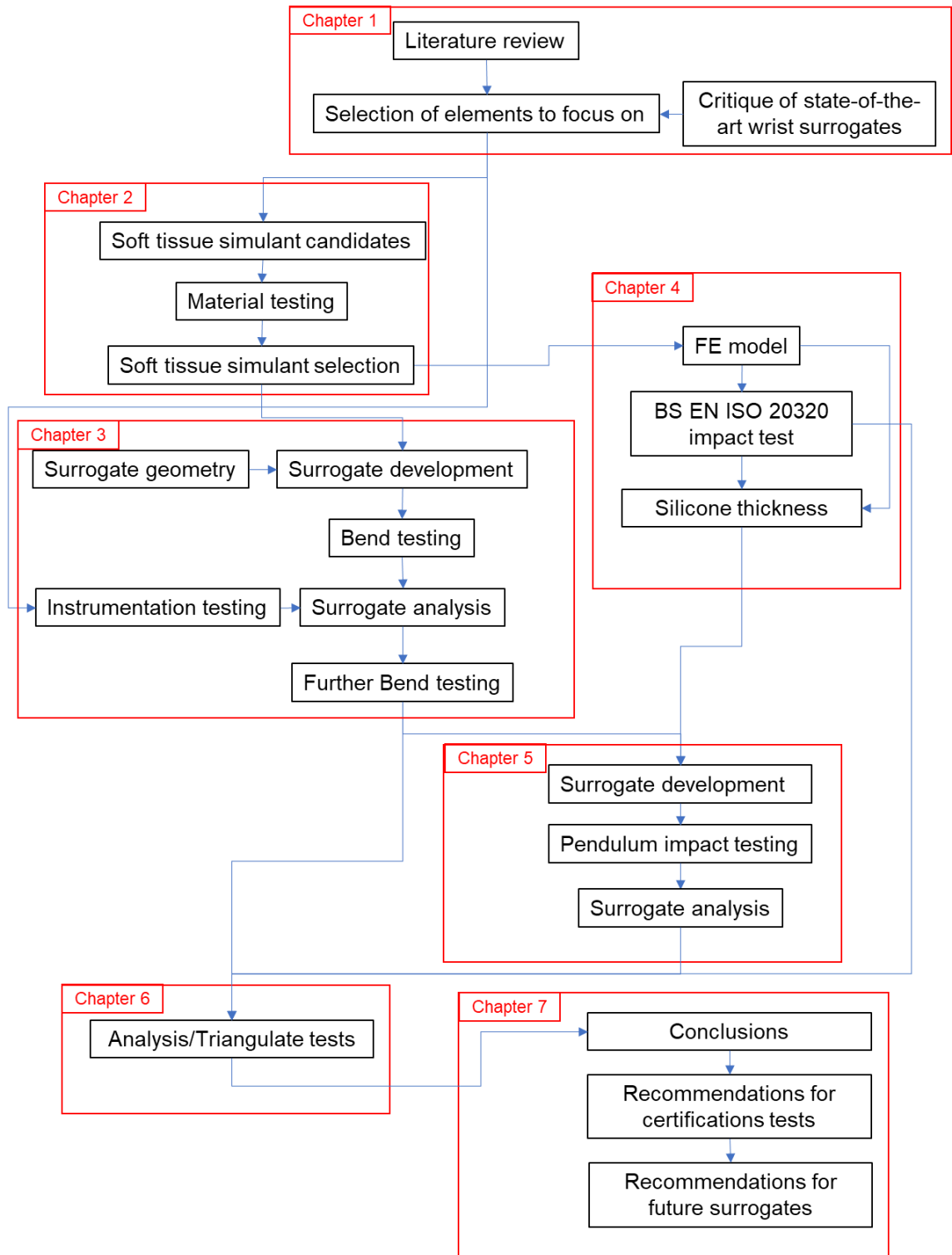
Figure 1-1: Thesis flow chart.

2. <u>Literature Review</u>

2.1   Introduction

This chapter reviews the literature in regards to the development of a wrist surrogate to support the testing of snowboarding wrist protectors. The first section (snowboarding and injury) assesses and evaluates the potential of wrist injuries amongst snowboarders. The next section (prevention) addresses protective equipment intended for preventing snowboarding wrist injuries and certification tests for such devices. The third section introduces surrogates for testing protective equipment, and the fourth section covers considerations for developing such surrogates. The final section critiques the current state-of-the-art wrist surrogates for testing snowboarding wrist protectors, followed by an overall conclusion.

2.2   Snowboarding and Injury

Snowboarding is a popular sport, with an estimated 10-15 million participants worldwide, and it is particularly popular among adolescents and younger adults (Michel *et al*., 2013). Michel *et al*. (2013) provided an overview of snowboarding injuries, stating that snowboarding injury risk has been reported as high as 8 injuries per 1,000 snowboarding days, resulting in lost riding days and substantial health-care costs. Furthermore, Michel *et al*. (2013) stated that the wrist is the most common site of injury for snowboarders, accounting for 35-45% of all snowboarding injuries. The risk of wrist injury during snowboarding can be attributed to the typical mechanism of a fall when riding a snowboard. When an inexperienced snowboarder loses balance, instinctively they often fall with their arms stretched out in an attempt to break the fall, which puts them at increased risk of sustaining an upper extremity injury (Figure 2-1a and b) (Kim and Lee, 2011; Maurel *et al*., 2013; Yamauchi *et al*., 2010). Indeed, over 90% of upper extremity injuries during snowboarding are thought to be due to a fall, either forwards or backwards (Idzikowski *et al*., 2000). The highest risk group has been reported to be novice snowboarders and beginners (Idzikowski *et al*., 2000; Kim *et al*., 2012). A distal radius fracture is the most common wrist injury amongst snowboarders, resulting from a compressive load applied to a hyperextended (outside the normal

range of motion) wrist (Figure 2-1c), and such injuries are seen after both backwards and forward falls (Michel *et al.*, 2013; Basques *et al.*, 2018; Robinson *et al.*, 2021).

Injury risks during snowsports are often estimated by reviewing accident reports collected within or near ski resorts. These statistics are often based on cases that were medically treated on-site or in nearby medical centres, and thus underreporting must be assumed. The true incident of wrist injuries is possibly higher, particularly minor injuries, such as sprains, that can go untreated.
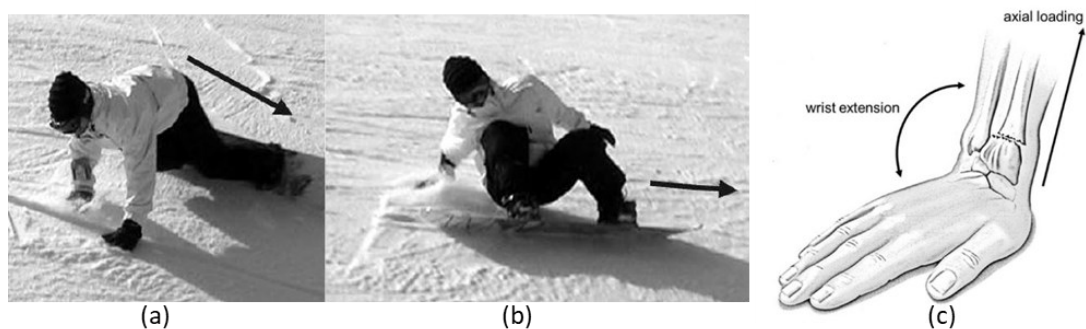
Figure 2-1 Snowboarding wrist injury scenarios, (a) forward fall, (b) backward fall, (c) distal radial fracture. Images (a) and (b) from Yamauchi et al. (2010) and (c) from Michel et al. (2013).

The wrist complex as a whole is considered to be biaxial, with motions of extension / flexion and ulnar / radial deviation (Figure 2-2). Table 2-1 reports the normal (non-injurious) ranges of motion of the wrist and forearm from various studies, with a maximum wrist extension of 85° stated. Wrist motion in one direction is thought to affect the motion capability in the other direction, i.e. lower range for flexion / extension when coupled with ulnar / radial deviation. Li *et al*. (2005) found the wrist could extend to 60° without ulnar / radial deviation, or 30° ulnar deviation without flexion or extension, but a combination of 60° extension and 30° ulnar deviation was unattainable. Due to the complexity of the wrist joint, there are many factors involved in a fracture, including the amount of radial / ulnar deviation, the amount of energy absorbed, the point and direction of load application and the strength of the bones and ligaments (Whiting and Zernicke, 2008). Idzikowski *et al*. (2000) found wrist injury severity to vary with snowboarding experience. Wrist fractures occurred predominantly in beginners. Intermediate to advanced snowboarders tended to have injuries from higher-energy falls, resulting in

scaphoid fractures and more severe distal radial fractures. Lunar or perilunar fractures and dislocations were reported in the expert group, resulting from backwards falls following an attempted aerial manoeuvre.

(a)   (b)
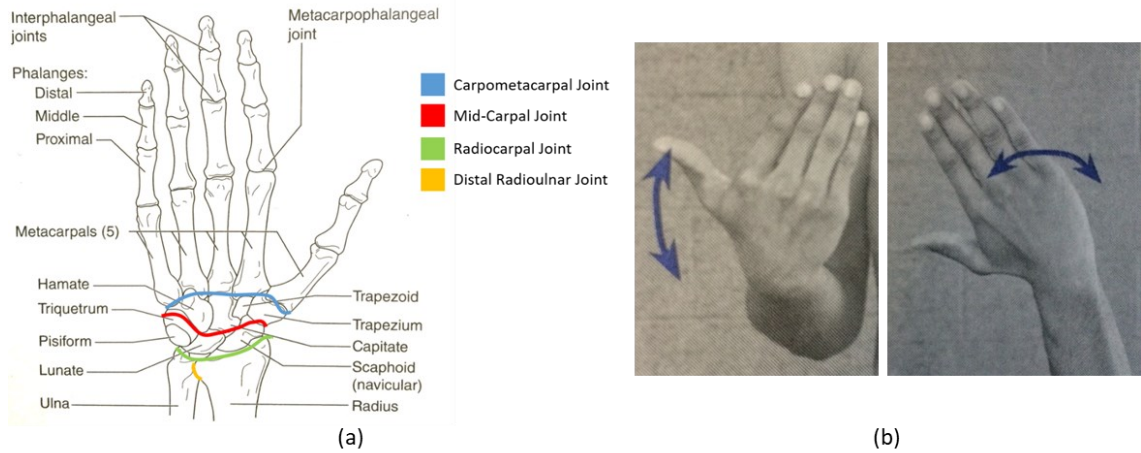
Figure 2-2 Wrist anatomy, (a) wrist anatomy, (b) wrist motion; left flexion/extension, right radial/ulnar deviation. Images adapted from Shultz (2010).

Table 2-1 Reported range of motion of the wrist and forearm from various studies. Some state a maximum value, others state a range. All values are in degrees

Flexion	Extension	Radial deviation	Ulnar deviation	Forearm pronation	Forearm supination	Participants	Reference
90	70	20	30	80-85	90	n/a	Shultz *et al.,* 2010
65-85	60-85	15-21	20-45	150 range		n/a	Levangie and Norkin, 2005
n/a	n/a	n/a	n/a	80-90	80-90	n/a	Whiting and Zernicke, 2008
41	67	20	35	n/a	n/a	10 ♂, Age 28.3 ± 4.9 years	Li *et al.,* 2005
67	73	n/a	47	n/a	n/a	35 ♂, Age 23 ± 4.5 years	Marshall *et al.,* 1999
72	79	21	46			19 ♀, Age 22.4 ± 4.8 years	
						109 ♂, Age	Boone and Azen, 1979
78	76	22	37	77	83	≤ 19 years	
75	74	21	35	75	81	> 19 years	
73 ± 14.7	**75 ± 5.5**	**21 ± 0.7**	**39 ± 6.2**	**82 ± 6.1**	**86 ± 4.1**	**Mean ± Standard Deviation**	

To gain knowledge of wrist injury mechanisms and fracture thresholds, researchers have impact tested cadaveric arms (Table 2-2). From the five cadaver studies reported in Table 2-2, the mean fracture threshold was 2,713 ± 636 N (mean ± standard deviation), with a cadaver fracture range of ~1,000 to 4,000 N. Lehner *et al.* (2014) simulated worst case forward and backwards falls in snowboarding, using the laboratory experiments mimicking forward and backwards falls of Schmitt *et al.* (2012) for validation. A 50th percentile adult of 1.80 m height and 78.4 kg weight was simulated, and peak impact forces of 3500 N for backwards falls and 1950 N for forward falls were reported. These peak impact forces lay within the reported cadaver fracture range in Table 2-2. To gain more knowledge on the mechanics of falling onto an outstretched arm, Giddins and Giddins (2021) studied videos (from Youtube©) of skateboarders falling (non-injurious), and measured wrist angles (Figure 2-3). Following initiation of the fall (Figure 2-3a), the arms aligned parallel to the ground with the wrist initially extended to ~40 to 50° and the fingers flexed. As the hands approached the ground (Figure 2-3b) the fingers started to hyper-extend. To allow this hyperextension of the fingers the wrist flexion reduced to ~30° (Figure 2-3c). From all the videos (50 falls), a mean maximum wrist extension of 80° (range 50 to 110°) was measured at impact (Figure 2-3d). While the fall mechanism in snowboarding may differ to skateboarding, this study provides useful information as a starting point to gain more knowledge on fall mechanics. Greenwald *et al.* (2013) used an instrumented glove to measure wrist impact forces and angles during non-injurious snowboarding falls. The instrumented glove was worn by 20 snowboarders (mean body mass 61.7 kg) and recorded data for 128 non-injurious falls. The mean maximum wrist extension was 80.2 ± 15.8°, which is similar to the values reported by Giddins and Giddins (2021) for non-injurious skateboarding falls. The mean maximum force was 266.0 ± 232.4 N was found, which was unsurprisingly lower than the values reported to fracture a cadaveric wrist/forearm (Table 2-2) because the falls were non-injurious.

Table 2-2 Laboratory cadaver forearm impact studies.

Forearm Cadaver	Test Setup	Test conditions	Fracture Threshold (N)	Reference
12 specimens Age: 20-68 years		Impact: 2.80 m/s 40° dorsiflexion, 10° internal rotation Drop height: 40 cm Effective mass: 23 kg	2,821 ± 763 (mean ± SD)	Greenwald *et al.,* 1998
48 specimens Age: 19-79 years		Impact: 2.66-3.12 m/s 60-80° dorsal flexion	1,030 to 4,315	Fryman, 1967
21 specimens Age: 49-91 years		Displacement: 0.00042 m/s 90° dorsiflexion	1,640 ± 980 (mean ± SD)	Spadaro *et al.,* 1994
36 specimens Age: 69-83 years		Displacement: 0.025 m/s 75° dorsal flexion, 10° internal rotation	3,390	Myers *et al.,* 1991
40 specimens Age: n/a		Displacement: 0.025 m/s 75° dorsal flexion, 10° internal rotation	1,470 to 4,116	Giacobetti *et al.*, 1997
30 specimens Age: 50-96 years		Impact: 2 m/s Radius mounted at 75°	2,963 ± 1,274 (mean ± SD)	Zapata *et al.*, 2017
Mean ± SD: **Range:**			**2,713 ± 636** **~1,000 to 4,000**	
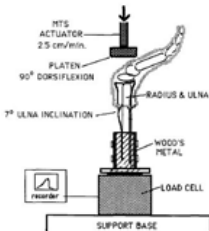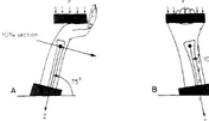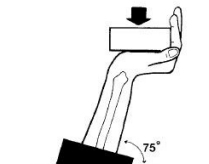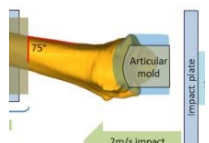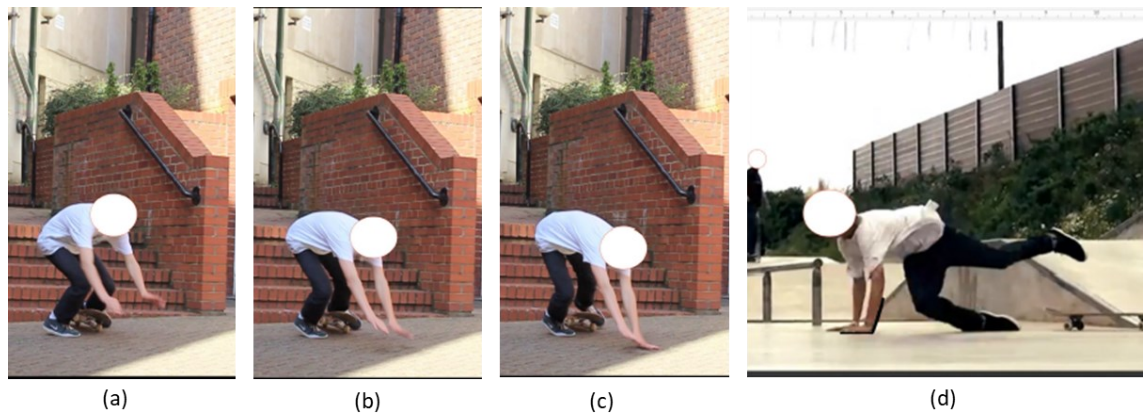
Figure 2-3 Images of skateboarders falling (non-injurious) onto an outstretched wrist from Giddins and Giddins (2021). Images show how wrist angles were measured (a) at the initiation of a fall, (b) as the hands approached the ground, (c) prior to impacting the ground, and (d) at impact.

2.3   Prevention

2.3.1   Wrist Protection and Standards Result

Wrist protective equipment are available for snowboarders. It is proposed that a snowboarding wrist protector prevents hyperextension of the wrist and limits impact forces imposed (Michel *et al*., 2013). Wrist protectors vary in length (short/long), wearing style preference (e.g. integrated into a glove, under the glove, over the glove), and use of protective elements (splints, palmar padding) (Figure 2-4) (Newton-Mann *et al*., 2018). The intended role of any splint/s are to prevent wrist hyperextension and absorb energy upon impact, whilst not over restricting motion during normal use. The intended role of any palmar padding is to limit impact force (Michel *et al*., 2013). Snowboarding injury records often lack detail of protective equipment usage and design, hindering knowledge of wrist protector usage and which designs, if any, work best. Senner *et al.* (2018) simulated child, adolescent and adult falls in snowboarding to determine the main functions of wrist protector elements for reducing impact force and wrist extension. A range of models were simulated with different versions of protective elements, e.g. no wrist protector, dorsal splints, palmar splints, both dorsal and palmar splints, protector/splint lengths, and palmar padding thickness. It was found that long protectors/splints reduced wrist extension by 18.6 to 25.4%, as opposed to short protectors/splint, which only reduced wrist extension by 11.3%. Protector palmar padding was found to be more efficient at reducing axial force at the wrist than reducing wrist extension, whereas padding thickness did not have a significant

effect. It was concluded that protectors with long dorsal and long dorsal and palmar versions offered the most effect, reducing both axial load and the resulting wrist extension. Michel *et al*. (2013) produced a white paper calling for a standard for snowboarding wrist protectors.

Certification tests for sports personal protective equipment (PPE) typically measure performance in terms of forces transmitted through the item during an impact test. Peak force usually needs to fall below a set value for the product to pass the test and gain certification. Such certification tests outlined within standards (e.g. BSI, ISO) tend to use rigid (i.e. metal) anvils or surrogates made from stiff material (i.e. plastic). The tests must be highly repeatable and the setups must usually be multifunctional to work with other PPE, allowing test houses to test various products without needing lots of specialist equipment. Ankrah and Mills (2003) state that impact energies in many certification tests are not justified, suggesting that they are often unrealistically low to prevent damage to test equipment, rather than matching to conditions experienced in sporting environments. The simple nature of certification tests can restrict the development of better procedures with more specialist equipment, instrumentation and human body / limb surrogates. To appease test houses, new certification tests typically need to utilise current test equipment, instrumentation needs to be user friendly, and surrogates need to be easy to make and offer a repeatable response.

BS EN 14120:2003+A1:2007[2] describes the certification tests for roller sport wrist protectors intending to reduce the risk of injuries caused by abrasion and provide stabilisation of the wrist. Michel *et al*. (2013) identified BS EN 14120:2003 as a starting point for a snowboarding wrist protector standard, as it addresses the core features of wrist protection, i) controlling wrist extension (identified through a bending test), and ii) managing impact energy (identified through a drop test). Michel *et al* (2013) claimed that modifications to the tests in BS EN 14120:2003 would be required for them to be applied to wrist protectors for snowboarding. In

---

[2] Protective clothing - Wrist, palm, knee and elbow protectors for users of roller sports equipment - Requirements and test methods

particular, they identified the need to test fingered gloves and to test at snowsports relevant temperatures.

Figure 2-4 Examples of different types of snowboarding wrist protectors available. (Images from Newton-Mann (2018) and Michel et al. (2013)).

Previous research by Adams (2018) and Newton-Mann (2019) has assisted the development of a standard for snowboarding wrist protectors. Adams (2018) critiqued BS EN 14120:2003 and developed a quasi-static bend test (Adams *et al.*, 2016) and a "pendulum style" impact test (Adams *et al.*, 2021), to evaluate the performance of snowboarding wrist protectors. Newton-Mann (2019) developed an finite element (FE) model of the pendulum impact test, in efforts to distinguish between different snowboarding wrist protector designs. Subsequently, BS EN ISO 20320:2020 was published.

2.3.2 Quasi-static Bend Test

The quasi-static bend test developed by Adams *et al.* (2016) (Figure 2-5) measures the stiffness of snowboarding wrist protectors when fitted to a wrist surrogate (consisting of a stiff hand and forearm part connected with a hinge joint). The surrogate was mounted to a mechanical test device, with a cable connecting the load cell to the hand via a pulley. Vertical displacement of the load cell applied a torque around the wrist joint, pulling the hand backwards. The wrist surrogate that the protector was fitted to was manufactured from a stiff material (i.e. polymer). Adams *et al.* (2016) found the strapping tightness of the wrist protectors on the surrogate to influence the measured stiffness in this test, and suggests it should be accounted for in future work. The quasi-static bend test of Adam *et al.* (2016) applied a relatively low magnitude load (typical values < 100 N) quasi-statically (200 mm/min, ~1°/s), and whilst this facilitates an understanding of product stiffness, it does not fully account for protectors with rate dependent materials (Adams *et al.*, 2016). It is also unclear how the specific results from such a bend test may relate to the ability of a wrist protector to prevent injuries.

1. Load cell
2. Wire joiners
3. Pulley
4. Instron flexure fixture
5. Arm prosthesis
6. Wrist protector
7. Hand prosthesis
8. Karabiner
9. Cable
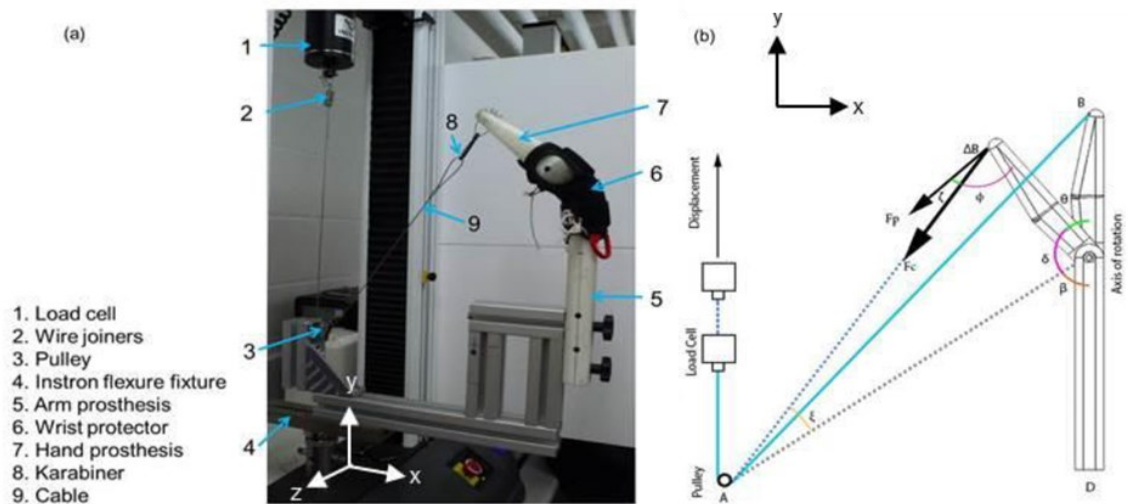
Figure 2-5 Quasi-static bend test (a) photo of test, (b) schematic. Images from Adams et al. (2016).

2.3.3 Pendulum Impact Test

Adams (2018) developed a pendulum impact test (Figure 2-6), designed to mimic the test conditions of Greenwald *et al.* (1998) (Table 2-2), but with a wrist surrogate rather than a cadaveric forearm. The rig included potentiometers to measure angular position of the pendulum arm and surrogate hand relative to the forearm, and a dynamometer to measure impact forces. A high-speed camera was synchronised to the instrumentation and used to film the impact. Adams (2018) used the rig for impact energies of 40 J, which was claimed to simulate worst-case scenarios. Newton-Mann (2019) modified this rig to achieve a broader range of impact energies, for comparative analysis against an FE model, by reducing the mass of the pendulum arm. This rig is probably too specialist for implementation within a test within a standard and subsequent use in a test house.
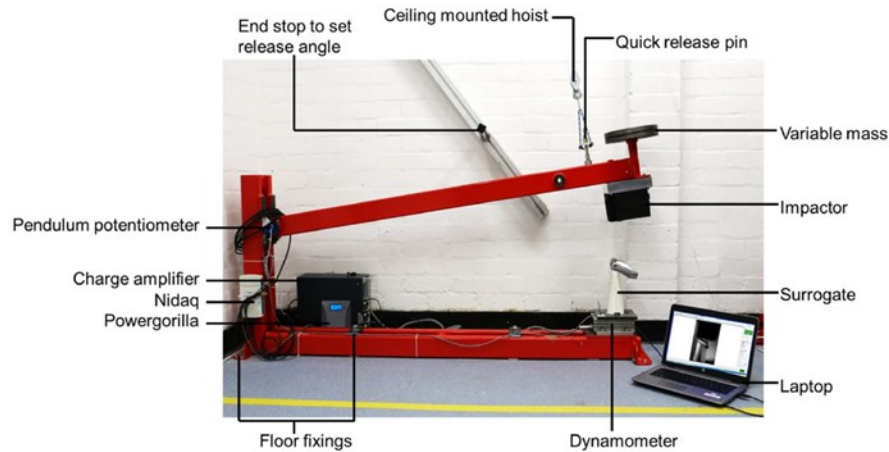
Figure 2-6 Pendulum impact rig. Image from Adams (2018).

The two test rigs developed by Adams (2018) were available for use during this current project. The wrist surrogates developed in this project will be designed to be compatible with both of these test rigs. This approach presents a good opportunity to assess and evaluate the effect of a more biofidelic novel surrogate in comparison to those developed by Adams (2018), to use when testing snowboarding wrist protectors.

2.3.4 BS EN ISO 20320:2020

BS EN ISO 20320:2020 consists of an impact strength, impact performance, and limitation of wrist extension test. The impact strength test is based on the previous BS EN 14120:2003, and tests the protectors component parts. The limitation of wrist extension test (Figure 2-7a) is a simplified version of the quasi-static bend test of Adams *et al* (2016), which measures the stiffness of the protector. Two torques are applied around the wrist joint: 5 Nm (Torque 1) and then 8 Nm (Torque 2). The protector passes the test if Torque 1 causes within 50 to 75° of wrist extension, and Torque 2 causes within 55 to 80° of wrist extension, with at least a 5° increase when Torque 2 is applied. The limitation of wrist extension test uses a "geometric style" surrogate (based on anthropometric data) made of stiff materials (polyamide or similar material, as stated in BS EN ISO 20320:2020).
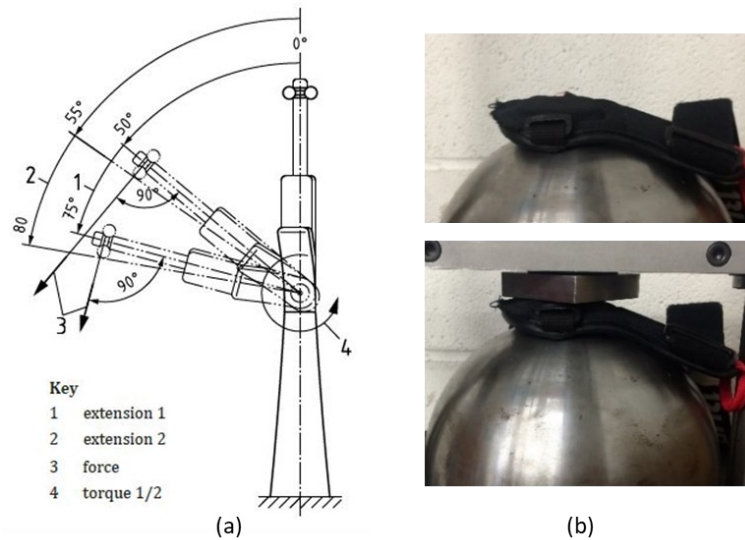
Figure 2-7 Example images of BS EN ISO 20320:2020 tests, (a) limitation of wrist extension, (b) impact performance (image taken by the author).

The impact performance test (Figure 2-7b) is based on the one in BS EN 14120:2003, and determines the ability of the palmar region of the protector to limit impact force. A circular test area (⌀ 40 mm) is located on the protector palmar side, which is mounted (held down by weights) to a rigid hemispherical anvil (100 mm radius with 100 mm radius of curvature), and impacted by a drop mass (2.5 kg, 40 by 40 mm striking face). The protector passes the test if the peak force does not exceed 3 kN, when impacted at either 3 J (small protector), 4 J (medium protector) or 5 J (large protector). Schmitt *et al*. (2011) impact tested a range of wrist protection (fingered gloves with integrated protectors, snowboarding wrist protectors and inline skating wrist protectors) against BS EN 14120:2003 and reported a mean peak force of 3,396 ± 1809 kN, which was above the 3 kN pass mark. Furthermore, some protectors were impacted at lower energies (1 to 3 J) as they did not exhibit impact protection within the impact test area, and a higher mean peak force of 5,745 ± 1,760 kN was observed.

A key limitation of the current test method is the rigid hemispherical anvil, which is not a true representation of a hand and wrist. In addition, it is also likely that some protectors would need to be modified via cutting or stretching them to fit the anvil, as observed by Schmitt *et al.* (2011). A more viable setup would allow the protector to be held in a more realistic position on a wrist surrogate, like the one in the limitation of wrist extension test.

Whilst a standard for snowboarding wrist protectors, BS EN ISO 20320:2020, has recently been published (April 2020), it is uncertain as to whether products have yet been certified. The lack of certified snowboarding wrist protectors and the various designs available has resulted in limited knowledge as to which product meets the minimum performance criteria. Therefore, it is likely that the level of protection varies between wrist protector designs (Schmitt *et al*., 2012, Adams *et al*., 2021).

2.4   Human Surrogates

To develop a good understanding of injury mechanisms and thresholds, it is essential to develop effective injury countermeasures (i.e. PPE) (Crandall *et al*., 2011;McIntosh, 2012). To assess injury risk and prevention measures, surrogates (Table 2-3) are sometimes adopted to better understand and represent human response to impacts, and are widely used in the automotive, defence, medical, and sports industries (Payne *et al*., 2016). Typically, surrogates used in the sports industry consist of simplified geometries and stiff materials (e.g. plastic). Such surrogates provide a basic representation of the human body, and are well suited for test houses to reduce complexities and potential variability. The main limitation of surrogates made from stiff material is that they do not reflect a true representative of the compliance of a human limb, and may prevent protective equipment from deforming under impact in the same way as it would when worn by a human (Payne, 2015). A biofidelic surrogate models the response of a human limb, and is arguably crucial in the development and testing of sports PPE (Payne *et al*., 2014). Biofidelic surrogates have greater potential to improve the assessment and design of PPE in relation to real life scenarios. Surrogates for body regions without joints, such as a shin or thigh could be manufactured simpler than those with a joint, such as a knee, wrist or ankle. A list of advantages and limitations for each type of surrogate are reported in Table 2-3.

Table 2-3 Types of surrogates (informed by Crandall et al., 2011; Payne et al., 2016).

Surrogate (Human or Synthetic)	Description	Uses	Advantages	Limitations
Human: Cadaver	Deceased human body/limb	Occupational safety. Athletics. Transportation. Military applications	Exact anatomical structures	Ability to produce comparable response and injury depends on tissue, rigidity due to storage, age condition. Ethics approval required. High cost. Specialist expertise/facilities.
Synthetic: Anthropometric test device (ATDs) i.e. Hybrid Test Dummy (Humanetics, 2009)	Mechanical analogue that aims to match the anthropometry, articulations and structural response of humans	Assessment of fatality risks in crash tests in the automotive industry	Highly instrumentation – sensors to record accelerations, forces and displacements of impacts experienced by the body in a crash	Oversimplified joints. Sensors primarily focused on head and spinal injuries. Stiff materials due to high durability requirements to sustain multiple high energy impacts. High cost
Synthetic: Anvils	Manufactured from metal. Utilise a range of geometries such as simple pucks, cylindrical and hemispherical or half-cylinder shapes of varying size and curvature to represent the outer surface geometries of human limb segments	Certification tests to assess PPE	Repeatable. Reproducible. Low cost. Compatible with test equipment	Unrepresentative geometries. Constraint to a large base, preventing it from recoiling in a manner similar to that observed in the body. Poor representation of impacts in actual sporting events
Synthetic: Sports surrogates	Designed to represent a human limb or body part i.e. thigh, wrist, head	The testing of sports PPE for research purposes or for implementation to certification tests	More complex geometries and materials can be explored, alongside the addition of instrumentation.	Some sports surrogates developed more than others. Simplified geometries and joints. Lack of human data for validation.

Previous wrist surrogates for assessing wrist protectors vary in type and their biofidelity (Table 2-4). The main limitations of such wrist surrogates is that they predominantly use stiff materials (not a true reflection of human structure/composition) and basic representations of the joint (i.e. a hinge). Adams *et al* (2021) suggested that future research should focus on increasing the biofidelity of wrist surrogates. Their suggestions include, i) a more advanced hinge joint accounting for the influence of muscle and tendons, ii) more degrees of freedom, and iii) incorporating a thin layer of compliant material as a basic representation of skin. Adding compliant material to the wrist surrogate could enhance protector fit and limit unwanted slippage during testing (Adams *et al*., 2018). Adding a layer of compliant material could also reduce the stiffness of the surrogate and allow energy absorption through compression of this material, making it a closer representation to the forearms used in cadaver testing (Adams, 2018).

Table 2-4 Synthetic wrist surrogates. Images from reference or otherwise stated.

Surrogate description	Image	Products tested	Key Features	Limitations	Reference
BS EN 14120 wrist surrogate. Rectangular cross-section forearm and paddle-like hand.		Roller sports wrist protectors	Wooden hand. Metal forearm. Low friction hinge joint. Small, medium, large variations based on body mass.	No fingers – cannot test glove integrated protectors. Single axis joint. Rigid materials. Basic geometry. Missing dimensions to recreate.	BS EN 14120:2003
BS EN ISO 20320:2020 wrist surrogate. Simplified geometric representation of a hand-arm		Snowboarding wrist protectors in a quasi-static bend/limitation of wrist extension test	Two machined fingers. 3D printed Nylon hand and forearm. Low friction hinge joint. Geometry based on anthropometric data. Small, medium, large variations based on anthropometric data	Stiff materials. Single axis joint. Low surface friction – slippage of the protector during testing	Adams *et al.,* 2016; BS EN ISO 20320:2020 Image taken by author of Adam's (2018) surrogate.
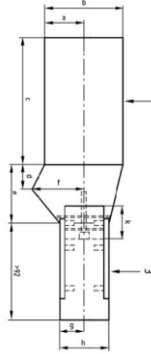
Wrist surrogate with dimensions from a 3D scan of a human hand and arm		Snowboarding wrist protectors in a pendulum impact test	Geometry (close to) 50th percentile male human hand and arm. CNC machined hand. Metal forearm core with 3D printed Nylon casing. Potentiometer to measure wrist angle. Mounted to a force platform. No fingers – excluded due to impact occurring on palm	Rigid materials. Central core protrudes when the wrist is fully extended. Single axis joint. Low surface friction – slippage of the protector during testing	Adams, 2018; Adams *el al.,* 2021
Hand model made of body filler (mix of resin and hardener) coupled with a 3 mm rubber layer		4 wrist protector prototypes	3 mm layer to model compliance of the human hand. Cast of a left hand	Wrist joint not represented	Maurel *et al.,* 2013

Forearm/hand complex of the enhanced air bag interaction (EAI) arm (crash test dummy)		5 testing conditions: bare hand, wrist guard, sorbothane glove, air cell, air bladder	Inbuilt instrumentation (load cell, potentiometer). Covered with a polymer to simulate arm flesh	Stiff materials not representative of a human	Kim *et al.,* 2006
Instrumented surrogate wrist/forearm falling onto a force plate		Evaluations of an instrumented glove's measurement accuracy	Surrogate arm modelled from a human hand. Constructed from 80 Shore A cast polyurethane	Single axis joint	Greenwald *et al.,* 2013

Surrogates have previously been developed for other human limbs to assess the effectiveness of associated protective devices (Table 2-5). In some cases, these surrogates have more developed or biofidelic features such as embedded instrumentation and soft tissue simulants. However, to the authors knowledge, none of these features have been applied to wrist surrogates and specifically in relation to snowboarding.

Table 2-5 Sports surrogates. Images from reference or otherwise stated.

Surrogate description	Image	Uses	Key Features	Limitations	Reference
Multi-material synthetic thigh surrogate for sports impacts		Cricket ball and knee impact tests	Anatomically contoured. Polydimethysiloxane (PDMS) multi-layered soft tissue simulants. Sawbone® femur	Fabrication time. Nothing to directly compare against for validity	Payne *et al.,* 2016
Human foot/ankle complex. Hollow aluminium tibia connected to a rigid foot made of epoxy		Rotational traction on an indoor playing surface	Torsional stiffness of the ankle could be modified. Foot could rotate about the tibia axis	Only ankle rotation is considered – no additional degrees of freedom. Development would be to incorporate a biofidelic knee joint	Villwock *et al.,* 2009
Thigh model. Femur represented by two pieces of stainless steel. Silastic 3483 used for soft tissue		Impact force attenuation of thigh pads	The soft tissue simulant was selected based on peak deceleration of the striker matching model prediction	Only an area representing the anterior mid-thigh was impacted	Hrysomallis, 2009

Instrumented human head surrogate		Impact evaluation of helmets	Skull and brain geometry determined from Magnetic resonance imaging (MRI) scans. 3D printed from ABS plus-P430 by Stratasys Ltd. Many sensors – nine triaxial accelerometers, ten pressure sensors	Future work required to optimise the surrogate reliability and validate the behaviour with and without helmets	Petrone *et al.,* 2018
Fiberglass model leg containing a synthetic tibia that had been calibrated against human cadaver specimens	n/a	Soccer shin guards	Simulated the elastic properties of human bone	No representation of a soft tissue/skin layer	Francisco *et al.,* 2000
Frangible surrogate leg. Anatomically correct bones from CT scans, synthetic knee and ankle ligaments encased in ballistic gelatine		Landmine blasts	Geometrically accurate bones. Cartilage, tendons and soft tissue represented by silicone, elastic materials and pig-skin gelatine. Instrumented with strain gauges and load cells	Single use surrogate	Bergeron *et al.,* 2001
Lower leg model		Stud impact on football shin guards	Sawbone® tibia. Soft tissue substitute Senflex 435 foam	Only front section/bone (tibia) of the lower leg modelled	Ankrah and Mills, 2003
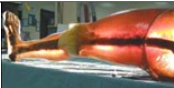
			– similar indentation resistance as human soft tissue in the ankle area. 2 mm thick SkinFx silicone rubber cosmetic skin held the components together during impact. 6 Tekscan™ Flexiforce sensors to determine load distribution		
Ankle surrogate consisting of aluminium casting of the ankle bones with a layer of foam to represent the soft tissue		Stud impacts on a protected ankle surrogate - replicating ankle impacts in football	Cast of a Sawbone® left foot. 2 mm layer of ESI foam to simulate skin. Five force sensors on the foam skin cover. The soft tissue was characterised by conducting compression tests on participants' ankle tissue.	No flexibility at joints between the ankle bones	Ankrah and Mills, 2004
Artificial lower limb		Impact testing of shin guards for field hockey, with and without a sock	Artificial leg was mounted over a hardened metal anvil with a flat impact area, so the top surface of the anvil was flush with the top surface of the limb	Surrogate was only used for mounting the shin guard, only the flat metal impact area was tested. No material properties were given	Ruznan *et al.,* 2017
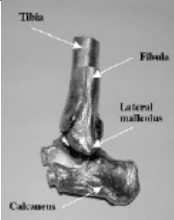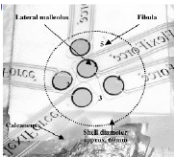
Leg surrogate including artificial knee joint. Incorporated the bones of the thigh, lower leg, hip, six knee ligaments, ten muscles and the muscle volume		Measures the stresses in the leg/knee, for performance measurement in sports safety equipment e.g. ski binding release and knee braces. Test rig enables quasi-static application of external loads	Aluminium tibia and femur bone. Prosthetic components for the joints. Muscles modelled by steel ropes and instrumented with force sensors. Muscle force set by a tensioning unit. Ligaments made of polyester and instrumented with force sensors. Muscle volume three layer coat of thermoplastic.	One degree of freedom on surrogate ankle - external loads applied to fixed surrogate foot.	Nusser *et al.*, 2016
Knee flexion surrogate - upper and lower leg made of silicone, connected by a hinge joint		Used as a test rig. Determining whether flexible sensors integrated into underwear can measure knee angles for performance measurements in sports safety equipment	Flexion and extension powered by a pneumatic cylinder. Rotary sensor to measure amplitude and velocity of knee movement.	Current system only addresses flexion and extension, limited to the knee flexion range.	Hermann *et al.*, 2020
Biofidelic human shoulder surrogate		For testing padded clothing in rugby union	Steel half cylinder, with a synthetic 10 mm muscle layer and 5 mm skin and adipose layer	Simplified geometry to represent the shoulder bones	Hughes *et al.*, 2021

Destructible headform		For testing sports impacts	CT and MRI scans used for head geometry.	Implementing a more sophisticated brain simulant to measure the motion of the brain during impact	Stone *et al.*, 2021
			Triaxial linear accelerometer and angular rate sensors.		
			3D printed in ABSp430.		
			250A gelatine powder to replicate human tissue.		
			Silastic 3483 to replicate soft tissue.		

2.5 Surrogate Development Considerations

To develop a more novel realistic, biofidelic wrist surrogate than the current state-of-the-art, the key design factors of a surrogate need to be studied. Key design factors for a wrist surrogate are, i) the external and internal anatomical measurements of the wrist, ii) the surrogate geometry, iii) the materials used to represent human soft tissue, iv) the manufacturing method, v) the measurement techniques and instrumentation, and vi) any finite element (FE) modelling techniques used to assist in the development of the surrogate. Within this current project there are many routes for surrogate development that could be taken. The key wrist surrogate design factors will be studied and prioritised to identify and justify the approach this project will take.

The progression towards a more novel biofidelic wrist surrogate should be incremental, with validation against previous work and comparison against current wrist surrogates. Such an approach will make it possible to determine whether research developments made are indeed improvements that could help improve the knowledge of wrist injury mechanisms, and the effectiveness of wrist protectors. It is important to note the difference between a surrogate intended for use in certification tests and a surrogate used for research purposes, and how this might influence the balance between simplicity, repeatability and biofidelity. A surrogate for use in certification tests needs to be simple and highly repeatable in terms of both manufacturing and testing. Therefore, the balance between both surrogate biofidelity and surrogate repeatability needs to be more weighted towards repeatability in certification tests, whereas, as this is a PhD research study, developments can be more complex and weighted more towards biofidelity. Developments intended to improve the biofidelity of the surrogate can be explored and tested, with the design later simplified to include only the most influential features for adoption into a certification test within BS EN ISO 20320:2020.

2.5.1 Anatomical Measurements of the Wrist

To develop a biofidelic wrist surrogate, the surrogate geometry is crucial. As such, it is necessary to determine the external dimensions, and internal structure of the human wrist. Anthropometry is the study of physical measurements of the human

body to determine differences in individuals and groups (Tilley, 2002). The BS EN 14120 surrogate sizes are based on body mass, whereas the BS EN ISO 20320 surrogate sizes were based on hand sizes. It was identified that surrogate B (medium) in BS EN 14120 was equivalent to a 15th percentile adult male, and thus anatomical datasets from Peebles and Norris (1998) and Pheasant and Halelgrave (2006) were scaled to represent a small (0.1[th] percentile), medium (15th percentile) and large (95th percentile) male hand and arm for the wrist surrogate in BS EN ISO 20320 (Adams, 2018). Some anthropometric data of the male forearm and hand is shown in Table 2-6, in which comparison can be made to the dimensions relating to the medium BS EN ISO 20320 surrogate. A schematic drawing of the surrogate and dimensions in BS EN ISO 20320:2020 from draft standard as of 15-05-2018 (BS EN ISO 20320:2020 had not been published and a draft of the standard was at the DS stage, when the standard was circulated to ISO members to vote and comment on before it was approved) are shown in Figure 2-8. The wrist surrogate developed in the later chapters correspond to these dimensions.

Table 2-6 Anthropometry of the male forearm. Dimensions in mm. Image from Diffrient et al. (1974).

Source	Percentile	A	B	C	D	E	F	G
Diffrient *et al.*, 1974	97.5	269	104	76	81	211	97	114
	5.0	254	94	69	76	191	89	104
	2.5	234	81	61	71	175	81	94
Tilley, 2002	99	274	n/a	n/a	84	213	102	117
	50	257			76	190	86	104
	1	234			69	168	78	94
Scaled from [1]Peebles and Norris, 1998; [2]Pheasant and Haslegrave, 2006; [3]Tilley, 2002; [4]BS EN 14120:2003 (dimensions used for BS EN ISO 20320:2020 surrogates)	95	312[3]	88[1]	66[1]	62[3]	204[4]	n/a	95[2]
	15	273[3]	69[1]	57[1]	56[3]	182[4]		82[2]
	0.1	245[3]	54[1]	50[1]	52[3]	160[4]		72[2]

Figure 2-8 (a) Schematic drawing and (b) dimensions, of surrogate from BS EN ISO 20320:2020 from draft standard as of 15-05-2018.

The wrist has fifteen bones, including five metacarpal bones, eight carpal bones (two rows of four), and the distal ends of the radius and ulna (Shultz *et al.*, 2010) (Figure 2-2a). Five main muscles act on the wrist joint, including the flexor carpi radius, palmaris longus, flexor carpi ulnaris, extensor carpi radialis longus and

29

extensor carpi ulnaris (Figure 2-9) (Shultz *et al.*, 2010). MRI scanning has been utilised to create an atlas of cross-sectional images of the human body (e-Anatomy, IMAIOS). The atlas states that the participant is a normal 45 year old male, but no other information is provided, such as their anthropometric measurements or whether they represented a certain size of person. Cross sectional images from e-Anatomy at locations along the wrist and forearm are displayed in Figure 2-10.
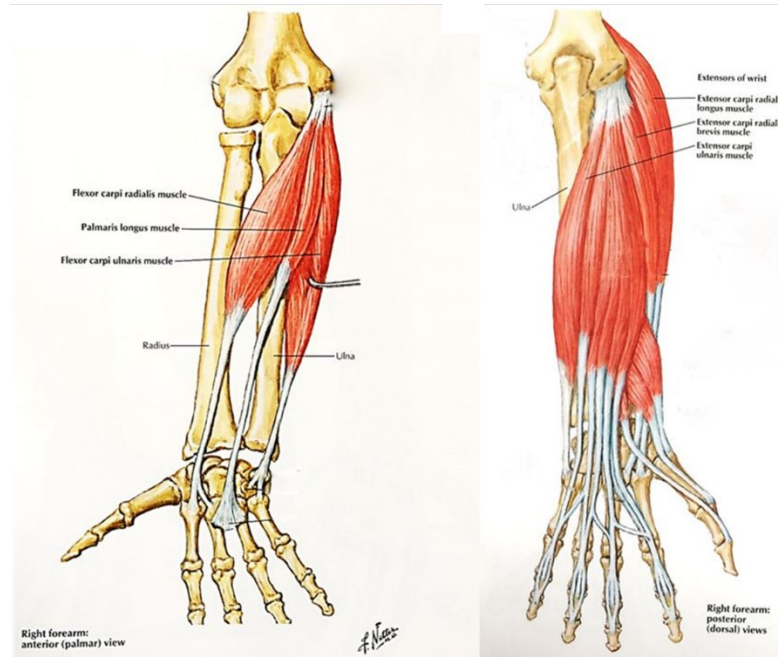
Figure 2-9 Main Muscles of the right forearm. Left anterior, Right posterior. Images adapted from Netter (2014).
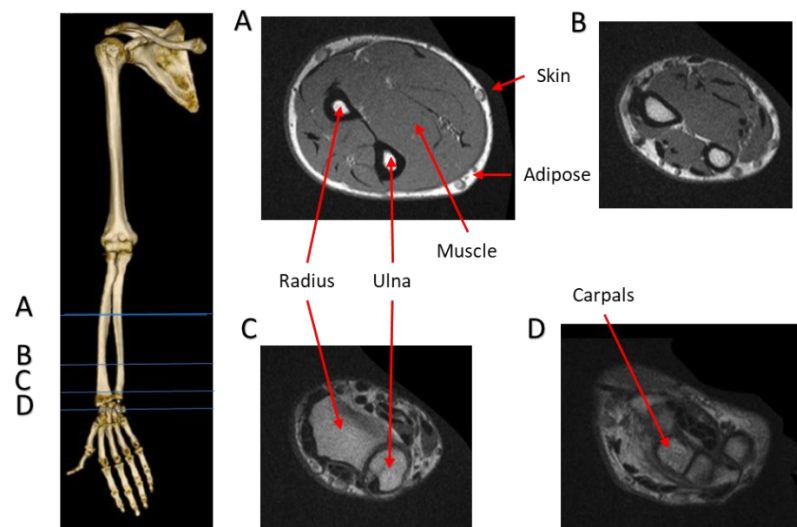
Figure 2-10 MRI cross-sectional images of the upper extremity (Micheau et al., 2017, e-Anatomy, IMAIOS).

The main components of the hand and forearm are the skin, adipose tissue, muscle and bone (labelled in Figure 2-10) (Clarys and Marfell-Jones, 1986). To determine the mass of each component of the hand and forearm, Clarys and Marfell-Jones (1986) portioned six cadavers into skin, adipose tissue, muscle and bone. The overall mass of the hand and forearm was stated as 1,091.65 g (Table 2-7).

Table 2-7 Forearm and hand components masses (Clarys and Marfell-Jones, 1986).

	Component	Mass in g, (%)
Forearm	Skin	63.8 (8)
	Adipose	181.1 (24)
	Muscle	397.8 (52)
	Bone	121.7 (17)
	Total	746.4
Hand	Skin	59.55 (17)
	Adipose	77.25 (23)
	Muscle	111.95 (31)
	Bone	96.5 (28)
	Total	345.25
Overall Total		**1091.65**

Muscle volume is typically measured using MRI, bioelectrical impedance analysis (BIA), or directly measured from cadavers (Stahn *et al.*, 2007; Clarys and Marfell-Jones, 1986). The mean ± SD muscle volume from five published articles (Stahn *et al.*, 2007; Holzbaur *et al.*, 2007; Clarys and Marfell-Jones, 1986; Vidt *et al.*, 2012; Miyatani *et al.*, 2001) for the forearm was 527 ± 44 cm^3, whereas the (upper) arm was $1,183 \pm 55$ cm^3 (Figure 2-11a). The mean ± SD of the flexor muscles (275 ± 20 cm^3) was larger than for the extensor muscles (150 ± 23 cm^3) (Holzbaur *et al.*, 2007; Vidt *et al.*, 2012) (Figure 2-11a). A comparison was also made between the muscle volume of the forearm and of the thigh (Figure 2-11b). The forearm has 83% less muscle volume than the thigh, due to the size of the muscle and demand (e.g. muscle power), so less soft tissue simulant would be required for a surrogate wrist than for a surrogate thigh, such as the one developed by Payne (2015). Payne (2015) did not state the volume of soft tissue simulant used in his thigh surrogate, although it was approximated here as 1,219 cm^3 from the dimensions of the

cylindrical surrogate FE model (276 mm height, ⌀70 mm), which is low in comparison the reported values in Figure 2-11.
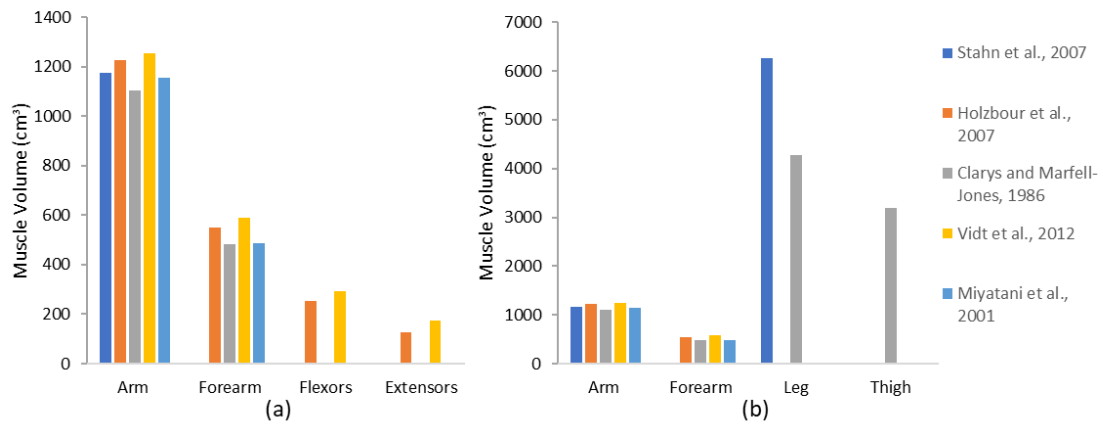
Figure 2-11 Reported muscle volumes of (a) the upper extremity and (b) comparison between upper extremity, leg and thigh.

Orsted *et al*. (2017) states that the thickness of the epidermis (outermost layer of the skin) ranges from thin (0.5 mm i.e. eardrum) to thick (6 mm i.e. the sole of the foot) depending on its location on the body. Skin and soft tissue thicknesses of the wrist and forearm are displayed in Table 2-8, and are typically measured using ultrasound techniques. The mean skin thickness for the forearm and hand from the literature were 1.2 ± 0.4 mm and 1.4 ± 0.1 mm respectively (Table 2-8). Ivarinen *et al*. (2011) reported tissue thicknesses within the forearm of 2.1 ± 0.3 mm, 2.1 ± 2.3 mm and 10.3 ± 1.9 mm for skin, adipose and muscle, respectively. Choi and Robinovitch (2011) measured the thickness of soft tissue over the palm region. A mean soft tissue thickness of 7.7 mm was found in the high BMI group, reducing to 6.9 mm in the low BMI group. Such knowledge of skin thicknesses around the hand and forearm (Table 2-8) could inform a suitable choice of skin and soft tissue simulant thickness in a wrist surrogate. It appears that a skin/soft tissue simulant with a thickness of around 1 to 2 mm around the hand and forearm, increasing to around 7 to 8 mm around the palm region, would be suitable for a wrist surrogate.

Table 2-8 Forearm and hand skin thickness.

Location	Thickness (mm) (mean ± SD)	Participants	Measurement technique	Source
Forearm skin	2.1 ± 0.3	7 ♂	B-mode ultrasound imaging	Iivarinen *et al.,* 2011
	2.1 ± 2.3	2 ♀		
		Age: 31±8 years		
Forearm muscle	10.3 ± 1.9	Mass 84±10 kg		
		Length of ulna bone: 29±2 cm		
Ventral forearm	~0.9	30 ♂, 30 ♀	Suction system with an ultrasound scanner	Diridollou *et al.,* 2000
		Age: 28±6 years		
Ventral forearm	0.80 to 1.00	8 ♂,	Ultrasonic echography	Escoffier *et al.,* 1989
	0.68 to 0.74	9 ♀		
	(digitised by author from the graph)	Age: 20-30 years		
Radial aspect of the forearm	1.3 ± 0.02	51 ♂,	Radiographic method	Black, 1969
	1.1 ± 0.005	53 ♀		
		Age: <65 years		
Forearm flexor	1.02 ± 0.10	44 ♂,	Pulsed ultrasound	TAN *et al.,* 1982
	0.81 ± 0.08	36 ♀		
		Age: 21-30 years		
Forearm flexor	1.11 ± 0.05	3 ♂, Age: 24-31 years		
Forearm extensor	1.29 ± 0.08			
Radial aspect of the forearm	0.75 to 1.16	10 ♂ and ♀	Pulsed ultrasound	Alexander and Miller, 1979
		Age: 24-37 years		
Forearm extensor	1.36 ± 0.25 (♀)	8 ♂, 10 ♀	Ultrasound scanner	Olsen *et al.,* 1995
	1.42 ± 0.14 (♂)	Age: 24-41 years		
Forearm flexor	1.12 ± 0.19 (♀)			
	1.31 ± 0.13 (♂)			
Hand dorsal	1.26 ± 0.18 (♀)			
	1.50 ± 0.14 (♂)			
Palm	1.50 ± 0.52 (♀)			
	1.48 ± 0.45 (♂)			

Mean skin thickness of the forearm: 1.2 ± 0.4
Mean skin thickness of the hand: 1.4 ± 0.1

Previous studies that have included a compliant layer to represent skin or soft tissue on a sports surrogate have typically used a thickness of ~3 mm. Maurel *et al.,* (2013) added a 3 mm thick rubber layer to model the compliance of the human hand on a hand surrogate for assessing the impact performance of wrist protection designs. An appropriate material and thickness was determined based on results from an impact test of various forms of foams and rubber substrates placed between the hand model and load cell. Payne (2015) selected a 3 mm thickness for the skin on a thigh surrogate, determined from reported thicknesses of 0.9 to 3.3

mm. Ankrah and Mills (2003) used a 2 mm thick silicone rubber layer to simulate the skin on the shin, and to hold the surrogate components together. Furthermore, Ankrah and Mills (2004) used a 2 mm thick ESI foam to simulate skin over the ankle. The thickness of 2 mm was selected because it had similar indentation resistance as human soft tissue in the ankle area, as measured with participants.

Spartacus *et al.*, 2021 recently conducted a study measuring the *in-vivo* stiffness of the palm. The soft tissue thickness over the trapezium was measured with the wrist at three angles (0°, 45° and 65°), and indentation tests were performed at two frequencies (0.2 Hz and 20 Hz) to 50% of the participants soft tissue thickness. Participants were put into three groups depending on soft tissue thickness (< 2.5 mm, 2.5 to 3.0 mm and > 3.0 mm). Palmar tissue thickness was positively correlated with weight, height, and BMI, and was different between males and females. The average male tissue thickness was 20% greater than females. The response of the soft tissue in the palm was non-linear and rate dependent, with high variability between participants. Loading rate had the greatest effect on peak force and energy absorbed. Changing joint position introduced additional variability. Stiffness (at large deformation of 25 to 30%) ranged from 0.11 to 1.78 N/mm (0° wrist extension), 0.15 to 1.58 N/mm (45° wrist extension) and 0.15 to 1.15 N/mm (65° wrist extension) at the low frequency (0.2 Hz) and 0.19 to 2.45 N/mm (0° wrist extension), 0.24 to 7.15 N/mm (45° wrist extension) and 0.32 to 3.81 N/mm (65° wrist extension) at the high frequency (20 Hz).

2.5.2   Surrogate Shape

Payne (2015) argues that surrogates with biofidelic geometries should be used when testing protective equipment, so it maintains alignment and remains attached. Methods used to develop surrogates with human-like geometries include using anthropometric data, or taking a cast or scan of the corresponding body part. Adams *et al.* (2018) studied the effect of surrogate design on the measured stiffness of snowboarding wrist protectors. A simplified geometric representation of a hand and forearm (BS EN ISO 20320:2020 wrist surrogate) gave more consistent results than a rectangular cross-section forearm and a paddle-like hand (BS EN 14120:2003 wrist surrogate), and a hand and forearm based on a laser scan of a (almost) 50th

percentile male (pendulum impact test surrogate (Section 2.3.3)). The implications of relative differences in protector stiffness measurements between surrogates depend on the purpose of the test. When assessing the effect of design parameters on product performance, these relative differences between surrogates can cause issues (Adams *et al.*, 2018).

2.5.3 Skin and Soft Tissue Simulants

A surrogate made up of stiff materials does not truly represent the compliance of a human limb. Maurel *et al.* (2013) states that the elasticity of the tissues in the upper limb helps reduce the forces in a fall onto an outstretched arm, and thus the severity of injury. It is inferred that a human surrogate utilising soft tissue simulants will represent a better prediction of human response (Payne *et al.*, 2015; Adams, 2018).

Elastomers are generally considered to be good tissue equivalents due to their durability, consistent response and similar densities to organic tissue (Payne *et al.*, 2014). Silicone elastomers exhibit both hyperelastic and viscoelastic material behaviour, meaning they exhibit non-linear responses to deformation and strain rate dependencies. Sports surrogates traditionally have one soft tissue simulant to represent all tissues in the segment, whereas Payne *et al.* (2015) developed multi-material soft tissue simulants to represent the different structures within a thigh surrogate (Table 2-9). The silicone Silastic™ 3481 is often used to represent soft tissue in sports surrogates. The quasi-static compressive response of Silastic™ 3481 is compared to organic structural tissue in Figure 2-12. Silastic 3481 compares well with organic tissue in general, but does not match to any particular organic tissue (Payne *et al.*, 2015). Polydimethysiloxane (PDMS) silicones can be manipulated (by changing the concentrations of constituents) to match different tissue properties, which means they can be applied to simulate different tissues within a surrogate. Payne *et al.*, (2015) developed PDMS silicones to match the quasi-static compression of relaxed muscle, contracted muscle, skin, and adipose (Figure 2-13).

Table 2-9 Soft tissue simulants used in sports surrogates.

Simulant (generic / trade names)	Application	Properties/Reason	Reference
Ballistic gelatine	Soft tissue simulant for a frangible leg surrogate	Used as an international standard for the Wound Ballistic community to simulate human soft tissues	Bergeron *et al.*, 2001
Silastic™ 3481	Soft tissue for sports surrogates	Employed within the sports PPE industry	Payne *et al.*, 2014
	Soft tissue for a shoulder surrogate for testing rugby padded clothing		Hughes *et al.*, 2021
Silastic™ 3483	Soft tissue of a thigh surrogate	Peak acceleration of the simulant did not differ from the peak acceleration of the cadaver and human volunteer drop tests	Hrysomallis, 2007
	Soft tissue in a destructible headform	Typically used as soft tissue simulants. Product more repeatable results than ethyl vinyl acetate foams	Stone *et al.*, 2021
PDMS maxillofacial silicone	Multi-material (relaxed muscle, contracted muscle, skin, adipose) thigh surrogate for cricket impacts	Can manipulate the constitutive silicone compounds to tailor the mechanical properties to match the dynamic response of each organic tissue	Payne *et al.*, 2015
Plasil-Gel 01-30 A+B	Head surrogate: Different combination of components used to mimic the skin and the brain properties	Can be tuned according to necessities and moulding outcomes	Petrone *et al.,* 2018
Senflex 435	Soft tissue substitute for ankle and lower leg surrogates	Similar indentation resistance as human soft tissue in the ankle area	Ankrah and Mills, 2003; Ankrah and Mills, 2004
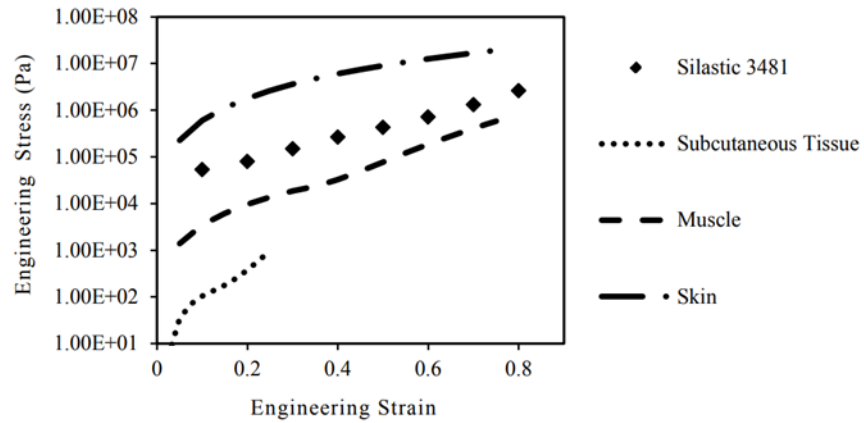
Figure 2-12 Quasi-static compressive stress-strain of Silastic 3481 compared to organic tissue (Payne et al., 2014). Log scale on the y-axis.
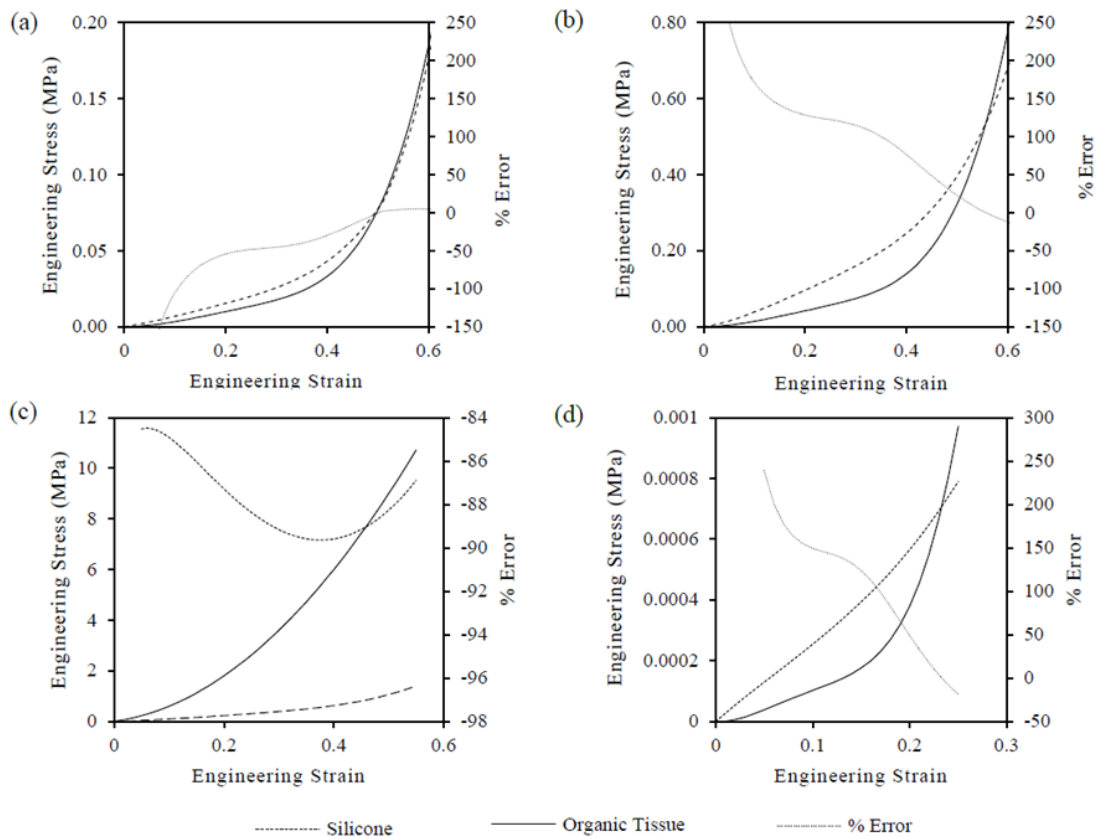
Figure 2-13 Quasi-static compressive response of bespoke PDMS silicones compared to organic tissue, (a) relaxed muscle, (b) contracted muscle, (c) skin, (d) adipose (Payne et al., 2015).

While using soft tissue simulants within a surrogate can increase biofidelity, the typically manual fabrication process of silicones creates challenges and limitations. Factors such as simplicity, reproducibility and repeatability of manufacture, and durability need to be considered. The benefits of using silicones in a wrist surrogate

must outweigh the limitations for their use to be worthwhile. As such, silicones could be added incrementally to determine the effect of different levels of compliance when testing wrist protectors. Furthermore, silicone can simply be moulded around a surrogate to achieve a specific geometry. Initially, the effect of a compliant layer to represent skin and potentially provide a better protector fit with less slippage during testing, could be determined. A simulant representing a skin layer on a wrist surrogate could be enough for the bend test, but a thicker layer representing soft tissue may be needed for impact testing.

The medical appliance industry has developed synthetic human tissue to replace live animals, cadavers and human participants for clinical training and surgical simulation. SynDaver™ (2020 online) manufactures synthetic human and animal tissue simulants, full bodies and body parts. Relevant products include a SynTissue(R) arm (includes all major skeletal, muscular and cartilaginous structures between the scapula and the fingers), adult skin (20 by 20 cm sheet with a thickness of 1 to 3 mm), and a muscular tissue plate (consisting of adult skin, subcutaneous fat and skeletal muscle) (Figure 2-14). The synthetic materials are validated by matching mechanical (tensile modulus, abrasion resistance, penetration force, coefficient of friction), physical and chemical properties to the tissue it is intended to mimic. The advantages of using SynDaver™ skin/muscle products in a wrist surrogate is that they come ready-made, they are pre-validated to match the tissue required, and they should be more consistent than manually mixed silicones, which is particularly important for use in test houses. The disadvantages include the specific storage techniques required, the cost (adult skin £30-40, muscle tissue £35-150), and it could be challenging to apply them to the specific geometry of a wrist surrogate. SynDaver™ products could be used during material testing, allowing for comparison with candidate simulants.
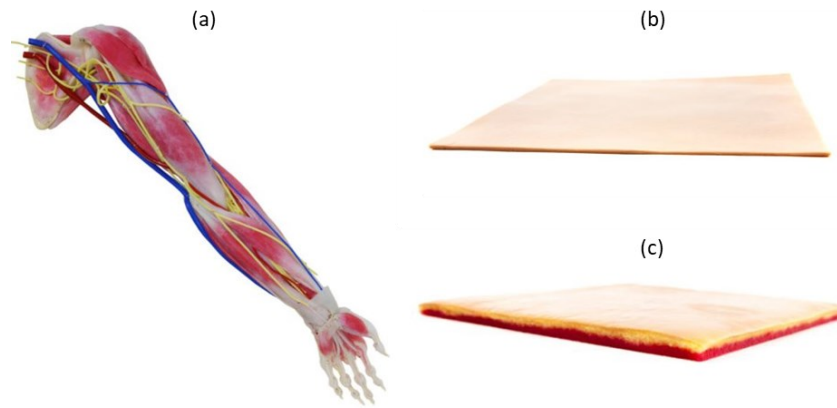
Figure 2-14 SynDaver^{TM} products: (a) SynTissue ® arm, (b) adult skin, (c) muscle tissue plate (SynDaver, 2020 online).

Bone models have been developed mainly to help train doctors and improve their skills. One supplier of these is Sawbone® (Pacific Research Laboratories Ltd., Washington, USA). Studies have used bone models, typically a Sawbone® tibia, when developing a surrogate for PPE testing (Francisco *et al*., 2000; Ankrah and Mills, 2003; Ankrah and Mills, 2004; Payne *et al*., 2016). The fourth generation composite from Sawbone® is the most recent version and performs within the biological range of healthy adult bones with respect to quasi-static flexural and torsional rigidity, with lower variability than cadaver specimens (Gardner *et al*., 2010). The tensile and compressive mechanical properties of fourth generation composite Sawbones® compared with organic bone is presented in Table 2-10. The loading response of viscoelastic material like bone is rate dependent, with a measurable increase in stiffness with increasing loading rate (Greenwald *et al*. 1998). So while the Sawbone® composite has a similar quasi-static response to organic bone (Table 2-10), under impact, in a sporting scenario, the response may differ (i.e. organic bone will increase in stiffness and the composite bone may not). Relevant Sawbone® products for a wrist surrogate include a radius, ulnar, hand, hand with wrist ligaments, and hand and wrist with moveable carpals (Table 2-11).

Table 2-10 Tensile and compressive mechanical properties of 4th generation Sawbone® composite and organic bone. Reproduced from Payne (2015), original data from Heiner (2008).

	4th generation Sawbone®	Organic bone
Tensile elastic modulus (GPa)	16.0	17.0
Tensile strength (MPa)	107	130
Compressive elastic modulus (GPa)	16.6	17.0
Compressive strength (MPa)	154	170

Table 2-11 Available Sawbone® products of the hand, wrist and forearm (Sawbone®, 2017 online).

Part	Approximate Cost (£)	Image
Radius, fourth generation	135	
Ulnar, fourth generation	135	
Hand, fourth generation	181	
Hand with wrist ligaments, solid white plastic	87	
Hand and wrist with moveable carpals, solid foam	48	

While bone models from a supplier such as Sawbone® may be well suited for use in a wrist surrogate as bone simulants, there are limitations. The high cost would be a concern if the surrogate was to be used in test houses, and more than one may need to be purchased if breaks or fractures occur, or damage occurring within the material, due to the test conditions (i.e. worst case scenario or bare hand scenario). The development of a wrist surrogate will be incremental, and although bone surrogates could be integrated into a wrist surrogate, they are a lower priority than a soft tissue layer.

2.5.4 New Technology and Manufacturing Processes

Three dimensional (3D) printing (or additive manufacturing) is being driven by the invention of new printable materials and associated processes (Chua *et al*., 2017). For biomedical engineering, 3D printing has applications such as biomodels, prostheses, surgical aids, implants, and scaffolds (Chua *et al*., 2017). 3D printing of thermoplastic polymers is relatively straightforward, as the extruded hot melt solidifies rapidly during printing. Printing with elastomeric polymers is more difficult as their precursors are normally liquid at room temperature, alongside their longer curing times (Roh *et al*., 2017). With advances in 3D printing, the materials that can be printed have evolved to include elastomeric and flexible materials (Qiu *et al*., 2018) (Table 2-12).

The 3D printing of soft tissue simulants, like silicones, could provide a repeatable and reproducible method of manufacturing, compared with manually moulded silicones. 3D printing surrogates containing elastomers could improve biofidelity, whilst offering manufacturing consistency. Furthermore, multi-material printing could be used to make a surrogate with a stiff core and flexible layer in one process.

Table 2-12 Examples of flexible 3D printable materials.

Material	Description	Tensile Strength (MPa)	Shore A Hardness	Elongation at Break (%)	Source
Agilus30	Durable rubberlike photopolymer capable of withstanding repeated flexing and bending	2.4-3.1	30-35 Scale A	220-270	Stratasys, 2017
Tango	Simulates rubber with different levels of elongation	0.8-1.5	26-28	170-220	
VeroFlex	used for flexible eyewear prototypes	43-64	75-85 Scale D	8-20	
NinjaFlex	Thermoplastic elastomers filament	4	85	660	NinjaTek, 2016

2.5.5 Measurement Techniques/ Instrumentation for Sports Surrogates

Instrumentation used in PPE certification test rigs typically includes accelerometers and load cells. For example, an accelerometer can be attached to the impactor to measure its acceleration as it strikes a PPE item mounted to an anvil secured to a

load cell/s for measuring the impact force. With instrumentation typically mounted on the test rig, and the widespread use of rigid anvils, there has been limited development of surrogates with inbuilt instrumentation. Instrumentation within a biofidelic surrogate could offer a means of measuring injury mechanisms (Payne *et al.*, 2016), providing feedback from the surrogate (local results) rather than just the energy absorbed by the PPE (global results).

Kim *et al.* (2006) used the forearm and hand of the anthropometric test device to measure the energy absorption of wrist protective devices. The forearm/hand was equipped with a load cell in both the wrist joint and the forearm, and a potentiometer in the wrist. Adams *et al.* (2021) incorporated a potentiometer into the wrist of the impact surrogate. The potentiometer was offset below the wrist joint, due to the limited space available at the joint, and connected via a toothed timing belt to the wrist joint shaft. The potentiometer was used to measure wrist joint angle and monitor wrist hyperextension during impact. Petrone *et al.* (2018) developed an instrumented human head surrogate. The head surrogate included nine tri-axial accelerometers, which were inserted into the silicone brain during casting, for exploring local behaviours during impacts. Further instrumentation included a tri-axis gyroscope at the centre of mass, and ten pressure sensors embedded in cavities in the skull.

Devices for measuring pressure often contain thin film piezoresistive sensors, creating a mobile pressure measurement system. Pressure sensors (Tekscan™ Flexiforce, Tekscan™ F-Socket 9811, Tekscan™ Model 9500, Tekscan™ F-Scan) have been used in sports impact studies, including human-on-human impacts in American Football (Halkon *et al.*, 2012) and baseball (Halkon *et al.*, 2014), face impacts from a boxer punch (Walilko *et al.*, 2005), ankle impacts in football (Ankrah and Mills, 2004), and stud impacts on shin guards (Ankrah and Mills, 2003). Measurements such as a pressure map of elbow and knee impacts, pressure and contact area of a punch, pressure distribution of shin guards during stud impacts, and peak pressure when pushed into the ankle tissue, were taken within these studies. Such pressure sensors are typically fitted between the PPE and body, mounted to the underneath of the PPE, mounted onto synthetic skin, or inserted

between layers of a surrogate. Payne (2015) showed that pressure sensors embedded within silicone layers of a surrogate can introduce artificial stress concentrations and affect the impact response. Adding pressure sensors to a wrist surrogate could be beneficial to monitor the interaction with the protector, quantify fit, set strapping tightness, and map areas of high pressure during testing (Adams, 2018). Measurements of high pressure caused by wrist protectors during impact testing, or pressure at specific points along the wrist/forearm, may provide a better insight into the wrist injury mechanism.

Strain gauges are used to measure displacement/deflection; when the conductive material of the strain gauge stretches, the resistance increases, generating a measurable change which is calibrated against a known increase in displacement. Strain gauges have been used to measure the deflection of sports equipment such as a golf club shaft during a swing (Milne and Davis, 1992), or a badminton racket during a stroke (Kwan *et al.*, 2010). Strain gauges are typically mounted to stiff bodies, whereas when mounted to a compliant material, most conventional strain gauges introduce artificial stiffness (Payne, 2015). Mounting a strain gauge to a bone of a surrogate forearm could be beneficial, whereas they would not be well suited for embedding or mounting to the surface of a wrist surrogate containing soft tissue simulants. Strain gauges could be mounted to the splints of wrist protectors, to measure deflection during testing.

Another method to measure displacement is Digital Imaging Correlation (DIC). A speckle pattern is added to the object of interest and a camera is used to film the corresponding test. There are commercial offerings, including GOM, which are capable of tracking these speckles, and calculating displacements with reference to a static reference. Payne (2018) used DIC when impact testing his thigh surrogate to determine the surface strain. DIC could be used to measure the deflection of wrist protector splints during the bend or impact test, although it may be impossible to film the splints directly if they are incorporated into the protector. Such testing could enable a comparison between how much the protector splints deflect, and the protector's stiffness and energy absorption. A comparison between different

protectors and splint lengths, as well as how the design of the wrist surrogate affects how the protector's splints deflect could be determined.

2.5.6   FE Modelling

Finite Element (FE) modelling is a tool that can be used to predict and explain the structural response of the anatomy under various conditions. The validity of an FE model is dependent on the quality of model with regards to geometry and material properties, and thus its predictive capabilities are enhanced by the input of experimental data (Crandall *et al.*, 2011). FE models are widely used to simulate sports impact scenarios as a development from a mass striker (i.e. stiff anvil) in experimental tests, to impact scenarios experienced in play, taking into account the connected bony masses and soft tissues of the striker/player.

FE models have been used to simulate sports impacts, such as the impact loading of the distal radius in forward falls (Burkhart *et al.*, 2014), and used alongside the development of sports surrogates, using the experimental testing to validate the FE model. Alongside the development of the ankle and shin surrogate in Table 1.5, Ankrah and Mills (2004) simulated stud impacts on a protected ankle, and stud impacts on shin guards (Ankrah and Mills, 2003). Newton-Mann (2019) developed FE models of two snowboarding wrist protectors, simulating the pendulum impact test rig setup of Adams (2018). FE models can be used as a design tool to determine the levels of complexity at which appreciable differences in response are attained, preventing engineering of overly complex surrogates. Payne *et al*. (2015) used FE modelling as a design tool to assess the influence of soft tissue layers and surrogate shape on the mechanical response of a thigh surrogate. FE modelling of multi-bone joints, such as the wrist and ankle, poses several challenges due to the number of anatomical connections, complex geometry, non-linear properties of supporting soft tissue structures and the inter-relationship between these components (Gíslason *et al.*, 2010; Freutel *et al.*, 2014).

Material models are used to describe the multi-dimensional material behaviour based on material constants derived from experimental tests. The selection of a suitable material model and determination of appropriate parameters influences the accuracy of results. Ogden is a commonly used hyperelastic model to describe

the material behaviour of soft solids that are both isotropic and incompressible, and thus is suitable for modelling soft tissue. The model proposes that the strain energy function (W) is based on the principal stretches (λ1, λ2, λ3), with the material parameters; μ describing the shear behaviour and α describing the strain hardening. The Ogden model is represented in Equation 1 (Ogden, 1972). The n term in the equation refers to the number of α and μ pairings, with more pairings indicating a more complex material curve.

$$W = \sum_{n=1}^{N} \frac{\mu_n}{\alpha_n} \left(\lambda_1^{\alpha_n} + \lambda_2^{\alpha_n} + \lambda_3^{\alpha_n} - 3 \right)$$

<div align="right">Equation 1</div>

Another commonly used hyperelastic model is Mooney-Rivlin. The Mooney-Rivlin model observes rubber's response is linear under simple shear loading conditions (Equation 2). The Mooney-Rivlin model is extended by developing W as a polynomial series (Equation 3).

$$W = C_1(I_1 - 3) + C_2(I_2 - 3)$$

<div align="right">Equation 2</div>

Where C1 and C2 are material parameters and I1 and I2 are strain invariants (Marckmann and Verron, 2006).

$$W = \sum_{i=0,j=0}^{\infty} c_{ij}(I_1 - 3)^i (I_1 - 3)^j$$

<div align="right">Equation 3</div>

The material model parameters used for bone and soft tissue in previous FE models of human limb surrogate are presented in Table 2-13. These material model parameters could be used in a wrist surrogate FE model, or they could be compared against those used in developed simulants within a wrist surrogate.

Table 2-13 Material model parameters for human bone and soft tissue.

Component	Model	Model parameters	Density (kg/m^3)	Young's Modulus (GPa)	Poisson's Ratio	Associated paper
Soft tissue of leg	Ogden (two term)	$\mu_1 = \mu_2 = 200$ kPa, $\alpha_1 = 2$, $\alpha_2 = -2$, $D = 1.0 \times 10^{-9}$ Pa^{-1}	n/a	n/a	n/a	Ankrah and Mills, 2003
Tibia	Elastic	n/a	n/a	11.5	0.4	
Ankle bone	Linear elastic	n/a	n/a	10	0.3	Ankrah and Mills, 2004
Lunate / scaphoid	Linear elastic	n/a	1,060	3	0.38	Burkhart *et al.*, 2014
Skin	Ogden	$\mu = 2.20 \times 10^6$ $\alpha = 12$	1,110	n/a	n/a	Payne *et al.*, 2015
Adipose	Ogden	$\mu = 1.70 \times 10^3$ $\alpha = 23$	1,100	n/a	n/a	
Relaxed muscle	Ogden	$\mu = 3.63 \times 10^4$ $\alpha = 45$	920	n/a	n/a	
Cortical bone	Ogden	$\mu = 4.58 \times 10^9$ $\alpha = 25$	1,880	n/a	n/a	
Cortical bone, Tibia/fibula	Linear elastic	n/a	1,850	17	0.3	Smolen and Quenneville, 2017
Plantar soft tissue	Ogden	$\mu = 24.72$ kPa $\alpha = 8.39$	1,000	n/a	0.49	
Cortical bone	Linear elastic	n/a	2,000	18	0.2	Gislason *et al.*, 2009
Cartilage	2 parameter Mooney Rivlin	$C_{10} = 4.1$ MPa $C_{01} = 0.4$ MPa	n/a	n/a	n/a	Gislason *et al.*, 2010

Creating an FE model of the developed wrist surrogate alongside the test procedure and parameters, and including the snowboarding wrist protector being tested, is outside the scope of this current project. FE modelling, however, will be used throughout the project as a design tool for the wrist surrogate.

2.6 Critique of State-of-the-art Wrist Surrogates

As a final stage in preparation for developing a wrist surrogate, the main elements of current state-of-the-art wrist surrogates have been critiqued to help prioritise and identify the specific ones to focus on for this project. The current state-of-the-art surrogates are the BS EN ISO 20320 surrogate and the impact surrogate of Adams (2018). Action priority matrix's are suitable when there are many elements to prioritise (Slack, 1994). The two surrogates have each been split into 10

elements, which were subjectively rated by the author on their current performance, level of importance, and challenge associated with improving them (Table-2-14 and Table-2-15). The surrogate elements were then imputed into an action priority matrix (Figure-2-15), where they fall into one of four categories within the matrix; quick wins (high impact combined with low effort), major projects (high impact and high effort), fill ins (low impact and low effect), and hard slogs (low impact but require high effort). The two surrogates were critiqued separately due to differences between some elements, whereas, the action priority matrix combines both surrogates.

Table 2-14 Critique of bend test surrogate. Images from Adams (2018) or taken by the author of Adam's (2018) surrogates (permission granted).

Elements	Author rated current performance /10	Importance	Difficulty
Mounts	9/10 Additional surrogate base and clamp on fingers attach to testing machine	High Enable consistency of testing and setup	Low Can be adapted to suit test setup
Instrumentation	0/10 None on the surrogate	High Could provide more feedback of the wrist response during testing	Medium Integration could reduce biofidelity and protector fit
Mass	5/10 Medium surrogate mass (including fingers): 1116.1 g (mass of hand and forearm from Table 1.7 1,092 g)	Medium Should be a representation of human wrist mass. Importance of hand is higher than arm during bent testing (as arm is static)	High Specific weight difficult to achieve due to combination of materials, geometry and instrumentation
Fingers	7/10 Steel fingers. Repeatable. Currently machined separately, which adds an extra step (added time, cost and could introduce uncertainties)	Low Allow testing of integrated glove protectors	Low Can easily adapt geometry
Joint Type	7/10 Single axis hinge joint	High Should be a representation of human wrist joint	High Complexity of wrist joint
Range of Motion	7/10 Current range 180°+ (flexion / extension)	High Representation of human wrist range of motion	Low Simple to change joint dimensions. Addition of stoppers on joint. (Identifying the injury range is more challenging)
Geometry	7/10	High Representation of human wrist size in three categories	High Variation in surface features between humans

	Simplified geometric surrogate based on anthropometric data. Small, medium, large		
From BS EN IS0 20320			
Material Additive manufactured polyamide hand and forearm, steel fingers	5/10 Not representative of compliance of human wrist. Ideal for test houses - consistent, repeatable	High Representation of human wrist soft tissue	High Issues with repeatability. Complex to manufacture. Simulants required
Surface Finish/Friction	3/10 Slippage of wrist protector during testing	High Fit of protector throughout testing needs to be consistent	Low Addition of surface texture/higher friction surface material
Joint Stiffness	1/10 Low friction joint. Start angle set by protector	High Representation of human wrist joint stiffness	High Accurate representation of human wrist stiffness, variation

Table 2-15 Critique of impact test surrogate. Images from Adams (2018) or taken personally of Adam (2018)'s surrogates (permission granted).

Elements	Author rated current performance /10	Importance	Difficulty
Mounts	7/10 Surrogate central core attached to base. Some unwanted movement observed by Adams (2018) during testing	High Enable consistency of testing and setup	Low Can be adapted to suit test setup
Instrumentation	4/10 Potentiometer, dynamometer	High Could provide more feedback of the wrist response during testing	Medium Integration could reduce biofidelity and protector fit
Mass	5/10 Steel hand, additively manufactured polyamide forearm casting, steel core	Medium Representation of human wrist soft tissue	High Specific weight difficult to achieve due to combination of materials, geometry and instrumentation
Fingers	0/10 No fingers (except for setting the hand angle before testing)	Low Not part of initial contact during impact	Low Addition of fingers
Joint Type	7/10 Single axis hinge joint. Belt to connect to potentiometer. Core protrudes	High Representation of human wrist joint	High Complexity of joint
Range of Motion	7/10 Current degrees 180°+ (flexion / extension)	High Representation of human wrist range of motion	Low Simple to change joint dimensions. Addition of stoppers on joint. (Identifying the injury range is more challenging)
Geometry	7/10 3D scan of human hand and forearm Only one size	High Representation of average human wrist	High Variation in surface features between humans
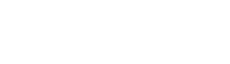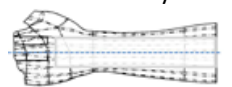
Materials	5/10	High	High
Steel hand, additive manufactured polyamide forearm casing, steal core	Unrepresentative of compliance of human wrist. Ideal for test houses - consistent, repeatable	Representation of human wrist soft tissue	Issues with repeatability. Complex to manufacture. Simulants required.
Surface Finish/Friction	3/10	High	Low
	Slippage of wrist protector during testing	Fit of protector throughout testing needs to be consistent	Addition of surface texture/higher friction surface material
Joint Stiffness	1/10	High	High
	Low friction joint. Start position set by protector.	Representation of human wrist joint stiffness	Accurate representation of human wrist stiffness, variation
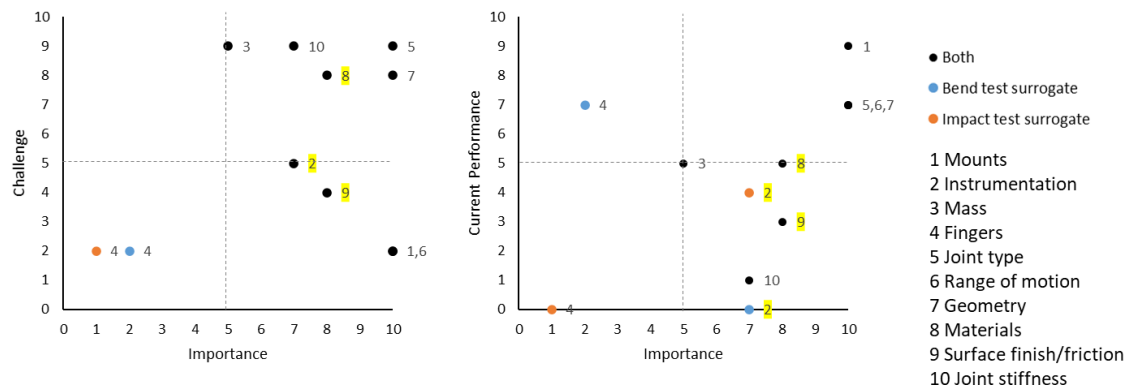
Figure 2-15 Action priority matrix of bend and impact test surrogate.

Highlighted in the action priority matrix (Figure 2-15) are three elements; materials, instrumentation and surface finish/friction. These elements have been identified as high importance, but vary in challenge level. Furthermore, they lie towards the lower end of current performance. These three elements have been reported in Section 2.5, and have been chosen as the elements this current project will focus on with the goal of improving the existing test model.

2.7   Chapter Summary

The need for a better wrist surrogate for improved assessment of the wrist injury mechanism and the effectiveness of wrist protection has been established. Studies highlight wrist injuries as a problem amongst snowboarders. The testing of wrist protection has suggested that wrist protectors probably work, however, the specific work on the wrist injury mechanism is missing.

Falling onto an outstretched arm was attributed to wrist injuries in snowboarding. The maximum non-injurious wrist extension was reported as 85°, with wrist angles of ~30° to 50° reported at the initiation of a fall but prior to impact. A fracture threshold of ~1,000 to 4,000 N was reported from cadaver impact studies. Wrist angles and fracture loads can inform the design and test parameters for wrist surrogates.

Current wrist surrogates consist of stiff materials that do not represent the compliance of a human wrist complex, and are underdeveloped compared to other sports surrogates. The development of the wrist surrogate for assessing

snowboarding wrist protection and snowboarding wrist injuries is the next step enhancing the work of Adams (2018) and Newton-Mann (2019) on the development of snowboarding wrist protector tests and FE models. Subsequent wrist surrogates will be designed for use in the quasi-static bend test and pendulum impact test previously developed by Adams (2018), although adaptations to these tests will be required to create a more biofidelic surrogate model.

Based on the literature review, the idealised solution to move towards reality from where we currently are, is to implement soft tissue simulants and instrumentation within a wrist surrogate, while using FE modelling as a design tool. Maxillofacial silicones have been identified as a starting point for developing surrogate compliance and protector fit. Pressure sensors could monitor the interaction between protector and surrogate, set strap tightness and map areas of high pressure during testing. FE modelling is useful for validation, justification and as a design tool for the development of the wrist surrogate.

Progression towards more biofidelic surrogates should be incremental, and constantly validated. Repeatability and reproducibility (during testing and manufacture) of a wrist surrogate needs to be considered for implementation into certification tests, and hence 3D printing techniques may be appropriate over manual fabrication. Therefore, a balance between surrogate biofidelity and surrogate repeatability is needed. An improved biofidelic wrist surrogate coupled with instrumentation will bridge the gap in knowledge of the effectiveness of wrist protection components and their protective capabilities, allowing for better assessment and design of protective equipment.

3. <u>Identification of Suitable Soft Tissue Simulants for a Wrist Surrogate</u>

3.1　Introduction

As highlighted in the literature review in Chapter 2, to improve the biofidelity of the current wrist surrogate (i.e. BS EN ISO 20320:2020), skin and soft tissue simulants were proposed. The aim of this current chapter was therefore to identify a suitable skin/soft tissue simulant to be used for the wrist surrogate. Previous soft tissue simulants used within sports surrogates reported within the literature have included Silastic™ 3481 and Silastic™ 3483 to represent soft tissue of the anterior thigh (Hrysomallis, 2007) and soft tissue in a headform (Stone *et al.*, 2021). Senflex 435 foam has also been used to represent soft tissue of the shin (Ankrah and Mills, 2003) and ESI foam to represent skin over the ankle (Ankrah and Mills, 2004). Other materials such as ballistic gelatine have been incorporated to represent the soft tissue of the leg (Bergeron *et al.*, 2001), and Polydimethysiloxane (PDMS) silicones to represent the different tissue constructs in the thigh (Payne *et al.*, 2015).

Silicone elastomers are considered to be good tissue equivalents due to their durability, ease of use, can be coloured to natural skin tissue, repeatable response and similar densities to organic tissue. Maxillofacial silicones are composed of PDMS silicone, which have previously been used in a thigh surrogate (Payne, 2018), and are commonly used for facial prosthetics in reconstructive science due to its ideal material properties (Hatamleh and Watts, 2010). PDMS silicone can be manipulated to match different tissue properties, and thus Payne (2018) developed PDMS silicone to represent relaxed muscle, contracted muscle, skin and adipose to create a biofidelic thigh surrogate. Maxillofacial silicones were therefore taken forward in this current project (as stated in Chapter 2 Section 2.7), and material testing of candidate maxillofacial silicones was conducted. The stress strain relations of the candidate silicones was compared to those in the current published literature, and one was selected for use in a wrist surrogate. Selection criteria was based on the repeatability of the silicone response, the agreement of this response

with values of organic tissue and soft tissue simulants in the literature, and the feasibility of using the silicone within the wrist surrogate.

3.2   Methods

3.2.1   Silicone Fabrication

Maxillofacial silicones M511 and Z004 (Technovent, Bridgend UK) were selected as candidate skin/soft tissue simulants in a wrist surrogate. M511 and Z004 consists of two-parts (part A - polymer, filler and catalyst, part B - cross linker and polymer) platinum (vinyl addition) cured silicones. M511 is a 10:1 (i.e. 10 g part A to 1 g part B) and Z004 is a 1:1 (i.e. 10 g part A to 10 g part B), with a working time of 1 hr and a cure time of 1 hr (M511) or 1.5 hr (Z004) at 100℃ for both silicones. M511 is a versatile silicone, as the cured properties can be modified by adding softener M513 (Technovent, Bridgend UK), which reduces the hardness from about 15-20 Shore A to about 10 Shore A, according to the manufacturer's guidelines (Appendix H Section 9.8.1). Z004 has a higher Shore A hardness than M511, typical value 40, which is suitable for finger and facial prosthesis where extra strength is needed (Hatamleh and Watts, 2010).

Alongside the fabrication of the M511 and Z004 silicones, two further M511 blends (M511 *s-blend* and M511 *r-blend*) were fabricated. M511 *s-blend* was fabricated by adding the softener M513 to M511 (at a ratio of 1:1 with part B, i.e. if 10 g of part A was weighed out, 1 g of part B was added and 1 g of softener was added). M511 *r-blend* was the same as M511, except it was cured at room temperature (~20℃) for 24 hrs, rather than in the oven at 100℃ for an hour. When implementing the silicone into a wrist surrogate, it may be unfeasible to put the surrogate into an oven set at 100℃ to cure the silicone due to the surrogate's size, or other materials or components which could distort, which would create variability within the surrogates if replications were made. Therefore, it is important to also determine the silicone material properties when cured at room temperature. The datasheets (Appendix H Section 9.8) did not specify that M511 and Z004 could be cured at room temperature, but Mehta and Nandeeshwar (2017) state that they are both room temperature vulcanizing silicone. Pilot work indicated that Z004 did not cure at room temperature within 24 hrs. This suggests that Z004 is heat cured based,

and highlights a mistake within the paper of Mehta and Nandeeshwar (2017), and after contacting other sources the material is heat cured based. All silicone blends were unpigmented within the current study.

Material property tests of the silicones were conducted for compression, tensile, stress relaxation and impact testing. Initially, steel moulds were manufactured for moulding the compression samples, and a mould sheet was made for the tensile test sample preparation (Figure 3-1). Tensile samples were then punched out of the fabricated sheet of silicone. The compression sample process was also used for the stress relaxation and impact testing.

The silicone test sample fabrication process was as follows:

1. Parts A and B were poured into a container (~50 g for each mould). Weighing of constituents to 0.1 g accuracy.
2. The mixture was vacuum mixed (FINOVAC 10423, FINO, Germany) for 90 seconds.
3. The mould was sprayed with Polyvinyl Acetate releasing agent.
4. The bottom plate was then secured via dental sticky wax by the use of a gas flame to hold the plates securely together. The silicone mixture was then poured into the frame.
5. Finally the top plate of the mould was secured (a 0.5 kg mass was placed onto the top plate to hold in position), and the mould was heated to 100℃ in a laboratory oven until cured (1 hr M511 and 1.5 hr Z004 respectively).
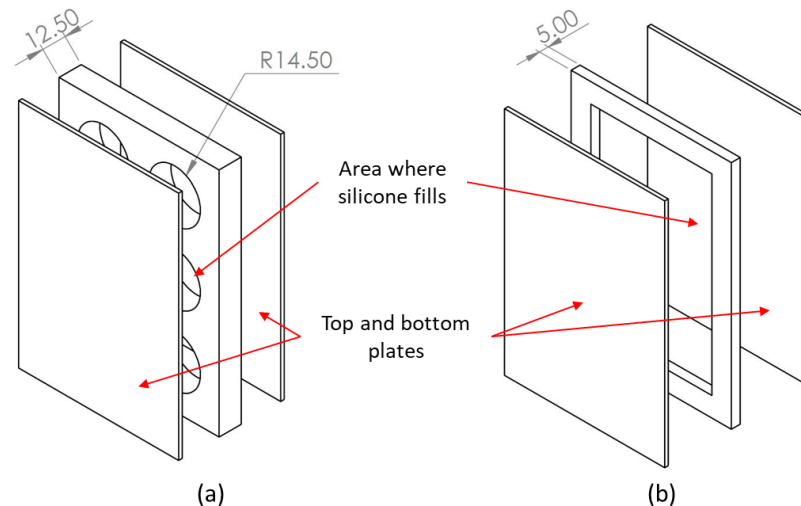
Figure 3-1 Exploded diagram of steel mould for (a) compression samples (as prescribed in ASTM D 95-03) and (b) sheet that tensile samples were punched out from (dimensions in mm).

3.2.2   Material Characterisation

3.2.2.1.   Compression

Six compressive test samples, as described in ASTM D 95-03 ($\varnothing$ 29 mm cylinder, 12.5 mm height), were moulded for each of the four silicones (Figure 3-1a). Compression tests were conducted using a Hounsfield HK10S tensometer (Tinius Olsen Limited, Surrey, UK) equipped with a 1,000 N load cell (0.5% or 5 N accuracy). A pre-load of 1 N (approach speed of 1 mm/min) was applied to each sample before testing to ensure the plates and samples were in contact. The load was then zeroed after the preload period.

Samples were compressed, between two lightly greased plates, to 55% strain to obtain stress vs. strain data at displacement rates of 3, 30 and 300 mm/min (strain rates of 0.0042, 0.042 and 0.42 s^{-1}). The three strain rates were chosen along a logarithmic scale base of 10, in line with previous research for the testing of sports materials for incorporation into an FE model (Pugh *et al*., 2010; Ranga and Strangwood, 2010). The Hounsfield HK10S tensometer (Tinius Olsen Limited, Surrey, UK) is capable of displacement rates of up to 500 mm/min, but due to limitations on the maximum acceleration, a maximum displacement rate of 300 mm/min was chosen. To compress samples at a higher strain, an Instron® Universal testing machine, capable of displacement rates up to 1,000 mm/min was used (1.39 s^{-1}). The Instron was fitted with a 5 kN load cell with an accuracy of ±5 N. Samples

were compressed at a strain rate of 0.42 s^{-1}, for comparison to the Hounsfield machine, and also at 1.39 s^{-1} to 55% strain. Three samples of each silicone were compressed three times, with a rest period of 6 minutes between tests, to observe any stress softening, sample repeatability and rate dependence effects (nine compressions of each sample across the three strain rates). The displacement rate sequence was from low to high. A further three samples of each silicone were tested at displacement rate sequence high to low to determine if there were any testing order effects.

The Shore A hardness of each silicone blend was then measured using a Durometer (Shore Durometer Hardness Type A-2, ASTM D676, New York, USA) on each compression sample (24 samples in total). The Shore A hardness was measured three times for each sample to gain a mean value.

2.2.2.2. Stress Relaxation

Compression test samples were also subjected to stress relaxation testing (Instron® Universal test machine) to provide time-dependent (viscoelastic) data for future use in the material model as described in Chapter 5. The samples were compressed to a strain of 25 and 50% at the maximum displacement rate of the device (1,000 mm/min), where they were held for 100 seconds while the decaying force was measured (sample rate 1,000 Hz). The temporal force data was converted to temporal Young's modulus (E) data using the original sample dimensions and the constant strain applied (either 0.25 or 0.50). Equation 4 was then applied to calculate shear modulus (G), using the Poisson's ratio (v) measured using Digital Image Correlation (DIC) (described in Section 3.2.2.2).

$$G = \frac{E}{2(1+v)}$$

Equation 4

3.2.2.2.   Impact Testing

The silicone compression samples were then impact tested to determine their impact performance, and to obtain high strain rate stress vs. strain data. Impact testing was conducted using a bespoke drop rig (Figure 3-2), consisting of a flat-

faced 2.5 kg drop mass (striking face of 60 x 60 mm) on a guided rail. Four synchronised load cells (208C05 ICP force sensor, sample rate 20,000 Hz) were integrated into the flat base plate, and connected to an oscilloscope (picoscope, Picotech 4824) via a signal conditioner (PCB Piezoelectronics 480B21 3-channel and 480E09 1-channel). Load cell voltage was converted into force using the calibration factors provided by the manufacturer and summed. Impacts were filmed for a visual aid with a high-speed camera (Phantom Micro R111, Vision Research UK Ltd, Bedford, UK) fitted with a zoom lens (Nikon AF Nikkor 24-85mm 1:2.8-4 D, Nikon Corporation, Japan). The camera was set at a capture rate of 10,000 fps, a resolution of 512 × 320 pixels, and was synchronised with the load cells via the oscilloscope and a manual trigger button. Impact energies of 1, 1.5, 2 and 2.5 J (drop heights 0.041, 0.062, 0.082, 0.102 m) were tested. ISO BS EN 20320:2020 specifies impact testing with a wrist protector at 4 J, so impact energies < 4 J were chosen for testing of silicone in isolation (i.e. the silicone will be beneath the protector when testing protectors).
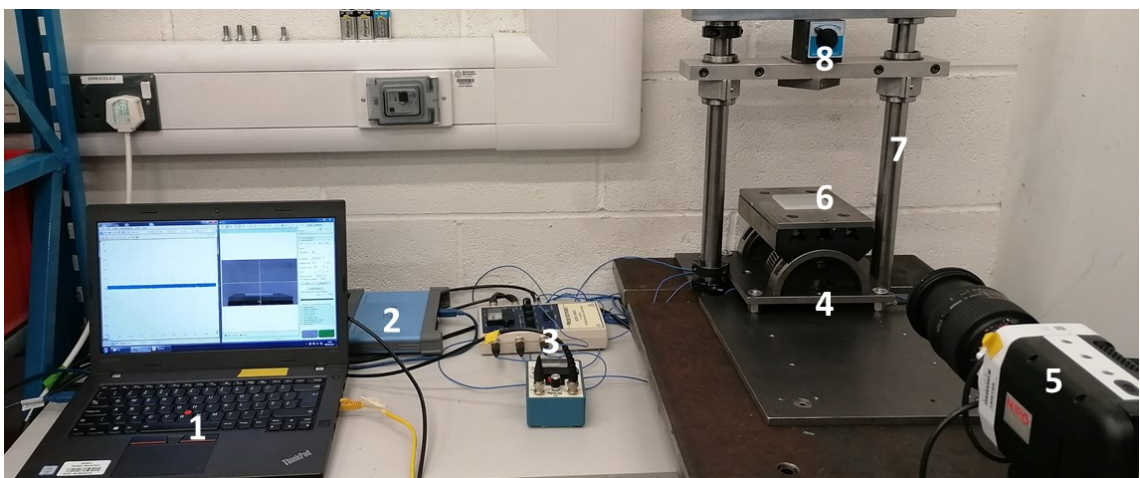
Figure 3-2 Bespoke drop rig. 1- Laptop, 2- Picoscope digital oscilloscope, 3- Signal conditioner (note there is two - a three-channel and a one-channel), 4- Force plate, 5- High-speed camera, 6- Sample, 7- Slide rails, 8- 2.5 kg drop mass.

To account for the effect of friction acting between the guide rails and the drop mass on estimates of the impact velocity from conservation of energy calculations using the drop height, measurements of the velocity of the drop mass just before impact were taken from the high-speed video footage (using Phantom Cine Viewer). Video's were calibrated using the known height of the compressive sample, using the 'Instant Measurement' function within Phantom Cine Viewer

Application. DIC software (GOM Correlate 2017, GOM GmbH, Braunschweig, Germany) was used to track the vertical displacement of the drop mass (via a tracking point), and velocity was calculated from the time and distance data 0.0005 s before impact.

To obtain high strain rate stress vs. strain data, the load cell data from the impact testing was used (Shepherd *et al*, 2020; Burbank and Smith, 2012). A second-order polynomial trend line was fitted to the initial section (0 to maximum force) of the force vs. time data. Smoothed acceleration vs. time data was generated from the equation of the trend line, and the trapezius method was applied in MS Excel® to obtain a strain vs. time relationship. Strain rate during sample loading was approximated from the gradient of a linear trend line fitted to the strain vs. time data. Example graphs displaying the process of obtaining stress vs. strain relationships from impacts on the silicone are included in the Appendix A (Section 9.1). Maximum displacements were calculated and compared to those measured in the video footage (using Phantom Cine Viewer) to check for their accuracy (41 mm drop height; velocity 0.9 m/s; energy of 1 J, calculated maximum displacement of 4.90 mm compared to a measured maximum displacement of 4.74 mm).

3.2.2.3.   Tensile

From the outcomes of Sections 3.2.2.1 to 3.2.2.2 (compression, stress relaxation and impact testing) the following tensile tests were conducted on the M511, Z004 and M511 *r-blend* silicones.

Tensile dogbone samples, as described in BS ISO 37:1994 (gauge length 35 mm and width 6 mm), were stamped out of a 5 mm thick sheet for each silicone (Figure 3-1b). Tensile tests were conducted using a Hounsfield HK10S tensometer (equipped with a 1,000 N load cell, as per Section 3.2.2.1). A pre-load of 1 N (approach speed of 1 mm/min) was applied to each sample before testing to remove any 'slack' in the samples. The load was zeroed after the preload period.

Two tensile samples of each silicone were tested at the same strain rates as the compression samples (0.0042 and 0.042 s^{-1}). The highest compressive strain rate of 0.42 s^{-1} was unattainable with the Hounsfield for the tensile samples. Samples were

placed in pneumatic grips (HT400, Tinius Olsen LtD) with a clamping pressure of ~100 kPa (15 psi), and stretched to a strain of 55% (pilot testing found that the samples remained within their elastic limit when stretched to a strain of 55%). Each sample was tested three times, with a rest period of 6 minutes between tests.

The tensile sample gauge length of 35 mm was selected to facilitate full-field strain measurement using DIC software. Speckle patterns were applied directly to the central region of the face of the tensile samples before testing using matt black acrylic spray paint. A camera (Phantom Micro R110, as per Section 3.2.2.2), set to capture rate of 24 fps and a resolution of 1,280 × 800 pixels, was used to film the pattern as the samples were stretched (Figure 3-3). To obtain Poisson's ratio, the axial strain was plotted against the transverse strain (obtained from the video footage using DIC), and a straight line was fitted (up to 10% strain). Poisson's ratio was taken as the gradient of the trend line multiplied by -1.
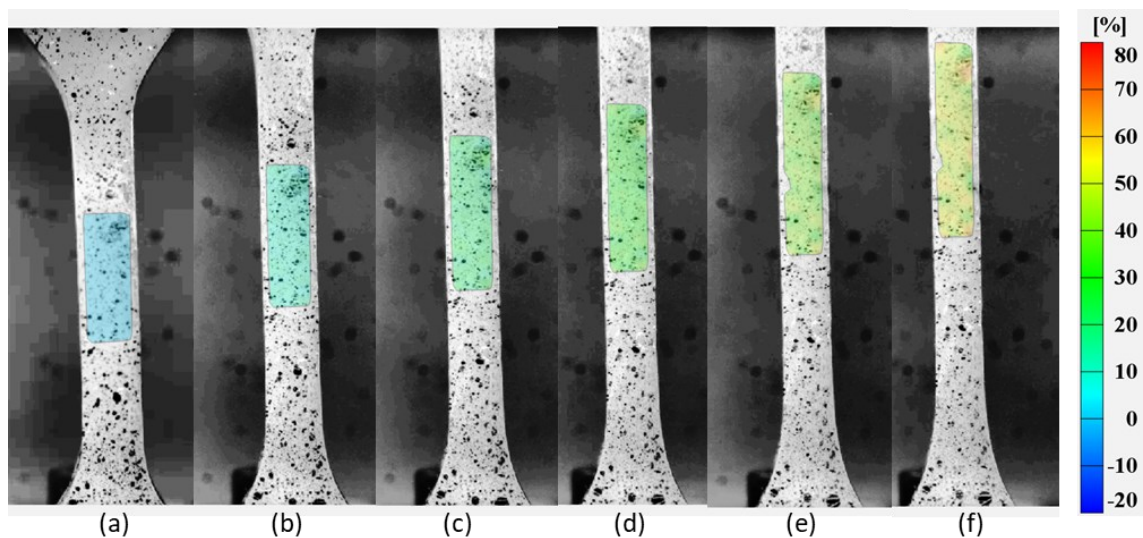
Figure 3-3 Example analysis of tensile sample using DIC software, showing axial strain at (a) 0% strain, (b) 10% strain, (c) 20% strain (d) 30% strain, (e) 40% and (f) 50%.

3.2.2.4.   Coefficient of Friction

From the outcomes of Sections 3.2.2.1 to 3.2.2.3, the following coefficient of friction test was performed for the M511 *r-blend* silicone.

Typical fabric used for the inner surface (in contact with the skin) of snowboarding wrist protectors is polyester and neoprene (Newton-Mann, 2019). To determine whether the coefficient of friction between silicone and such wrist protector fabric

was comparable to reported values between skin and similar fabrics, the coefficient of friction between M511 *r-blend* and polyester, and between M511 *r-blend* and neoprene was measured using a sled procedure. A 5 mm thick M511 *r-blend* sheet was attached (adhesive) to the base, and the fabric (polyester, neoprene - sourced from disassembled protectors from Newton-Mann (2019)) was attached (adhesive) to the bottom of the sled (Figure 3-4a). A mass was added to the sled (either 100, 200 or 300 g) and hanging masses were added in increments (5, 10, 50 and 100 g) until the sled began to move, and the masses were recorded. Each sled mass was tested three times. Mass of sled vs. hanging mass added, was plotted (Figure 3-4b), and the coefficient of friction was calculated by dividing the frictional force by the normal force.

(a)   (b)
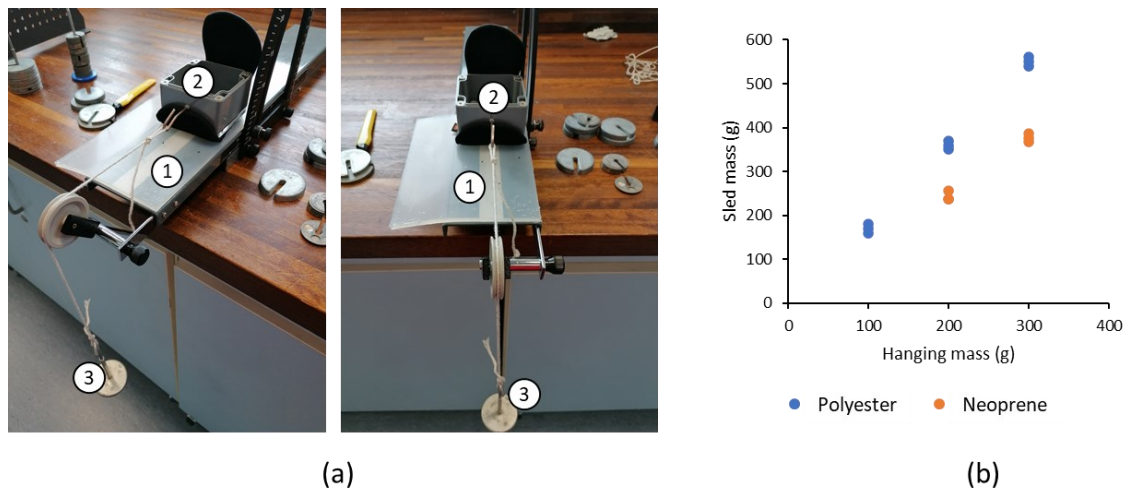
Figure 3-4 Coefficient of friction (a) test set up, 1 - base, 2 - sled, 3 - hanging mass. (b) hanging mass vs. sled mass for the 3 trials for the two protector fabrics.

3.3   Results

The measured Shore A hardness of each silicone was as follows (mean ± SD): M511 19 ± 0.9, Z004 26 ± 1.1, M511 *r-blend* 22 ± 1.1, M511 *s-blend* 12 ± 1.3. The Shore A hardness results are consistent with the expected values. Z004 had the highest Shore A hardness, and adding softener to M511 (M511 *s-blend*) reduced the Shore A hardness, agreeing with the manufactured guidelines. Curing M511 at room temperature (M511 *r-blend*) marginally increased its Shore A hardness.

The compressive stress vs. strain relationships comparing intra reproducibility (of the same sample) (Figure 3-5) and inter reproducibility (between samples) (Figure

3-6) of M511 and Z004 for the low strain rates (0.0042, 0.042 and 0.42 s^{-1}) are displayed. The compressive stress vs. strain relationship comparing all four silicone blends across all strain rates are displayed in Figure 3-7. The M511 and Z004 samples each showed consistent results between the three repeated compression tests (Figure 3-5). Z004 tended to have a steeper stress vs. strain curve than M511, suggesting it was stiffer, which was expected, as Z004 has a higher Shore A Hardness. No distinct evidence of stress softening was shown by either M511 or Z004 (Figure 3-5). M511 and Z004 showed consistency between samples, although Z004 had more varied stress values at maximum compression (55% strain) (0.85 to 1.10 MPa) than M511 (0.65 to 0.75 MPa) (Figure 3-6).

The compressive stress vs. strain curves for all silicones (M511, Z004, M511 *r-blend* and M511 *s-blend*) were also consistent across the strain rates imparted with the Hounsfield device (0.0042 to 0.42 s^{-1}) (Figure 3-7). There was discrepancy between the stress vs. strain curves obtained using the Hounsfield and Instron devices at 0.42 s^{-1} strain rate, suggesting inconsistency between the two test devices. M511 stress vs. strain relations were similar to those for the M511 *r-blend* (Figure 3-7a vs. c), whereas, the M511 *s-blend* showed a shallower stress vs. strain curve (Figure Figure 3-7a vs. d), as expected when softener is added. The high strain rate stress vs. strain data obtained from the 1, 1.5, 2 and 2.5 J impacts are shown alongside those from the quasi-static compression tests in Figure 3-7. The 1, 1.5, 2 and 2.5 J impacts were found to relate to an (estimated) strain rate of 60, 75, 90 and 100 s^{-1} respectively. Comparison between the low-speed compression test data (0.004, 0.042, 0.42 and 1.39 s^{-1}) and the impact test data (60, 75, 90 and 100 s^{-1}) confirmed that the silicone response was rate dependent, stiffening when it was compressed quicker.
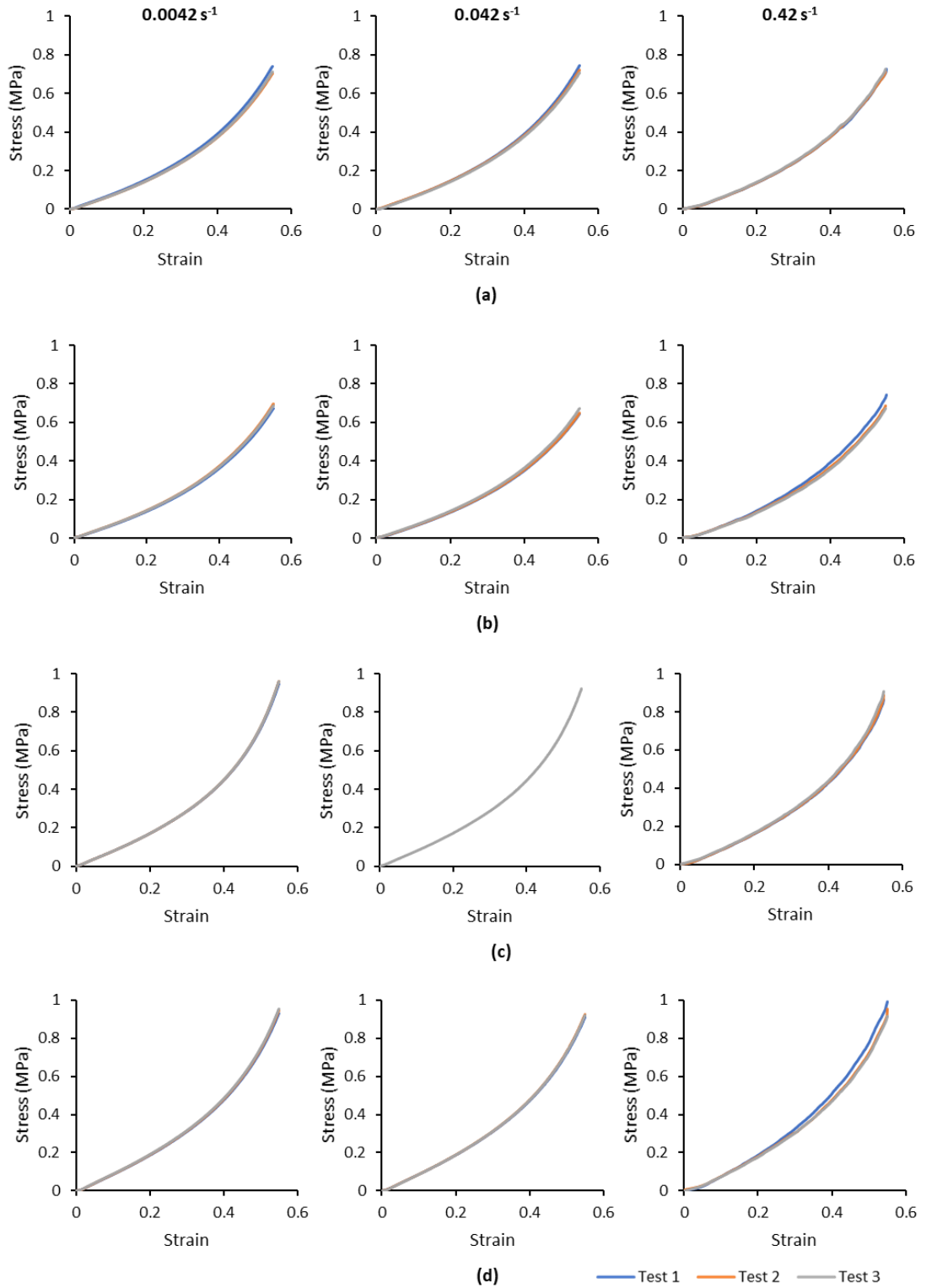
Figure 3-5 Compressive stress-strain data for intra reproducibility of (a) M511 tested low to high strain rate, (b) M511 tested high to low strain rate, (c) Z004 tested low to high strain rate, and (d) Z004 tested high to low strain rate, at strain rates 0.0042 s⁻¹ (left), 0.042 s⁻¹ (middle) and 0.42 s⁻¹ (right).
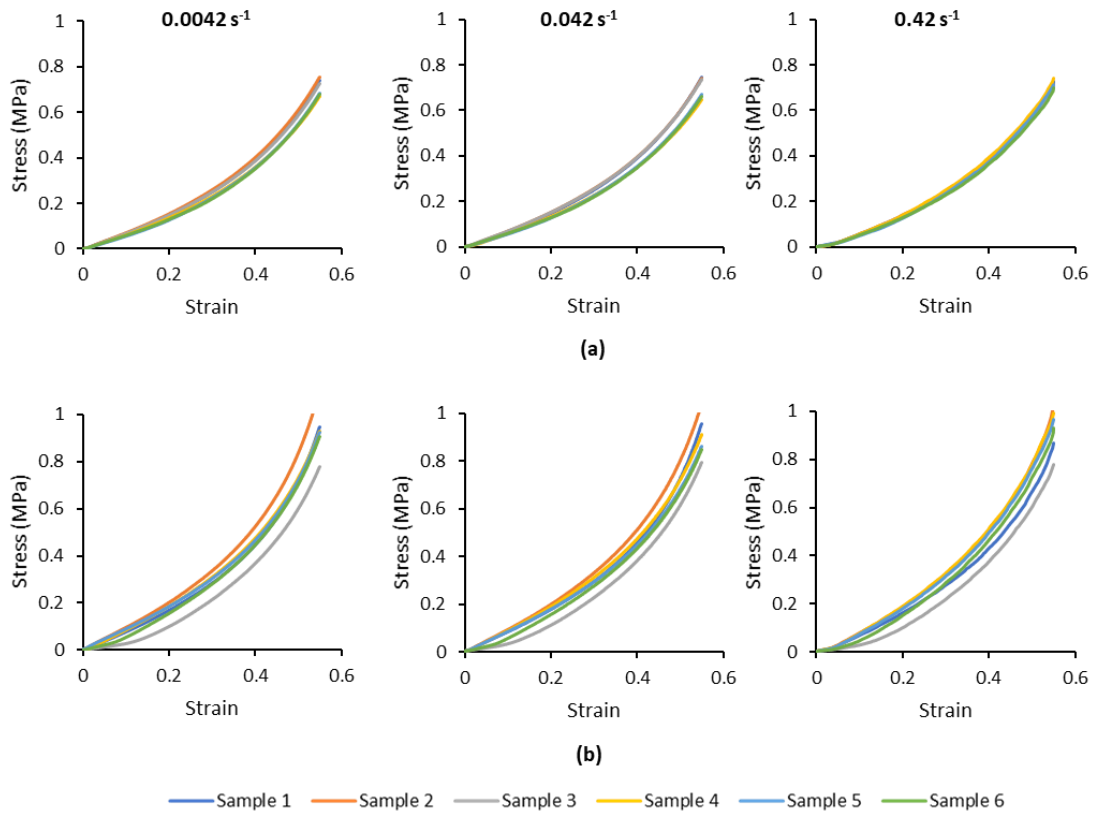
Figure 3-6 Compressive stress-strain data for inter reproducibility of (a) M511 and (b) Z004, at strain rates 0.0042 s⁻¹ (left), 0.042 s⁻¹ (middle) and 0.42 s⁻¹ (right).
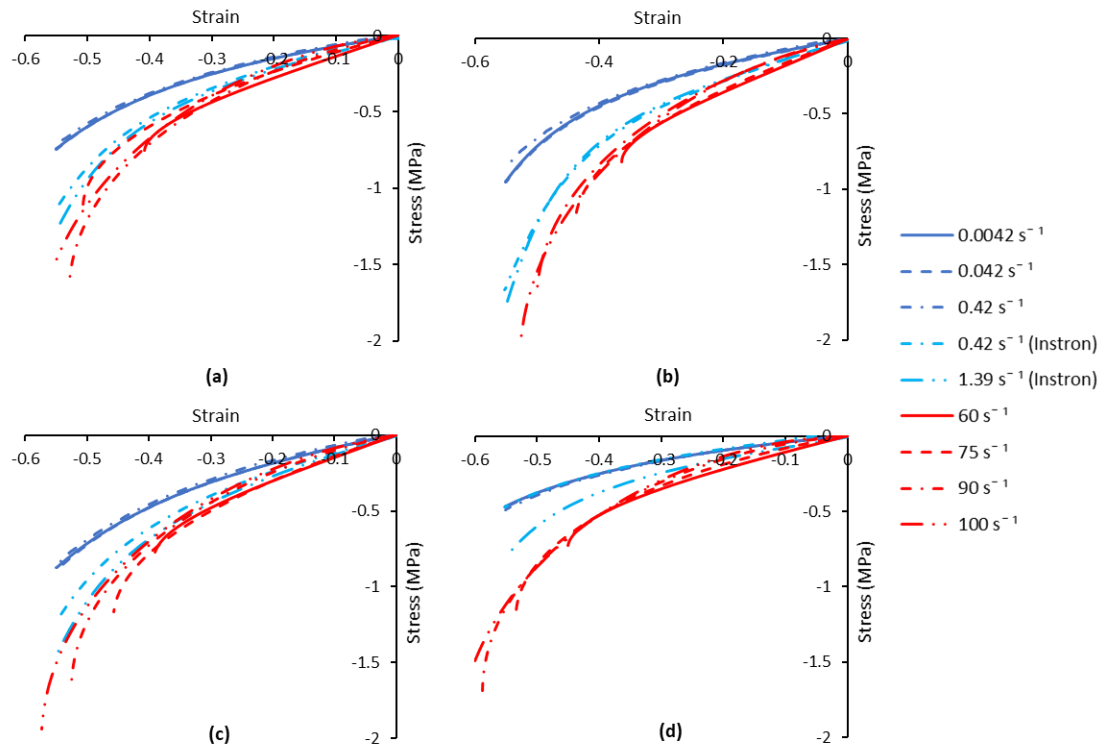
Figure 3-7 Compressive stress-strain data for (a) M511, (b) Z004, (c) M511 r-blend and (d) M511 s-blend at different strain rates for compressive samples under quasi-static compression (blue) and impact tests (red).

The four candidate silicones (M511, Z004, M511 *r-blend*, and M511 *s-blend*) were then plotted alongside the quasi-static (< 0.2 s^{-1}) compressive stress vs. strain response of organic tissues and Silastic 3481™ from Payne *et al*. (2014) (Figure 3-8). As highlighted earlier within this chapter Silastic™ 3481 has previously been used in a study by Hrysomallis (2007) for a sports surrogate. It is typically used as a general representation of organic tissue, whereas the quasi-static compressive stress vs. strain response between each organic tissue differ as shown in Figure 3-8. The maxillofacial silicones shows stress vs. strain relationships similar to Silastic™ 3481, indicating that they provide a good general representation of organic tissue, specifically between skin and muscle tissue.
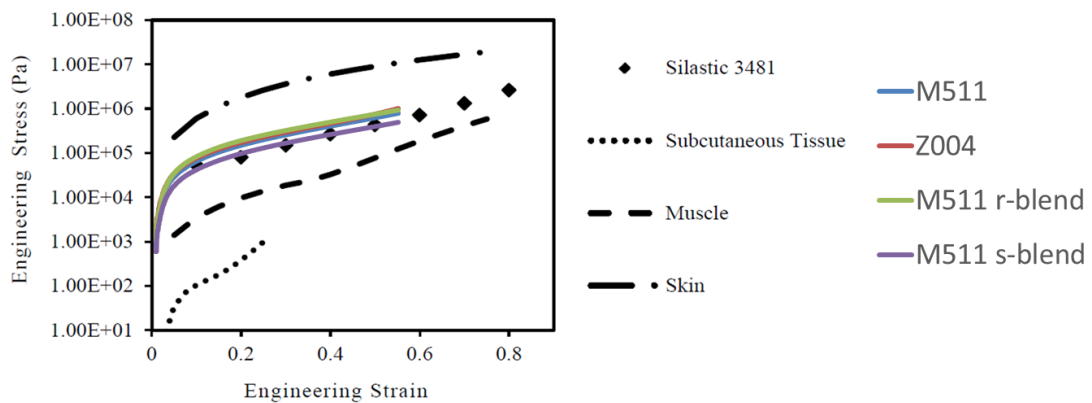
Figure 3-8 Compressive stress vs. strain of the candidate silicones (M511, Z004, M511 r-blend and M511 s-blend) compared to Silastic™ 3481 and organic tissues (subcutaneous tissue, muscle and skin) (adapted from Payne et al., 2014). Note the log scale for the y-axis.

The shear modulus response of the compression samples from the stress relaxation test over a logarithmic scale of time is shown in Figure 3-9 for strains of 25 and 50%. All silicones showed a more pronounced decay in shear modulus when held at 50% strain compared to 25% strain. Z004 showed the largest decay of ~0.4 MPa (40%) from a maximum of ~1.0 MPa at 50% strain. M511 and M511 *r-blend* showed a decay of ~0.2 MPa (25%) from a maximum of ~0.8 MPa, whereas M511 s-bend showed the smallest decay of ~0.1 MPa (20%) from a maximum of ~0.5 MPa. At 25% strain, shear modulus decayed by <0.05 MPa (10%) in all silicones.
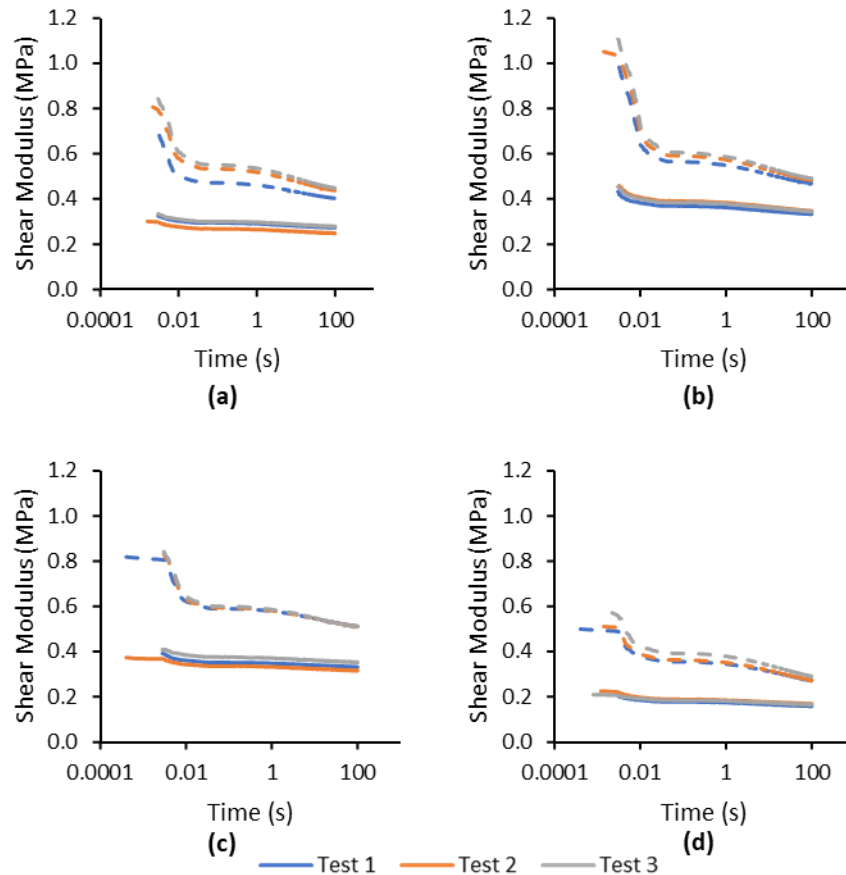
Figure 3-9 Shear modulus vs. time data from the stress relaxation of compression samples (a) M511, (b) Z004, (c) M511 r-blend and (d) M511 s-blend, at 20% (solid lines) and 50% (dashed lines) strain.

The temporal forces from impacting the candidate silicones at energies of 1, 1.5, 2 and 2.5 J are presented in Figure 3-10. Velocities of 0.86, 1.10, 1.33 and 1.55 m/s were measured from the 1, 1.5, 2 and 2.5 J impact videos (mean difference of 5%). The peak impact forces increased with the impact energy, and ranged from 564 to 1,449 N for M511, 582 to 1,432 N for M511 *r-blend*, 545 to 1,440 N for M511 *s-blend* and 580 to 1,503 N for Z004. Z004 gave the highest impact forces of all the silicones for all four impact energies (average of ~4% higher). The common theme in terms of stiffness of the silicones (M511 *s-blend* < M511 < M511 *r-blend* < Z004) has been shown throughout the compression, stress relaxation, impact testing and hardness test.
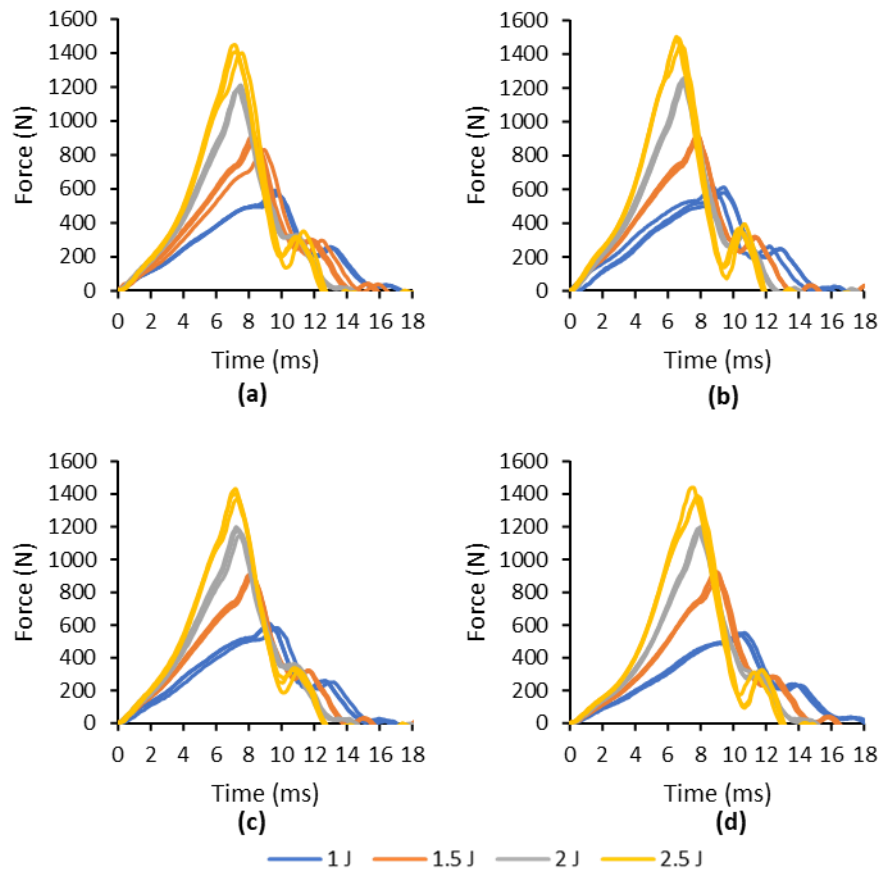
Figure 3-10 Force vs. time results from impact testing (a) M511, (b) Z004, (c) M511 r-blend, and (d) M511 s-blend, at four impact energies from 1 to 2.5 J.

Natural skin had the stiffest stress strain relations in comparison to subcutaneous tissue and muscle (Figure 3-8). As the candidate soft tissue simulants had stress strain relation between that of natural skin and muscle, it is suggested that silicones with a stiffer stress strain relation provide a better representation of skin. M511 *s-blend* has proven to have the softest response throughout the compression, stress relaxation, impact testing and hardness test. Due to this, alongside the extra step required for its manufacture (addition of M513 softener), it was chosen to discontinue the testing with M511 *s-blend*. Therefore, Z004, M511 and M511 *r-blend* were taken forward for tensile testing.

The tensile stress vs. strain of M511, Z004 and M511 *r-blend* are displayed in Figure 3-11. Z004 had a steeper stress vs. strain curve than M511 and M511 *r-blend*. The stress vs. strain relations between M511 and M511 *r-blend* were similar. The stress vs. strain curves for the silicones were similar between the two strain rates tested (0.044 and 0.0042 s^{-1}). The tensile results agree with those for the compressive

results; Z005 had the steepest stress vs. strain curve, and a similar stress vs. strain result was found between M511 and M511 *r-blend*.
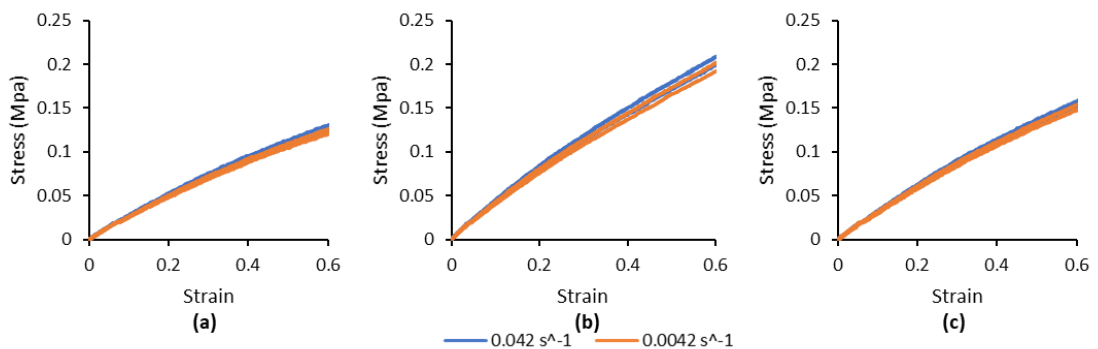
Figure 3-11 Tensile stress-strain data of (a) M511, (b) Z004 and (c) M511 r-blend, at the two strain rates.

DIC provided a Poisson's ratio of 0.48 ± 0.01 for the silicone samples (Figure 3-12, Table 3-1), although, these values were determined during quasi-static tensile testing and in theory could move closer towards incompressibility (0.50) at higher strain rates (Mott *et al.*, 2008).
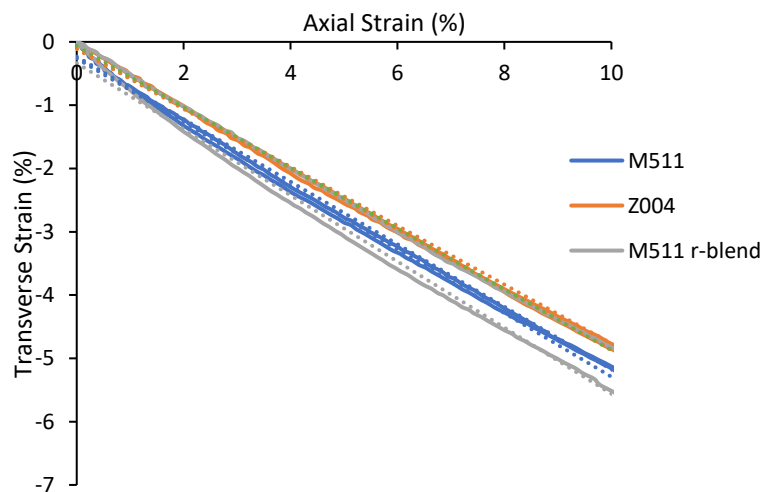
Figure 3-12 Transverse strain vs. axial strain for a M511, Z004 and M511 r-blend tensile samples at a strain rate of 0.042 s-1. Solid lines indicated linear trend lines.

Table 3-1 Poisson's Ratio of silicone samples provided from DIC.

Silicone	Gradient of Trend line (Poisson's Ratio)
M511	0.50
	0.49
Z004	0.46
	0.47
M511 *r-blend*	0.52
	0.48

The coefficient of friction between M511 *r-blend* and polyester was 0.56, whereas the coefficient of friction between M511 *r-blend* and neoprene was 0.81.

3.4   Discussion

In general, the results from the quasi-static and impact testing indicate the two maxillofacial silicones, M511 and Z004, had similar material characteristics. Consistent results between repeats and between samples were shown for all silicones for the compression tests, with no distinct evidence of stress softening. All four silicone blends (M511, Z004, M511 *r-blend* and M511 *s-blend*) were rate dependant, and provide a general representation of organic tissue, specifically showing stress strain reactions between that of skin and muscle. The stress strain relations align with previous studies using Silastic™ 3481 (Hrysomallis, 2007), a general soft tissue simulant used within sports surrogates.

Z004 had a higher Shore A Hardness than all the M511 blends (M511, M511 *r-blend* and M511 *s-blend*), in line with the manufacturer's guidelines and findings from Hatamleh and Watts (2010) (all unpigmented specimens). A Shore A hardness of 26 ± 1.1 was measured for Z004, however higher values of 40 and 36.44 ± 1.81 were reported in the datasheet and measured by Hatamleh and Watts (2010). The measured Shore A Hardness of M511 (19 ± 0.9) aligned with the manufacturer's guidelines (15-20), whereas Hatamleh and Watts (2010) measured a lower Shore A Hardness (12.64 ± 1.79), which aligner more with the Shore A Hardness measured here for M511 *s-blend* (12 ± 1.3). M511 *r-blend* had a marginally higher Shore A Hardness than M511.

The common theme in terms of stiffness of the silicones was shown throughout the material characterisation tests. Z004 was the stiffest, and M511 was stiffer when cured at room temperature and, as expected, softened when softener M513 was added (M511 *s-blend* < M511 < M511 *r-blend* < Z004). Z004 therefore had steeper stress strain relations for compression and tensile, and highest impact force in the impact tests, compared to the M511 blends. Z004 also showed the largest decay in shear modulus in the stress relaxations tests.

A higher coefficient of friction was found between M511 *r-blend* and neoprene than between M511 *r-blend* and polyester (0.81 vs. 0.56). Vilhena and Ramalho (2016) reported a coefficient of friction of ~0.7 between skin (ventricle forearm) and polyester, which was similar to that measured here between the M511 *r-blend* and polyester. Andreopoulos and Polyzois (1994) measured the frictional properties of a maxillofacial elastomer (Cosmesil HC2) compared to skin, and reported a mean value of 0.22 for skin and 0.20 for the elastomer. This suggests that maxillofacial silicones provide a good representation of skin tissue in terms of coefficient of friction.

Overall, M511 was observed to be slightly less viscous than Z004, as it was easier to pour into the mould when making the test specimens. M511 could also be cured at room temperature (M511 *r-blend*) unlike Z004, which should make it easier to implement it onto the surrogate. From the findings of this chapter, it was decided that M511 *r-blend* was the most suitable of the candidate materials to take forward to represent soft tissue within the wrist surrogate for improved biofidelity within this study.

3.5   Chapter Summary

Maxillofacial silicones were identified as suitable soft tissue simulants for the wrist surrogate. Four candidate maxillofacial silicones (M511, Z004, M511 *r-blend*, and M511 *s-blend*) (Technovent, Bridgend UK) were selected, and material characterisation in the form of compression, tensile, stress relaxation, impact testing and hardness testing, were performed. The material properties of these silicones were similar to each other and compared well to organic tissue (between

skin and muscle) and to previous simulants used to represent skin/soft tissue (Silastic™ 3481) within the literature. The common theme in terms of stiffness of the silicones was shown throughout material characterisation tests (M511 *s-blend* < M511 < M511 *r-blend* < Z004).

All M511 blends (M511, M511 *r-blend* and M511 *s-blend*) were less viscous than Z004, making them easier to pour into the moulds, and furthermore, could be cured at room temperature (M511 *r-blend*). M511 *r-blend* was selected as a more suitable soft tissue simulant for a wrist surrogate than the other candidates. The next chapter of this thesis will investigate implementing M511 *r-blend* on a wrist surrogate to improve its biofidelity properties enhancing previous work within the area of wrist surrogate research and injury.

4. <u>Effect of Surrogate Surface Compliance on the Measured Stiffness of Snowboarding Wrist Protectors</u>

4.1 Introduction

The previous chapter identified M511 maxillofacial silicone (Technovent, Bridgend UK) as a suitable candidate for the skin/soft tissue simulant of a wrist surrogate. M511 (cured at room temperature) will be used for the rest of this PhD project, and throughout the thesis it will now mainly be referred to simply as "silicone". This current chapter investigates the effect of introducing an outer layer of silicone to an otherwise stiff (plastic) wrist surrogate on the bending stiffness of snowboarding wrist protectors, creating a more bespoke biofidelic model. The wrist surrogate's geometry was defined, and a suitable silicone thickness to represent a skin was selected, based on values from the current literature. A wrist surrogate consisting of a stiff core and silicone outer layer (defined as the compliant surrogate) was fabricated, alongside a comparable stiff surrogate. The bend test protocol from Adams *et al*. (2016) was used to test the stiffness of two styles of snowboarding wrist protector on the developed compliant surrogate and the comparable stiff surrogate, to determine the effect of surrogate surface compliance. A repeatability study was also performed to determine the repeatability of the bend test, and to see whether adding the outer layer of silicone made the test more repeatable. This chapter documents the fabrication of the surrogates, a pilot test of the bend test with the new surrogates, and repeatability testing of the bend test.

4.2 Surrogate Geometry

The wrist surrogate consisted of a hand and forearm connected with a low-friction hinge at the wrist joint, allowing a wrist extension of ~90°. Two steel fingers protruded from the hand to facilitate load application to extend the wrist, and fitting of gloves / protectors integrated into gloves. The geometric wrist surrogate geometry (BS EN ISO 20320:2020 surrogate) was selected for this PhD project over other candidates, as i) it is based on anthropometric data, ii) it can be communicated in an engineering drawing, and iii) it has been shown to provide more repeatable measurements in a bend test than both a simpler hand and

forearm and a hand and forearm based on a laser scan of a human arm (Adams *et al.*, 2018). When this wrist surrogate geometry was selected (August 2018), BS EN ISO 20320:2020 had not been published and a draft of the standard was at the design stage (DS). The DS stage was when the standard was circulated to ISO members to vote and comment on before it was approved. The selected dimensions of the wrist surrogate used in this PhD project therefore correspond to those of the medium surrogate from the draft standard as of 15-05-2018.

The geometry of the BS EN ISO 20320:2020 medium surrogate (as per 15-05-2018) was created in CAD (Solidworks, 2019, Dassault Systems) using the schematic drawing and associated dimensions (Chapter 2 Section 2.5.1, Figure 2-8). Some aspects of the schematic drawing were undefined, such as the joint dimensions and the lofts between surfaces (see highlights on Figure 4-1). Incorrect joint dimensions can result in a surrogate with a limited range of flexion-extension motion at the wrist, which does not comply with the specified testing procedures in BS EN ISO 20320:2020. Joint dimensions were, therefore, assigned to ensure the surrogate joint had the required range of motion (0° to at least 80° wrist extension) (as shown in Figure 4-2).
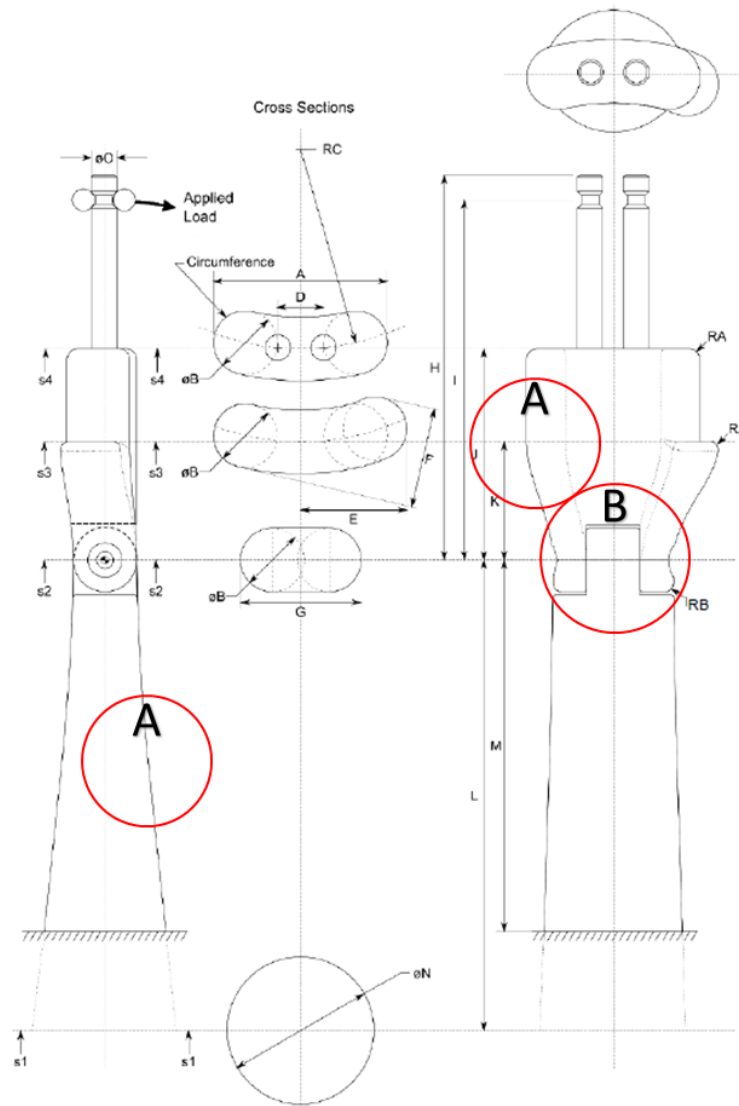
*Figure 4-1 Highlighted undefined areas of the BS EN ISO 20320:2020 schematic drawing (as per 15-05-2018). A -
loft between surfaces undefined as to whether these are straight or curved lines, B - joint not dimensioned.*
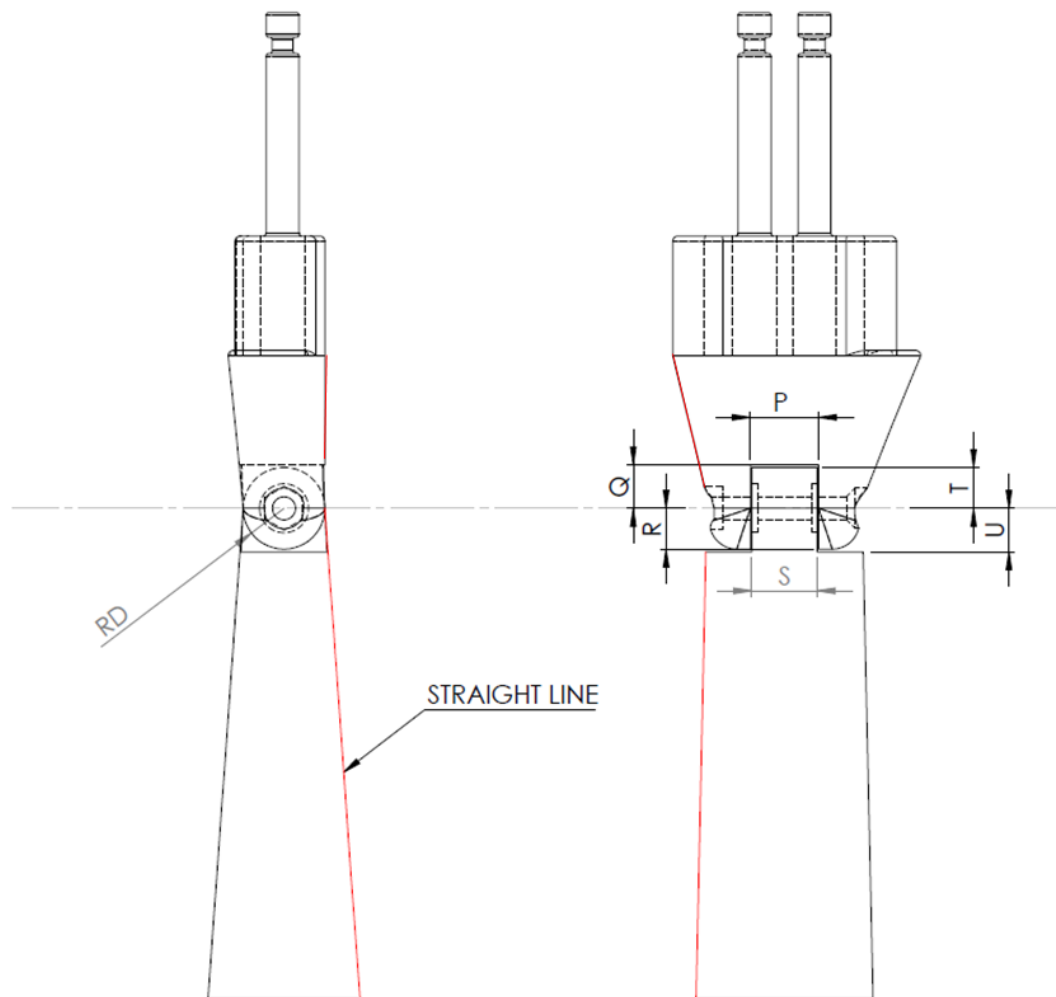
Surrogate Size		Dimensions (mm)					
	RD	Hand			Forearm		
		P	Q	R	S	T	U
S	12	25	13	12	24	12	13
M	15	25	16	15	24	15	16
L	19	25	20	19	24	19	20

Figure 4-2 Additional information to BS EN ISO 20320:2020 schematic drawing (as per 15-05-2018). Updated schematic drawing with the joint dimensioned and the loft of the forearm defined as straight (top), alongside associated joint dimensions to ensure the required range of motion is achievable (bottom).

4.2.1 Compliant Layer

An outer layer of silicone was applied to the wrist surrogate to represent skin. From Chapter 2, the literature review highlighted that the mean skin thickness around the hand and forearm reported in the published studies was 1.4 ± 0.1 mm and 1.2 ±

0.4 mm respectively (Chapter 2 Table 2-8). Studies that have implemented a compliant layer onto a sports surrogate (thigh, ankle and hand) to simulate skin have used a 2 to 3 mm thickness (Ankrah and Mills, 2003; Payne, 2015; Maurel *et al.*, 2013). Payne (2015) selected a 3 mm thickness for the skin on a thigh surrogate based on reported thicknesses in the literature. Maurel *et al.* (2013) selected a 3 mm thickness to model the compliance of soft tissue in the hand for a hand surrogate, based on results from an impact test. Ankrah and Mills (2003) opted for a 2 mm thickness for the skin on an ankle surrogate, as it gave a similar indentation resistance to measurements collected on participants for the soft tissue in the ankle area. As the bend test only involves low-speed extension of the wrist joint (< 3°/s as stated by Adams *et al.* (2021)) and does not involve any impact testing, a silicone layer representing just the skin and not the underlying soft tissue was deemed sufficient. A silicone layer of 3 mm thickness was selected to represent skin on a wrist surrogate.

4.3   Surrogate Fabrication

The compliant surrogate consists of a stiff core and a 3 mm thick silicone outer layer. To develop the surrogate hand and forearm cores, the *loft-cut* function was used on the CAD models from Section 4.2 to reduce the periphery of the hand and forearm by 3 mm (Figure 4-3). Five holes of 3 mm diameter were added through the hand and forearm core to allow the silicone to pass through and achieve a full mechanical bond. The hinge joint region was not edited, this was to maintain full range of motion without influencing joint friction.

1- holes for mechanical bond

(a)   (b)
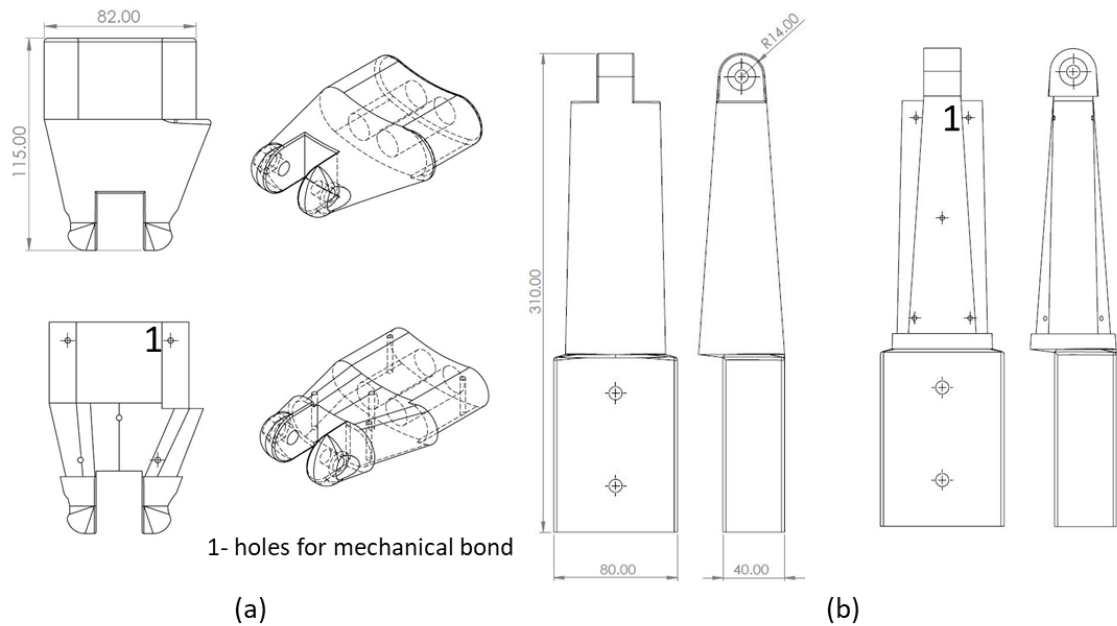
Figure 4-3 CAD diagram of (a) hand (top) and hand core (bottom), (b) forearm (left) and forearm core (right). Points marked "1" indicate the holes for mechanical bonds.

Moulds, based on the external geometry of the surrogate hand and forearm CAD models from Section 4.2, were created in CAD using the *cavity* function. When fitted around the surrogate cores, the mould created a 3 mm thick cavity for the silicone to fill during fabrication (Figure 4-4). The moulds had a 5 mm diameter hole (towards the bottom of the dorsal side) to allow the silicone to be inserted into the cavity (Figure 4-4 point 2), four 3 mm diameter cylindrical supports (two on each side protruding into the cavity) to ensure the cores sat central in the cavity (Figure 4-4 point 3), and 6 mm diameter holes at each corner, so the two halves could be bolted together around the surrogate core (Figure 4-4 point 4). All parts were additively manufactured (Markforged X7, Markforged, Massachusetts, USA) in Onyx™ filament (short carbon fibre reinforced polyamide). Onyx™ was selected as a suitable material as it offers a high strength-to-weight ratio (due to being reinforced with carbon fibre), and therefore reduces potential deflection of the surrogate forearm during testing. A mounting block, consisting of a cuboid (dimensions 115 × 80 × 40 mm) with two 8 mm diameter holes, was incorporated into the bottom of the surrogate forearm for attachment to the bend test rig (Figure 4-4), as done by Adam *et al*. (2016).

1- holes for mechanical bond, 2- hole for silicone insertion, 3- cylindrical supports, 4- hole for bolting halves together

(a)   (b)
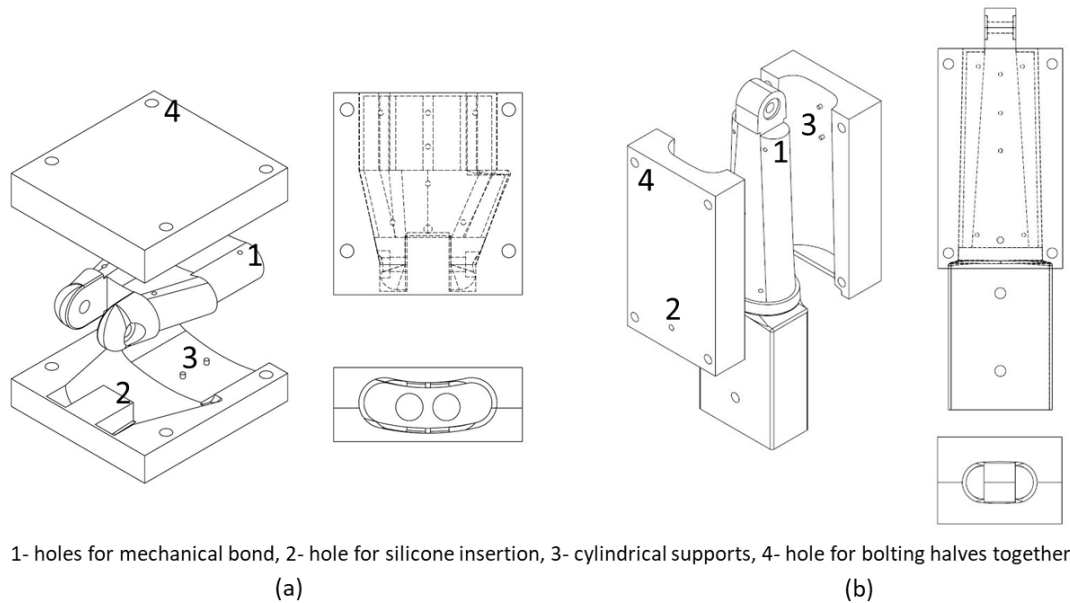
Figure 4-4 CAD drawing showing exploded view, front view and top view of (a) hand core and mould, (b) forearm core and mould.

The moulds were bolted around the hand and forearm cores and mounted in preparation for silicone insertion (Figure 4-5a). The silicone was fabricated (as per Chapter 3 Section 3.2.1), the mixture was then transferred into a 10 mL syringe, and introduced to the silicone cavity via the hole in the mould (Figure 4-5b). This method of syringing the silicone into the mould from the bottom, was selected to reduce the possibility of bubbles forming and creating potential porosity during the curing process of the silicone. The mould was then left for 24 hours at room temperature (~20°C) to cure. The surrogate was then removed, and any excess silicone along the mould joint was cut away by the use of a Stanley knife, being careful not to damage the silicone sleeve. The steel machined fingers were inserted into the top of the hand, and the hand and forearm hinge joint was assembled (Figure 4-5c).

(a) (b) (c) (d)

3 mm silicone outer layer
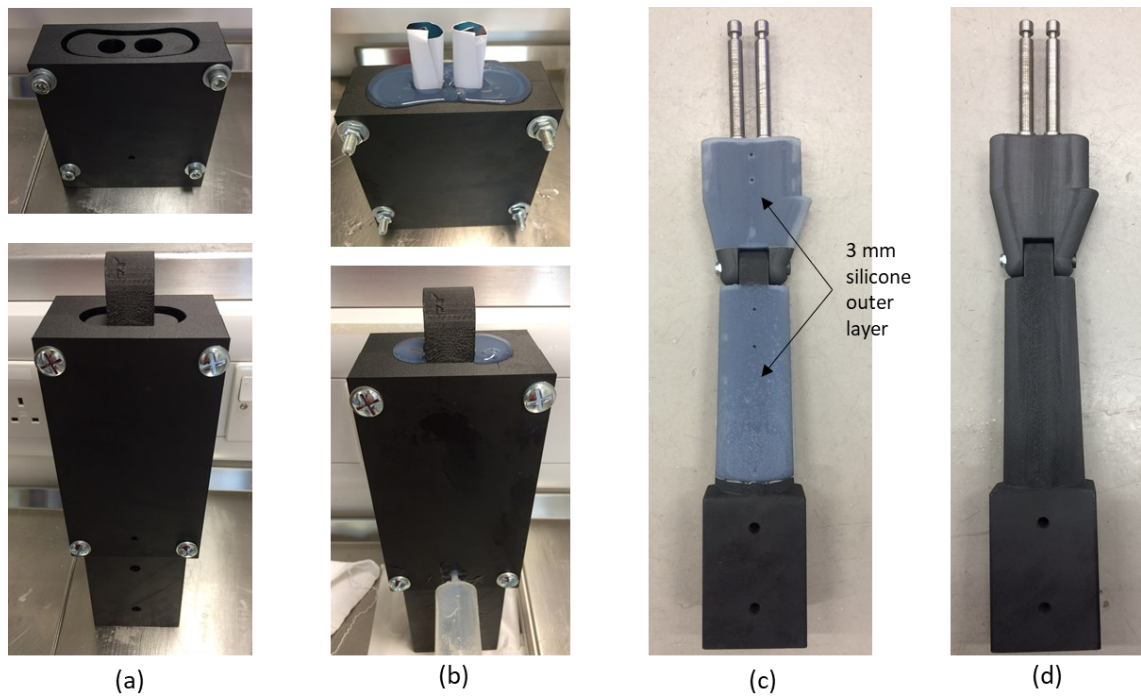
Figure 4-5 Images of (a) the prepared moulds (b) silicone moulding procedure (c) finished compliant surrogate and (d) comparable stiff surrogate.

A comparable stiff wrist surrogate was additively manufactured from the CAD model from Section 4.2 (Onyx™ filament, Marksforged X7) (Figure 4-5d). The hand and forearm parts of both surrogates were additively manufactured in the same orientation to maintain consistency in part strength. The maximum wrist extension of both surrogates was 90°. Components were weighed (Mettler Toledo PE11, UK) and stated in Table 4-1. Compared to its stiff counterpart, the mass of the compliant surrogate was more similar to that of an actual hand and forearm, as reported by Clarys and Marfell-Jones (1986). A true comparison cannot be made between the mass of the surrogates and an actual hand and forearm, however, as the former did not include the entire forearm. The difference in mass of the hand between the two surrogates resulted in a negligible difference of 0.63 Nm in the torque produced when the hand was at 90° wrist extension (calculated using the mass and distance to the CoM).

Table 4-1 Surrogate component masses.

Surrogate Part	Mass (g)		
	Compliant surrogate	Stiff surrogate	Clarys and Marfell-Jones (1986)
Hand	135.9	84.1	345.3
Forearm	349.0	268.7	746.4
Fingers	308.2		n/a
Hinge joint fasteners	32.3		n/a
Total	**825.4**	**693.3**	**1,091.7**

4.4 Bend Test Pilot Test

4.4.1 Protectors

During this thesis, two styles of snowboarding wrist protector (both adult medium)
were tested. The protectors were labelled as the, i) short protector - Burton©
(Burton Sportartikel GmbH, Innsbruck, Austria) and ii) long protector - Flexmeter™
double sided (Demon United, Nijmegen, The Netherlands). These protector designs
have been investigated by others, and Newton-Mann (2019) characterised their
materials. Both styles of protector consist of palmar and dorsal fabric, palmer and
dorsal splints, and two straps (top and bottom). The length of the short protector
was ~140 mm, with high density polyethylene (HDPE) splints of ~50 × 5 × 4 mm. The
length of the long protector was ~210 mm, with high impact polypropylene (PP)
splints of ~200 × 60 × 2 mm. The short protector also had palmar padding (~30 × 30
× 7 mm) consisting of a stiff plastic shell (HDPE) and polyurethane foam (PU). The
long protector had a detachable PP skid plate (~78 × 55 × 3 mm) on the palmar side.
This skid plate was removed before impact testing the long protectors (Chapter 5
and 6) as it was considered to be intended for roller sports rather than
snowboarding where wrist protectors are typically worn underneath gloves.

4.4.2 Methodology

The short and long snowboarding wrist protectors (right hands) were tested in the
bend test following work published by Adams *et al*. (2018). This was to evaluate as
to whether the addition of the compliant layer to the wrist surrogate had any effect
on the measured stiffness of the protectors. The surrogate was fastened to a
bespoke rig, developed by Adams *et al*. (2016), with the forearm vertical and the

palm facing away from the uniaxial test machine (Hounsfield HK10S, Tinius Olsen Limited, Surrey, UK) (Figure 4-6). A 2 mm diameter steel cable was connected to the distal end of the surrogate fingers (via a 148 g clamp) to the test machine load cell (1 kN load cell) via a pulley (Harken 22 mm micro block, Hampshire, UK). Positive vertical displacement of the load cell (test speed - 200 mm/min) applied an extension torque to the surrogate wrist via the cable, pulling the hand backwards (mimicking wrist extension) and bending the protector (angular velocity ~0.9 °/s (0.016 rad/s)). Specific manual measurements of the rig were required for data analysis; i) A - horizontal distance from pulley to arm centre, ii) B - vertical distance from pulley to point of load application, iii) C - vertical distance from axis of rotation to point of load application, and iv) D - fingers to point of load application (Figure 4-6).

(a)   (b)
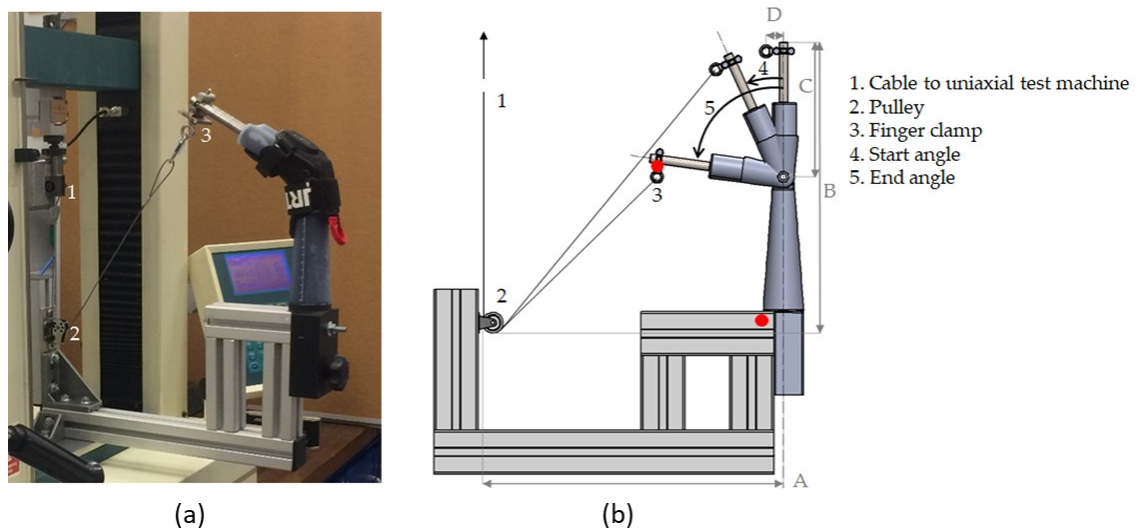
Figure 4-6 (a) Bend test setup, (b) schematic (A, B, C, D indicate manual measurements required for data analysis, and the two red dots indicate where markers were placed to track protector movements for video analysis.

Before testing and data collection, the linear displacement of the load cell required to give the desired final wrist extension of ~80° needed to be established, to prevent the surrogate reaching its extension limit of 90°. A used short protector was fitted to the stiff surrogate on the rig to determine the required load cell displacement (136 mm) to extend the surrogate wrist from its starting angle (~40° with the finger clamp contributing a torque of ~0.16 Nm) to ~80°. Each test trial involved; (i) fitting the protector to the surrogate on the rig, (ii) connecting the

finger clamp and cable, (iii) measuring the start angle of the wrist, (iv) applying a linear displacement of the load cell of 136 mm at a speed of 200 mm/min, (v) measuring the end angle of the wrist.

Load and linear displacement were recorded by the test device at a sample rate of 25 Hz. The start and end angles of the wrist were measured for each trial with a digital inclinometer placed on the fingers (PRO360, SPI, Swiss Precision Instruments, Switzerland. Accuracy ±01°, Resolution 0.1°). Three conditions were used for protector strap tightness; loose, moderate and tight. Strap tightness was established for each condition by (Figure 4-7, from Adams, 2018); (i) putting the protector on the surrogate, (ii) holding the surrogate horizontal, (iii) hanging either a 1, 2 or 3 kg mass from the straps of the protector, (iv) rotating the surrogate around its long axis to tighten the straps, (v) marking the position of the straps for future reference. Strap tightness for each protector was set before testing using the marks established with the hanging masses.

To determine the effect of protector strap tightness, six protectors of each style (short, long; labelled A to F) were tested, with two of each tested at each strapping condition on each surrogate (three strapping conditions across two surrogate-protector pairings - 24 different combinations). Three repeated tests were performed for each surrogate-protector-strapping combination, with a minute long rest period between repeats (total of 72 tests). For example, short protector A was tested at loose strapping condition on the stiff surrogate for three repeats, and then tested on the compliant surrogate for three repeats, equating to a total of six tests performed on that protector (Table 4-2). Protectors were defined as either: new (untested) or used (after three tests on a surrogate). To limit the potential effect of protector degradation after testing on the first surrogate, surrogates were alternated between combinations, so one new protector of each style was tested at each strapping condition on each surrogate (15 minute rest between each test surrogate). This meant there was a longer rest period between going from a new to used protector (15 vs 1 minute). Protectors were re-positioned and re-strapped between tests.
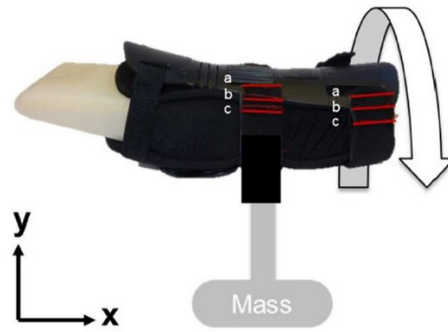
Figure 4-7 Schematic of the procedure used to set protector strap tightness (Adams, 2018).

Table 4-2 Table showing the test order of each protector (A to F), with each row equating to a total of six tests.

Protector		Strapping Conditions	Test surrogate 1 (3 repeats) Protector defined as new	Test surrogate 2 (3 repeats) Protector defined as used
Short	A	Loose	Stiff	Compliant
	B	Loose	Compliant	Stiff
	C	Moderate	Stiff	Compliant
	D	Moderate	Compliant	Stiff
	E	Tight	Stiff	Compliant
	F	Tight	Compliant	Stiff
Long	A	Loose	Stiff	Compliant
	B	Loose	Compliant	Stiff
	C	Moderate	Stiff	Compliant
	D	Moderate	Compliant	Stiff
	E	Tight	Stiff	Compliant
	F	Tight	Compliant	Stiff

A camera (Chapter 3 Section 3.2.2.2) filmed the test side-on, recording footage of wrist extension. The camera filmed at a resolution of 1,280 × 800, with a capture rate of 24 Hz, and was calibrated from an image taken of a measuring tape on the test rig (Figure 4-8). Markers were placed on the rig to track protector movement for manual video analysis (Figure 4-6, Figure 4-8). The first test for each surrogate-protector combination (24/72 tests) was filmed (i.e. repeats 2 and 3 for each combination were not filmed).
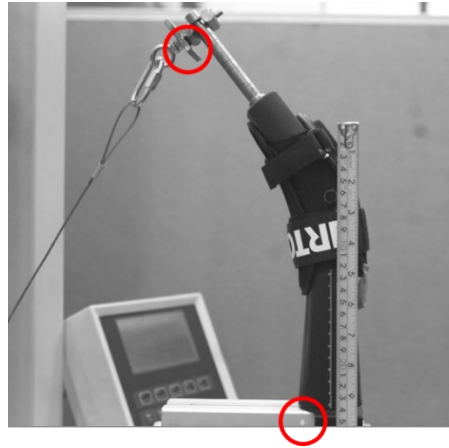
Figure 4-8 Image from the camera for calibration. The tape measure is positioned vertically on the surrogate forearm, and the red circles highlight the markers on the rig.

4.4.3   Data Analysis

Load and displacement values obtained were converted to torque and angle, respectively, using trigonometry equations as stated in Adams *et al*. (2016) (start and end angle, and manual measurements in Figure 4-6 were required for this process). A Matlab (vR2018a, Mathworks®, USA) script using the *fit* function with the nonlinear least-squares algorithm was used to curve fit and filter the torque vs. angle data. Statistical analysis was used to compare surrogates at each strapping condition (for each protector). The mean torque values at 75° wrist extension (upper wrist extension range (Shultz *et al*., 2015; Levangie *et al*., 2000)) were compared using two-sample t-tests, at a significance level of $p<0.05$, using Minitab (v18 statistical software). Effect sizes were calculated using Pearson's correlation coefficient (small ±0.2, medium ±0.5, large ±0.8 effect size (Sullivan and Feinn, 2012)).

If protector slippage was observed in the videos, measurements were taken between a feature on the protector and a marker on the rig, using Phantom Cine Viewer (as per Chapter 3 Section 3.2.2.2).

4.4.4   Results

In 31 tests (86% of cohort), the compliant surrogate gave higher torque values at 75° wrist extension than the stiff surrogate (Figure 4-9). The five test exceptions when the stiff surrogate gave higher torque values than the compliant surrogate occurred on repeated tests on the short protector, and four of these were on the

third repeat for a given strapping condition. Significant differences at 75° wrist
extension ($p < 0.05$) occurred between the surrogates when fitted with the long
protector at all strapping conditions (Table 4-3). All cases demonstrated a medium
to large effect size (Table 4-3). The torque required to extend the wrist to 75°
tended to decrease with test repeats, indicating the stiffness of the protectors
decreased with testing (Figure 4-9). In most cases (15/16, 94%) for the first test on
both a new and used protector, the torque required to extend the wrist to 75°
increased with strap tightness (Figure 4-9). Torque values increased with wrist
extension (Figure 4-10). When analysing across wrist extension angles (Figure 4-10),
the torque required to extend the wrist varied with strap tightness. A small torque
(<1 Nm) is displayed at 40° (Figure 4-10), due to tension in the cable at the start of
each test. The long protector gave higher torque values for a given wrist extension
angle than the short protector (Figure 4-9 and Figure 4-10), as expected (Adams *et
al.*, 2016; Adams *et al.*, 2018). The torque values observed from Adams *et al.* (2018)
(equivalent to moderate strap tightness) fell between those measured during this
study under moderate and tight strapping conditions on the stiff surrogate (shown
by the red lines in Figure 4-10).
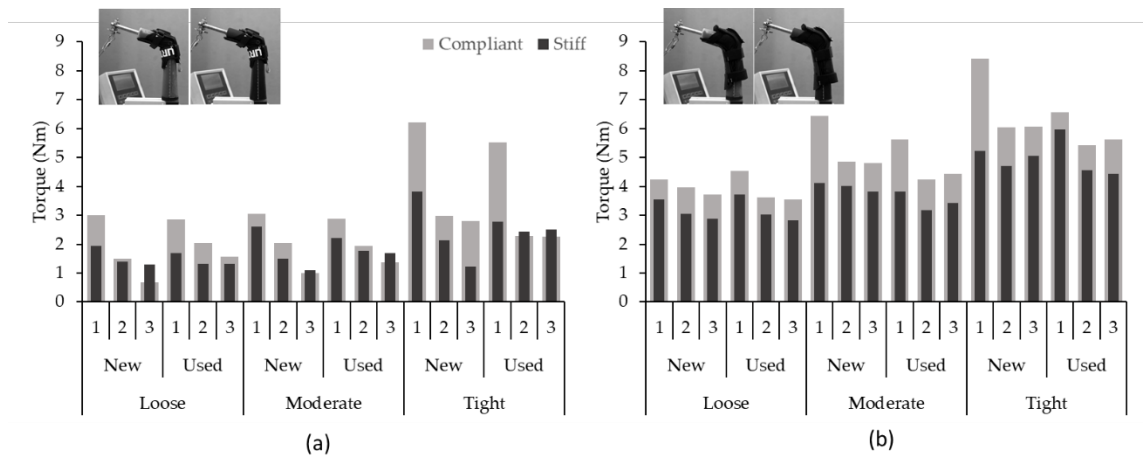
*Figure 4-9 Torque at 75° wrist extension for (a) short and (b) long protector. The x-axis indicates the test repeat,
protector condition, and strapping condition.*

*Table 4-3 Statistical test results and effect sizes between surrogates for torque measurements at 75° wrist
extension (* indicates a significant difference).*

Protector	Strapping Condition	p-value Compliant-Stiff	Effect Size
Short	Loose	0.267	0.832 (large)
	Moderate	0.568	0.789 (medium)
	Tight	0.161	0.748 (medium)
Long	Loose	0.005*	0.857 (large)
	Moderate	0.004*	0.782 (medium)
	Tight	0.021*	0.845 (large)
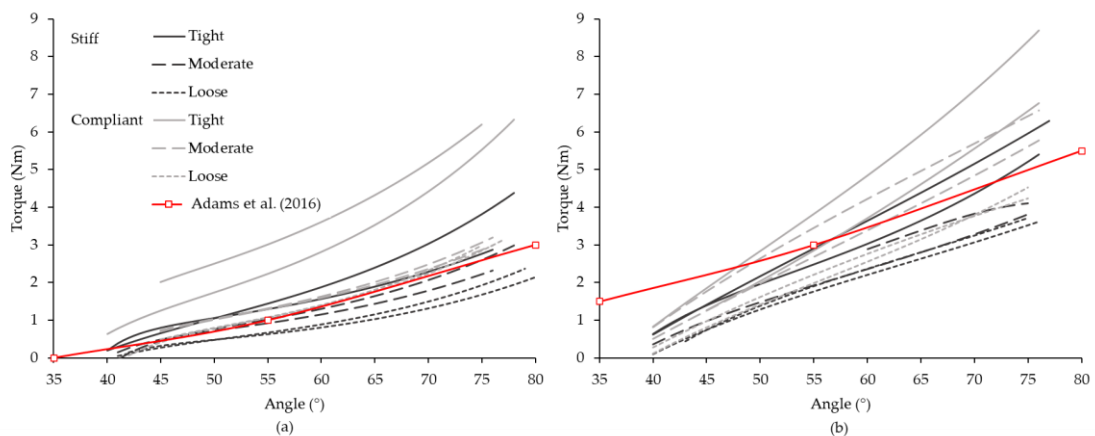
*Figure 4-10 Torque vs. angle for Test 1 of a new and used protector at each strapping condition (tight - solid line,
moderate - broken line, loose - dotted line), for (a) short and (b) long protector, plotted alongside previous data
(red line) adapted from Adams et al. (2016).*

Visual inspection of videos found that the dorsal side of the short protector slipped
more on the stiff surrogate than on the compliant surrogate (under moderate and
tight strapping conditions). Measurements on the video frames (start and end
angle) showed the top of the dorsal side of the new short protector slipped 13 mm
towards the fingertips on the stiff surrogate, compared to 8 mm on the compliant
surrogate (both under moderate strapping condition) (Figure 4-11). Slippage also
occurred at the same location on the used short protectors under moderate
strapping condition (9 mm stiff vs. 7 mm compliant surrogate), and the short
protector under tight strapping condition (new protector - 14 mm stiff vs. 10 mm
compliant surrogate, and used protector - 16 mm stiff vs. 7 mm compliant
surrogate). Whilst the short protector slipped in a similar manner under loose

strapping condition, no clear differences were observed between the surrogates. The long protector was not observed to slip in any test.

| | | | | |
| (a) | (b) | (c) | (d) | (e) |
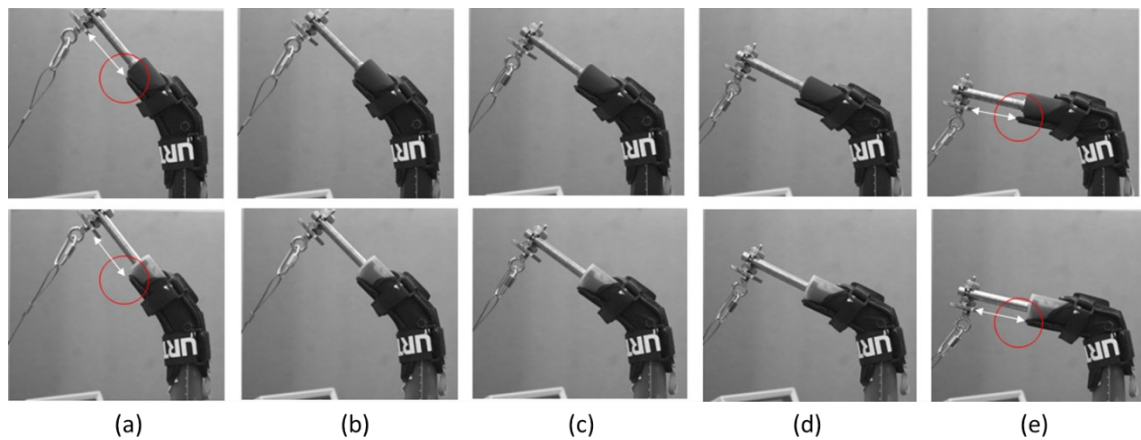
Figure 4-11 Video sequence at (a) 0 s, (b) 10 s, (c) 20 s, (d) 30 s, (e) 40 s of the short protector on the stiff (top) and compliant (bottom) surrogate. All at the moderate strapping condition. Red circles highlight protector slippage. White lines indicate measured distance.

4.4.5   Pilot Test Discussion

In general, the compliant surrogate gave higher torque values for a given wrist extension angle for both protectors. At 75° wrist extension, the compliant surrogate gave higher torque values in 86% (31/36) of tests (Figure 4-9). The difference in torque values between the surrogates may have been due to the silicone increasing the friction between the protector and surrogate, although this was not measured. The silicone had similar frictional properties to skin (Chapter 3 Section 3.3), but the frictional properties between the protector materials and the stiff surrogate have not been assessed.

Video analysis showed the top of the dorsal side of the short protector slipped (Figure 4-11) a mean of 5 ± 2.9 mm more during testing when fitted to the stiff surrogate under moderate and tight strapping condition compared to the compliant surrogate. Indeed, Adams *et al*. (2016) suggested that adding a compliant layer could limit unwanted movement during testing. The reduced slippage of the short protector on the more biofidelic compliant surrogate may have caused the splints to engage more during testing, explaining the increased torque required to extend the wrist. However, it was unclear from the video capture as to whether protector slippage occurred at other locations on the surrogates. Synchronised cameras viewing different regions of the protectors could enable more insight into protector

slippage during bend testing. A second camera was, therefore, incorporated into
the repeatability study in Section 4.5. The incorporation of strain gauges on
protector splints could provide valuable insight into how much they bend during
testing on different surrogates. Strain gauges were not incorporated into the
repeatability test, as this was outside the scope of this study on the surrogate, but
future work focussing on protector performance should consider using them.

The stiffness of the protectors decreased during repeat tests, indicating they
degraded. The difference in torque values between the first and second (repeat)
test of a new protector ranged from 0.5 to 3.2 Nm (short protector) and 0.3 to 2.4
Nm (long protector) at 75° wrist extension (Figure 4-9). After the longer rest period
(15 minutes) when going from a new to used protector, the protectors appeared to
have partially recovered, with differences in torque values between the first test of
a new protector and the first test of a used protector ranging from 0.2 to 1.0 Nm
(short protector) and -0.7 to 1.9 Nm (long protector) at 75° wrist extension. All of
the second and third tests (new and used protectors) showed differences in torque
values of under 1 Nm, but due to the protectors degrading, these torque values are
not a true indication of protector stiffness when new. New protectors, or longer
rest periods before repeat testing, should be used in future tests to limit the
influence of protector degradation on results. Due to the influence of protector
degradation on repeated test results, it is unclear whether the repeatability of the
test was improved by adding the compliant outer layer. The repeatability study in
the Section 4.5 includes a longer rest period between test repeats, and uses
coefficient of variance as a measure of surrogate repeatability.

At 75° wrist extension, the torque values for the short and long protector under
moderate strapping conditions on the stiff surrogate were 2.6 and 4.1 Nm
respectively (Figure 4-9). Torque values of ~2 Nm (short protector) and ~5 Nm (long
protector) were reported at 75° (based on line connecting points from Adams *et al*.
(2018) Figure 4) by Adams *et al*. (2018) for an equivalent surrogate geometry and
protector strapping condition. The torque values reported in Adams *et al*. (2018)
under moderate strapping conditions fell between those observed within this study
for moderate and tight strapping conditions (Figure 4-10). As the same method to

set protector strap tightness was used, this indicates potential issues in achieving a set strap tightness between operators.

An improved method to provide increased control and reduced variability during testing of protector strap tightness could include the embedding of pressure sensors in the surrogate. The use of flexiforce pressure sensors (A201, Tekscan Inc, South Boston, USA) were trialled for measuring protector strap tightness and pressure at specific points along the forearm during bend testing. Four flexiforce sensors were trialled in different locations on the surrogate (directly under the protector straps, and in three locations along the dorsal side of the forearm), both on the outer surface of the surrogate and embedded in the surrogate (under the compliant layer). Due to uneven contact / non-uniform pressure distribution between the protector and surrogate, coupled with the 0.2 mm thickness of the sensors, consistent pressure values were unattainable (trial study presented in Appendix B (Section 9.2)). Pressure sensors were, therefore, not incorporated into Section 4.5.

4.4.6   Pilot Test Conclusion

Adding a 3 mm thick compliant outer layer to a wrist surrogate gave higher torque values in a bend test for a given wrist extension angle, relative to a stiff surrogate. This observation indicates that the compliant layer increased the surrogate-protector stiffness. The torque required to extend the wrist on both the stiff and compliant surrogate increased with protector strap tightness. Protectors degraded with repeated tests when a rest period of 1 minute was used. 15 minute rest periods between repeats will be used in Section 4.5 to reduce the effect of protector degradation on results, and to determine whether adding a compliant layer reduces variance of results and improves the overall repeatability of the test. A short protector slipped more during testing when fitted to a stiff surrogate compared with a compliant surrogate, whereas a long protector was not observed to slip in any tests. A second camera will be used in Section 4.5 to gain more insight into protector slippage.

4.5 Repeatability of the Bend Test

Testing of the stiffness of snowboarding wrist protectors via the bend test in
Section 4.4 was conducted on one test day. Having all testing on the same day /
session does not provide any information on the repeatability of the test.
Therefore, to determine the intra-repeatability of the bend test, the bend test was
repeated across three test days, each a week apart, with the same operator. Based
on the results from the pilot test, the procedure was improved for the repeatability
test, such as by having a longer rest period between test repeats and an additional
camera to measure protector slippage. The purpose of this repeatability study,
alongside determining the intra-repeatability of the bend test, was to assess the
variance of the two surrogates, with regards to test repeats, test days, and
protector strap tightness. Similar repeatability testing has been conducted on golf
clubs, to determine the reliability of a golf clubhead and ball velocity over repeated
testing sessions (Turner *et al*., 2020), and on measurements of wrist joint angles in
boxing, by conducting test-retest studies which involved recalibration between test
sessions (Gatt *et al*., 2020).

4.5.1 Method

The following five changes were made to the bend test procedure of Section 4.4.2:

1. a rest period of at least 5 minutes between repeats (additional pilot testing
   indicated that a 2 minute rest period was adequate, so a 5 minute rest period
   was deemed plenty) and a 15 minute rest period between surrogates, to reduce
   the effect of protector degradation on result,
2. the maximum wrist extension angle was increased to 85° (previously 80°), to
   create a wrist angle range of ~40 to 85°,
3. a second camera viewing the dorsal side of the protector was synchronised with
   the side-on camera (viewing wrist extension) to gain a better insight into any
   protector slippage (Figure 4-12 point 5),
4. markers were added to the protectors to measure protector and strap
   movement in video footage from testing,

5. the mass of the finger clamp was reduced from 184 to 54 g (reducing its effect on torque measurements to ~0.06 Nm at the starting angle 40°) (Figure 4-12 point 3).

The same wrist protectors from Section 4.4.1 were used for this repeatability study (short and long protectors, labelled A to F). The same markers for strap tightness were used for protector strapping. Three test days were conducted, each a week apart, with all equipment packed away and re-setup between test days. The room temperature was recorded at the start and end of each test day.

(a)   (b)
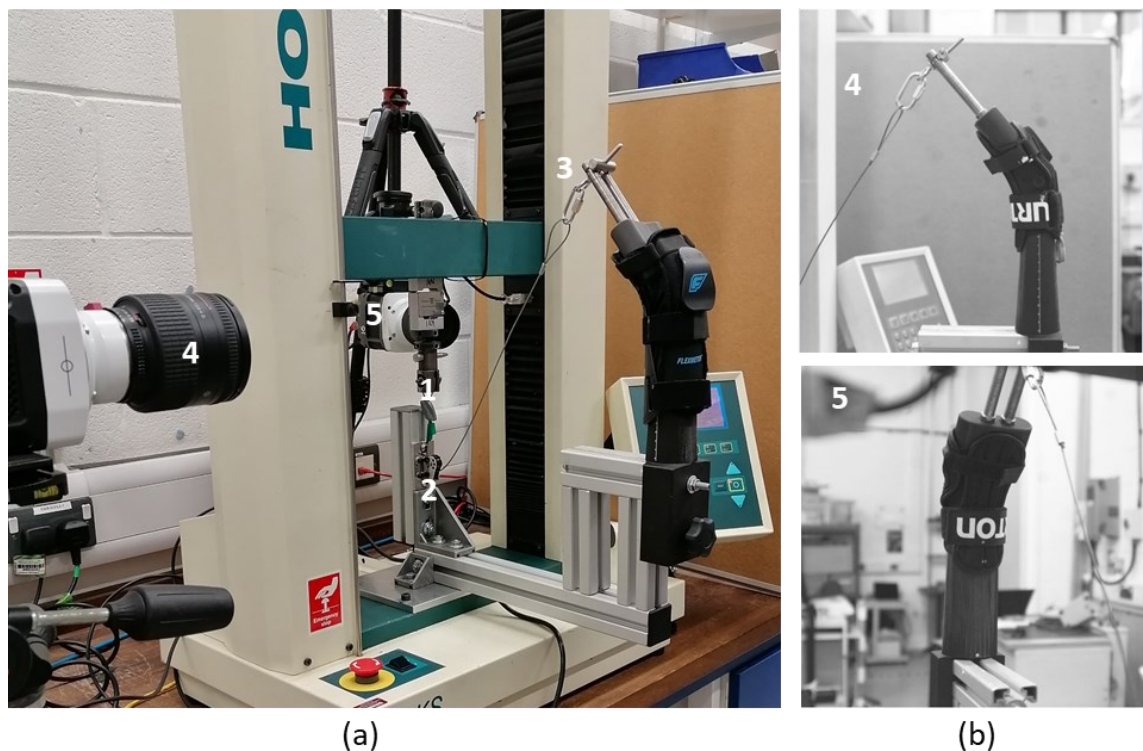
Figure 4-12 Bend test setup with additional camera. (a) test setup with a long protector on the stiff surrogate, (b) view from cameras (top - camera one, bottom - camera two). 1 - cable to uniaxial test machine, 2 - pulley, 3 - finger clamp, 4 - camera one viewing wrist extension, 5 - camera two viewing dorsal side of protector.

4.5.2   Data Analysis

The mean and standard deviation (SD) of the torque values at 5° intervals from the filtered (following Matlab script as per Section 4.4.3) torque vs. angle data, were calculated (six repeats for each surrogate-protector-strapping condition). The relationship between wrist extension angle and torque was studied for four cases: 50, 55, 75 and 80°. These four wrist extension angles relate to each extremity of the pass criteria for the medium surrogate in BS EN 20320:2020; when a torque of 5

Nm is applied the wrist angle should be between 50 and 75°, and when the torque is increased to 8 Nm the wrist angle should be between 55 to 80°. Thus, the lowest specified value from the torque of 5 Nm and the highest from the 8 Nm were taken to gain the full range of degrees of movement.

General linear model (GLM) univariate analysis was performed using SPSS statistical software (IBM® SPSS® Statistics Premium 27) at a significance level of $p < 0.05$ to determine the main effects and surrogate interaction ($\eta p^2 > 0.01$ small effect, $\eta p^2 > 0.06$ medium effect, $\eta p^2 > 0.14$ large effect (Richardson, 2011)). Torque was set as the dependent variable and surrogate, protector, angle, strapping condition, and test day as the independent variables. To determine the effect of the independent variable on the surrogates individually, further GLM univariate analysis was performed with the surrogates split up (removing surrogate as an independent variable). Box plots were used to display the distribution of the data. The coefficient of variance was calculated for each condition (protector, surrogate, angle, strapping condition).

4.5.3 Results

The room temperature recorded at the start and end of each test day was: test day 1 - 19.9℃ (start) and 21.2℃ (end), test day 2 - 17.6℃ (start) and 18.8℃ (end), test day 3 - 19.2℃ (start) and 20.8℃ (end). The highest and lowest room temperature was 21.2℃ and 17.6℃ respectively, equating to a difference in room temperature of 3.6℃. Such minor changes in temperature were unlikely to affect the following results.

In all cases (72/72), the compliant surrogate gave higher mean torque values than the stiff surrogate across all four wrist extension angles (50°, 55°, 75° and 80°) (Figure 4-13), which followed the results obtained from Section 4.4. The torque values at the four angles fluctuated between test repeats within a test session (Figure 4-14) and the mean torque values fluctuated between the three test days (Figure 4-13). The difference in torque values at 75° wrist extension between the first and second (repeat) test of a new protector, and between the first test of a new protector and first test of a used protector were similar (0.01 to 0.99 Nm compared to 0.01 to 1.66 Nm (short protector), 0.01 to 2.24 Nm compared to 0.07

to 2.64 Nm (long protector)) across all test days (Figure 4-14). Torque values
increased with both wrist extension and strap tightness (Figure 4-13 and Figure
4-15), following the results from Section 4.4. The long protector gave higher torque
values for a given wrist extension angle than the short protector, also following the
results from Section 4.4 (Figure 4-13 to Figure 4-15).
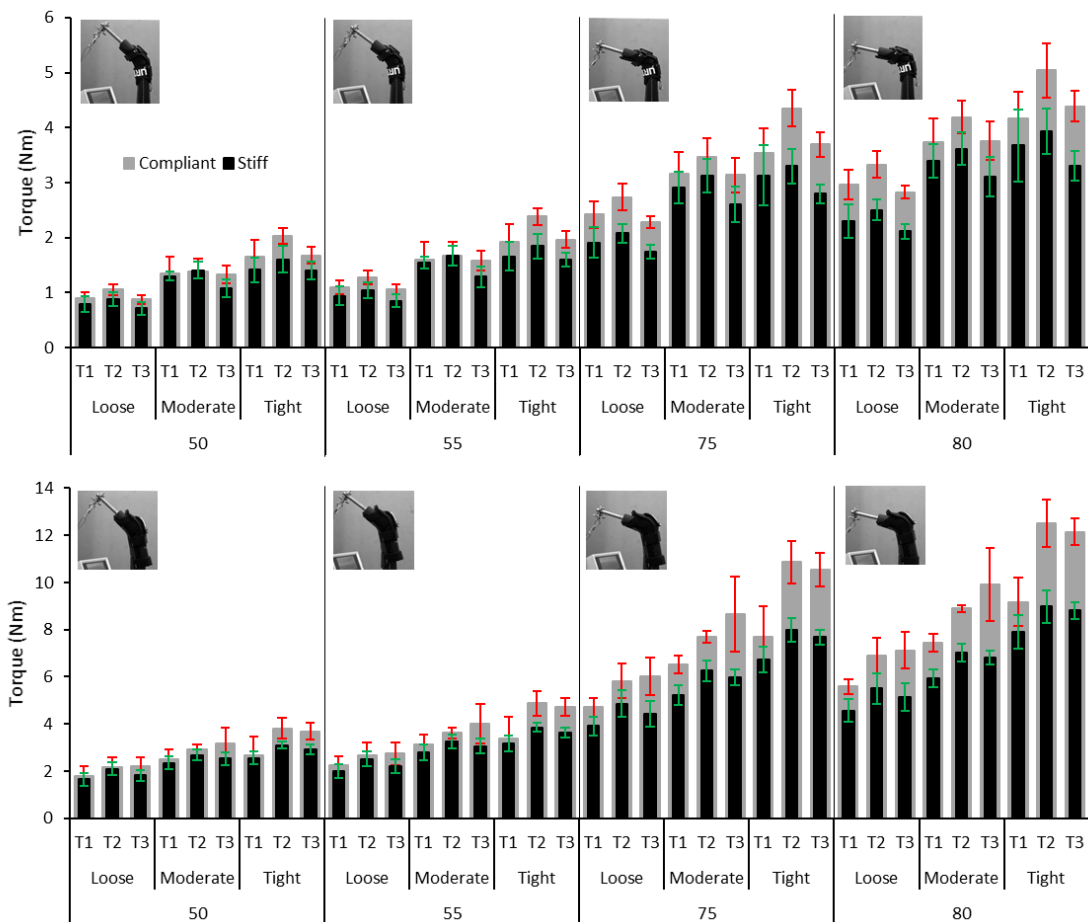
Figure 4-13 Mean torque at 50°, 55°, 75° and 80° wrist extension at each test day (T1- day 1, T2- day 2, T3- day 3) for the short protector (top) and the long protector (bottom) (error bars showing mean ± SD).
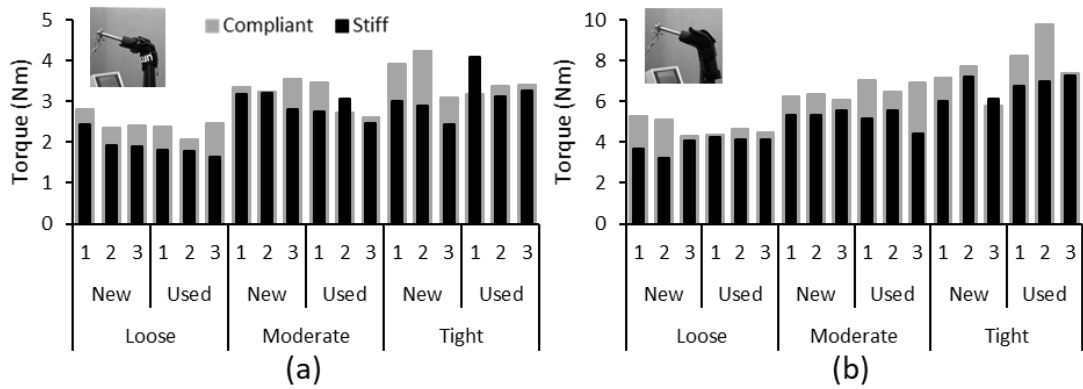
Figure 4-14 Example of torque at 75° wrist extension for (a) the short protector and (b) the long protector on test day 1. Torque values at 75° wrist angle for all test days are reported in the Appendix C Section 9.3.

When comparing the torque vs. angle results with the pass criteria of BS EN ISO 20320 (when a torque of 5 Nm is applied, the wrist angle should be between 50 and 75°, and when a torque of 8 Nm is applied, the wrist angle should be between 55 to 80°. i.e. the torque vs. angle curve has to pass through both horizontal dotted lines to pass, and for the stiff surrogate only) (Figure 4-15), the short protector did not meet the pass criteria in any test, and the long protector only met them at the tight strapping condition (on test days 2 and 3). When the protectors did not meet the pass requirements of BS EN ISO 20320, this was because the surrogate-protector stiffness was too low.
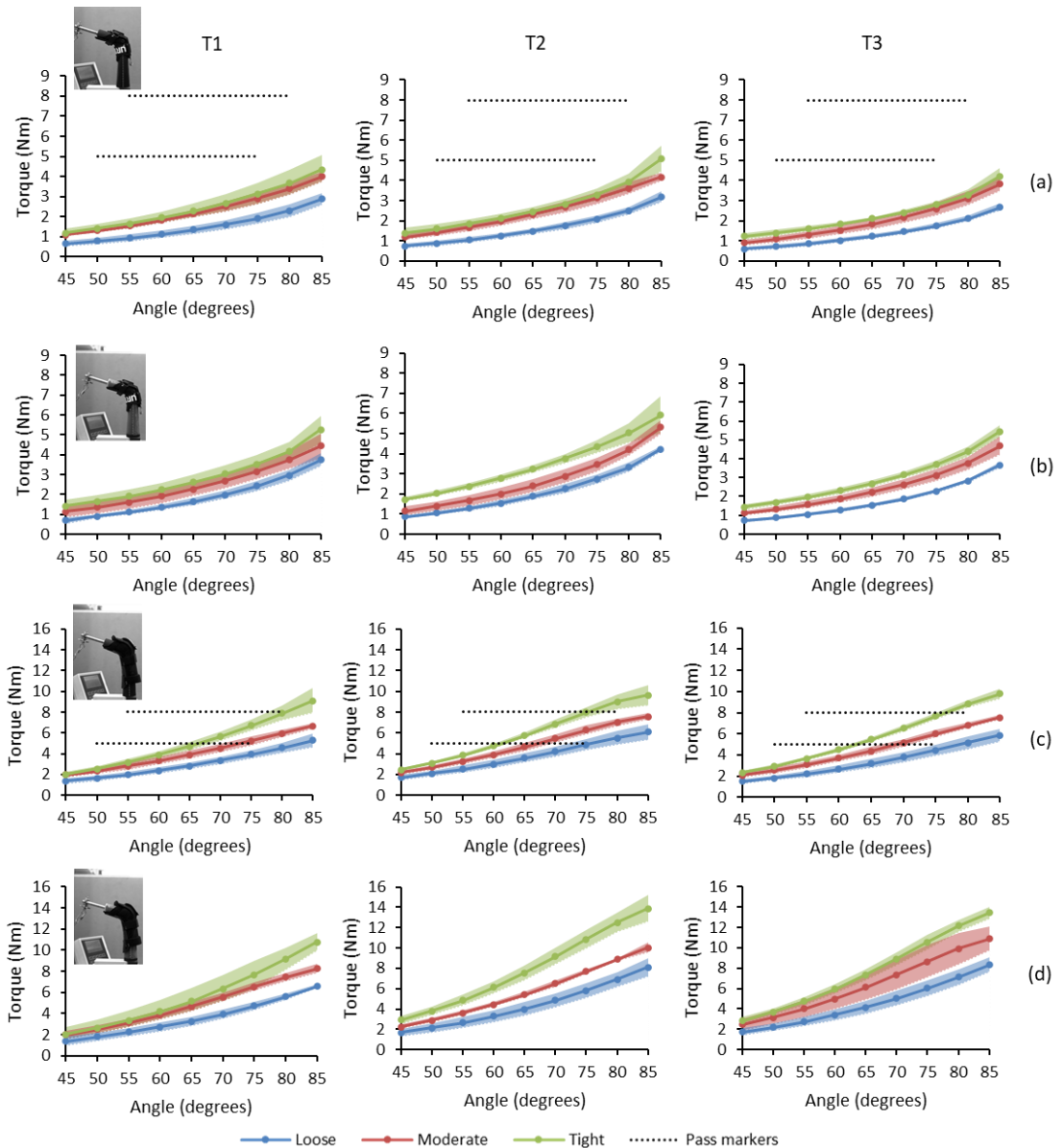
Figure 4-15 Torque vs. angle for the three test days (columns T1, T2, T3) and four surrogate-protector conditions: (a) stiff short, (b) compliant short, (c) stiff long, (d) compliant long. Shaded region indicates the SD. The dotted horizontal lines (Pass markers) indicate the pass criteria for BS EN ISO 20320:20200 for the medium surrogate. Note only the surrogate-protector conditions with the stiff surrogate meet the conditions of the standard.

Observations from the videos showed that protector slippage occurred on, i) the top of the dorsal side of the short protector (towards the surrogate fingers), ii) the bottom of the dorsal side of both the short and long protector (towards the base of the surrogate forearm), and iii) the two straps of the long protector (Figure 4-16). Due to the additional camera, more slippage locations were identified than in the pilot test. Measurements of protector slippage (in mm, expected accuracy ± 1 mm) on the video frames (start and end) across the three test days showed that both the short and long protector slipped further on the stiff surrogate than on the

96

compliant surrogate. The short protector slipped 13.8 ± 2.7 mm on the stiff surrogate compared to 12.5 ± 1.9 mm on the compliant surrogate (towards the surrogate fingers), and 6.5 ± 2.8 mm on the stiff surrogate compared to 5.4 ± 2.0 mm on the compliant surrogate (towards the base of the surrogate forearm). The long protector slipped 13.8 ± 3.3 mm on the stiff surrogate compared to 12.2 ± 3.0 mm on the compliant surrogate (top strap), 15.1 ± 4.3 mm on the stiff surrogate compared to 13.1 ± 3.9 mm on the compliant surrogate (bottom strap), and 19.1 ± 3.7 mm on the stiff surrogate compared to 17.8 ± 3.1 mm on the compliant surrogate (towards the base of the surrogate forearm). Although protectors appeared to slip less on the compliant surrogate than when on the stiff surrogate, the protector slippage between surrogates was not significant (statistical analysis in Appendix D (Section 9.4.1). The largest protector slippage difference between surrogates occurred at the same location on both protectors; the bottom of the dorsal side, at loose strapping condition (Figure 4-16b, c).

| (a) | (b) | (c) | (d) |
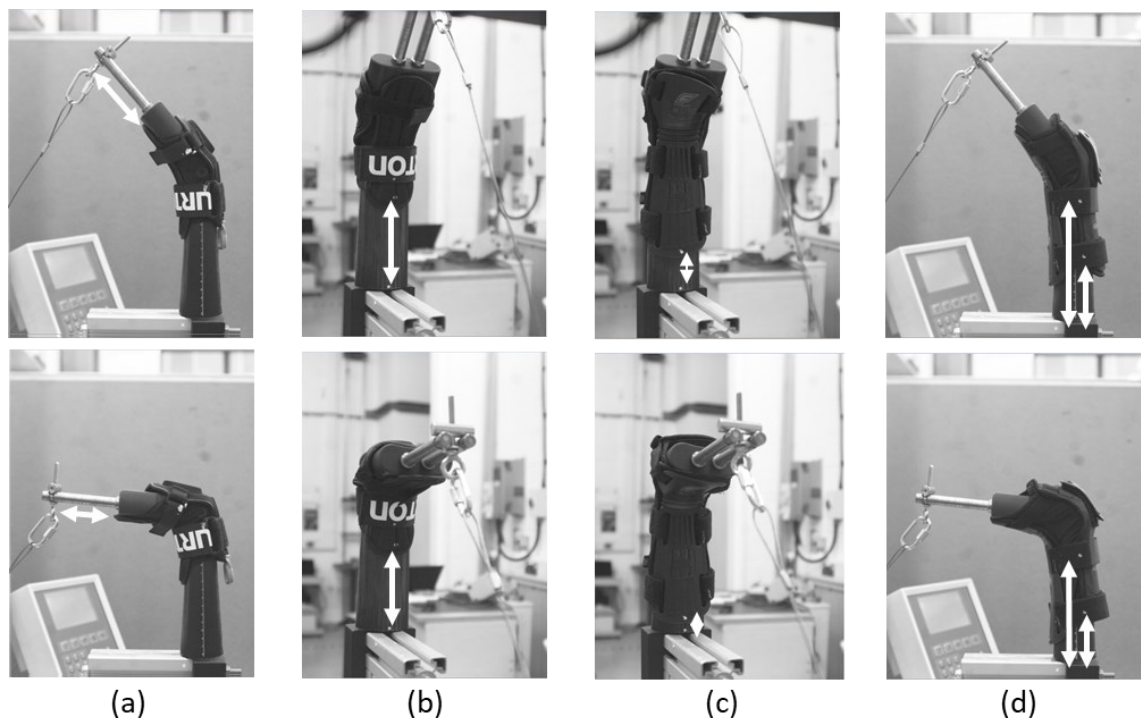
Figure 4-16 Video stills at start (top) and end (bottom) of test, showing observed protector movement when on the stiff surrogate: (a) top of the dorsal side of the short protector, (b) and (c) bottom of the dorsal side of the short and long protector, (d) the two straps of the long protector.

The GLM univariate analysis showed all the main effects and surrogate interactions were significant ($p < 0.05$) (Table 4-4). The main effects (surrogate, protector, angle,

strapping condition and test day) all showed a large effect ($\eta p^2 > 0.14$). Angle had the largest effect ($\eta p^2 = 0.94$), followed by protector ($\eta p^2 = 0.92$), strapping condition ($\eta p^2 = 0.77$), surrogate ($\eta p^2 = 0.49$), and finally test day ($\eta p^2 = 0.31$). The surrogate interaction between protector ($\eta p^2 = 0.17$) and between angle ($\eta p^2 = 0.26$), had a large effect, whereas the surrogate interaction between strapping condition ($\eta p^2 = 0.06$) and between test day ($\eta p^2 = 0.08$) had a medium effect.

The GLM univariate analysis for the surrogates individually, showed significant ($p < 0.05$) main effects (Table 4-5 and Table 4-6). Angle had the largest effect ($\eta p^2 = 0.95$ (stiff), 0.93 (compliant)), followed by protector ($\eta p^2 = 0.94$ (stiff), 0.91 (compliant)), strapping condition ($\eta p^2 = 0.82$ (stiff), 0.75 (compliant)) and finally test day ($\eta p^2 = 0.29$ (stiff), 0.37 (compliant)). The effect of the protector, angle, strapping condition, and test day were similar between surrogates (0.03 to 0.08 difference in ηp^2). The effect of the hand angle and protector was marginal between surrogates (~0.025 difference in ηp^2), whereas the strapping condition had a slightly larger effect on the stiff surrogate than the compliant surrogate (0.07 difference in ηp^2), and the test day had a slightly larger effect on the compliant surrogate than the stiff surrogate (0.08 difference in ηp^2).

Table 4-4 General linear model univariate between subject effects.

Source	df_1	df_2	F	*p-value*	Partial Eta Squared (ηp^2)
Surrogate	1	720		< 0.001	0.49 (large effect)
Protector	1	720		< 0.001	0.92 (large effect)
Angle	3	720		< 0.001	0.94 (large effect)
Strapping condition	2	720		< 0.001	0.77 (large effect)
Test day	2	720		< 0.001	0.31 (large effect)
Surrogate*Protector			$F_{(1, 720)} = 150.96$	< 0.001	0.17 (large effect)
Surrogate*Angle			$F_{(3, 720)} = 83.68$	< 0.001	0.26 (large effect)
Surrogate*Strapping condition			$F_{(2, 720)} = 21.95$	< 0.001	0.06 (medium effect)
Surrogate*Test day			$F_{(2, 720)} = 32.13$	< 0.001	0.08 (medium effect)

Table 4-5 General linear model univariate between subject effects for the stiff surrogate.

Source	df_1	df_2	F	*p-value*	Partial Eta Squared (ηp^2)
Protector	1	360	5567.23	< 0.001	0.94 (large effect)
Angle	3	360	2241.99	< 0.001	0.95 (large effect)
Strapping condition	2	360	813.38	< 0.001	0.82 (large effect)
Test day	2	360	72.26	< 0.001	0.29 (large effect)

Table 4-6 General linear model univariate between subject effects for the compliant surrogate.

Source	df_1	df_2	F	*p-value*	Partial Eta Squared (ηp^2)
Protector	1	360	3740.56	< 0.001	0.91 (large effect)
Angle	3	360	1632.35	< 0.001	0.93 (large effect)
Strapping condition	2	360	536.56	< 0.001	0.75 (large effect)
Test day	2	360	106.17	< 0.001	0.37 (large effect)

Box plots in Figure 4-17 display the distribution of the data for each surrogate for each of the independent variables (angle, protector, strapping condition and test day). In general, the spread of data was negatively skewed for all independent variables and for both surrogates, indicating that the values on the upper end of the scale (higher torque values) were more variable. The median torque value at 75° and 80° lies above the 50° and 55° boxes (Figure 4-17a), indicating that these groups were different. Torque at 75° and 80° had a larger range than at 50° and 55° for both surrogates. The median torque value for the long protector lies above the short protector box for both surrogates (Figure 4-17b), indicating that these groups were different. The torque range for the long protector was larger than for the short protector when fitted to both the compliant and stiff surrogate. The torque range was larger for both the moderate and tight strapping conditions than for the loose strapping condition (Figure 4-17c). The spread of data between test days was similar, whereas the median value fluctuated between test days (Figure 4-17d).
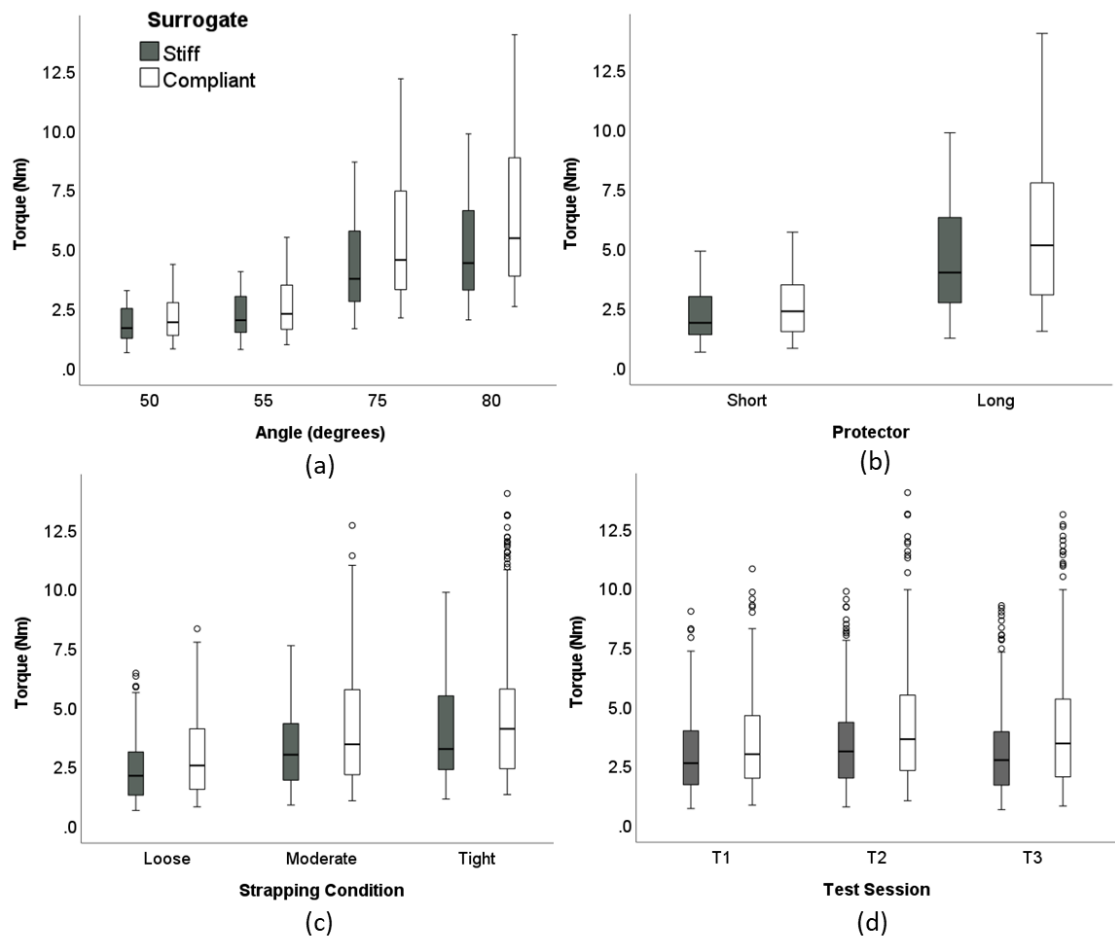
Figure 4-17 Box plots of the torque values for (a) angle, (b) protector, (c) strapping condition and (d) test day for each surrogate. The box plots display the minimum, first quartile, median, third quartile, maximum and outliers (data points).

The coefficient of variance for each surrogate-protector-strapping condition for the four angles of interest at each test day, and the mean for each angle across the test days and each surrogate-protector condition, are shown in Table 4-7. The compliant surrogate had marginally less variation with the short protector (13% vs. 14%), whereas it had more variation with the long protector (18% vs. 11%). The largest coefficient of variation across the three test days occurred at 50° and 55° wrist extension (22%) when the long protector was tightly strapped on the compliant surrogate. The smallest coefficient of variation occurred with the long protector on the stiff surrogate, at moderate strapping condition at 80° wrist extension and at tight strapping condition at both 75° and 80° wrist extension (9%).

*Table 4-7 Coefficient of variance (CV) for each surrogate-protector condition at each strapping condition across
all test days at the four angles of interest.*

Protector	Surrogate	Angle	Coefficient of Variance (%)			
			Loose	Moderate	Tight	Mean CV
Short	Stiff	50	18	15	15	14
		55	16	15	13	
		75	12	13	14	
		80	12	11	14	
	Compliant	50	13	17	15	13
		55	13	15	15	
		75	11	11	13	
		80	10	10	12	
Long	Stiff	50	17	11	11	11
		55	16	11	10	
		75	14	10	9	
		80	13	9	9	
	Compliant	50	21	19	22	18
		55	20	18	22	
		75	16	17	18	
		80	14	15	16	

4.5.4   Discussion - Repeatability of the Bend Test

The addition of a 3 mm thick skin tissue simulant to an otherwise stiff wrist
surrogate increased the surrogate-protector stiffness of two snowboarding wrist
protectors in a quasi-static bend test. However, the magnitude of the change in
stiffness could not be reliably quantified due to poor repeatability between test
days. Although, torque increased with both wrist angle and strap tightness (Figure
4-13 to Figure 4-15), which builds on the results from Section 4.4, and indicates that
the trend of results was repeatable. Torque values fluctuated between test repeats
on the same day and between test days (Figure 4-13 and Figure 4-14), indicating
the test was not highly repeatable. The measured stiffness of the protectors was
similar between the first and second (repeat) test of a new protector, and the first
test of a new and the first test of a used protector, in contrast to the results from
the pilot test (Section 4.4). This finding suggests that with a sufficient rest period (of
at least 5 minutes) between test repeats, the influence of any protector
degradation can be limited, i.e. the protectors recovered.

Strapping condition had a large effect ($\eta p^2 > 0.14$) on torque values for both surrogates, but the effect was similar between surrogates (0.82 ηp^2 stiff vs. 0.75 ηp^2 compliant surrogate), indicating that adding the skin simulant did not reduce the protector's sensitivity to strap tightness. This further highlights the need for the strap tightness to be controlled when testing, and ideally in BS EN ISO 20320:2020, such as a minimum strap tightness requirement. BS EN ISO 20320:2020 currently states that the protectors should be strapped as per the manufacturer's instructions, and perhaps requirements for what needs to be included in these instructions should be added in a revision of BS EN ISO 20320:2020. The long protector (on the stiff surrogate) only met the pass criteria of the standard (a torque of 5 Nm should cause between 50 and 75° of wrist extension, and a torque of 8 Nm should cause between 55 and 80° of wrist extension) when tightly strapped (on test day 2 and 3). The implication of this finding is that whether protectors pass or fail the standard could depend on how tightly the operator sets the straps. The short protector (on the stiff surrogate) did not meet the pass criteria of the standard under any strapping condition across the three test days, but these protectors have been tested before (Section 4.4), and therefore these results may not be a true indication of the protector's stiffness when new.

Test day had a large effect ($\eta p^2 > 0.14$) on torque values for both surrogates (0.29 ηp^2 stiff vs. 0.37 ηp^2 compliant surrogate), further indicating that the test was not repeatable. The similar effect of test day between surrogates indicates that adding a skin simulant did not reduce the variability of torque values between test days. Relatively poor repeatability was found with one operator, and the repeatability between operators could be worse, although this was not tested, and would fall under further work.

Both protectors slipped more on the stiff surrogate than when on the compliant surrogate, as found in Section 4.4, but the measured differences were not significant. The second camera enabled more insight into protector slippage of the long protector and other locations of the short protector. No further interpretation can be made on the effect of protector slippage on results. The lower coefficient of friction between the silicone and short protector inner fabric (polyester) compared

to the silicone and long protector inner fabric (neoprene) (0.56 vs. 0.81) (Chapter 3, Section 3.3) suggests why the short protector slipped in more locations than the long protector. However, it is unclear why the long protector tended to slip further than the short protector.

The coefficient of variance provided insight into the repeatability of protector stiffness testing on the surrogates. Repeatability of the surrogates varied between the two protector styles tested, with mean coefficient of variances of 13% (short protector) and 18% (long protector) for the compliant surrogate, and 14% (short protector) and 11% (long protector) for the stiff surrogate. This indicates that the repeatability of the surrogates were similar between the two styles of protectors tested, although further testing with more protector designs is recommended. There was no clear trend on the repeatability of different protector strapping conditions.

4.5.5   Conclusion

The results from the repeatability test further the findings from the pilot test in Section 4.4. Adding a 3 mm thick compliant outer layer to an otherwise stiff wrist surrogate increased the measured surrogate-protector stiffness of the snowboarding wrist protectors in a quasi-static bend test, but the magnitude of the change in stiffness could not be reliably quantified due to poor repeatability between test days. Strap tightness and test day both had a large effect on torque values. As such, the measured torque values from the bend test were not repeatable between test repeats nor test days, but the trend of the results between the various test conditions was repeatable. Adding a 3 mm thick skin tissue simulant to an otherwise stiff surrogate did not reduce the protector's sensitivity to strap tightness on torque results, nor did it reduce the variance of torque values between test repeats and test days.

4.6   Chapter Summary

The medium wrist surrogate from BS EN ISO 20320:2020 as per the draft standard on 15-05-2018 (geometric surrogate from Adams *et al.* (2016)) was critiqued, and amendments were made to finalise the wrist surrogate's geometry for testing.

Amendments included accounting for some missing dimensions around the surrogate's joint and undefined lofts between surfaces.

A 3 mm thick silicone layer was selected to represent skin on a wrist surrogate, based on reported skin thickness from literature and skin simulant thicknesses used by others to add compliance to sports surrogates. A wrist surrogate consisting of a 3 mm thick silicone outer layer and a stiff core was developed, and the effect of surrogate surface compliance on the measured stiffness of snowboarding wrist protectors was investigated. Furthermore, the intra-repeatability of a bend test, based on the one described in BS EN ISO 20320:2020, was determined, along with the variance of the two surrogates with regards to test repeats, test days, and protector strap tightness, and coefficient of variance for each condition.

Stiffness increased with both the surrogate wrist extension angle and the protector strap tightness. The bend test was found to have poor repeatability, as stiffness fluctuated between test days, however, the trend of results between test conditions was repeatable. A 5 minute rest period between test repeats was sufficient for limiting the effect of protector degradation on stiffness results.

Adding a skin simulant to an otherwise stiff wrist surrogate increased the surrogate-protector stiffness of the short and long snowboarding wrist protectors in a quasi-static bend test. Protectors showed variability between test repeats and test days, and were sensitive to strap tightness when tested on both a stiff and compliant wrist surrogate.

A key recommendation for the first revision of BS EN ISO 20320:2020 is to include a more repeatable test for measuring the quasi-static stiffness of the protectors. The results presented here indicate that strap tightness can determine whether a protector meets the pass requirements of BS EN ISO 20320:2020. The effect of strap tightness on the bend test needs to be reduced or accounted for somehow, but this is not straightforward. As a first step, it is recommended that a revision of BS EN ISO 20320:2020 should include requirements on what needs to be included in the strapping instructions provided by the protector manufacturer.

The novelty of this chapter was the use of maxillofacial silicone on a wrist surrogate, and the testing of snowboarding wrist protectors in a bend test, when on the developed compliant surrogate. Testing protectors on the compliant surrogate gained knowledge on the effect of developing the biofidelity of the wrist surrogate, informing the use of biofidelic surrogates for the testing of sports PPE. The repeatability study of the bend test furthered the work of Adams *et al.* (2016) and Adams *et al.* (2018) on the bend test, and the implications for BS EN ISO 20320:2020. The limitations of this chapter were that only two styles of wrist protector were tested, and thus the trends found are only current for those protectors. The degradation of the silicone was not extensively assessed, and thus its suitability for implementing into the standard was not determined. Furthermore, only the medium sized wrist surrogate was tested, and thus the testing of the small and large sized surrogates is required for further evaluation of the bend test and BS EN ISO 20320:2020.

This chapter determined the effect of surrogate surface compliance on the measured stiffness of snowboarding wrist protectors in a bend test developed by Adams *et al.* (2016), relating to the limitation of wrist extension test from BS EN ISO 20320:2020. The effect of surrogate surface compliance in an impact scenario has not been established. The effect of including a compliant layer on an otherwise stiff anvil will be explored within the impact test from BS EN ISO 20320:2020 in Chapter 5, and then the effect of adding a compliant layer to a wrist surrogate in the pendulum impact test developed by Adams (2018) will be explored in Chapter 6.

5. <u>Effect of Compliance on the Impact Performance of the Palmar Region of Snowboarding Wrist Protectors against BS EN ISO 20320</u>

5.1   Introduction

The previous chapter identified that adding silicone (M511 maxillofacial silicone, Technovent, Bridgend, UK) to a wrist surrogate increased the measured surrogate-protector stiffness in a bend test. The bend test is quasi-static and does not assess the impact performance of wrist protectors. This chapter will determine the effect of adding an outer layer of silicone to an otherwise stiff anvil on the impact performance of the palm region of snowboarding wrist protectors. Unlike the previous chapter, the silicone layer in this chapter will represent both skin and the underlying soft tissue, so it will need to be thicker. The outcome of this chapter will inform the design of the final wrist surrogate that will be tested in the pendulum impact test developed by Adams (2018) in the next chapter.

To determine the effect of silicone thickness in different impact scenarios, an FE model was used to simulate a range of silicone thicknesses on three different shaped anvils. A flat anvil simulated the most basic scenario, a hemispherical anvil simulated the impact test in BS EN ISO 20320:2020, and a palm shaped anvil simulated an impact on a basic surrogate hand. The FE model allowed the effect of silicone thickness on the impact test results to be assessed virtually without the need to make samples of specific thicknesses (within 1 mm). Data from the silicone material testing (Chapter 3 Section 3.3) was used to develop the FE material model. To check the accuracy of the models, the outputs were compared against those from experiments with a drop-tower impact test. To estimate the effect of a layer of silicone located under a palmar pad, the palmar pad from a short protector was incorporated into the FE model. The model of the pad was based on the work of Newton-Mann *et al.* (2018).

As there is limited published work characterising the impact performance of snowboarding wrist protectors against the impact test from BS EN ISO 20320:2020

(Chapter 2 Section 2.3.4) (Schmitt *et al.*, 2011), experimental impacts on the short and long protectors were performed. The effect of adding silicone to the prescribed anvil (hemisphere) on the impact performance of the short and long wrist protectors was investigated by replicating the BS EN ISO 20320:2020 impact test setup. The effect of introducing an anvil shaped more like a hand, as per the FE model, was also investigated.

This chapter documents, i) the development of an FE model to estimate the effect of silicone thickness on protector performance during an impact on the palmar region, ii) the impact testing of the short and long wrist protectors against BS EN ISO 20320:2020, and iii) the impact testing of the protectors on an anvil that is shaped more like a hand than the hemisphere prescribed in BS EN ISO 20320:2020, alongside the effect of adding a layer of silicone to these anvils.

5.2   FE Model - Effect of Silicone Thickness

5.2.1   Material Model Selection and Validation

An FE model for simulating the impact test on the cylindrical silicone sample from Chapter 3 Section 3.2.2.2 was created in ANSYS Workbench v182 using the LS-DYNA® add-in (Figure 5-1). Geometries of the drop mass, silicone sample and base plate were developed in SolidWorks and imported into ANSYS Workbench. The drop mass (60 × 60 × 5 mm) and base plate (80 × 80 × 3 mm) were defined as rigid bodies (MAT_RIGID), with material properties corresponding to structural steel (Ansys© library). Due to the lower volume of the drop mass in the model compared to the one in the experiment (which included the carriage), its density was artificially increased so the mass matched that of the drop mass in the experiment (2.5 kg).

The base plate was fully constrained and the drop mass was constrained in all but the z-axis and given initial velocities as measured from the experiment (Chapter 3 Section 3.3). Frictional surface-to-surface contacts (CONTACT_AUTOMATIC_SURFACE_TO_SURFACE) were defined between the drop mass and silicone sample, and the base plate and silicone sample, with a coefficient of friction of 0.4 (sensitivity study in Appendix E Section 9.5.1). A coefficient of

friction < 0.4 resulted in fluctuations in the force vs. time plots, and peak force plateaued after a coefficient of friction 0.4. A quadrilateral mesh with the default number of elements was applied to all geometries. The drop mass and base plate were assigned four mesh divisions on each edge (edge sizing), and a mesh with element size of 2 mm was assigned to the silicone sample following a mesh dependency study (mesh dependency study in Appendix E Section 9.5.1) (Figure 5-1).
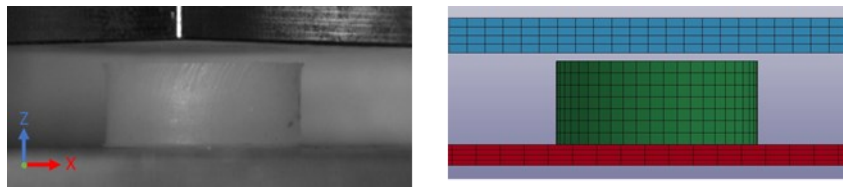
Figure 5-1 Experimental (left) and FE model (right) set up, displaying the silicone sample, drop mass and base plate.

To identify a suitable material model to assign to the silicone, four sets of stress vs. strain relations (from Chapter 3 Section 3.3) were trialled. The resulting outputs from the FE model were compared to the force vs. time result from the experimental impact test (Chapter 3 Section 3.3). The four stress vs. strain relations were: i) the 0.042 s^{-1} compression test data, ii) the 0.042 s^{-1} compression test data combined with the 0.042 s^{-1} tensile test data, iii) the 1.39 s^{-1} compression test data, and iv) the data obtained from the 2.5 J (~100 s^{-1}) impact on the compression sample (Chapter 3 Section 3.3). The four material datasets were imported into ANSYS Workbench v18.2 via the engineering data tab, a material model was selected and the curve fitting option was used to fit the material model to the data. The lowest residual and best visual match between the material model algorithm and the stress vs. strain data was used to determine the best fitted model for each dataset.

The Ogden (1st, 2nd and 3rd Order) and Mooney-Rivlin (2, 3 and 5 Parameter) material models were both trialled. Based on the curve fitting results, the Ogden 1st Order was selected for all four datasets (Residuals - 5.6, 28.8, 5.8, 0.6 for each dataset, respectively) (Figure 5-2). The material models were assigned a density of 1,072 kg/m³ (calculated from the mean sample mass) and a Poisson's ratio of 0.49 (sensitivity study in Appendix E Section 9.5.1). Following results from initial

simulations, frequency independent damping (shear modulus damping values), G and SIGF, were used to improve agreement with experimental data (G 47; SIGF 0.01). The shear modulus (G) was calculated using a maximum Young's modulus of 140 MPa (maximum Young's modulus of human skin tissue (Kalra *et al.*, 2016, Jacquemoud *et al.*, 2007)) (Chapter 3 Equation 4), and a limit setting of 0.01 (LS-DYNA® Model Volume-Ⅱ) for damping (SIGF) was applied.
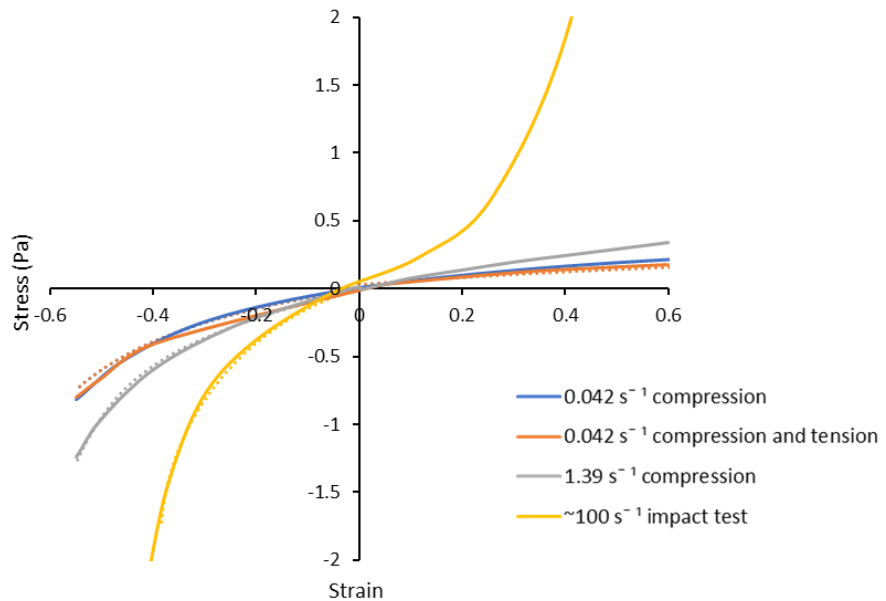
Figure 5-2 Stress vs. strain of the four datasets (dotted lines) and the material model curve fits (solid lines) for those datasets. The material models were plotted by taking individual points along the curve fit displayed in the engineering data tab (in ANSYS Workbench).

The four material models were applied to the FE simulation of a 1.0, 1.5, 2.0 and 2.5 J impact, and the temporal forces were compared with those from the experiments (Figure 5-3). The 0.042 s^{-1} compression and 0.042 s^{-1} combined compression and tension stress vs. strain curve fits for the Ogden material model were similar (Figure 5-2), which was reflected in the similar temporal forces results from the FE simulations of the impact test (Figure 5-3). For the 0.042 s^{-1} compression and the 0.042 s^{-1} combined compression and tension material models, broad agreement was obtained between the simulation and the experiment. The simulation with ~100 s^{-1} material model, which had the steepest stress vs. strain curve (Figure 5-2), overpredicted the peak force from the experiment at all impact energies, indicating the material in the model was too stiff. The simulation with the 1.39 s^{-1} material model, which had intermediate stiffness (Figure 5-2), provided the best agreement

to the experimental data in terms of peak force across the four impact energies
(error percentage for peak force was 4.3 to 6.7% across the four impact energies
and the error percentage for time to peak force was 19.0 to 30.6%). Based on these
results, the 1.39 s^{-1} material model was selected to be taken forward, and the
coefficients are presented in Table 5-1. At maximum deformation, the experimental
impact and 1.39 s^{-1} FE model were visually similar (Figure 5-4).

Pilot simulations with a Prony series (calculated from the stress relaxation data
(Chapter 3 Section 3.3)) combined with the stress strain data overpredicted the
peak force during 1 J impact simulations, even without shear modulus damping
(refer to Appendix E Section 9.5.2 for more information). Hence the material
models used only the quasi-static stress strain data without the stress relaxation
data.
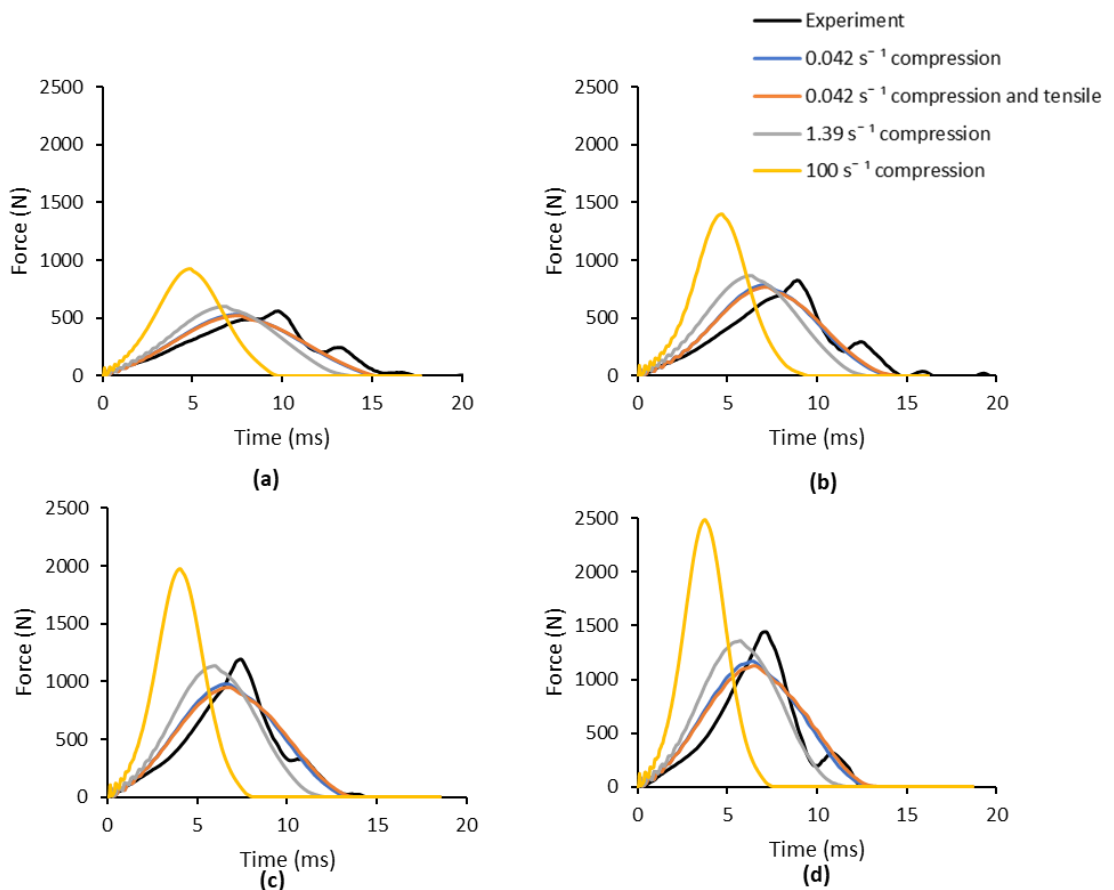
Figure 5-3 Force vs. time of the four material models compared to the experimental impact energies (a) 1 J, (b) 1.5 J, (c) 2 J and (d) 2.5 J for a silicone compressive sample (12.5 mm thickness) impacted on a flat anvil.

Table 5-1 Specific material model generated and used for the silicone.

Material model Ogden 1st Order	Coefficient value	
	MU1 (Pa)	A1
	2.6167E+5	2.1217

Property	Value
Poisson's ratio	0.49
Density (kg m^{-3})	1,072
G	47
SIFG	0.01
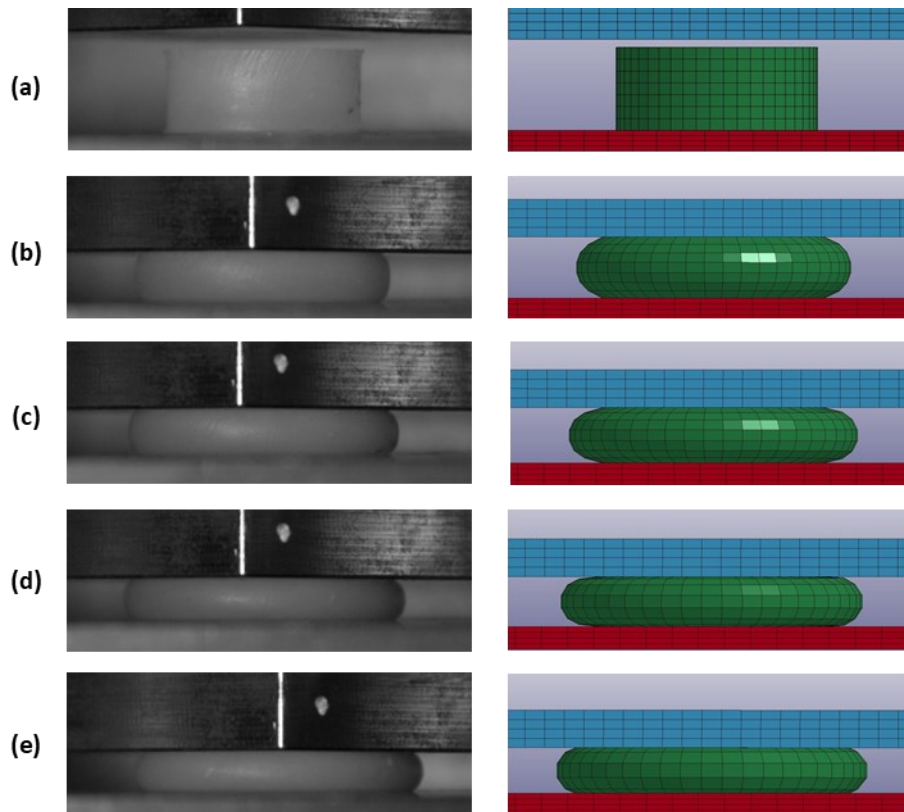
Figure 5-4 Visual comparison of maximum deformation between experimental impact test (left) and FE model (right) at (a) start position, and for impact energies (b) 1 J, (c) 1.5 J, (d) 2 J, (e) 2.5 J.

To compare the silicone (M511) material model developed here with the PDMS silicones used by Payne (2015) to represent different tissues within the thigh, their PDMS material models were input into the FE model of a 1 J impact. FE modelling was used for this comparison as the scenarios from experimental data differed. Only one impact energy was simulated for this comparison as it was assumed the temporal force would extrapolate across impact energies, as shown in Figure 5-3.

The PDMS material models consisted of a prony series without damping (Table 5-2). Force vs. time results for a 1 J impact showed that the silicone response fell between that of PDMS skin and PDMS adipose (Figure 5-5). This result was expected as M511 showed stress strain relations between that of organic skin and muscle (Chapter 3 Section 3.3), of which Payne's (2015) PDMS silicones simulated.

Table 5-2 PDMS material models (Payne, 2015).

	Ogden 1st Order Coefficients			Prony Series			Poisson's ratio
	μ	α	D	i	$g(i)$	$k(i)$	τ	
PDMS skin	5.92×10^5	2.61	-	1	2.67×10^{-2}	-	8.51×10^{-1}	0.476
				2	8.07×10^{-3}	-	4.04×10^1	
	Mooney-Rivlin Coefficients							
	D_{10}	C_{01}	C_{10}					
PDMS muscle	-	4.25×10^2	1.57×10^4	1	1.28×10^{-1}	-	3.52×10^{-1}	0.490
				2	5.29×10^{-2}	-	8.07	
				3	3.39×10^{-2}	-	7.61×10^1	
PDMS adipose	-	2.55×10^3	9.19×10^3	1	1.39×10^{-1}	-	7.51×10^{-5}	0.492
				2	1.70×10^{-1}	-	3.07	
				3	7.41×10^{-2}	-	7.90×10^1	
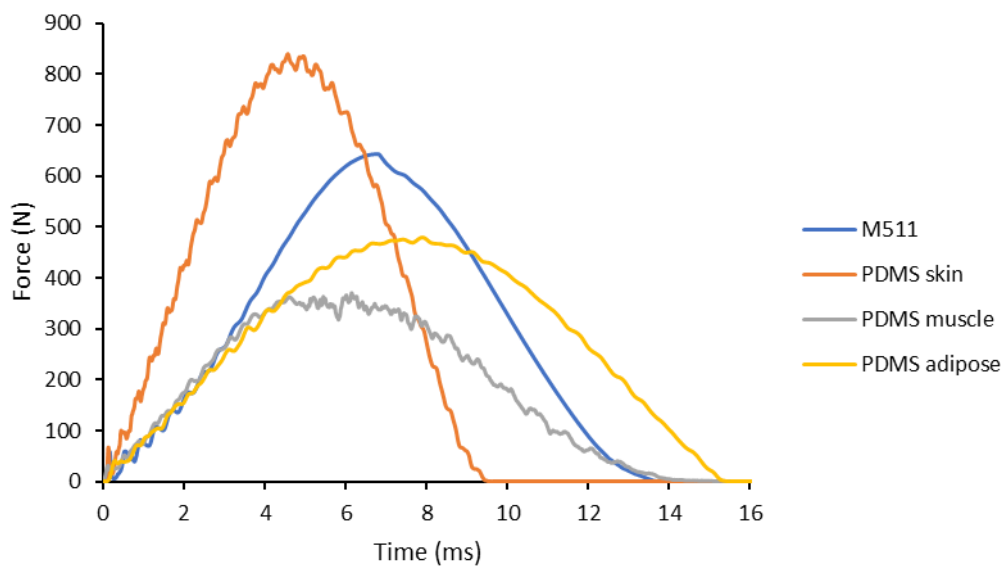
Figure 5-5 Force vs. time comparison between the silicone (M511) and PDMS silicones used by Payne (2015), in an FE model 1 J impact.

5.2.2 Model

Previous studies have used a 3 mm thick layer of compliant material to represent a soft tissue layer on a sports surrogate (Maurel *et al.*, 2013; Payne, 2015), whereas

the thickness of soft tissue in the palm area has been reported as 7 to 8 mm (Choi and Robinovitch, 2011). Based on this previous work, silicone thicknesses of 1 to 10 mm were tested in the FE model to predict the effect of silicone thickness on impact force. The silicone was positioned on three anvils (flat anvil, hemispherical anvil, palm anvil) and impacted at 4 J, corresponding to the impact energy in the BS EN ISO 20320:2020 impact test, and 10 J, the lowest impact energy used by Newton-Mann (2019) when testing a wrist protector on the pendulum drop rig of Adams (2018). Experimental impacts of 5, 8 and 10 mm thick silicone samples (silicone samples of 3 and 5 mm thickness were layered, approximately 60 × 60 mm) on all three anvils (flat, hemisphere, palm) were conducted at 4 and 10 J to further check the accuracy of the FE model predictions.

The silicone material model (Table 5-1) was applied to the silicone sample (56 × 56 mm) and the parameters (material model and mesh) from the previously described model (Section 5.2.1) were used for the drop mass (relating to the prescribed impactor striking face in BS EN ISO 20320:2020) and flat anvil. The hemispherical anvil was as per the dimensions stated in BS EN ISO 20320:2020 (Chapter 2 Section 2.3.4), and the palm anvil was as per the surrogate hand (Chapter 4 Section 4.2). The hemispherical and palm anvil geometries were edited to remove regions away from the impact area, to simplify the models without changing the results of the simulations (Figure 5-6). A tetrahedral mesh was applied to the hemispherical (130,533 elements) and palm (14,011 elements) anvil (difference in element number due to volume difference between anvils). To determine the effect of silicone thickness when positioned under a protective pad, the palmer pad of a short snowboarding wrist protector was also added to the FE model. The palmer pad material model from Newton-Mann *et al*. (2018) was input into the FE model (cross-validation in Appendix E Section 9.5.3) and a tetrahedral mesh (12,564 elements) was applied (Figure 5-6). Pilot simulations found the silicone sample had to be increased to 70 × 70 mm on the palm anvil (without the pad), to prevent the drop mass impacting the sides of the palm before the silicone (this was not an issue on the other anvils nor when the palmar pad was added, so the original size was used). The effect of also increasing the silicone sample on the flat and

hemispherical anvil was checked with the model (for a few cases), and found to
have a negligible (~2%) effect on peak force.
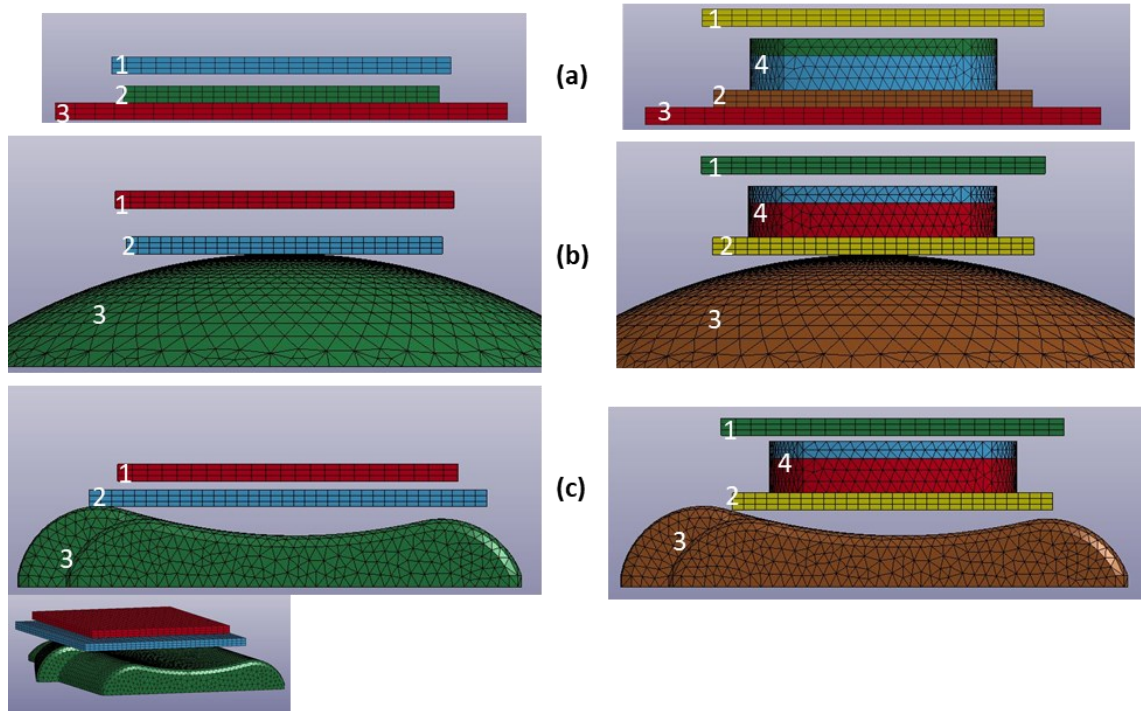
*Figure 5-6 FE geometries of silicone impact on the (a) flat anvil, (b) hemispherical anvil and (c) palm anvil.
Geometries include 1- drop mass, 2- silicone sample, 3- anvil (flat, hemisphere or palm), 4- palmer pad
(geometries on the left side). Note the silicone sample on the palm anvil (without the palmar pad) was larger to
prevent the drop mass impacting the sides of the palm before making contact with the silicone.*

To determine the effect of silicone thickness on impact forces, force vs. time and
silicone thickness vs. peak force were plotted for each silicone thickness impacted
on each anvil at energies of 4 and 10 J (Figure 5-7 and Figure 5-8). Peak force
decreased and impact duration increased as the silicone thickness increased from 1
to 10 mm (Figure 5-7). The FE model results were in good agreement with the
experimental impacts (5, 8 and 10 mm silicone sample impacted on each anvil) (see
Appendix E Section 9.5.4 for further graph) at 4 J (Figure 5-7), but at the higher
impact energy (10 J), the trend of results from the experiment in terms of the anvil
shape did not match the FE model. At 10 J, the experimental data showed that the
hemispherical anvil caused a higher force than the flat and palm anvil across the
different silicone thicknesses, whereas the FE model predicted the flat anvil to
cause the highest force.
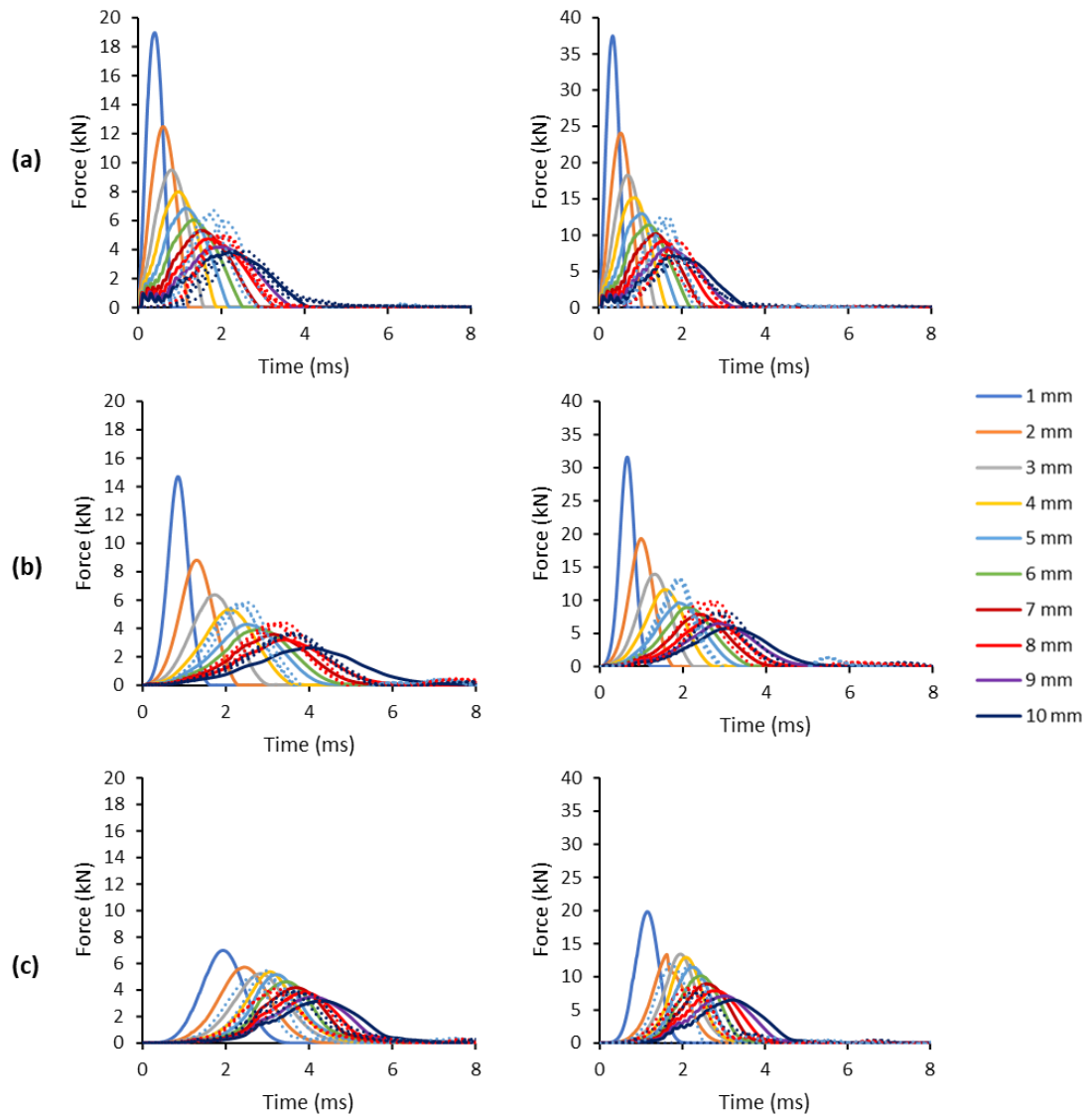
Figure 5-7 Force vs. time results for a 4 J (left) and a 10 J (right) impact for anvils (a) flat, (b) hemispherical, (c) palm, with various silicone thicknesses from 1 to 10 mm. Dotted lines show experimental impact results for comparison.
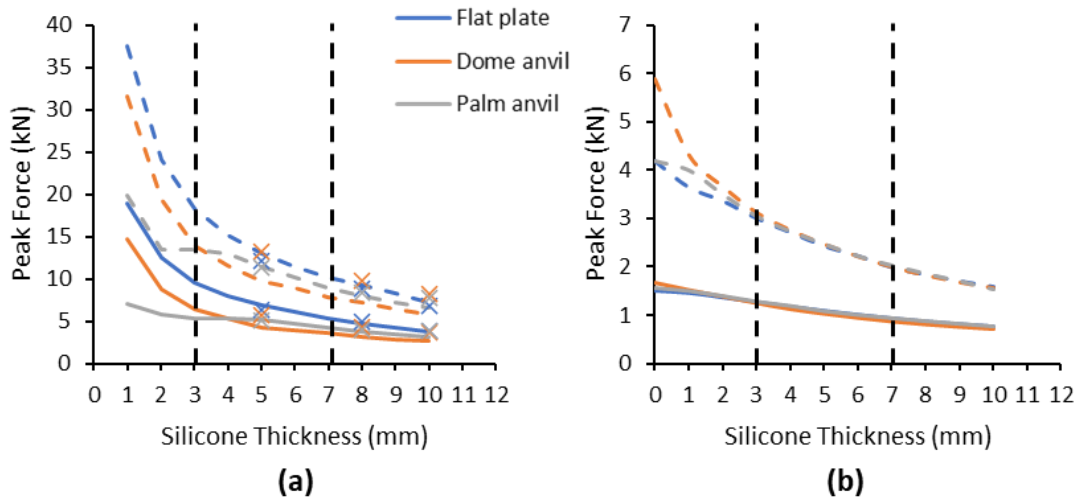
Figure 5-8 Peak force vs. silicone thickness for each of the three anvils. (a) anvil and silicone, (b) anvil, palmer pad and silicone. Solid curve indicates a 4 J impact, dashed curve indicates a 10 J impact. The markers (×) indicate experimental data. The black vertical dashed lines indicate previous silicone thickness used on surrogates (3 mm) and the measured soft tissue thickness of the palm (~7 mm) (Choi and Robinovitch, 2011; Maurel et al., 2013; Ankrah and Mills, 2013; Payne, 2015).

When impacted on the flat anvil and the hemispherical anvil, a large force reduction was predicted when the thickness of the silicone sample was increased from 1 to 3 mm (flat anvil - 9.5 kN (50%) at 4 J and 19.2 kN (51%) at 10 J, hemispherical anvil - 8.3 kN (57%) at 4 J and 17.7 kN (56%) at 10 J), whereas the force difference between an 8 and 10 mm thick silicone sample was marginal (flat anvil - 0.9 kN (19%) at 4 J and 2.0 kN (21%) 10 J, hemispherical anvil - 0.6 kN (18%) at 4 J and 1.3 kN (19%) at 10 J) (Figure 5-7 and Figure 5-8a). A similar trend was observed for impacts on the palm anvil, but the force reduction with increasing silicone thickness was smaller than for the other two anvils (1 to 3 mm - 1.7 kN (25%) at 4 J and 6.3 kN (32%) at 10 J; 8 to 10 mm - 0.6 kN (16%) at 4 J and 1.4 kN (17%) at 10 J). These results indicate that adding even a 2 to 3 mm thick compliant layer to a rigid surrogate could noticeably reduce impact force.

The reduced effect of silicone thickness on the palm anvil could have been due to the variable surface (i.e. curvature) of the palm compared to the flat and hemispherical anvil, which resulted in different areas of high effective plastic strain on the silicone sample (Figure 5-9). When impacted on the palm anvil (at 4 J), only specific areas of the silicone were under high effective plastic strain (sides of the palm anvil), as opposed to when on the flat and hemispherical anvil, in which most (centre top of the hemispherical anvil) or all (on the flat anvil) of the sample was

116

under high effective plastic strain. This phenomena could explain why the peak
force with a 1 mm thick silicone sample clearly differed between the palm anvil and
the flat and hemispherical anvil, as opposed to with a thicker (7 mm) silicone
sample, in which the areas of high effective plastic strain of the silicone were similar
between anvils, corresponding with similar peak force values.

As expected, adding a palmer pad reduced peak force for all silicone thicknesses on
the three anvils (Figure 5-8b). The peak force reduction from adding a palmar pad
over a 1 mm thick silicone sample impacted at 4 J was 17.5 kN (92%) on the flat
anvil, 13.2 kN (90%) on the hemispherical anvil, and 5.5 kN (79%) on the palm anvil.
A similar force reduction at 10 J was found when a palmar pad was added (33.8 kN
(90%) hemispherical anvil, 27.3 kN (86%) hemispherical anvil, 15.8 kN (80%) palm
anvil). In contrast, placing a 1 mm thick silicone sample under a palmar pad reduced
the peak force by only 2.9 to 8.9% at 4 J and 4.5 to 26.7% at 10 J in comparison to
the palmar pad in isolation across the three anvils. These results indicate that
adding a palmer pad reduces impact force, and thus could reduce injury risk,
although this would need to be confirmed in further work.
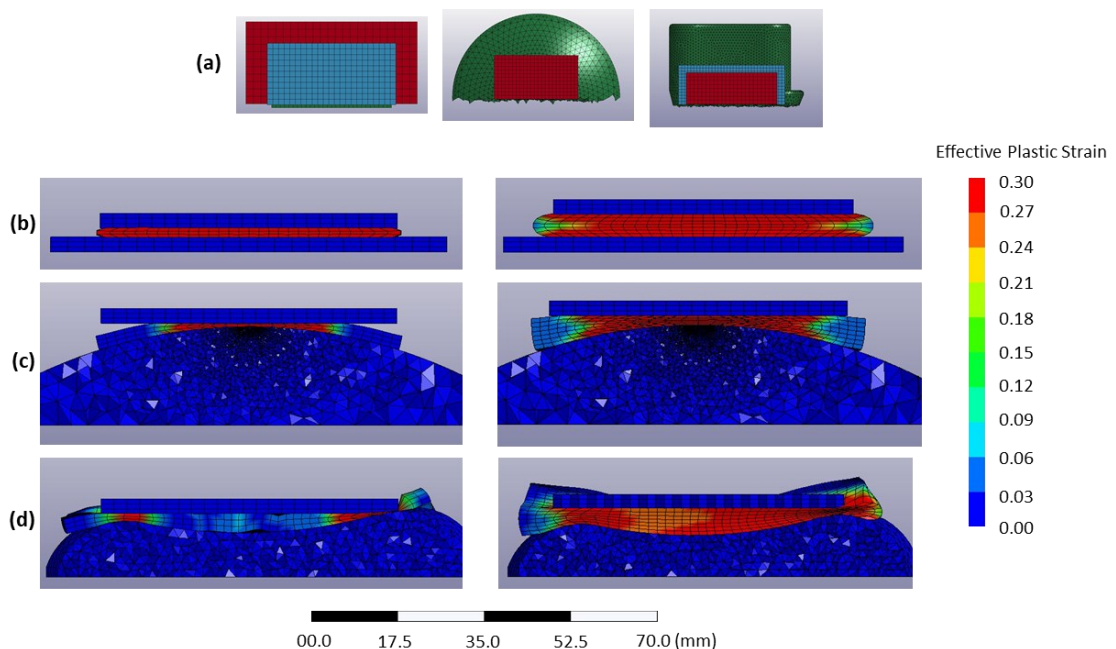
*Figure 5-9 Cross-sectional ((a) location of cross-section) comparison of effective plastic strain at maximum
deformation of a 3 mm (left) and a 7 mm (right) silicone sample impacted at 10 J on (b) flat anvil, (c)
hemispherical anvil and (d) palm anvil.*

Adding a 3 mm thick silicone layer to an anvil substantially reduced peak force in comparison to a 1 mm thick layer when impacted in isolation (mean force reduction across all avils of 6.5 kN at 4 J and 14.4 kN at 10 J compared to a 1 mm silicone layer) and when impacted in combination with a palmer pad (mean force reduction across all anvils of 0.3 kN at 4 J and 1.7 kN at 10 J compared to without silicone). Based on these findings, alongside previous studies (Maurel *et al*., 2013; Payne, 2015), it is suggested that 3 mm of silicone would be a suitable minimal thickness for use in a wrist surrogate impacted at low energies <10 J, to have a meaningful effect on peak force. Likewise, a silicone thickness >5 mm would be suitable for high energy impacts (>10 J), as a 1 to 3 mm silicone thickness would likely have limited effect on force reduction. The peak impact force began to plateau with a 7 mm thick silicone thickness, with a ~20% change in force between an 8 and 10 mm thick sample, so the effect of increasing the thickness of a silicone layer in a wrist surrogate beyond 7 mm may be marginal (<10% for each extra 1 mm added). A 7 mm silicone thickness also aligns with the measured soft tissue thickness of the palm region (Choi and Robinovitch, 2011).

5.3   Impact Testing against BS EN ISO 20320:2020

5.3.1   Test Method

To determine the impact performance of the palmar region of the short and long snowboarding wrist protectors, they were impact tested as defined in BS EN ISO 20320:2020. An anvil shaped more like a hand was introduced to the test, along with the addition of a 5 mm silicone layer to determine the effect of adding compliance to the impact test. The palm anvil also made it possible to gauge protector fit and whether any palmar padding was in an appropriate location and provided sufficient coverage. A silicone thickness of 5 mm was the median thickness tested in the FE model in Section 5.2.2 on the three different anvils, and thus was deemed a suitable starting point for adding compliance in experimental impacts of the full protector palmar region.

Impact tests were performed on the bespoke drop rig (Chapter 3 Section 3.2.2.2) (drop mass and hemispherical anvil as per BS EN ISO 20320:2020) (Figure 5-10a). A palm anvil (as per palmar surface in Chapter 4 Section 4.2) was fabricated (CNC) in

aluminium (Figure 5-10b). The anvils were fixed to the base plate. Silicone samples (60 × 60 × 5 mm) were fabricated (as per Chapter 3 Section 3.2.1) to add a compliant outer layer to both anvils.

A circular impact area (⌀ 40 mm) was located on the protectors and four impact locations were marked on the protectors (as per BS ISO EN 20320:2020) (Figure Figure 5-10c). Protectors were cut down both sides to enable the test area to be positioned on the anvil (Figure 5-10c). The skid plate on the long protector was removed, as stated in Chapter 4 Section 4.4.1. To secure the protectors but allow some compliance, they were held down by three 100 g masses on the hemispherical anvil, and four elastic bands passing under the base plate for the palm anvil (Figure 5-10a, b). The protectors were impacted once at each test location (four impacts) at an impact energy of 4 J. A foam sample (Plastazote LD60, 10 × 40 × 40 mm) was tested as a control material (as used by Imam (2021) as a control foam as a basic representation of rugby padding). The control material was used to determine whether the response (in terms of impact performance) of a snowboarding wrist protector due to a change in anvil shape or compliance, could be predicted using a generic foam that is similar to those typically used in sporting PPE. If such a generic foam can indeed be used to represent the palmar padding of a wrist protector, cost could be saved as products would not need to be purchased and dismantled for testing, and it would also be easier to investigate the effect of padding size on impact performance. For the tests involving the compliant layer, the silicone sample was placed between the anvil and protector / control material (Figure 5-10c).
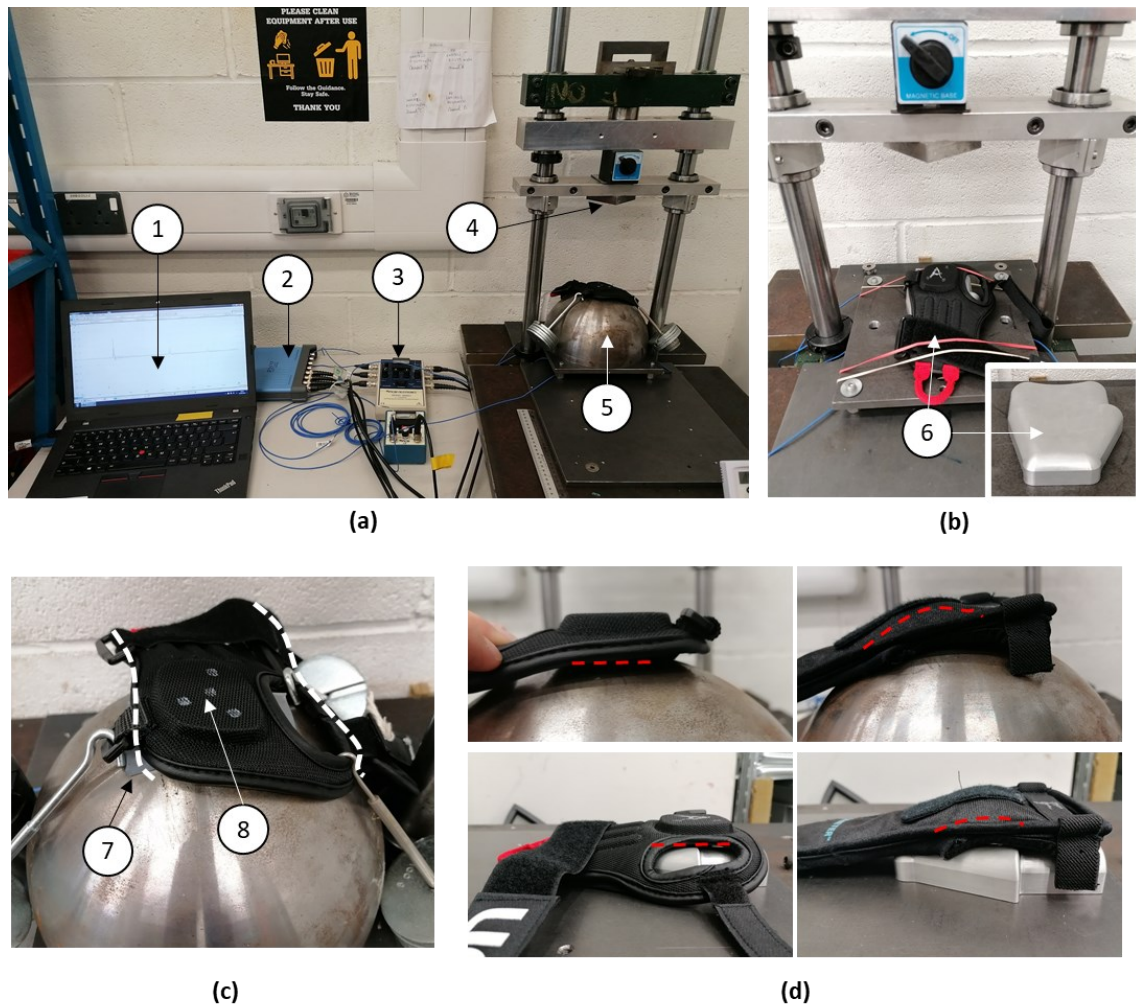
Figure 5-10 Bespoke drop rig with (a) hemispherical anvil and (b) palm anvil, showing projectors held down by masses for the hemispherical anvil, and elastic bands for the palm anvil. (c) shows the test location markers, position of silicone sample between anvil and protector, and white dashed lines indicating where the protectors were cut to be positioned on the anvil. (d) shows a close up of the fit of the protectors to the anvils, with red dashes lines highlighting the shape of the protector. 1-laptop, 2-picoscope, 3-signal conditioners, 4-drop mass, 5-hemispherical anvil, 6-palm anvil, 7-silicone sample, 8-test location markers.

To test inter repeatability between protectors, ten protectors of each style (short, long; labelled A to J) were tested. The protectors had not previously been impact tested (although all had been previously bend tested). Four of each protector (protectors A, B, C, D) were tested on just the hemispherical anvil (both with and without silicone underneath), another four (protectors E, F, G, H) were tested on just the palm anvil (both with and without silicone underneath), and a further two (I and J) were tested on both of these anvils (both without silicone). To limit the potential effect of degradation of the silicone and protector on the findings, protectors were alternated between silicone or anvil combinations. All protectors were tested eight times; four impacts (one at each of the four test locations) on the

anvil with silicone and four impacts without silicone, or, four impacts on the hemispherical anvil and four impacts on the palm anvil (10 minute rest between tests). A different silicone sample was used for each protector (five silicone samples; labelled 1 to 5) and these were each impacted a total of 16 times (Table 5-3). Room temperature was recorded at the start, middle and end of testing (testing was done in one day). Four foam samples (control samples) (labelled 1 to 4) were tested following the same test procedure.

Table 5-3 Table of test order, including the control foam samples. For example, with the hemispherical anvil, short protector A was tested with silicone for four impacts, and then without silicone for four impacts, giving a total of eight impacts for each row of the table.

Anvil	Protector		Test 1 (4 impacts)	Test 2 (4 impacts)
Hemispherical	Short	A	Silicone 1	No silicone
		B	Silicone 2	No silicone
		C	No silicone	Silicone 1
		D	No silicone	Silicone 2
	Long	A	Silicone 3	No silicone
		B	Silicone 4	No silicone
		C	No silicone	Silicone 3
		D	No silicone	Silicone 4
	Foam	1	Silicone 5	No silicone
		2	No silicone	Silicone 5
Palm	Short	E	Silicone 1	No silicone
		F	Silicone 2	No silicone
		G	No silicone	Silicone 1
		H	No silicone	Silicone 2
	Long	E	Silicone 3	No silicone
		F	Silicone 4	No silicone
		G	No silicone	Silicone 3
		H	No silicone	Silicone 4
	Foam	3	Silicone 5	No silicone
		4	No silicone	Silicone 5
Both	Short	I	Hemispherical	Palm
		J	Palm	Hemispherical
	Long	I	Hemispherical	Palm
		J	Palm	Hemispherical

5.3.2 Data Analysis

Load cell voltage was converted into force using the calibration factors provided by
the manufacturer and summed, as per Chapter 3 Section 3.2.2.2, and peak force for
each condition was determined. Peak force is of interest as BS EN ISO 20320 defines
a force limit (3 kN) which the protectors must not exceed, depending on protector
size range. The mean, standard deviation (SD) and coefficient of variation (CV) were
calculated for each protector tested with silicone (four tests) and without silicone
(four tests), and for all protectors tested on the same anvil with silicone (16 tests)
and without silicone (16 tests). GLM univariate analysis was performed as per
Chapter 4 Section 4.5.2, with the same values for identifying significant differences
and categorising effect sizes. Peak force was set as the dependent variable and
anvil, protector and silicone (with or without) as the independent variables. To
determine the effect of the independent variable on the anvils individually, further
GLM univariate analysis was performed with the anvils split up (removing anvil as
an independent variable).

5.3.3 Results

The room temperature recorded at the start, middle, and end of the day was:
19.3℃ (start), 20.2℃ (mid) and 20.4℃ (end), which corresponds to a change in
temperature of about 1℃ and was not deemed to affect the following results.

The mean peak force across the four short and the four long protectors tested on
the hemispherical anvil without silicone was 2.75 ± 0.55 and 3.08 ± 0.51 kN
respectively (Figure 5-11a). Out of the four test locations on the four short
protectors, 9/16 (56%) tests met the pass criteria for the standard (peak force
under 3 kN) (two protectors met the requirements at all four impact locations, one
protector failed all impact locations, and one protector met the requirements at
one impact location), whereas only 6/16 (38%) tests met the pass criteria for the
long protector (none of the protectors passed at all four impact locations). The
standard does not specify whether the peak force of only one, or all, impacts must
be under 3 kN for the protector to pass, and this could be clarified in the next
revision.
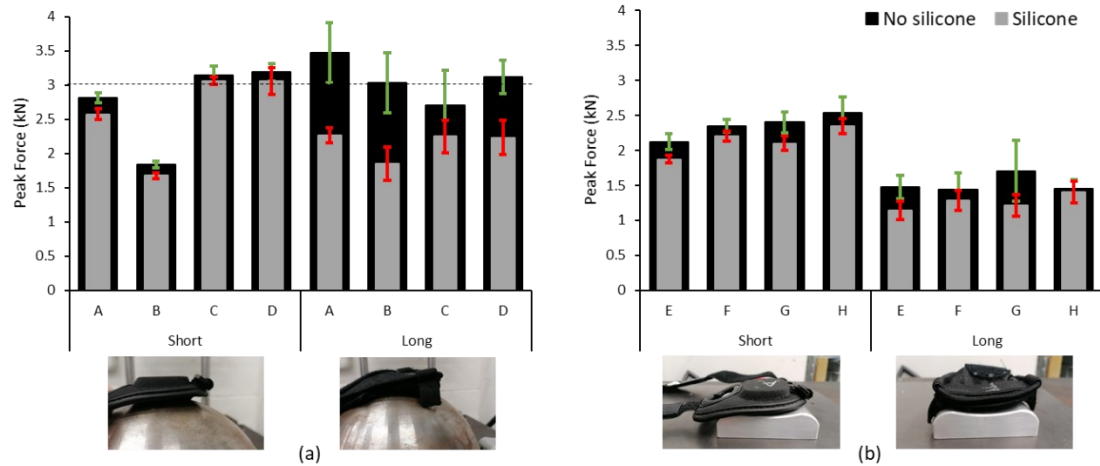
Figure 5-11 Peak impact force for testing with and without silicone for (a) short protector and long protector tested on the hemispherical anvil, and (b) short and long protector tested on the palm anvil. The x-axis indicates the protector tested (A to D; E to H). The black dotted horizontal line indicates the BS EN ISO 20320:2020 pass threshold (error bars showing mean ± SD).

Adding silicone to the hemispherical anvil reduced the mean peak force by 6% for the short protector (2.59 ± 0.58 kN) and 30% for the long protector (2.15 ± 0.28 kN). Testing the protectors on the palm anvil (without silicone) further reduced the mean peak force of the short and long protectors by 9 and 29% respectively, compared to testing on the hemispherical anvil with silicone (short protectors 2.35 ± 0.22 kN, long protectors 1.52 ± 0.29 kN) (Figure 5-11b). Moreover, adding silicone to the palm anvil reduced the mean peak force of the short and long protector by 9 and 17% respectively (short protector 2.13 ± 0.19 kN, long protector 1.26 ± 0.18 kN). When adding silicone to the anvils, or impacting on the palm anvil, the ranking of the protectors changed, i.e the long protector was better at limiting impact force than the short protector, as opposed to when impacted on the hemispherical without silicone as per BS EN ISO 20320:2020, where the short protector was better at limiting impact force than the long protector, which is interesting.

The FE model (Section 5.2.2) predicted a force reduction of 38% (639 N difference) when adding a 5 mm thick silicone sample below a short protector's palmar pad for a 4 J impact on the hemispherical anvil, and a force reduction of 31% (481 N difference) when on the palm anvil. For the experimental impacts, a mean force reduction of 156 N (5%) for the short protector and 932 N (30%) for the long protector was found when adding a 5 mm thick silicone layer to the hemispherical anvil. A mean force reduction of 223 N (9%) for the short protector and 260 N (17%)

for the long protector was found when adding a 5 mm silicone layer to the palm anvil (for the experiment).

When tested on the hemispherical anvil (without silicone), there was a larger CV of peak force between the short protectors than the long protectors (20 vs. 16%), whereas there was a larger CV of peak force between the test locations of long protectors (ranged from 8 to 19%) compared to the test locations of short protectors (ranged from 3 to 4%) (Table 5-4). Adding silicone to the hemispherical anvil marginally increased the CV of peak force between the short protectors (22 vs. 20%) and decreased it between the test locations of short protectors (ranged from 2 to 6%). Whereas, adding silicone slightly reduced the CV of peak force between the long protectors (13 vs. 16%) and between the test locations of long protectors (ranged from 5 to 13%).

When tested on the palm anvil, the CV of peak force between short protectors reduced, compared to the hemispherical anvil (9 vs. 20%) (Table 5-4). In contrast, the CV of peak force between long protectors slightly increased when tested on the palm anvil compared to the hemispherical anvil (19 vs. 16%). Adding silicone to the palm anvil followed the same trend as adding silicone to the hemispherical anvil for the long protector.

The GLM univariate analysis showed all the main effects and anvil interactions were significant ($p < 0.05$) (Table 5-5). The main effects (anvil, protector, silicone) were all large ($\eta p^2 > 0.14$). Anvil had the largest effect ($\eta p^2 = 0.54$), followed by protector ($\eta p^2 = 0.26$), and then silicone ($\eta p^2 = 0.21$). The anvil interaction with protector ($\eta p^2 = 0.21$) had a large effect, whereas, the anvil interaction with silicone had a small effect ($\eta p^2 = 0.04$).

The GLM univariate analysis for the anvils individually, showed significant ($p < 0.05$) main effects (Table 5-6 and Table 5-7). Silicone had a large effect on both anvils ($\eta p^2 = 0.23$ for both). Protector had a large effect on the palm anvil ($\eta p^2 = 0.79$), and no effect on the hemispherical anvil ($\eta p^2 = 0.003$).

Table 5-4 Coefficient of variance (CV) for each protector-anvil condition with and without silicone.

Anvil		Coefficient of Variation (%)			
		Short		Long	
	Protector Sample	No Silicone	Silicone	No Silicone	Silicone
Hemisphere	A	3	3	13	5
	B	3	2	15	13
	C	4	2	19	11
	D	4	6	8	11
	Mean CV	20	22	16	13
Palm	E	5	3	11	11
	F	4	3	17	11
	G	6	5	25	13
	H	9	5	8	11
	Mean CV	9	9	19	14

Table 5-5 General linear model univariate between subject effects.

Source	df_1	df_2	F	*p-value*	Partial Eta Squared (ηp^2)
Anvil	1	120		< 0.001	0.54 (large effect)
Protector	1	120		< 0.001	0.26 (large effect)
Silicone	1	120		< 0.001	0.21 (large effect)
Anvil*Protector			$F_{(1, 120)} = 32.57$	< 0.001	0.21 (large effect)
Anvil*Silicone			$F_{(3, 120)} = 4.69$	< 0.001	0.04 (small effect)

Table 5-6 General linear model univariate between subject effects for the hemispherical anvil.

Source	df_1	df_2	F	*p-value*	Partial Eta Squared (ηp^2)
Protector	1	60	0.18	< 0.001	0.003 (small effect)
Silicone	1	60	18.30	< 0.001	0.23 (large effect)

Table 5-7 General linear model univariate between subject effects for the palm anvil.

Source	df_1	df_2	F	*p-value*	Partial Eta Squared (ηp^2)
Protector	1	60	219.23	< 0.001	0.79 (large effect)
Silicone	1	60	17.71	< 0.001	0.23 (large effect)

When comparing peak force values between anvils (without silicone), the long protector showed a larger mean peak force difference between anvils (62%) than the short protector (4%) (Figure 5-12a). A larger difference in impact time was also shown between anvils for the long protector (~3.3 ms) than for the short protector (~0.3 ms) (Figure 5-12b and c).
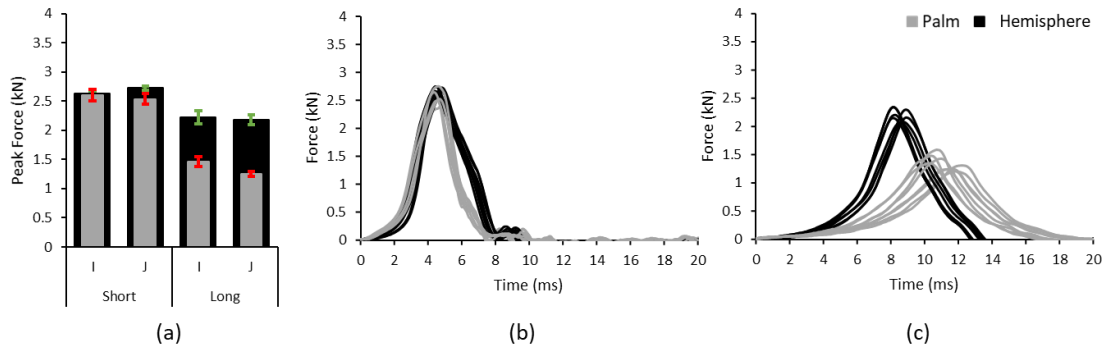
Figure 5-12 Comparison of (a) peak impact force between anvils (palm and hemisphere), and temporal force for (b) short protector and (c) long protector between anvils. The x-axis for the comparative peak force graphs indicates the protector tested (I and J) (error bars showing mean ± SD).

During pilot testing of the control foam on the palm anvil without silicone, it was found that a foam sample of 40 × 40 × 10 mm (Figure 5-13 point 1) caused the drop mass to impact the sides of the palm during impact (Figure 5-13 point 2), causing a large peak force (metal-on-metal impact). A similar result was found with the FE model (Section 5.2.2), where the silicone sample had to be increased due to the drop mass striking the sides of the palm. The size of the foam sample was therefore increased to 60 × 60 × 10 mm (Figure 5-13 point 3), to prevent the metal-on-metal impact (Figure 5-13 point 4). This was not an issue when testing with the hemispherical anvil.

The mean peak force of the control foam when tested on the hemispherical anvil without silicone was 2.68 ± 0.47 kN (Figure 5-14). The mean peak force of the control foam when tested on the palm anvil without silicone was 1.25 ± 0.11 kN (Figure 5-14). Adding silicone to the hemispherical anvil reduced the mean peak force of the control foam by 33% (1.79 ± 0.26 kN), and adding silicone to the palm anvil reduced the mean peak force of the control foam by 12% (1.09 ± 0.07 kN). The difference in mean peak force between anvils for the control foam was 54% without silicone, and 39% with silicone.
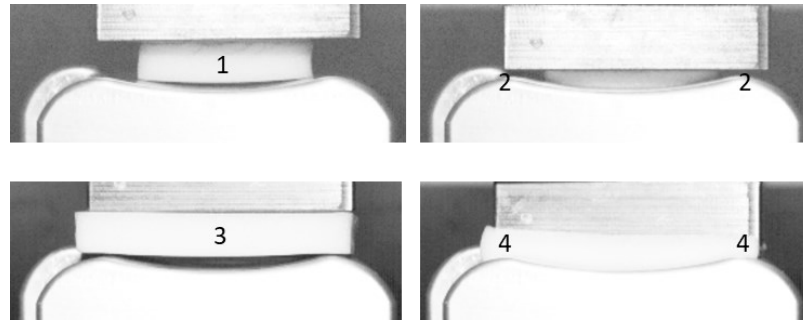
Figure 5-13 Example images from a high-speed camera showing a 40 × 40 × 10 mm foam sample (1) impacted on the palm anvil, causing the drop mass to impact the sides of the palm (2), and a 60 × 60 × 10 mm foam sample (3) impacted on the palm anvil, preventing the metal-on-metal impact (4).
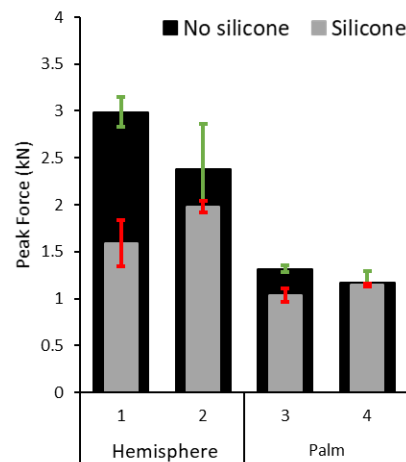
Figure 5-14 Peak impact force of the control foam tested with and without silicone on the hemispherical and palm anvil. The x-axis indicates the foam sample tested (1, 2, 3, 4) (error bars showing mean ± SD).

5.3.4 Discussion

The long protectors had a higher mean peak force than the short protectors when impacted on the hemispherical anvil without silicone (3.08 vs. 2.75 kN), as per BS EN ISO 20320:2020. This result indicates that the short protectors were better at limiting impact force than the long protectors when on the hemispherical anvil. Indeed, the short protectors met the pass criteria of BS EN ISO 20320:2020 (peak force below 3 kN) more often than the long protectors. In contrast, the short protectors had a higher mean peak force than the long protectors when impacted on the palm anvil without silicone (2.53 vs. 1.52 kN). This finding indicates that the long protectors were better at limiting impact force than the short protectors when on an anvil that was shaped more like a hand. Both protector styles, however, were better at limiting impact force when on an anvil shaped more like a hand than when on the hemispherical anvil. This indicates that anvil shape is important, and should

127

be appropriately accounted for in BS EN ISO 20320:2020. Furthermore, the GLM univariate analysis found that anvil shape had a larger effect than silicone on peak impact force.

The long protector was found to be more sensitive to the different shaped anvils, with a mean peak force difference of 62% between the hemispherical and palm anvils, compared to only 4% for the short protector. This finding could be due to the fit of the protectors to the anvils. The short protector lay flat on both anvils, whereas the long protector's curved palmar splint affected the fit of the protector to the anvils (Figure 5-10d). The arc of the long protector's palmar splint conformed to the shape of the palm anvil more so than for the hemispherical anvil.

Adding a 5 mm thick silicone layer to the anvils reduced the peak force of the long protectors more so than for the short protectors (long protector 30% (hemisphere) and 17% (palm), short protector 6% (hemisphere) and 9% (palm)). The lack of dedicated palmar padding on the long protector could mean that the silicone acted in a similar way to a palmar pad, reducing the impact force, whereas the short protector already had a palmer pad, so the silicone had less of an effect.

There was a larger CV of peak force between short protectors than between long protectors when tested on the hemispherical anvil (without silicone) (20 vs. 16%), indicating that there was more variability between short protectors than long protectors. The large variance between short protectors suggests that the palmar pads vary between protectors, as observed by Newton-Mann *et al*. (2018). This inconsistency in palmar padding has implications for BS EN ISO 20320:2020, as one short protector from the batch may pass the standard due to its specific palmar pad within the protector, whereas this may not represent the batch as a whole. Adding a 5 mm thick silicone sample did not reduce the variability in peak force between short protectors.

There was a larger CV of peak force between test locations on the long protectors compared to the short protectors (short protector ranged from 3 to 9%, long protector ranged from 8 to 25%), indicating that there was more variability between test locations on the long protector than on the short protector. Adding a

5 mm thick silicone layer to the anvils slightly reduced the CV of peak force
between test locations, although the variation was still larger for the long protector.
This finding was expected as the short protector specifically had a palmer pad that
covered the test area, whereas the long protector consisted of different materials
(supporting foam, soft gel, D3O™ and palmar splint (Newton-Mann, 2019)) within
the palmar area. The short protector's test area lay flat on the hemispherical and
palm anvil (at all impact locations), whereas the long protector's test area lay with a
slight arc (which was in a different position depending on the test location) due to
its shape.

The force reduction predicted by the FE model due to adding a 5 mm thick silicone
sample under a short protector's palmar pad impacted at 4 J on the hemispherical
anvil (38%, 639 N) was larger than for the experimental test of a (full) short
protector impacted on the hemispherical anvil at 4 J (6%, 156 N). The difference
could be due to inaccuracy in the model of the pad, and also because the model did
not include other aspects of the protector, such as the backing foam which can
further reduce impact force (Newton-Mann, 2019).

The control foam performed similarly to the long protector in terms of force
reduction due to adding silicone to the hemispherical anvil (33%) and the palm anvil
(12%), and peak force difference between anvils (54%). This means that the control
foam did not provide a good representation of the short protector. The control
foam, therefore, did not provide a general representation of both protector styles.

Testing on the palm anvil could help to determine whether a palmar pad was large
enough to cover the palm region, as if the pad was too small, the drop mass would
impact the sides of the hand. In contrast, it is difficult to determine whether a
palmer pad offers sufficient coverage when testing on the hemispherical anvil as
prescribed in BS EN ISO 203230:2020.

5.3.5   Conclusion

The short wrist protector limited peak force better than the long wrist protectors
when impacted on a rigid hemispherical anvil following BS EN ISO 203230:2020. As
noted in the literature review (Chapter 2), the prescribed anvil (hemisphere) is

clearly not representative of a wrist. Incorporating an anvil shaped more like a hand
into the impact test described in BS EN ISO 20320:2020 reduced the peak impact
force of both the short and long protector, and reduced the variability between
short protectors. As also noted in the literature review, the elasticity of the soft
tissue in the upper arm can reduce the force in a fall, suggesting that an impact
featuring a metal anvil and drop hammer is not representative of a real life fall
scenario. Introducing compliance into an impact test would add biofidelity, with an
expected energy dissipation, which was found in the results presented here. Adding
a compliant layer on the anvils reduced the peak impact force of both the short and
long protector.

5.4   Chapter Summary

An FE model was used to predict the effect of silicone thickness on impact force, by
simulating 4 and 10 J impacts of 1 to 10 mm thick silicone samples on three
different shaped anvils (flat, hemisphere, palm). A material model for the silicone
was selected from the material characterisation data from Chapter 3, and
experimental impacts were used for validation. Maximum force decreased, and
then plateaued, and impact duration increased as silicone thickness increased from
1 to 10 mm on all three anvils. A large force reduction was predicted between a 1
and 3 mm thick silicone layer (~53%), whereas the force began to plateau at 7 mm,
resulting in a marginal change in force between an 8 to 10 mm thick silicone layer
(~18%). A silicone thickness of 3 mm was selected as a suitable minimal thickness
for use in a wrist surrogate intended for low energies impacts (<10 J), whereas a ~7
mm silicone thickness would be suitable for higher energy impacts (>10 J).

A wrist protector palmar pad (Newton-Mann *et al*., 2018) was added to the FE
model to determine the effect of silicone thickness between a pad and the anvil.
The pad substantially reduced force for all silicone thicknesses and the different
shaped anvils, indicating that a palmar pad could reduce injury, although further
work is needed to determine this.

The impact performance of the palmar region of snowboarding wrist protectors
was determined by conducting experimental impacts following the test procedure

in BS EN ISO 20320:2020. The short protector was better at limiting impact force than the long protector, and as a result, more tests on the short protectors met the pass criteria of BS EN ISO 20320:2020 (peak force below 3 kN). As the short protector specifically had a palmar pad, this result was not unexpected. As the prescribed anvil (hemisphere) in BS EN ISO 20320:2020 is not representative of a hand, impact performance testing of the wrist protectors on an anvil shaped more like a palm was also conducted. Both protectors were better at limiting impact forces when on the palm shaped anvil, and furthermore the variance between short protectors was reduced, indicating that anvil shape is important in a linear impact test. While the hemispherical anvil is well suited for sports PPE certification tests, as the operator can easily position the product so the impactor strikes in the intended location, it is not always so easy to secure the PPE to it, particularly without cutting or otherwise damaging the product. Indeed, it was easier to fit the protectors to the palm anvil, although as the components of wrist protectors are typically sewn together to form a sleeve, and the anvil was fixed to the base plate of the test rig, they still needed to be cut to access the palmar side for testing. Furthermore, testing with the palm anvil determined whether a palmar pad offered sufficient coverage, which was impossible with the hemispherical anvil. Future work could develop a hand / wrist shaped anvil that protectors could be fitted to without the need for them to be cut or otherwise damaged or dismantled.

Compliance was introduced into the impact test to add biofidelity, and to understand its effect on the protectors ability to limit impact force. Adding a compliant layer to the hemispherical and palm anvil reduced the impact peak force for both protectors, without increasing the variability.

The novelty of this chapter was the use of an FE model to determine the effect of silicone thickness on impact force when between a wrist protector palmar pad and rigid anvil, and the testing of snowboarding wrist protectors against the impact test in BS EN ISO 20320:2020, alongside the addition of a compliant layer to this impact test and incorporation of an anvil shaped more like a palm. The impact testing of snowboarding wrist protectors against BS EN ISO 20320:2020 furthered the work of Schmitt *et al.* (2011) on the impact test procedure and ability of wrist protectors to

limit impact force. The addition of a compliant layer to the anvil and incorporation of a more representative anvil shape, gained knowledge on the effect of developing the biofidelity of the anvil for impact testing wrist protectors. This work also informed the use of biofidelic surrogates/anvils for impact testing and certification of sports PPE. The limitations of this chapter were that only two styles of wrist protector and only medium sized protectors were tested. To further determine the ability of wrist protectors to limit impact force and the implications for BS EN ISO 20320:2020, more protector styles and sizes need to be tested.

The addition of a 3 mm silicone outer layer to a wrist surrogate, with a thicker (~7 mm) silicone layer on the palmar region, could combine the results of increased protector stiffness from the bend test (Chapter 4) with the reduction of impact force on the palmar region found here, which could lead to reduced impact force in the pendulum impact test. The next chapter will first develop both a compliant (with silicone) and a stiff (without) surrogate suitable for impact testing in the pendulum impact test developed by Adams (2018). These two surrogates will then be used to determine the effect of using silicone as a skin and soft tissue simulant on the impact performance of the short and long protectors.

6. <u>Effect of Surrogate Compliance on the Impact Performance of Snowboarding Wrist Protectors</u>

6.1   Introduction

The previous chapter determined the effect of placing a layer of silicone over a rigid anvil during an impact test, in terms of force reduction. A silicone thickness of ~7 mm was determined to be suitable to represent the soft tissue of the palm in a wrist surrogate when impacted at energies >10 J. This chapter develops the compliant surrogate from the bend test (stiff core and 3 mm thick silicone outer layer) so it can be implemented into the pendulum impact rig developed by Adams *et al*. (2021). The original surrogate from the pendulum impact rig (based on a laser scan of a human hand and forearm, as detailed in Adams (2018)) was critiqued, and amendments were made to ensure that the compliant impact surrogate developed here would fit to the rig.

The compliant impact surrogate consisted of a central core, compliant hand (attached via a hinge joint to the central core), and compliant forearm casings (bolted around the central core). The compliant forearm casings consisted of a 3D printed stiff plastic core and a silicone outer layer. The impact performance of the short and long wrist protectors were tested following the pendulum impact test procedure from Newton-Mann (2019). These protectors were tested on both the compliant surrogate, and a comparable stiff surrogate. The stiff surrogate had the same size and shape as the compliant surrogate, with the 3D printed plastic forearm casing including the space occupied by silicone on the compliant surrogate. This chapter documents the development of the compliant surrogate specifically for use on the pendulum impact rig, the test procedure, and the impact performance of the short and long protectors.

6.2   Hypothesis

Chapter 4 demonstrated that adding a compliant outer surface to a wrist surrogate increased the measured stiffness of both the short and long wrist protectors in a bend test, compared to a stiff surrogate. The long protector was found to be stiffer than the short protector, as reported by both Adams *et al*. (2021) and Newton-

Mann (2019). Strapping conditions affected the measured stiffness of both protectors; as strapping tightness increased, the torque required to extend the wrist increased. The addition of the compliant layer to the wrist surrogate did not reduce the protector's sensitivity to strapping tightness on torque results. Based on these previous findings, it was hypothesised that:

1. Compared to the stiff surrogate, the compliant surrogate will,
    1.1. have a lower wrist angle for a given force, due to the silicone increasing the surrogate-protector stiffness.
    1.2. improve the measured impact performance of the short and long wrist protector, i.e. a lower peak force and slower wrist extension.
    1.3. have a lower force when the impactor strikes the uppermost of the hand at the start of the impact phase, due the silicone surrounding the end of the hand
    1.4. have a similar, or slightly lower, force and a similar, or slightly longer, contact time for the bare hand condition (no protector), as the silicone does not directly cover the wrist joint.
2. The long protector will have a lower peak force than the short protector under impact.
3. Increasing strapping tightness will reduce the wrist angle for a given force, but the effect between surrogates will be marginal.

6.3   Impact Surrogate Development

6.3.1   Critique of Current Test Rig and Surrogate

The pendulum impact rig developed by Adams *et al.* (2021) consists of a pendulum arm (steel box section) locked to a steel pivot shaft (potentiometer mounted), with a flat-faced impactor (aluminium plate and two neoprene blocks (polychloroprene, 50 Shore A hardness, Boreflex Ltd, Rotherham, UK), as per Newton-Mann's (2019) rig modifications). Adams published a PhD thesis detailing the development of this rig (Adams, 2018), some of which was published recently (Adams *et al.*, 2021). Generally speaking, the thesis will be referred to here as it contains more details than the corresponding paper. The surrogate geometry was based on a laser scan of a human arm (Adams, 2018), and consists of a steel central core bolted to the base

plate, an aluminium hand and a two-part forearm casing (laser sintered, PA12, Materialise). Wrist extension is measured by a (second) potentiometer mounted in the central core, which is offset from the wrist and connected via a toothed timing belt (Figure 6-1). The potentiometer was mounted in the central core because it was too big to fit in at the wrist joint.

A	Hand
B	Shaft
C	Bearing x2
D	Toothed timing pulley x2
E	Potentiometer
F	Toothed timing belt
G	Central metal core
H	Washer
I	Casing part 1
J	Slot in casing for potentiometer and wiring
K	Casing part 2
L	Fixing to bolt casing to central core
M	Hole to mount casing to central core
N	Finger slots
O	Base plate
P	Dynamometer
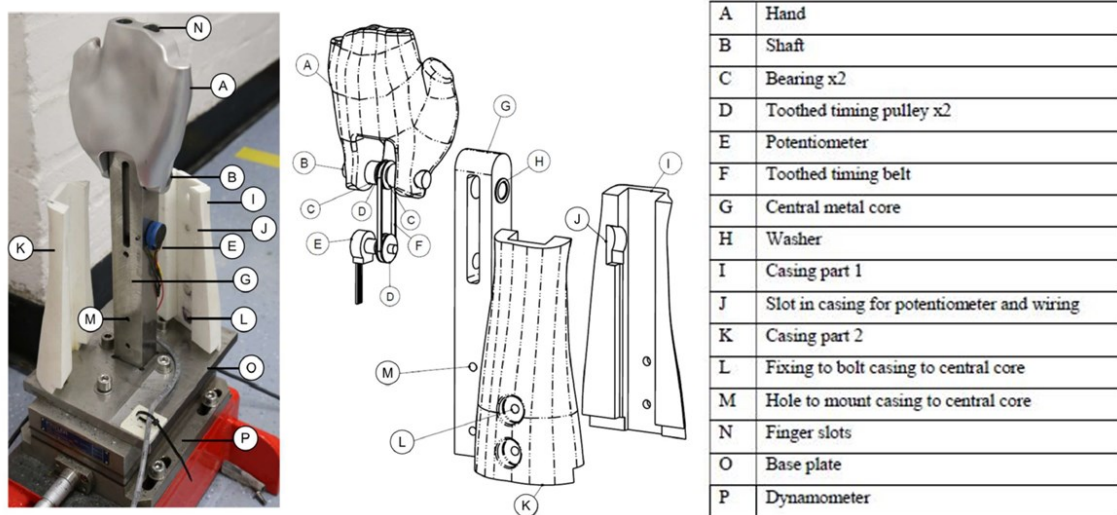
Figure 6-1 Pendulum impact surrogate from Adams (2018).

A simple way to implement a compliant impact surrogate onto the pendulum impact rig was thought to be to replace, i) the hand with a compliant one (i.e. with an outer layer of silicone), and ii) the forearm casings with versions similar to those developed for the compliant surrogate forearm in the bend test (see Chapter 4 Section 4.2). The geometry of the central core was recreated in CAD (as per the dimensions from Adams (2018)), and then aligned with that of the compliant surrogate (Chapter 4 Section 4.2) to determine the suitability of this approach. There were issues which meant this approach was unfeasible; i) the central core protruded during wrist extension, ii) the potentiometer protruded from the compliant forearm, and iii) the central core protruded at the top of the compliant forearm (Figure 6-2). For the compliant surrogate to be implemented into the pendulum impact rig, the central core was redesigned to enable it to fit with the compliant surrogate parts.
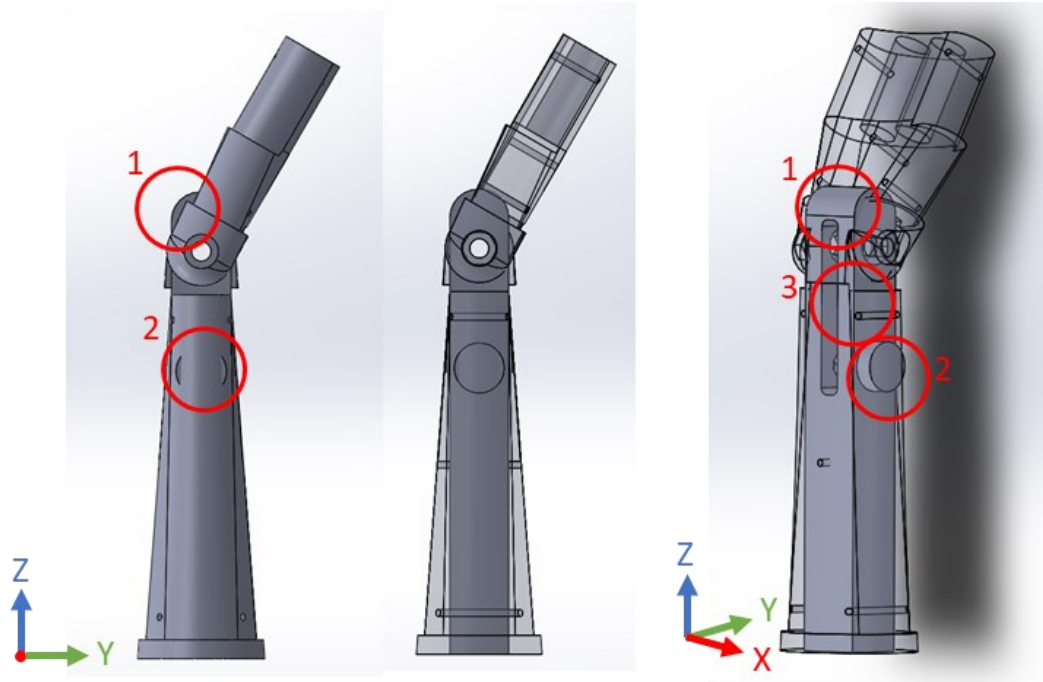
Figure 6-2 CAD model of the compliant hand and forearm overlaid onto the central core. The hand is at 30° wrist extension and the cylinder on the central core represents the potentiometer. The hand and forearm are shown as transparent on the central and right images. The red circles highlight the central core protruding through the hand during wrist extension (1), and the potentiometer (2) and central core protruding through the forearm (3).

6.3.2   Compliant Impact Surrogate Development

The central core was developed to allow a compliant hand and forearm to fit around it without it protruding. Amendments to the central core included; i) making the upper section narrower to prevent the central core and potentiometer from protruding through the forearm, and ii) making it shorter to prevent it from protruding through the hand during wrist extension. Following lessons learned from disassembling and reassembling Adams (2018) surrogate's potentiometer and toothed timing belt mechanism, the central core was developed to include a detachable side part (Figure 6-3 part 6). This side part allowed easier access to the toothed timing belt mechanism, and was attached to the central core by three bolts (M3) and two dowels (⌀ 3 mm) (Figure 6-3 part 7) to ensure alignment (Figure 6-3).

The toothed timing belt mechanism was similar to the one of Adams (2018). The hand and a timing pulley were locked to the shaft with two grub screws (⌀ 3 mm), and the second timing pulley was locked to the potentiometer shaft and connected to the wrist joint via a toothed timing belt. This arrangement meant the angular movement of the wrist joint was transferred to the potentiometer (Figure 6-3 and

Figure 6-4), allowing the hand angle to be measured. The bearings (Figure 6-3 part 2) were bush bearings manufactured from phosphor bronze (8 mm, 12 mm O.D), which are better suited for impact scenarios than roller bearings as used by Adams (2018). The pulleys (Figure 6-3 part 3) were machined from an aluminium toothed bar (22 tooth T2.5 toothed bar, Beltingonline, UK) as they were bespoke and included an extruded section to give easier access to the grub screw, which would otherwise be located under the timing belt. The potentiometer (10 kΩ rotary potentiometer, Vishay, 790-4378, RS Components, UK) (Figure 6-3 part 5) was selected as it was easier to source than the one used by Adams (2018), and was of the same specification, but smaller, allowing it to fit within the narrower forearm.
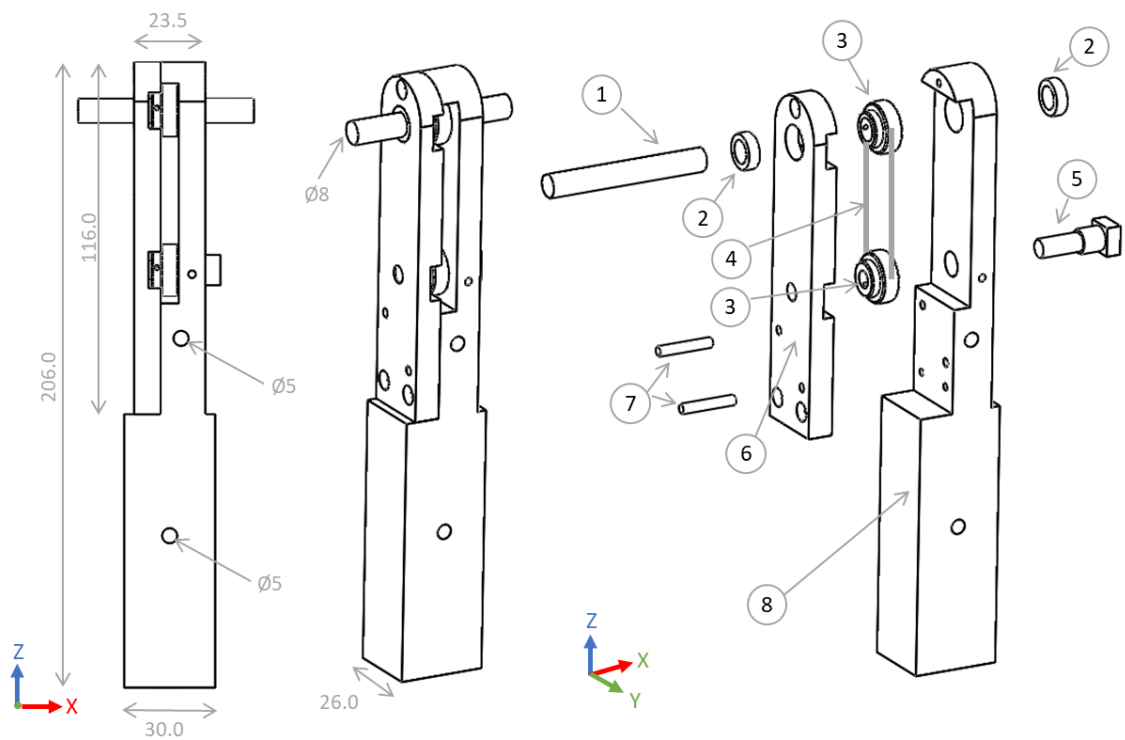
Figure 6-3 Assembly of central core. 1 - shaft, 2 - bearing, 3 - timing pulley, 4 - timing belt, 5 - potentiometer, 6 - central core side part, 7 - dowels, 8 - central core. Dimensions in mm.

The compliant impact surrogate consisted of a compliant hand and two compliant forearm casings (Figure 6-4). The forearm casings each consisted of a stiff core and silicone outer layer, which fitted around the central core. To develop the compliant surrogate parts, the compliant hand and forearm CAD models from Chapter 4 Section 4.2 were edited. The compliant hand core (Figure 6-4 part 1) was developed by; i) further reducing the palmar side of the hand to allow for a 7 mm thick outer

layer of silicone, ii) removing the finger holes, and iii) adding a 2.5 mm diameter tapped hole (Figure 6-4 part 4) to enable a grub screw to secure it to the shaft. The compliant hand, therefore, consisted of a stiff core with a 7 mm thick silicone outer layer on the palmar side and a 3 mm thick silicone outer layer elsewhere.

The compliant forearm casings (Figure 6-4 part 3) were developed by; i) applying the *Cavity* function in SolidWorks to cut away the section for the central core, ii) splitting the forearm into two to create two casings, iii) cutting a section for the potentiometer and wires, iv) cutting a section from the top of each casing where the surface was < 1 mm thick, and v) relocating the holes for the mechanical bond (Figure 6-4 part 6) to the sides. Two tapped holes ($\varnothing$ 5 mm) (Figure 6-4 part 5) were added through the forearm casings and central core, so these parts could be bolted together. The compliant forearm, therefore, consisted of two casings, each with a stiff core and a 3 mm thick silicone outer layer. Moulds, based on the external geometry of the surrogate, to create a cavity around the hand and forearm casings for the silicone to fill, were created following the same procedure as Chapter 4 Section 4.3.

The stiff hand and forearm casings were developed accordingly, with the same size and shape of the compliant surrogate, including the space occupied by the silicone (Figure 6-4c). One surrogate central core was made, and the compliant and stiff surrogate parts (hand and forearm casings) were interchangeable on this core. It was decided to make one central core with interchangeable parts, rather than two entirely separate surrogates, to make the setup more versatile, allowing future surrogate geometries to be easily applied and tested. Having just one central core also reduced manufacturing time and cost.
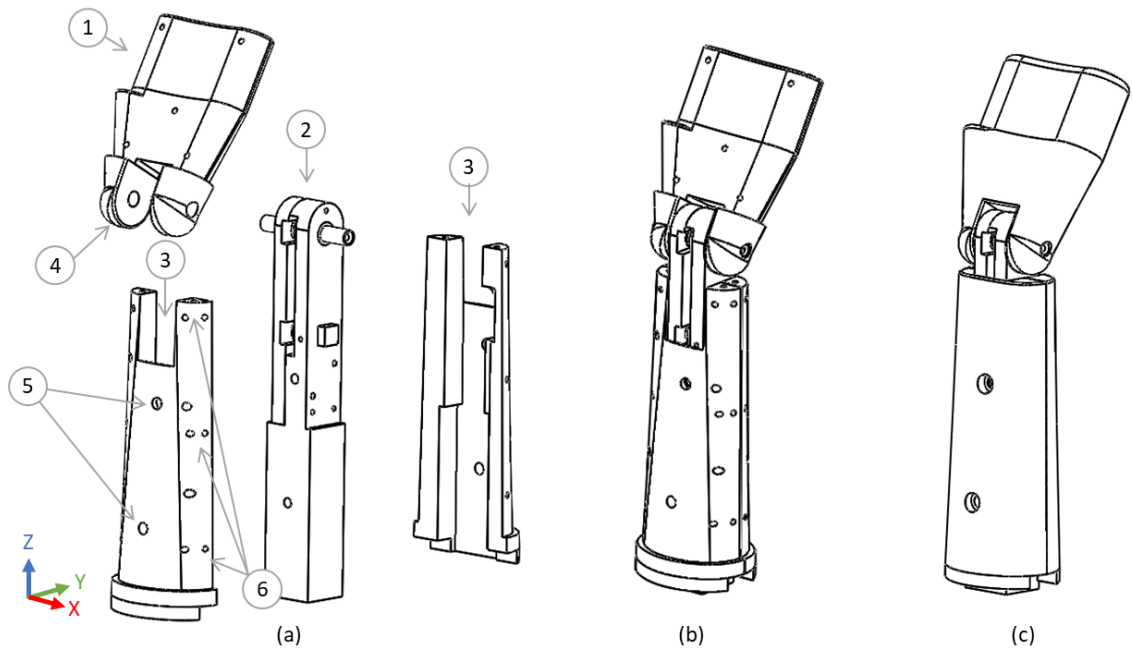
Figure 6-4 Compliant impact surrogate (a) exploded view and (b) assembly, and (c) stiff impact surrogate. 1 - hand core, 2 - central core, 3 - forearm casing, 4 - grub screw hole, 5 - holes for attachment to central core, 6 - mechanical bonds for silicone.

6.3.3 Compliant Impact Surrogate Fabrication and Assembly

The central core and central core side part were machined (SM3500 CNC milling machine, XYZ Machine Tools Ltd, Devon, UK) from mild steel. The compliant hand core and stiff hand were machined (CNC machine, VF-2, HAAS Automation Ltd, Norwich, UK) from 6061 aluminium. The forearm casings were all laser sintered (PA12, Materialise). The hand and forearm moulds were additively manufactured (PLA, Ultimaker, PrintCity, UK). The silicone was moulded around the surrogate hand core and forearm casing cores following the same procedure as Chapter 4 Section 4.3 (Appendix F Section 9.6.1) (Figure 6-5).

Components were weighed (Mettler Toledo PE11, UK) and stated in Table 6-1. The compliant parts were lighter because the silicone had a lower density than the aluminium of the hand and the plastic of the casings. The surrogate hands were ~100 g heavier than the reported mass of an actual hand by Clarys and Marfell-Jones (1986). As the surrogate forearm is fixed, the mass in comparison to an actual forearm is less important in this impact scenario.
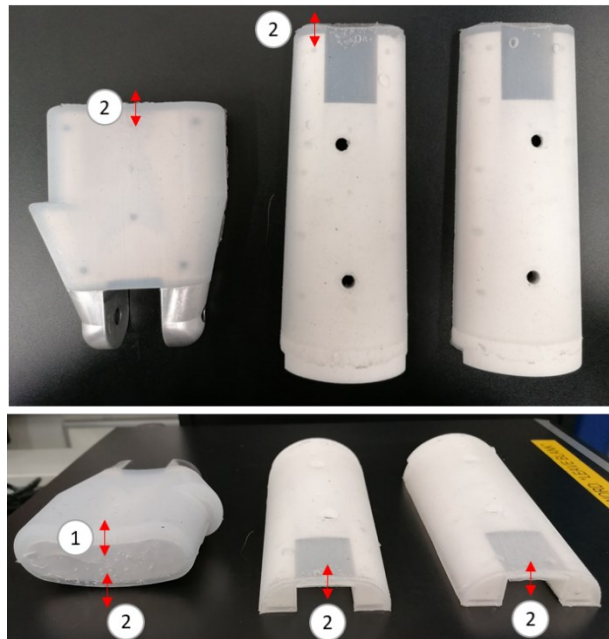
Figure 6-5 Compliant impact surrogate hand and forearm casings. 1 = 7 mm silicone thickness, 2 = 3 mm silicone thickness.

Table 6-1 Surrogate component masses.

Surrogate Part	Mass (g)		
	Compliant surrogate	Stiff surrogate	Clarys and Marfell-Jones (1986)
Hand	437.8	495.5	345.3
Forearm (excluding central core)	113.8	215.9	746.4
Total	**551.6**	**711.4**	**1,091.7**

The compliant impact surrogate was assembled by; i) bolting the central core to the base plate, ii) fitting the potentiometer, toothed timing belt mechanism and central core's side part, ii) attaching the hand and shaft, iii) fitting the grub screws to secure the hand and top timing pulley to the shaft, iv) attaching the forearm casings (Figure 6-6). A detailed step-by-step assembly procedure is provided in Appendix F Section 9.6.2. Interchanging the compliant and stiff hand and forearm casings on the central core (Figure 6-7) took ~15 minutes. A detailed step-by-step procedure of how to change between the stiff and compliant surrogate configurations is provided in Appendix F Section 9.6.3. Maximum wrist extension of the stiff surrogate was ~103°. The compliant surrogate could also reach a maximum wrist extension of ~103°, increasing to ~115° when the hand was forced backwards, causing the silicone near the joint to compress (Figure 6-7 red cross).
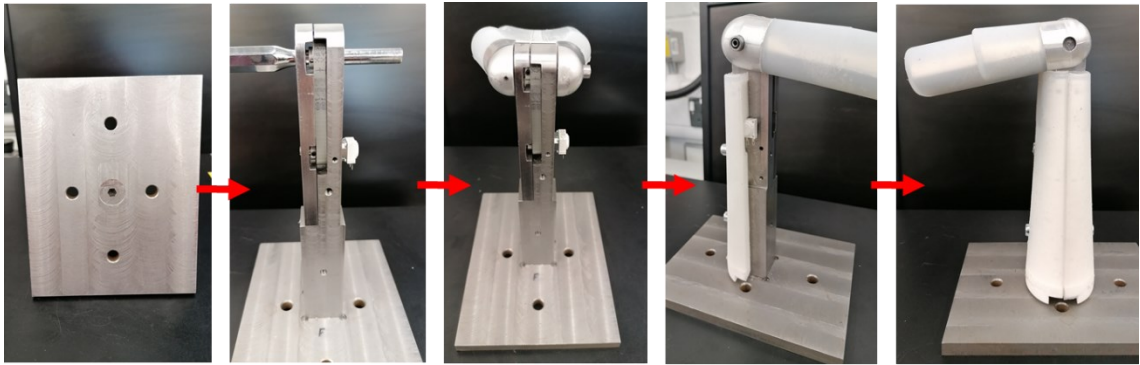
Figure 6-6 Compliant impact surrogate assembly procedure.
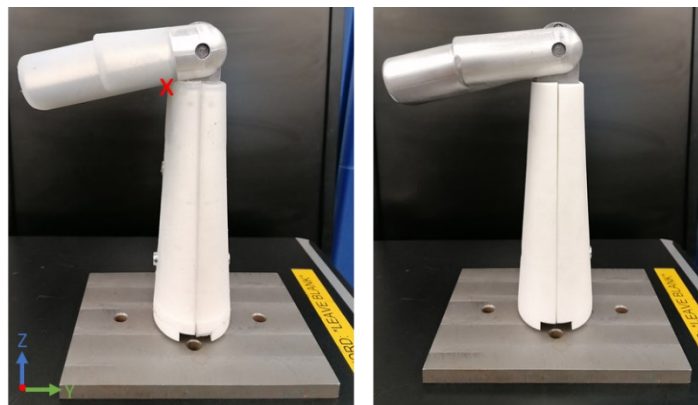
Figure 6-7 Compliant impact surrogate (left) and stiff impact surrogate (right). Red cross indicates the area of silicone which can compress when the hand is forced backwards, causing a higher maximum wrist extension to be reached than the stiff surrogate.

6.4 Rig Setup and Calibration

The pendulum impact rig was as per Chapter 2 Section 2.3.3 (Figure 2-6; Adams, 2018). The wrist surrogate base was mounted to a three-axis dynamometer (Kistler, 9257A, Switzerland) connected to a charge amplifier (FE-128-CA, Fylde, Preston, UK), which measured force. The focus of this study was on vertical force (z-axis) to compare with the cadaver fracture range from the literature, previous work by Newton-Mann (2018), and the linear impact test in BS EN ISO 20320:2020 (Chapter 5). The pendulum arm angle was measured by a potentiometer (6657, Bourns, Riverside, California, USA) and wrist angle was measured by the potentiometer mounted within the surrogate. The charge amplifier and both potentiometers were connected to a data acquisition device (DAQ) (USB-6211, National Instruments™, Austin, Texas, USA). Both potentiometers were driven by a stand-alone 8.4-volt power source (Powergorilla power bank, Powertraveller, Alton, UK).

A BNC cable with a t-splitter to a trigger button and two high-speed cameras (Chapter 3 Section 3.2.2.2; Phantom Micro R110, Vision Research UK; resolution 320 × 400 pixels, 10,000 fps) was also connected to the DAQ, with a 5 volt resistor input. The DAQ was triggered manually in the software (prior to impact), and the trigger button was used to manually trigger the cameras (upon impact). The trigger drops the signal for its channel to 0 volts, thus frame 0 of camera footage can be matched with the time step when the trigger channel reads 0 volts. The DAQ recorded all six channels at 20,000 Hz: force in x-, y- and z-axis, pendulum arm potentiometer, wrist potentiometer and the trigger.

The pendulum arm potentiometer and wrist potentiometer were calibrated using a digital inclinometer (Chapter 4 Section 4.4.2). The pendulum arm and surrogate wrist were set at various angles (measured by the inclinometer) while voltage readings were taken. Voltage and angular position were plotted and a linear trendline was fitted (Appendix G Section 9.7.1). The gradients of the trendlines fitted to both the arm potentiometer and the wrist potentiometer data differed to those reported by Adams (2018) and Newton-Mann (2019) because, i) a different potentiometer was used for the wrist surrogate and ii) the potentiometers were driven by a different power voltage. When the wrist potentiometer was driven by a higher power voltage (i.e. 24-volt as per Adams (2018) and Newton-Mann (2019)), the signal exceeded the 10-volt range of the data capture system and interfered with the signals from the other channels. Therefore, the power voltage to the potentiometer was reduced (8.4-volt) to ensure the signal stayed within the capture range.

The pendulum arm impactor consisted of a 10 mm thick aluminium plate (0.180 × 0.125 m), a 1 mm thick aluminium plate (0.180 × 0.125 m) with two neoprene blocks (0.130 × 0.125 × 0.020 m) attached (Adhesive, Evo-Stik Impact), and a 1 mm thick polypropylene sheet (0.130 × 0.125 m), as per Newton-Mann's (2019) modifications. The effective mass of the pendulum impact arm was calculated as its moment of inertia about the pivot divided by the distance from the pivot squared (Adams *et al.*, 2021). The effective mass of the pendulum arm bar in isolation was a

third of its mass (~2.5 kg), plus the mass of additional attachments (~2.0 kg) and the impactor (aluminium plate and neoprene blocks) (1.6 kg), totalling 6.1 kg.

6.5   Pilot Testing

Initial testing was undertaken to become familiar with the test rigs and to cross-check the results with previous work (Newton-Mann, 2019). The compliant surrogate was excluded from all pilot testing, to avoid potential degradation or damage of the silicone. Used short and long protectors were tested both on Adam's (2018) surrogate (scanned surrogate) and the stiff surrogate developed here. The results from this initial testing provided a comparison between the scanned (original) and the geometric (new) surrogate, and are presented in Appendix G Section 9.7.3. Peak impact forces from testing of the used protectors on the scanned surrogate were similar to values reported by Newton-Mann (2019) for new protectors, but the maximum wrist extension was higher. Peak force was higher for both protectors when tested on the geometric surrogate compared to the scanned surrogate. A higher wrist extension was observed for the scanned surrogate, which could be because it had a higher maximum possible wrist extension (~110°) than the geometric surrogate (~103°).

Adams (2018) and Newton-Mann (2019) repeatedly impacted protectors to see if they degraded. When Adams (2018) tested protectors of varying design three times each, the first impact had the lowest peak force for 72% of the tests, with the third one having the highest for 64% of the tests. Newton-Mann (2019) compared the peak force of five repeat impacts on each protector, with a 3 minute rest period between repeats. The first impact was unique (lowest peak force), repeats 2 and 3 were similar to each other, and repeats 4 and 5 gave a higher peak force than the rest. Averaging across all impact energies, a mean increase in peak force between the first and fifth impact of 42% (short protector) and 15% (long protector) was found. Based on this prior work, it was decided that three repeat impacts on each protector on each surrogate, with at least 5 minutes between repeats, would be suitable (i.e. a total of six impacts on each protector). Variability of results could also be introduced after changing the surrogate hand and forearm casings, i.e.

partially disassembling and reassembling the surrogate, as required when changing between the stiff and compliant configuration.

A pilot test was conducted to assess both protector degradation from repeated impacts, and also potential variability due to partially disassembling and reassembling the surrogate. A 5 minute rest period was introduced between impacts. This pilot test consisted of six repeat impacts on each protector, followed by a longer rest period when the surrogate was partially disassembled and reassembled, and then a further six impacts on each protector. A new protector of each of the two styles was tested on the stiff surrogate. The protectors were strapped to moderate condition (as per Chapter 4 Section 4.4.2) and the hand was set to a start angle of ~30°.

Adams (2018) and Newton Mann (2019) noted that the first impact on the neoprene impactor in isolation was unique compared to the following impacts, and therefore suggested that the neoprene should be conditioned with a single bare hand impact before testing. A bare hand impact was therefore conducted, i) before the testing (to condition the neoprene), ii) after six impacts on the short protector, iii) after six impacts on the long protector, iv) after the surrogate was part disassembled and reassembled, v) after a further six impacts on the short protector, and vi) at the end of testing (total of six bare hand impacts). Peak force for the bare hand impacts was compared to see if the neoprene was degrading.

Peak forces from Newton-Mann (2019) for impacts with a pendulum arm release (drop) height of 0.42 m lay within the range of cadaver fracture forces reported in the literature (~1,000 to 4,000 N) (Chapter 2 Table 2-2). Therefore, drop heights of 0.42 m were chosen for this PhD project to see where the peak force lies when using a compliance wrist surrogate, and whether it drops below the cadaver fracture range. A drop hight of 0.42 m lay within the range of drop heights used by Schmitt *et al.* (2012) in laboratory experiments with participants mimicking forward and backwards falls (0.125 to 0.815 m), and furthermore would translate to an impact velocity of ~2.87 m/s, which is towards the higher fall heights used in that study (range of 1 to 3 m/s). The drop height of 0.42 m gave an impact energy of 25 J. Force in the z-axis was calculated from the corresponding calibration factors from

Adams (2018), and peak force was compared between repeat impacts. Temporal force was compared between the first and last impact of the short and long protector, with peak force aligned at time (t) = 0 s for comparison.

6.5.1 Pilot Testing Results

Repeated testing tended to have a random effect on the peak impact force of the short and long protectors (Figure 6-8a). The very first impact on a protector did not give the lowest peak force, as expected (Adams, 2018; Newton-Mann, 2019). For the first impact after the longer rest period when the surrogate was partially disassembled and reassembled (first datapoint for each protector after the horizontal line on Figure 6-8a), the peak force was the lowest overall for both protectors (short protector 757 N (12%), long protector 1,000 N (11%)). The long protector had a lower coefficient of variation than the short protector for the 12 impacts (5.4 vs. 9.4%). The short protector showed a clear increase in peak force between the very first and second impact (1,332 N, 22%), and the first and second impact after the surrogate was partially disassembled and reassembled (1,616 N, 30%). Based on these findings, it was decided that with a longer rest period of 15 minutes between repeats, three repeat impacts on each protector on each surrogate (total of six impacts on each protector) would be suitable.

The shape of the temporal force trace between the first and last (12th) impact of both the short and long protector was similar (Figure 6-8b). An initial force spike of ~2,000 N (at ~0.03 s) was observed before peak force, due to the pendulum arm striking the top of the hand (as observed by Adams (2018) and Newton-Mann (2019)). In an attempt to reduce the size of this initial force spike, the start angle of the hand was increased by 5° to ~35° for future tests.

Consistency in the bare hand impacts results indicated that the neoprene impactor did not noticeably degrade during the pilot test, with a coefficient of variation of 6.0% for peak force. Bare hand impact peak forces were 10,212 ± 611 N, with a percentage difference between the first and last impact of 0.2%. Based on these results, three different neoprene impactors were used during the final testing, each changed after 24 impacts. The maximum difference in mass between the pairs of

the neoprene blocks used in the impactor was 27.6 g, which was considered to have a negligible effect on the impact energy of the pendulum.

(a)   (b)
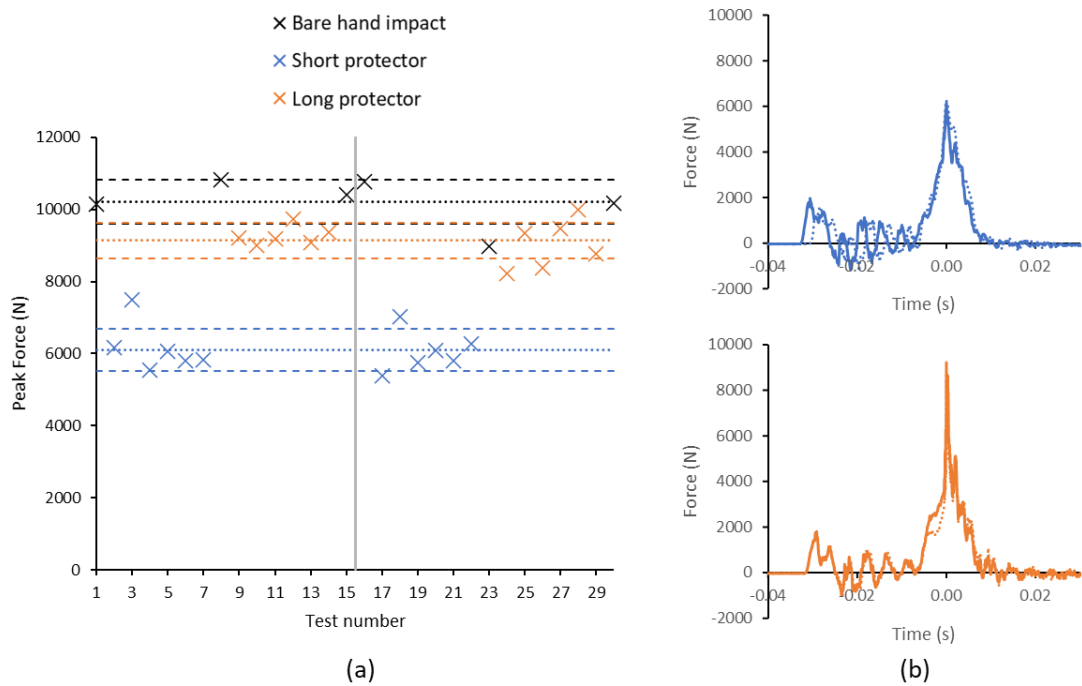
Figure 6-8 (a) Scatter graph showing the effect of 12 repeated impacts (6 impacts, followed by a further 6 impacts) on the short (blue) and long (orange) protector on the stiff surrogate at 30 J. The dotted line indicates the mean, and dashed lines indicate ± SD for each protector. The grey horizontal line indicates when the surrogate hand was partially disassembled and reassembled. (b) Temporal force comparing the first (solid line) and last impact (dotted line) of the short (top) and long (bottom) protector.

6.6   Final Testing

To monitor the silicone on the compliant surrogate, and to see if impact testing changed its condition, Shore A hardness tests (Shore durometer hardness type A-2, The Shore Instrument & MFG Co, New York, USA) on specific points on the surrogate palm and forearm casings (Figure 6-9) were taken after moulding of the silicone, before testing, and after testing. The hardness of the silicone could only be measured on flat surfaces, and thus the uppermost regions of the edges of the palm, and centrally along the forearm casings were chosen.

Figure 6-9 Location of the Shore A hardness tests on the compliant hand, conducted before and after testing. (a) top view and (b) front view.

The test conditions (surrogate-protector-strapping) were the same as for the bend test (Chapter 4 Section 4.4.2 Table 4-2). Six protectors of each style (short, long; labelled A to F) were tested, with two of each tested at each strapping condition (loose, moderate, tight (Chapter 4 Section 4.4.2)) on each surrogate (stiff, compliant) (three strapping conditions across two surrogate-protector pairings - 24 different combinations). The skid plate on the long protector was removed, as also done in Chapter 5. Three repeated tests were performed for each surrogate-protector-strapping combination (i.e. a total of 72 tests, with a 15 minute rest period between them). Protectors were defined as either: new (untested) or used (after three tests on a surrogate). Surrogates were alternated between combinations, so one new protector of each style was tested at each strapping condition on each surrogate. Protectors were re-positioned and re-strapped between tests. The testing was conducted over two days, with 36 tests on each day. The room temperature was recorded at the start and end of each test day.

Bare hand impacts were conducted during the testing to monitor the neoprene impactor, and for comparison between a protected and unprotected surrogate. The drop height of the pendulum arm was not changed between bare hand and protected impacts, therefore bare hand impacts related to a drop height of ~0.50

m. A bare hand impact was conducted, i) at the start of testing (new impactor) to condition the neoprene, ii) after eight impacts (a third of the way through testing), iii) after 16 impacts, and iii) at the end of testing (after 24 impacts) before the neoprene was changed (total of four bare hand impacts for each neoprene impactor).

Two synchronised high-speed cameras (Chapter 3 Section 3.2.2.2) were used to film the impact, one side-on to visually inspect hand angle (Figure 6-10 part 3), and the other viewing the dorsal side of the protector (Figure 6-10 part 4). The cameras filmed at a resolution of 320 × 400 pixels, a sampling rate of 10,000 fps, and were calibrated from an image taken of a measuring tape on the surrogate. Two LED lights provided lighting for the cameras (Figure 6-10 part 5). Markers were placed on the protectors (locations chosen based on observations from the bend test in Chapter 4) (Figure 6-11) to allow their movement to be measured on the video frames, by manually measuring the distance the marker moved from the frame at the start of the impact to the one at maximum wrist extension. The first test for each surrogate-protector combination (24/72 tests) was filmed, allowing the movement of new protectors to be measured during impact.
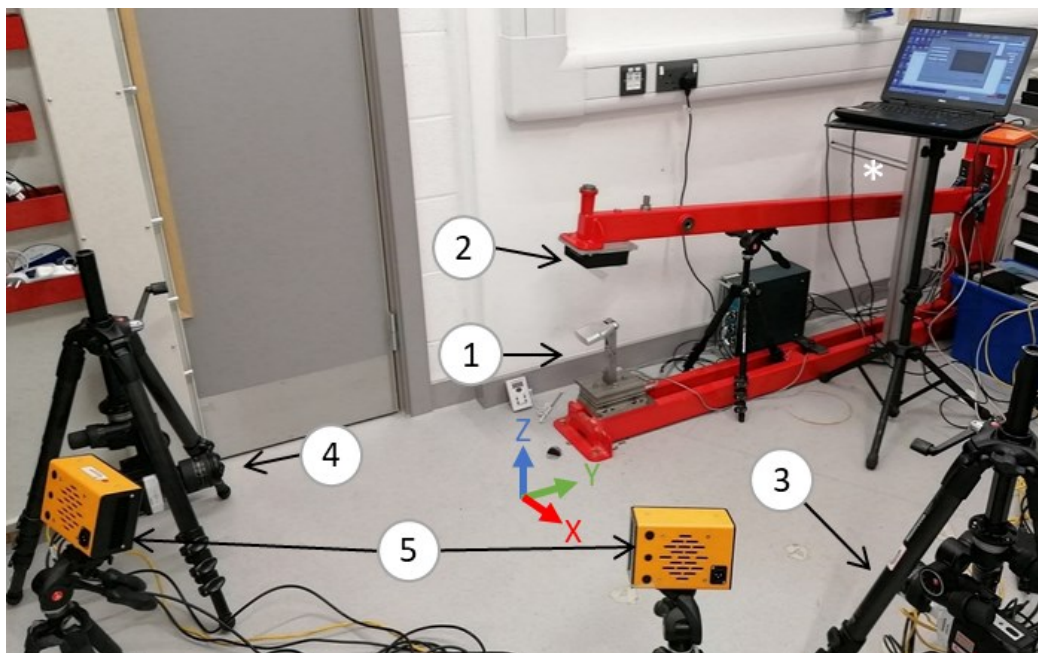
Figure 6-10 Impact test setup, showing the position of the high-speed cameras and lights. 1 - surrogate (without forearm casing), 2 - neoprene impactor, 3 - camera viewing wrist extension, 4 - camera viewing the dorsal side of the protector, 5 - LED lights. The pendulum arm was manually raised up to the horizontal bar (*) to set the release height, before being manually released.
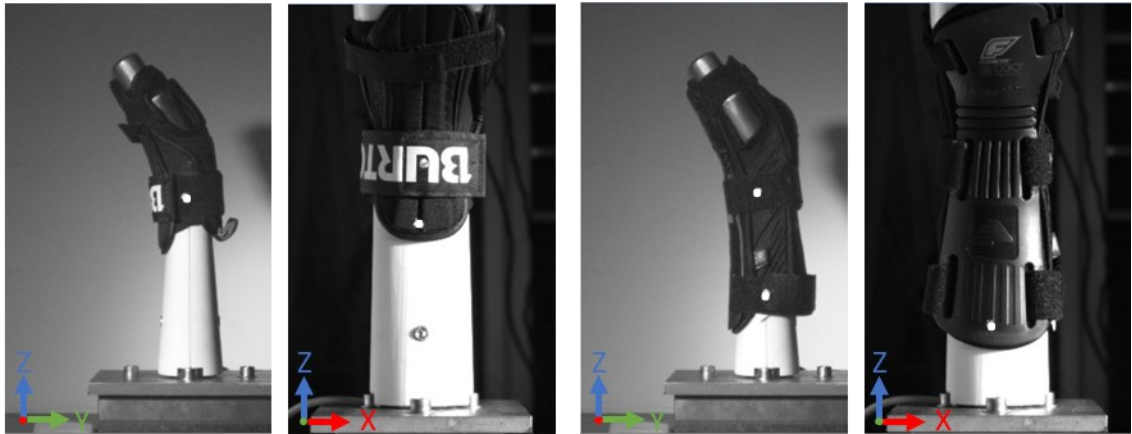
Figure 6-11 Location of markers (white dots) on protectors (left short, right long) for measurements of protector movement.

6.6.1 Data Analysis

Force in the z-axis, wrist angle and pendulum arm angle were calculated using the calibration factors. Data was low-pass filtered (4-pole phaseless Butterworth digital filter) at Channel Frequency Class 1,000 (1,650 Hz cutoff frequency) in MATLAB® (vR2017a, MathWorks®, USA), as per Newton-Mann (2019) who followed the guidelines of Weisang (2018). Examples of data with various levels of filtering are displayed in Appendix G Section 9.7.4. Temporal force, temporal wrist angle and force vs. wrist angle were plotted, with peak force aligned at time (t) = 0 s for comparison between surrogate-protector-strapping conditions. Key points in the traces for the first impact at moderate strapping condition for each surrogate-protector condition were matched to images from the cameras to help communicate and explain the results. Peak force was compared for all conditions. Angular velocity of the pendulum arm was calculated from the temporal pendulum arm angle to check consistency between tests (due to it being manually released, Figure 6-10).

GLM univariate analysis was performed as per Chapter 4 Section 4.5.2. Peak force was set as the dependent variable and surrogate (stiff, compliant), protector style (short, long), strapping condition (loose, moderate, tight) and protector condition (new, used) as the independent variables. To determine the effect of the independent variable on the surrogates individually, further GLM univariate

149

analysis was performed with the surrogates split up (removing surrogate as an
independent variable). Box plots were used to display the distribution of the data.

6.6.2   Results

The room temperature recorded at the start and end of each test day was: test day
1 - 21.6℃ (start) and 21.5℃ (end), test day 2 - 21.5℃ (start) and 21.8℃ (end),
equating to a range in measured room temperature of <1℃. As such, changes in
temperature during testing were not considered to have influenced the results
presented here.

The Shore A hardness of the silicone on the compliant surrogate across the eight
points measured was 26 ± 3.2 (mean ± SD). The silicone was softest straight after
moulding (Shore A hardness 22 ± 1.6), and hardened in the two months before
testing began (Shore A hardness 28 ± 2.2). There was no significant difference in the
Shore A hardness measurements taken before and after testing (details of statistical
test performed are provided in Appendix D Section 9.4.2). This finding indicates that
the hardness of the silicone did not change during the impact testing to a sufficient
extent to influence the results presented here. A significant difference in Shore A
hardness was, however, found between the measurements taken after moulding
and before testing, and after moulding and after testing. It is therefore
recommended that after the silicone is moulded, the surrogate should be left for a
specific time period before testing, to allow time for the silicone to naturally
harden.

The angular velocity of the pendulum arm at ~0.01 s prior to impact was 1.80 ± 0.06
rad.s^{-1} (CoV of 3%), suggesting that it was consistent between tests. The measured
angular velocity was ~6.5% lower than the theoretical angular velocity (1.926 rad.s^{-1}) calculated from the pendulum arm length and drop height.

The wrist potentiometer was found to be non-linear across its full mechanical
range, and furthermore, the calibration was non-linear across the wrist angle range
used in the test (Appendix G Section 9.7.1). Visual inspection of the videos and wrist
angle data indicated inconsistencies with the wrist potentiometer for the stiff
surrogate configuration. So wrist angles were manually measured on some of the

videos for both surrogate configurations, and compared against those from the potentiometer (Figure 6-12). Confidence in the manual measurements of the wrist angles was increased by taking many data points on multiple videos. For the compliant surrogate configuration, the angles measured on the video frames were within ±1° of the corresponding potentiometer value, and thus the values from the potentiometer were used. For the stiff surrogate configuration, a larger difference was found between the potentiometer and video measurements. The maximum wrist angle measured in the video footage was ~5 to 6° above the corresponding potentiometer value, indicating an error of ~6° at maximum wrist extension (103°). Calibration parameters from the video measurements were, therefore, applied to the output voltage from the potentiometer, rather than those obtained from the inclinometer, for the stiff surrogate configuration. A comparison between calibration trendlines for the different methods is displayed in Appendix G Section 9.7.2.

(a)   (b)   (c)   (d)
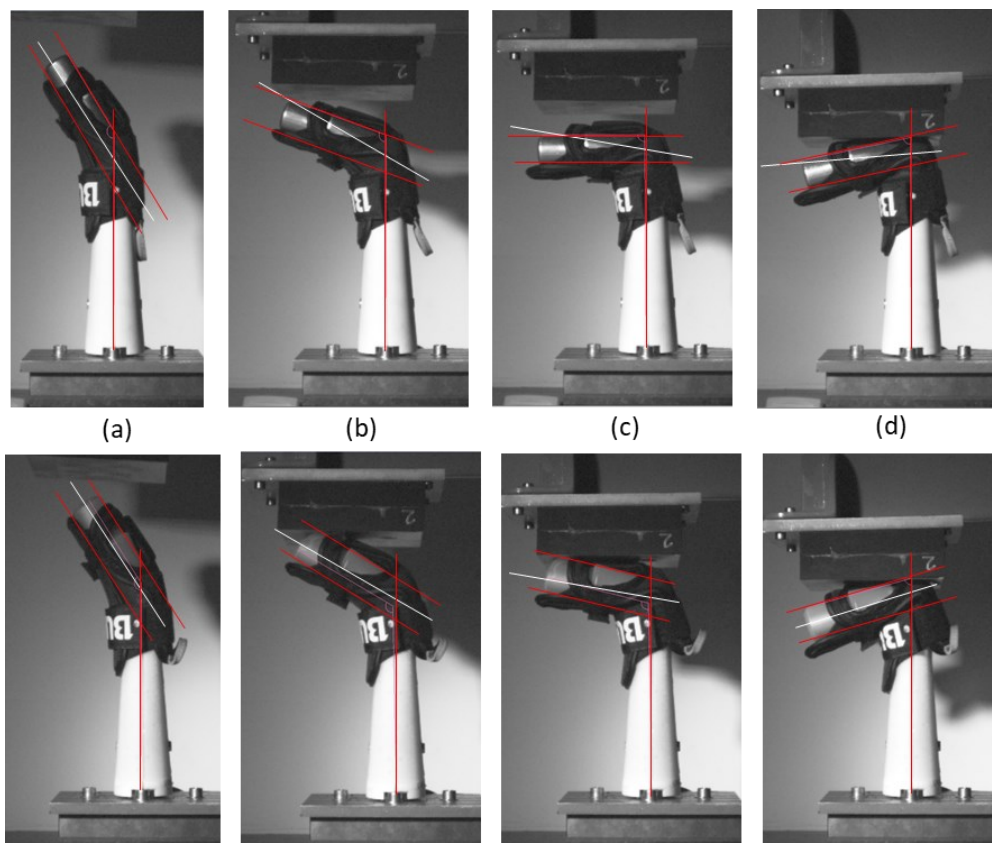
Figure 6-12 Example wrist angle measurements from the video frames of the short protector on the stiff (top) and compliant (bottom) surrogate at (a) start angle (~35°), (b) 60°, (c) 80° and (d) maximum wrist angle (stiff surrogate 97°, compliant surrogate 108°) according to the potentiometer. The red lines indicate the angle measured on the image, and the white line indicates the angle recorded by the potentiometer.

6.6.2.1.   Between bare hand conditions

Example temporal force, wrist angle and pendulum angle traces for a bare hand
condition of the stiff and compliant surrogate are displayed in Figure 6-13. The peak
force of the compliant surrogate tended to be slightly higher than for the stiff
surrogate (stiff 9,678 ± 72 N, compliant 10,051 ± 193 N). The stiff surrogate's wrist
stayed at ~101° throughout the impact, whereas as the pendulum arm struck the
compliant surrogate, the wrist extended to 115°, entering the range where the
silicone surrounding the joint was compressed (see Figure 6-7). The impact duration
for the compliant surrogate was longer than for the stiff surrogate (difference of
~0.0016 s). The bare hand impacts on the stiff and compliant surrogate produced a
loading curve with a similar slope to those of Newton-Mann (2018) for 0.56 m drop
heights (Appendix G Section 9.7.5). As the pendulum arm was not modified since
the work of Newton-Mann (2018), it was expected that bare hand impacts here
would produce a similar loading curve.
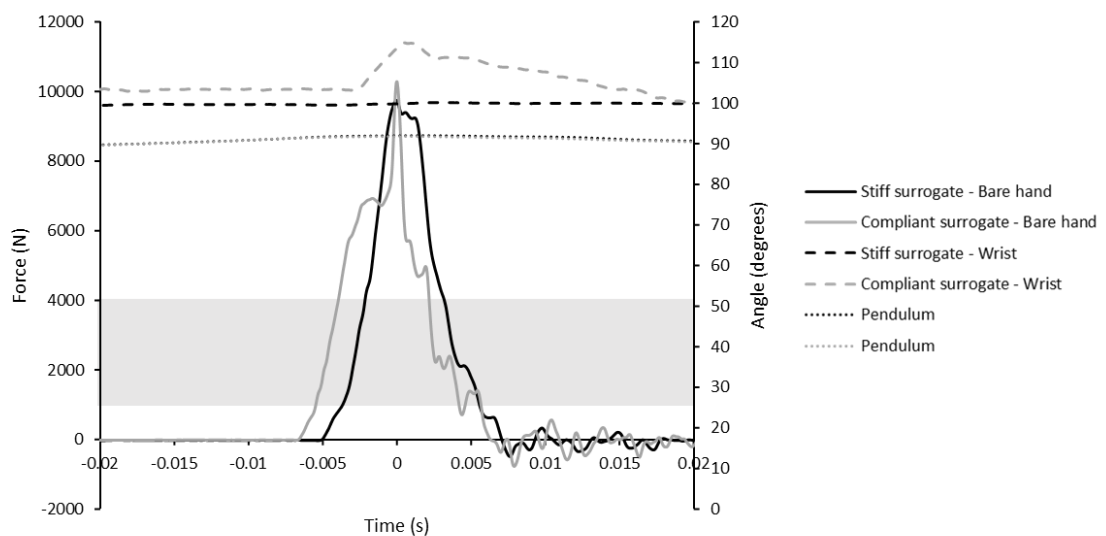
*Figure 6-13 Temporal force, temporal wrist angle and temporal pendulum angle trace for bare hand impacts on
the stiff and compliant surrogate. The horizontal grey box highlights the cadaver fracture range (Table 2-2).*

6.6.2.2.   Between surrogates

The temporal force, temporal wrist angle and force vs. wrist angle traces for the
short protector on the stiff and compliant surrogate, and the long protector on the
stiff and compliant surrogate are displayed in Figure 6-14 and Figure 6-15,
respectively. The cadaver fracture range (~1,000 to 4,000 N) (Table 2-2) and the
maximum non-injurious wrist extension (85°) (Table 2-1) are included in these plots

for comparison with the data. When the pendulum arm first struck both surrogates (point 1), there was an initial spike in force (point 2). Following this initial spike, there was a period of low force due to the wrist extending (point 3). During this period of low force, the pendulum arm broke contact with the stiff surrogate, whereas it remained in contact with the compliant surrogate, which reduced vibrations and kept the force above 0 N. For both surrogates, the force began to increase (point 4) as the protector splints and/or palmar pad engaged until peak force and maximum wrist angle were reached (point 5). After peak force, the pendulum arm started to rebound and the force returned towards 0 N as the hand began to return towards its initial position (point 6). Previous work by Adams (2018) and Newton-Mann (2019) showed similar traces for temporal force, temporal wrist angle and force vs. wrist angle, and similar images from video footage.
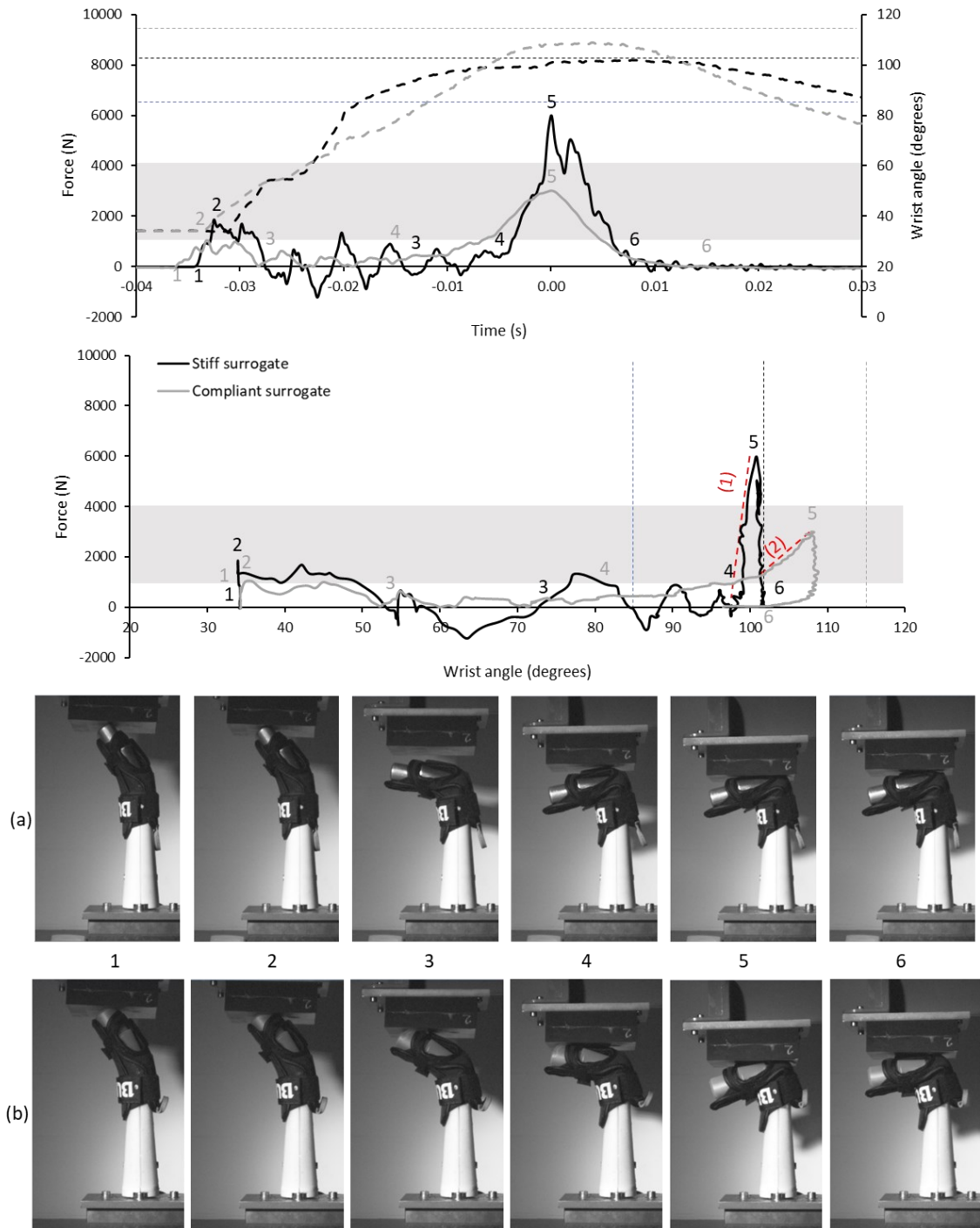
Figure 6-14 Temporal force and temporal wrist angle trace (top) and force vs. wrist angle (bottom) of the short
protector strapped at moderate condition on the stiff surrogate and compliant surrogate, alongside a sequence
of high-speed images which showcase the key points (a – stiff surrogate, b – compliant surrogate). The dashed
curves indicate the temporal wrist angle. The horizontal grey box highlights the cadaver fracture range (Table
2-2), the vertical blue dashed line indicates the reported non-injurious maximum wrist extension (Table 2-1), the
vertical black and grey dashed lines indicate the maximum wrist angle of the surrogates, and the red dashed
trend lines indicate the gradient, where (1) is 2,347 N/° and (2) is 249 N/°.
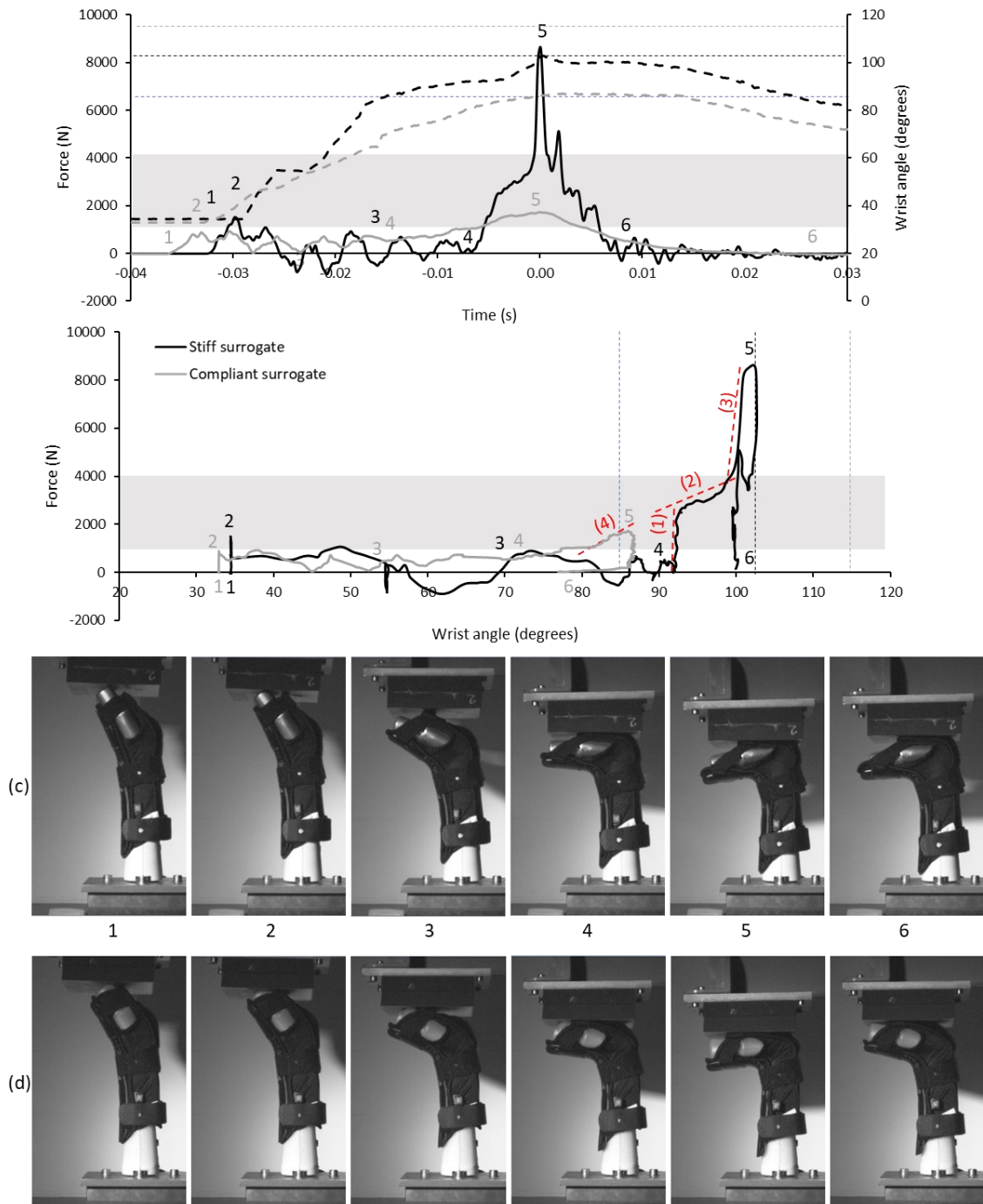
Figure 6-15 Temporal force and temporal wrist angle (top) and force vs. wrist angle (bottom) of the long protector strapped at moderate condition on the stiff surrogate and compliant surrogate, alongside a sequence of high-speed images which showcase the key points (c – stiff surrogate, d – compliant surrogate). The dashed curves indicate the temporal wrist angle. The grey box highlights the cadaver fracture range (Table 2-2), the blue dashed line indicates reported maximum non-injurious wrist extension (Table 2-1), the black and grey dashed lines indicate the maximum wrist angle of the surrogates, and the red dashed lines indicate the gradient, where (1) is 3,519 N/°, (2) is 154 N/°, (3) is 1,985 N/° and (4) 160 N/°.

For the short protector on the compliant surrogate (Figure 6-14), a relatively low force (~1,000 N) was required to displace the wrist to ~100°, following which a slightly sharper increase in force with m = 249 N/° was required to reach a

maximum wrist angle of ~108°, corresponding to peak force. In contrast, when on the stiff surrogate, a sharp increase in force with m = 2,347 N/° was required to displace the wrist from ~97 to 103°, corresponding to peak force and maximum wrist extension. For the long protector on the compliant surrogate (Figure 6-15), a relatively low force (~1,500 N) with m = 160 N/° was required to displace the wrist from ~80 to 85°, corresponding to peak force and maximum wrist extension. In contrast, when on the stiff surrogate, a sharp increase in force (to ~3,000 N) with m = 3,519 N/° was required to displace the wrist from ~92 to 94°, followed by a period of little change in force (~1,800 N) with m = 154 N/° between ~94 to 100°, after which a sharp increase in force with m = 1,985 N/° was required to reach a wrist angle of ~103° (maximum wrist extension), resulting in a three-part gradient to peak force.

The compliant surrogate reached a maximum wrist angle of 108° for the short protector (Figure 6-14) and 86° for the long protector (Figure 6-15). These results indicate that when tested on the compliant surrogate, it was only with the short protector that the wrist angle entered into the range where the silicone surrounding the joint was compressed by the hand as it was forced backwards, i.e. > 103° (see Figure 6-7). Whereas when on the stiff surrogate, both protectors reached the maximum possible wrist angle (103°), which explains the rapid increase in impact force observed in Figure 6-14 and Figure 6-15. The force up to 103° for the short protector on the compliant surrogate was 1,690 N, which increased to 2,998 N as the wrist extended to 108°.

Observation from video showed that the surrogate forearm deflected in the y-axis direction (Figure 6-16) after it was struck by the pendulum arm (between point 2 and 4, Figure 6-14 and Figure 6-15). Such forearm deflection was also observed by Adams (2018) and Newton-Mann (2019) when they tested with the scanned surrogate. To measure the angular displacement of the forearm, a point on it (on the line where the forearm casings joined) was measured in the video footage of the short protector between its initial position and the frame of maximum (horizontal) displacement using Phantom® CineViewer (Figure 6-16). Arm movement in the negative y-axis direction occurred after the initial contact of the

pendulum arm on both surrogates (Figure 6-14 and Figure 6-15 point 2). Movement
in the positive y-axis direction also occurred on the stiff surrogate as the wrist
extended and the pendulum arm broke contact (Figure 6-14 point 3). A forearm
angular displacement of 1.62° for the stiff surrogate and 1.06° for the compliant
surrogate was measured in the negative y-axis, and a forearm angular displacement
of 1.14° for the stiff surrogate was measured in the positive y-axis (no positive
movement for the compliant surrogate). Both the stiff and compliant forearm
returned to vertical as the pendulum arm connected with the protector (Figure 6-14
and Figure 6-15 point 4). Newton-Mann (2018) reported a deflection at the point of
axis rotation of the wrist (8.2 mm (+Y) and 5.8 mm (-Y)), which equates to an
angular deflection of 2.50° (+Y) and 1.77° (-Y) for the same impact conditions. A
measurement was not taken for the long protector as it obscured much of the
forearm.
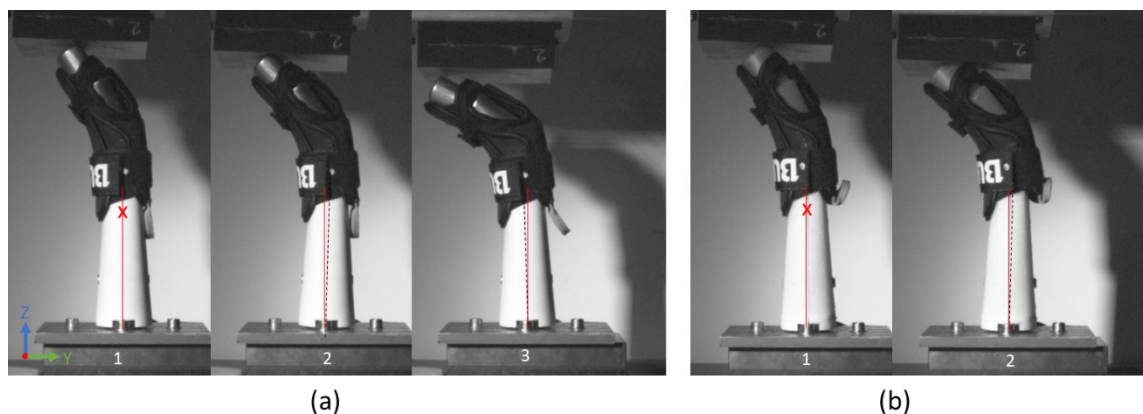
*Figure 6-16 Example of y-axis displacement for the short protector on the stiff (a) and compliant (b) surrogate at
(1) prior to impact, (2) maximum -y motion, (3) maximum +y motion. The red cross indicates the point that was
tracked.*

For both protectors, when tested (at moderate strapping condition) on the
compliant surrogate, a lower peak force was observed than when tested on the stiff
surrogate (short protector 2,999 vs. 5,982 N, long protector 1,733 vs. 8,645 N). The
time to peak force was longer when the protectors were impacted on the compliant
surrogate compared to the stiff surrogate (difference of 0.002 s for short protector
and 0.004 s for long protector when strapped at moderate condition). The wrist
angular velocity between the start angle (35°) and 85° (relating to the reported
maximum non-injurious wrist extension (Table 2-1)) was higher for the stiff

surrogate than for the compliant surrogate for both protectors (4,048 vs. 2,320 °/s short, 3,782 vs 1,661 °/s long).

The initial spike in force (Figure 6-14 and Figure 6-15 point 2), due to the pendulum arm striking the uppermost part the hand, was lower for the compliant surrogate than for its stiff counterpart (short protector ~975 vs. 1,854 N, long protector ~800 vs. 1,454 N). For both protectors when on the compliant surrogate, this initial force spike was below the cadaver fracture range, although the peak force (Figure 6-14 and Figure 6-15 point 5) did lay within that range. When on the stiff surrogate, both protectors' initial force spike lay within the cadaver fracture range, whereas the peak force exceeded that range. Both surrogates exceeded the reported maximum non-injurious wrist extension angle (85°) during testing of both protectors. Reported non-injurious maximum wrist extension (85°) occurred after point 3 (stiff surrogate) and after point 4 (compliant surrogate) when testing the short protector (Figure 6-14), whereas it occurred after point 4 when testing the long protector on both surrogates (Figure 6-15).

In all cases (72/72, 100%), the compliant surrogate gave lower peak force values than the stiff surrogate (Figure 6-17). Peak force tended to fluctuate with test repeats, and the first impact of a new protector had the lowest peak force in only 3/12 (25%) cases, which was similar to the results from the pilot testing (Section 6.5.1). The mean peak force of the long protector was higher than for the short protector when on the stiff surrogate (8,365 ± 365 vs. 6,816 ± 1,085 N), whereas the opposite was the case when on the compliant surrogate (3,095 ± 316 vs. 2,661 ± 574 N).
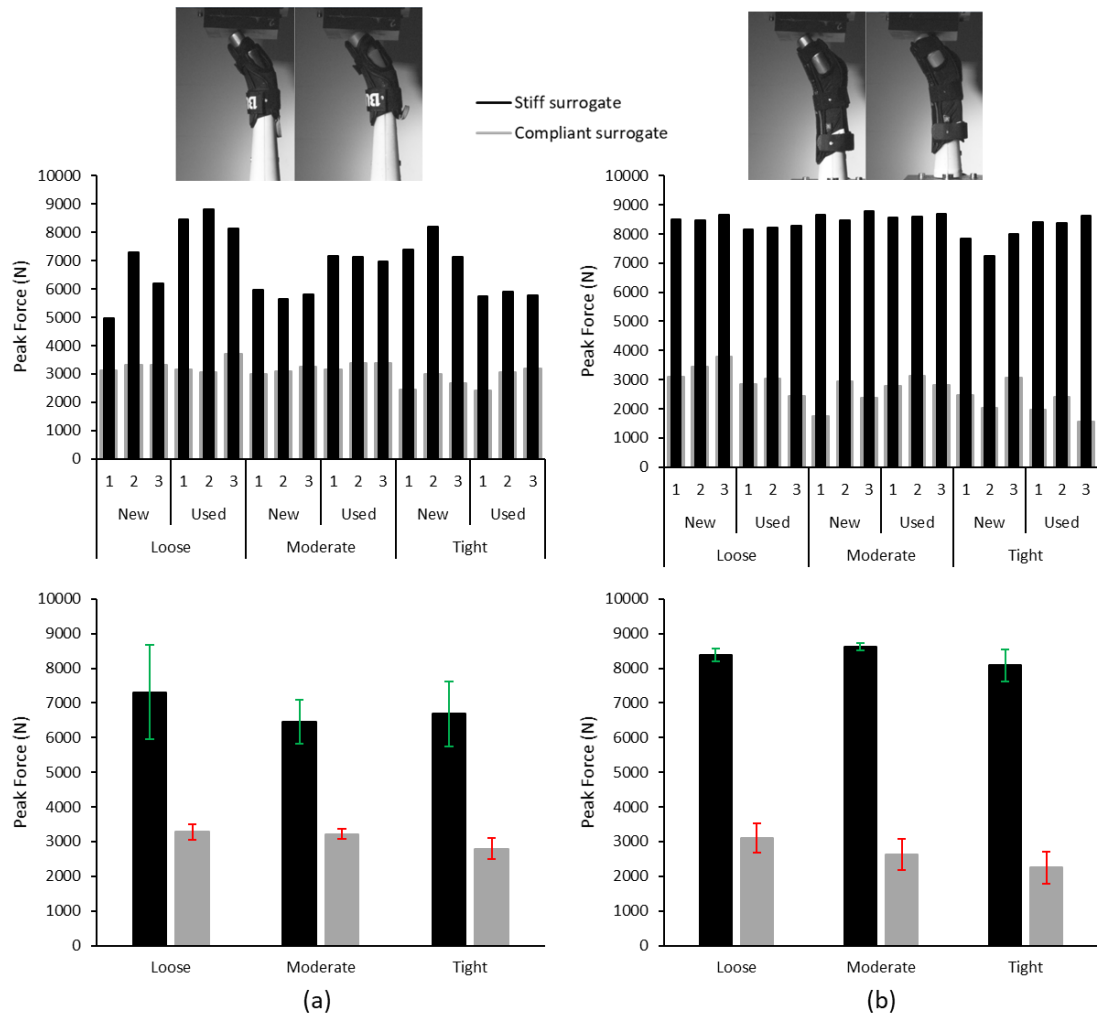
Figure 6-17 Peak force for all tests (top bar charts) of (a) the short and (b) the long protectors. The x-axis indicates the test repeat, protector condition, and strapping condition. The bottom bar charts show the mean peak force at each strapping condition (error bars showing mean ± SD).

6.6.2.3. Between strapping conditions

The results were dependent on the protector strapping condition (tightness) (Figure 6-18 and Figure 6-19). When strapped at the tight condition, both protectors on each surrogate tended to have a higher force for a set wrist angle once the pendulum arm connected with the protector (defined by point 4 on Figure 6-14 and Figure 6-15), compared to the loose and moderate conditions. When on the compliant surrogate, as strapping tightness increased, the maximum wrist angle tended to decrease for both protectors, and furthermore, mean peak force decreased (short protector - loose 3,280 ± 218 N, moderate 3,215 ± 140 N, tight 2,791 ± 304 N, long protector - loose 3,108 ± 429 N, moderate 2,628 ± 459 N, tight 2,247 ± 472 N). The gradients of the force vs. wrist angle traces were similar

between strapping tightnesses for both protectors on the compliant surrogate, although they diverged as they reached peak force and maximum wrist angle. In contrast, when on the stiff surrogate, the maximum possible wrist angle (103°) was reached for both protectors at all strapping conditions, and no clear trend of mean peak force was observed (short protector - loose 7,311 ± 1,358 N, moderate 6448 ± 639 N, tight 6,689 ± 941 N, long protector - loose 8,386 ± 178 N, moderate 8,628 ± 103 N, tight 8,082 ± 457 N). Strapping conditions did not affect where the initial force (defined by point 2 on Figure 6-14 and Figure 6-15) and the peak force lay relative to the cadaver fracture range (either within or above), nor when the surrogates exceeded the reported maximum non-injurious wrist extension angle.
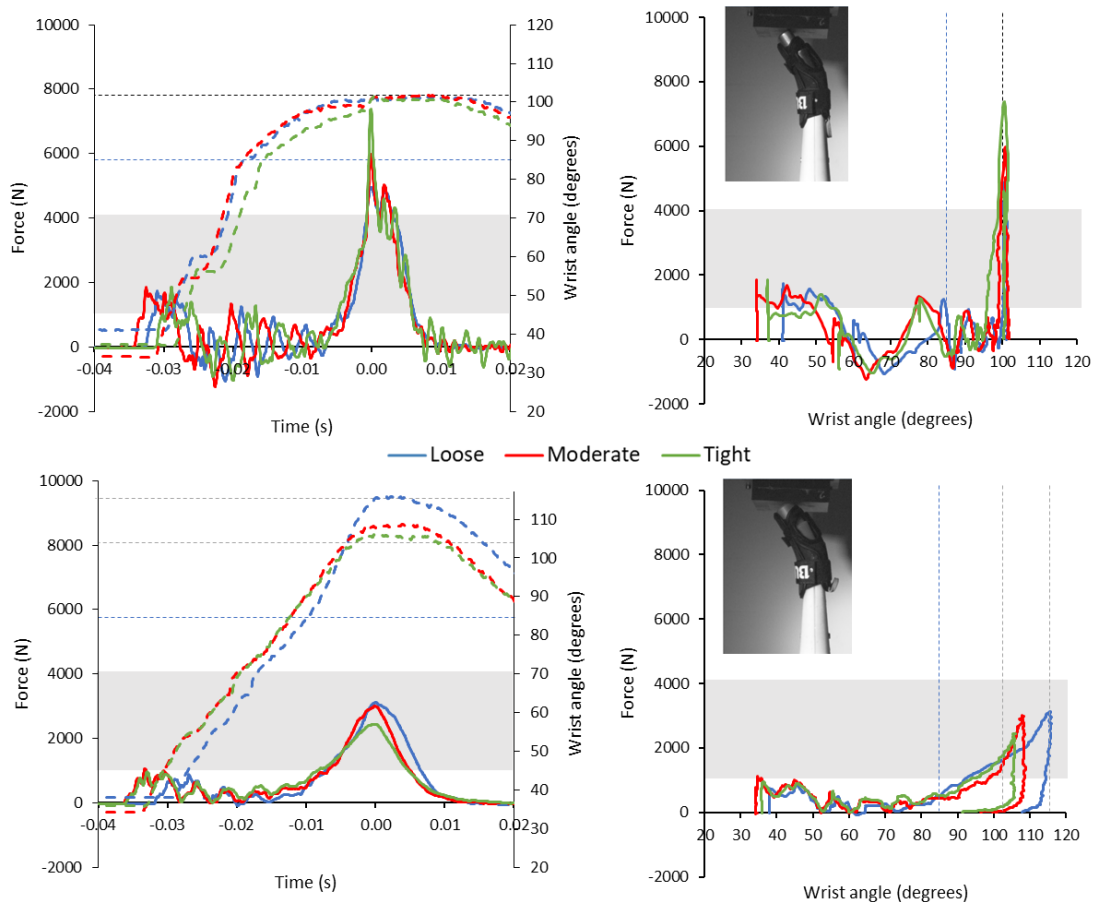
Figure 6-18 Temporal force and temporal wrist angle (left) and force vs. wrist angle (right) of the short protector between strapping conditions on the stiff surrogate (top) and compliant surrogate (bottom). The dashed curves indicate the temporal wrist angle. The grey box highlights the cadaver fracture range (Table 2-2), the blue dashed line indicates reported maximum non-injurious wrist extension (Table 2-1), and the black and grey dashed lines indicate the maximum wrist angle of the surrogates.
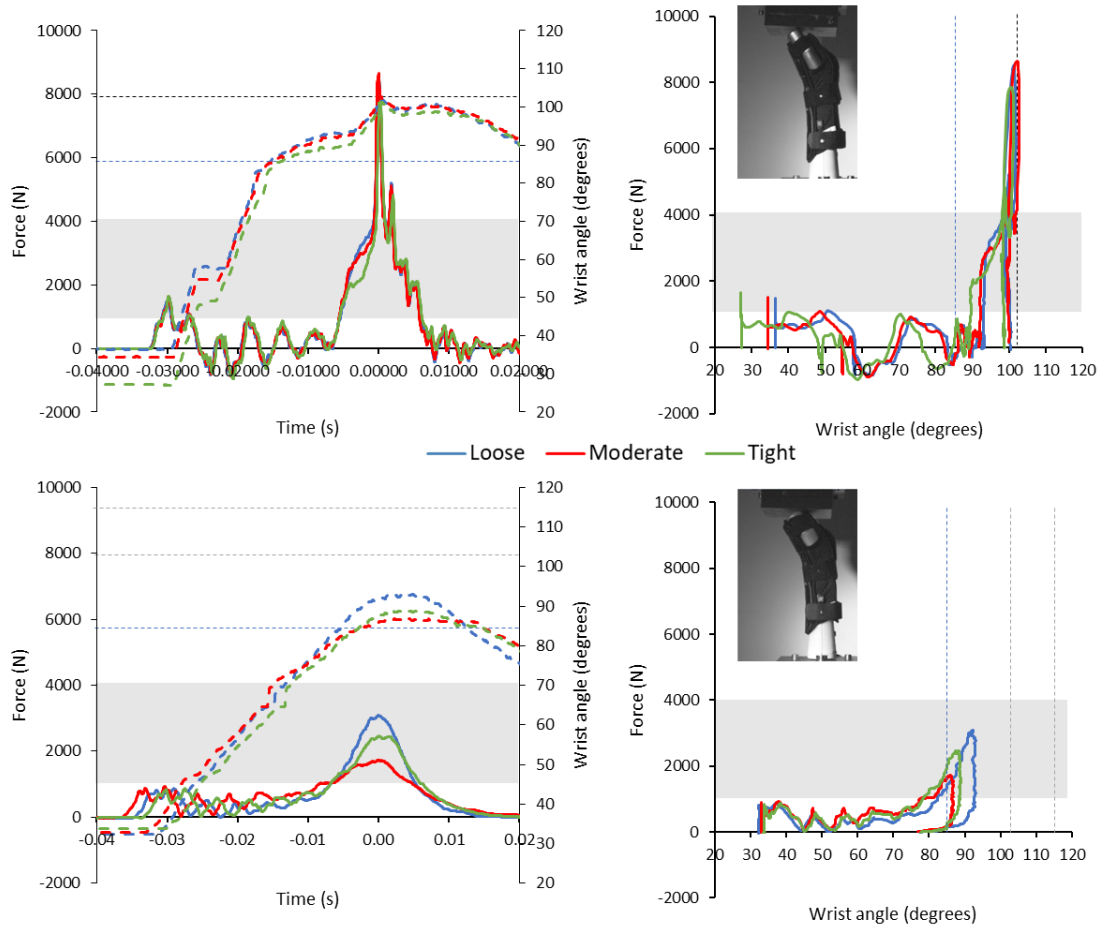
*Figure 6-19 Temporal force and temporal wrist angle (left) and force vs. wrist angle (right) of the long protector
between strapping conditions on the stiff surrogate (top) and compliant surrogate (bottom). The dashed curves
indicate the temporal wrist angle. The grey box highlights the cadaver fracture range (Table 2-2), the blue
dashed line indicates reported maximum non-injurious wrist extension (Table 2-1), and the black and grey
dashed lines indicate the maximum wrist angle of the surrogates.*

6.6.2.4. Protector slippage

Protector slippage locations were observed and then measured in the video footage
at, i) the bottom of the dorsal side of both protectors (towards the base of the
surrogate forearm), ii) the short protector strap, and iii) both straps of the long
protector (Figure 6-20). When comparing protector slippage between the initial
position and the one coinciding with the maximum wrist angle (stiff surrogate at
103° and compliant surrogate at 90° to 115°), the long protector slipped further on
the stiff surrogate than when on the compliant surrogate at all locations, whereas it
slipped further on the compliant surrogate than when on the stiff surrogate at all
locations when comparing protector slippage at equivalent wrist angles between
surrogate (long protector at 90°). In contrast, the short protectors' strap slipped
further on the stiff surrogate than when on the compliant surrogate, and the

bottom of the dorsal side slipped further on the compliant surrogate than on the stiff surrogate, when comparing slippage at both maximum angle and at equivalent angles (short protector at 103°). Protectors slipped less at the lower equivalent angle than at the maximum angle. Protectors tended to slip furthest when strapped at the loose condition, and the least when strapped at the tight condition. Significant differences of protector slippage between surrogates occurred on the short protector at the bottom of the dorsal side (at maximum wrist angle and at equivalent wrist angles) and at the strap (only when comparing equivalent wrist angles), and the effect size varied from small to medium (Table 6-2).

(a)   (b)   (c)   (d)
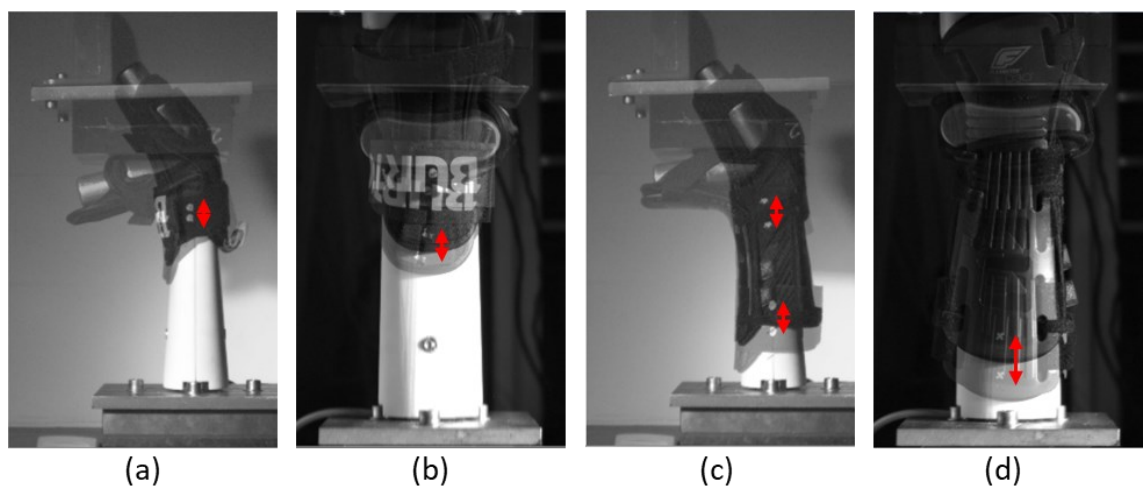
Figure 6-20 Overlaid video stills at the start and at maximum wrist extension, showing the protector movement on the stiff surrogate: (a) the short protector strap, (b) the bottom of the dorsal side of the short protector, (c) the top and bottom strap of the long protector and (d) the bottom of the dorsal side of the long protector.

Table 6-2 Protector slippage measurements (in mm) at maximum wrist angle (103° on the stiff surrogate and 90° to 115° on the compliant surrogate) and at an equivalent wrist angle, alongside statistical test results and effect sizes between surrogates for the protector slippage measured (* indicates a significant difference). Refer to Appendix D Section 9.4.3 for details on the statistical tests performed.

	Protector slippage location	Slippage measurement (mm)		p-value	Effect size
		Stiff surrogate	Compliant surrogate		
				Compliant-Stiff	
Short	Strap	6.2 ± 1.4	4.8 ± 0.9	0.314	0.244 (small)
			2.7 ± 0.9 (at 103°)	0.044*	-0.398 (small)
	Bottom	13.5 ±1.1	19.3 ± 1.8	0.018*	0.570 (medium)
			17.9 ± 1.0 (at 103°)	0.015*	0.175 (small)
Long	Bottom strap	21.5 ±1.4	18.3 ± 4.4	0.657	0.271 (small)
		13.9 ± 1.6 (at 90°)		0.102	0.231 (small)
	Top strap	19.8 ± 0.8	18.6 ± 3.5	0.382	0.728 (medium)
		13.0 ± 1.4 (at 90°)		0.265	0.902 (large)
	Bottom	21.8 ± 1.2	20.4 ± 3.3	0.611	0.876 (large)
		15.1 ± 1.5 (at 90°)		0.105	0.996 (large)

6.6.2.5.   Between protectors

Fitting a protector to the stiff surrogate reduced the peak force by ~39% (short protector) and ~11% (long protector) compared to the bare hand condition (Figure 6-21). Furthermore, fitting a protector to the compliant surrogate reduced the peak force by ~71% (short protector) and ~83% (long protector) compared to the bare hand condition. The short protector reached a higher wrist extension angle than the long protector when on the compliant surrogate, whereas both protectors reached the maximum possible angle (103°) when on the stiff surrogate. When on the compliant surrogate, both protectors had a similar force-angle gradient to peak force (249 vs 160 N/°), whereas on the stiff surrogate, the short protector had a single steep gradient to peak force (2,347 N/°), in contrast to the long protector, which had a three-part gradient to peak force (3,519, 154, 1,985 N/°), as observed in Figure 6-15. Both protectors exceeded the cadaver fracture range when on the stiff surrogate. When on the compliant surrogate, the short protector lay in the upper half of the cadaver fracture range (above 3,000 N), whilst the long protector lay in the lower half of that range (below 3,000 N). Both the stiff and compliant surrogates reached the reported maximum wrist angle (85°) earlier when fitted with the short protector compared to the long protector.
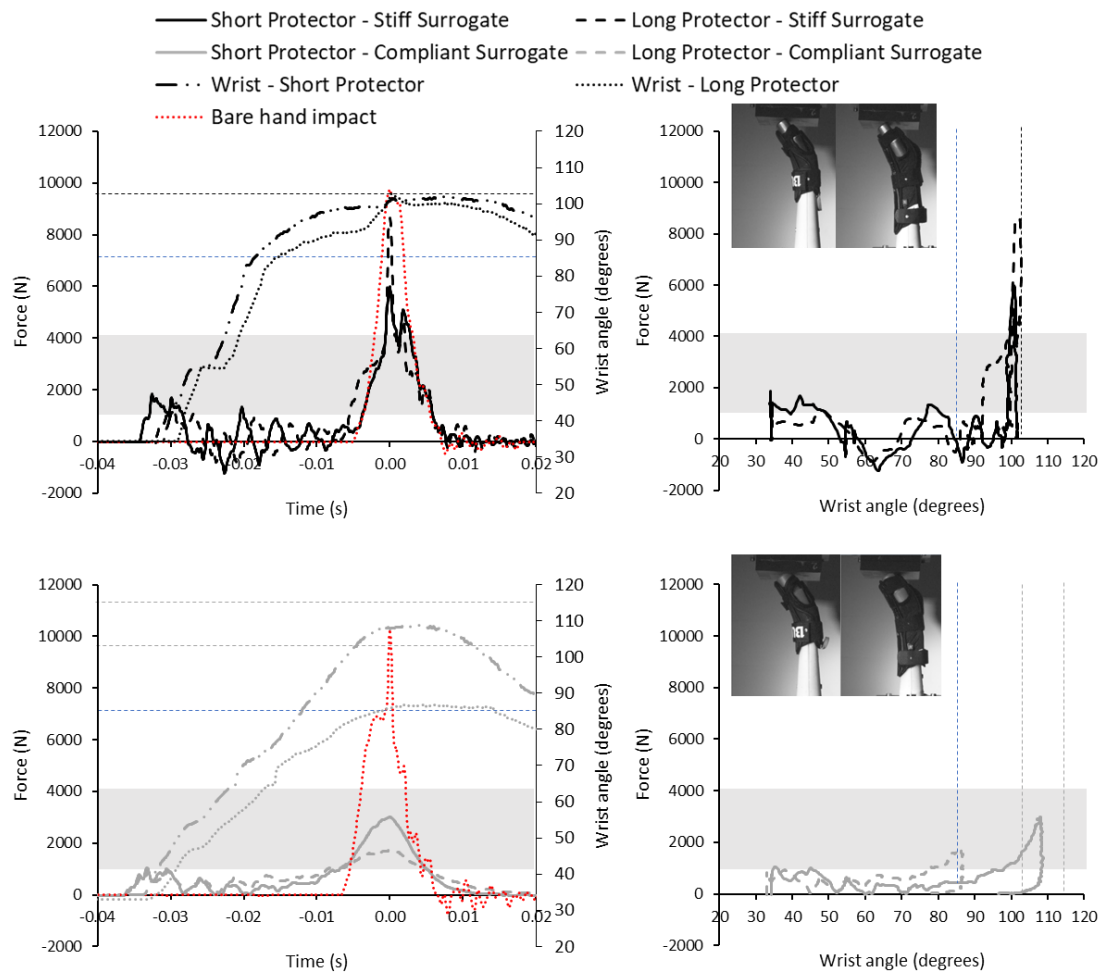
Figure 6-21 Temporal force and temporal wrist angle (left) and force vs. wrist angle (right) between protectors on the stiff surrogate (top) and compliant surrogate (bottom), alongside a bare hand impact on each surrogate. The grey box highlights the cadaver fracture range (Table 2-2), the blue dashed line indicates reported maximum non-injurious wrist extension (Table 2-1), and the black and grey dashed lines indicate the maximum wrist angle of the surrogates.

6.6.2.6. Statistical analysis

The GLM univariate analysis showed most main effects and surrogate interactions were significant ($p < 0.05$) (Table 6-3). The main effects (surrogate, protector style, strapping condition and protector condition) were all medium ($\eta p^2 > 0.06$) to large ($\eta p^2 > 0.14$). Surrogate had the largest effect ($\eta p^2 = 0.98$), followed by protector style ($\eta p^2 = 0.44$), strapping condition ($\eta p^2 = 0.36$) and finally, protector condition ($\eta p^2 = 0.07$). The surrogate interaction with protector style had a large effect ($\eta p^2 = 0.72$), whereas the surrogate interaction with protector condition had a medium effect ($\eta p^2 = 0.10$), and with strapping condition had a small effect ($\eta p^2 = 0.03$).

The GLM univariate analysis for the surrogates individually, showed that most of the main effects were significant (p < 0.05) (

Table 6-4 and Table 6-5). Protector style had a larger effect on the stiff surrogate than the compliant surrogate (ηp^2 = 0.84 vs. 0.36), and the strapping condition had a larger effect on the compliant surrogate than the stiff surrogate (ηp^2 = 0.48 vs. 0.25). Protector condition had the smallest effect on both the stiff and compliant surrogate (ηp^2 = 0.24 (stiff surrogate), and < 0.01 (compliant surrogate)), and was not significant on the compliant surrogate.

Table 6-3 General linear model univariate between subject effects (indicates significant result).*

Source	df₁	df₂	F	p-value	Partial Eta Squared (ηp^2)
Surrogate	1	48		< 0.001*	0.98 (large effect)
Protector style	1	48		< 0.001*	0.44 (large effect)
Strapping condition	2	48		< 0.001*	0.36 (large effect)
Protector condition	1	48		0.068	0.07 (medium effect)
Surrogate*Protector style			$F_{(1, 48)}$ = 120.21	< 0.001*	0.72 (large effect)
Surrogate*Strapping condition			$F_{(2, 48)}$ = 0.74	0.483	0.03 (small effect)
Surrogate*Protector condition			$F_{(1, 48)}$ = 5.20	0.027*	0.10 (medium effect)

Table 6-4 General linear model univariate between subject effects for the stiff surrogate (indicates significant result).*

Source	df₁	df₂	F	p-value	Partial Eta Squared (ηp^2)
Protector style	1	24	126.82	< 0.001*	0.84 (large effect)
Strapping condition	2	24	3.93	0.033*	0.25 (large effect)
Protector condition	1	24	7.44	0.012*	0.24 (large effect)

Table 6-5 General linear model univariate between subject effects for the compliant surrogate (indicates significant result).*

Source	df₁	df₂	F	p-value	Partial Eta Squared (ηp^2)
Protector style	1	24	13.67	0.001*	0.36 (large effect)
Strapping condition	2	24	11.14	< 0.001*	0.48 (large effect)
Protector condition	1	24	0.10	0.753	< 0.01 (small effect)

Box plots in Figure 6-22 were used to display the distribution of the data for each surrogate for each of the independent variables (protector, strapping condition and protector condition). The stiff surrogate showed more variation in peak force values than the compliant surrogate. The median peak force value for the long protector lay above the short protector box for the stiff surrogate (Figure 6-22a), indicating

that these groups were different. Furthermore, the median peak force value for the short protector lay above the long protector box for the compliant surrogate, likewise indicating that these groups were different. Peak force of the short protector varied more than for the long protector for the stiff surrogate, whereas the opposite was the case for the compliant surrogate. Moderate and tight strapping conditions had more varied peak force than the loose strapping condition on the stiff surrogate, whereas all strapping conditions had a similar peak force range on the compliant surrogate (Figure 6-22b). The spread of data between the protector condition was similar for both surrogates (Figure 6-22c).
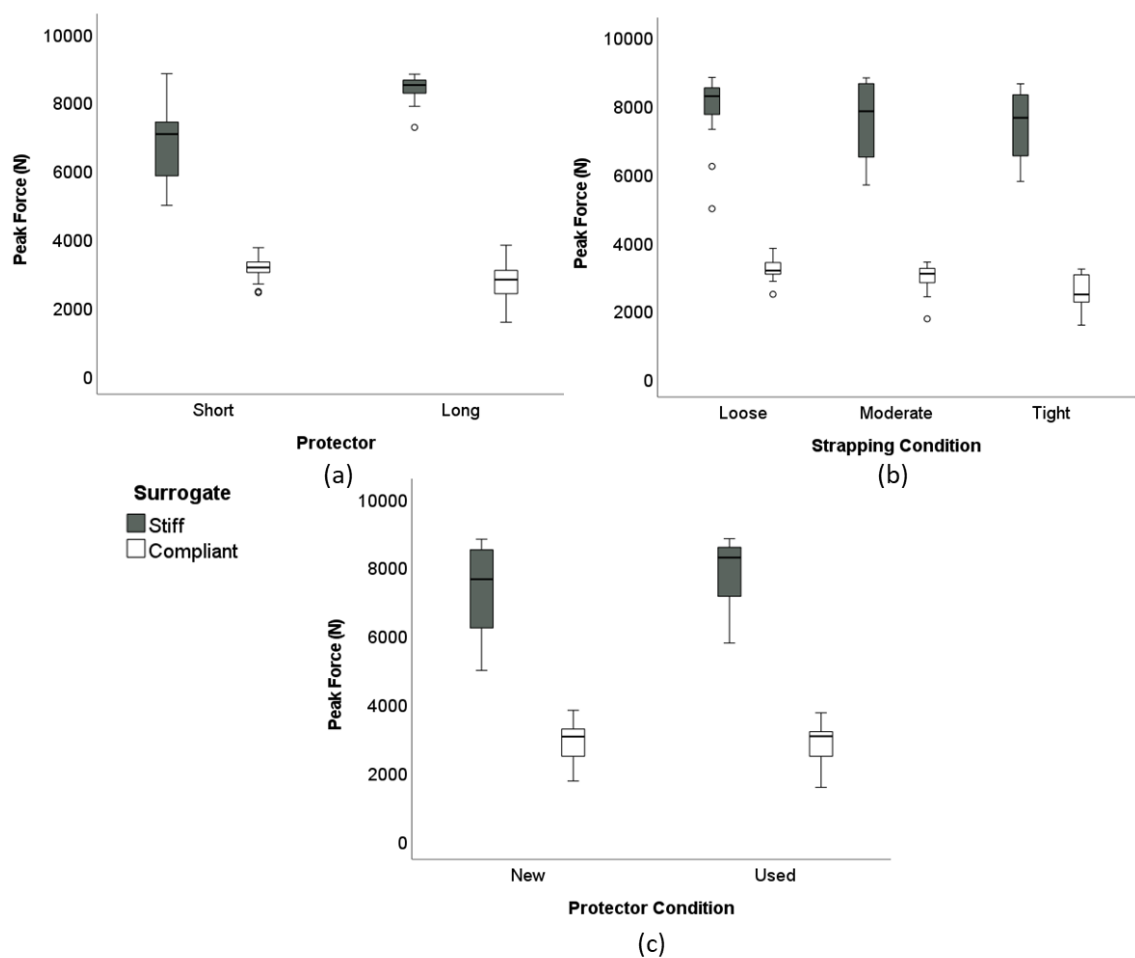
Figure 6-22 Box plots of the peak force values for (a) protector style, (b) strapping condition and (c) protector condition for each surrogate. The box plots display the minimum, first quartile, median, third quartile, maximum and outliers (data points).

6.6.3   Discussion

The temporal force, temporal wrist angle and force vs. wrist angle traces observed for the short and long protector on the stiff and compliant surrogate showed a

similar shape to those reported by Adams *et al*. (2018) and Newton-Mann (2019) (Figure 6-14 and Figure 6-15).

The bare hand impacts of the compliant surrogate had a slightly higher (4%) mean peak force than those of the stiff surrogate, although the mean impact duration of the compliant surrogate was ~3% longer than for the stiff surrogate. The higher force and longer impact duration of the compliant surrogate (bare hand condition) could be attributed to its wrist extending past 103° and into the range where the silicone surrounding the joint was compressing, as opposed to the stiff surrogate which remained at ~103° throughout the impact. The compliant surrogate (bare hand condition) was expected to have a slightly longer impact duration, as per the hypothesis 1.4 in Section 6.2, although the peak force of the compliant surrogate (bare hand condition) was expected to be lower than for the stiff surrogate.

Adding silicone to the surrogate further reduced the short and long protectors peak force compared to a bare hand condition (Figure 6-21), confirming hypothesis 1.2 in Section 6.2. The short protector reduced the peak force by ~39% (when on the stiff surrogate) and ~71% (when on the compliant surrogate), whereas the long protector reduced the peak force by ~11% (when on the stiff surrogate) and ~83% (when on the compliant surrogate). For the scenario tested here (25 J impact), the peak force values of both protectors when on the compliant surrogate lay within the cadaver fracture range (~1,000 to 4,000 N), and moreover, when on the stiff surrogate, the peak force values exceeded that range. Furthermore, the reported maximum non-injurious wrist extension angle (85°) (Table 2-1) was exceeded on both surrogates when testing both protectors.

Temporal forces for both protectors were lower when on the compliant surrogate, compared to the stiff surrogate, and furthermore, the time to reach peak force was longer. Testing on the compliant surrogate may, therefore, indicate that the protectors are more likely to prevent or reduce the severity of a wrist injury. Furthermore, the addition of silicone to the surrogate increased the surrogate-protector stiffness, having a lower wrist angle for a given force, confirming hypothesis 1.1. As such, surrogate design (in terms of surface materials) can influence the results when impact testing wrist protectors. It is, therefore,

recommended that any work reporting on impact testing of wrist protectors should clearly describe the surrogate used, so the results can be objectively compared with other studies and the work can be reproduced.

The initial spike in force due to the pendulum first striking the surrogate was ~46% lower on the compliant surrogate compared to the stiff surrogate (Figure 6-14 and Figure 6-15 point 2). The FE model in Chapter 5 (Section 5.2.2) predicted a 51% reduction in force due to increasing the thickness of silicone on a rigid anvil from 1 to 3 mm when impacting at 10 J, furthermore, a 73% reduction due to increasing the silicone from 1 to 7 mm (without a palmar pad). The reduction in force due to this initial contact between the pendulum and compliant surrogate, compared to the stiff surrogate, can be attributed to the silicone surrounding the end of the compliant surrogate hand, and confirms hypothesis 1.3 (Section 6.2). This initial contact caused a clear increase in force without a change in angle on both surrogates, suggesting that the initial hand position may be too upright. This suggests that increasing the wrist start angle by 5° from the pilot test to the final test (from 30 to 35°) did not have the desired effect, and the initial hand position may still be too upright and may not be representative of those where snowboarders injure their wrists (Chapter 2 Figure 2-1; Figure 2-3). Future work should consider larger start angles, which could be achieved by pulling the hand backwards before impact, and may require it to be tethered from behind with a cord. Furthermore, as the silicone reduced the initial force when the pendulum first struck the hand, future work with a compliant surrogate could look at reducing the amount of neoprene on the impactor, or removing it entirely. Indeed, a metal impactor without neoprene could be more suitable for use in test houses, as it would be simpler, lower cost, more durable and more repeatable. Such benefits would only be achieved if the corresponding compliant surrogate was also simple, low cost, durable and repeatable.

After the initial force spike corresponding to the start of impact, both protectors had force values fluctuating between positive and negative when on the stiff surrogate, whereas they had a steady positive increase in force when on the compliant surrogate (between point 2 and point 4 on Figure 6-14 and Figure 6-15).

The fluctuating force when protectors were on the stiff surrogate was because the forearm deflected in the y-axis direction after the initial contact and as the pendulum arm broke contact with the surrogate (Figure 6-16). The compliant surrogate remained in contact with the pendulum arm during this period, thus anchoring the top of the surrogate, and reducing the deflection of the forearm. The stiff surrogate hand had a ~50% higher angular velocity than the compliant surrogate hand after this initial contact, and thus broke away from the pendulum arm. This higher hand velocity could have been due to the higher initial impact force, whereas, the compliant surrogate may have gripped the pendulum arm due to higher friction between the silicone and impactor. The stiff hand was heavier than the compliant hand, so if all else was equal it would be expected to rotate slower. Friction between the hand and impactor was not measured, and this could be the subject of future work. A steady increase in force during this period was therefore observed when the protectors were on the compliant surrogate, as their protective elements were always engaged, as opposed to when on the stiff surrogate, where these elements were not engaged with the pendulum arm. In a fall scenario, the ground would be unlikely to break contact with the hand (Chapter 2 Figure 2-1; Figure 2-3) so it is thought that the compliant surrogate gave an impact scenario that was more like a fall than the stiff surrogate. Future work could study fall scenarios to better determine how snowboarders fall and the associated impact parameters, such as the angle of the wrist when it contacts the ground, to inform future impact testing.

A rapid increase in force to the peak value was observed when the short and long protectors were on the stiff surrogate, with a corresponding increase in wrist angle (Figure 6-14, Figure 6-15, Figure 6-18, Figure 6-19, Figure 6-21). This was due to the stiff surrogate reaching its maximum possible extension (103°), and thus the back of the hand contacted the central core. In contrast, when both protectors were on the compliant surrogate, a more gradual increase in force to the peak value was observed, with the surrogate reaching a higher wrist angle when testing the short protector (maximum 115°). The more gradual increase to peak force on the compliant surrogate could be due to the higher maximum possible wrist angle, and

furthermore, the silicone surrounding the joint compressing (at wrist angles >103°), and acting as a cushion. As such, this raises the question of whether it was the silicone surrounding the joint or the silicone on the palm and forearm of the surrogate that led to lower impact force values for the compliant surrogate in comparison to the stiff surrogate. The surrogates can be compared for impact force at 103° hand angle, and the contribution before and after the silicone behind the joint begins to compress can be determined. The peak force of the short protector strapped at moderate condition on the compliant surrogate increased by 77% as the wrist angle went from 103° to 108°, however the corresponding peak force for the stiff surrogate was still about twice as high.

Peak force fluctuated between test repeats, suggesting that the protectors had a sufficient rest period between impacts to reduce the effect of degradation. Similar results were found in the pilot test, and furthermore, the GLM analysis found that protector condition (new vs. used) had the smallest effect (ηp^2 = 0.07) on the peak force values out of the main effects (surrogate > protector style > strapping condition) (Table 6-3). The short protector had the most varied peak force values when on the stiff surrogate (CV 16%), whereas the range of values was similar between the short protector on the compliant surrogate, and the long protector on both surrogates (Figure 6-17 and Figure 6-22a).

Results were dependent on the strapping condition of the protectors. Protectors on the compliant surrogate generally behaved as expected; as strapping tightness increased, wrist angle reduced, implying the surrogate-protector combination was stiffer, and as a result peak force reduced (Figure 6-17 to Figure 6-19). Based on the results from the bend test, where torque values increased with strap tightness, it was expected that the surrogate-protector stiffness would be higher when the protectors were strapped tighter (as per hypothesis 3 in Section 6.2). Protectors on the stiff surrogate reached the maximum possible wrist angle (103°) at all strapping conditions, and no clear trend was found between the peak force values. GLM univariate analysis found that the protector strapping condition had a larger effect on peak impact force for the stiff surrogate than for the compliant surrogate (ηp^2 =

0.48 vs. 0.25), however it is suggested that strapping condition had a larger effect on wrist angle than peak force values.

Protector slippage occurred at two locations on the short protector (bottom of the dorsal side, and the strap) and three locations on the long protector (bottom of the dorsal side, and both straps). Protectors slipped less at the lower equivalent wrist angle between surrogates, compared to at the maximum wrist angle. This finding suggests that protectors slip further as wrist angle increases. The short protectors' strap slipped further on the stiff surrogate than the compliant surrogate, whereas the bottom of the dorsal side slipped further on the compliant surrogate than the stiff surrogate. No significant difference of protector slippage between surrogates was found for the long protector. Future work could look at this in more detail, but the results presented here indicate that the short protector slippage is more sensitive to surrogate material than the long protector.

The long protector had a higher peak force than the short protector when on the stiff surrogate (8,365 ± 365 vs. 6,816 ± 1,085 N). This finding is the opposite to what Newton-Mann (2019) observed when testing on the scanned surrogate, and rejects hypothesis 2 (Section 6.2), whereas Adams *et al*. (2021) observed the two protector styles to have similar peak forces. The disagreement with the previous work is likely due to the different surrogate (geometric vs. scanned) (Appendix G Section 9.7.3). Other reasons could include a different batch of protectors tested, and that the skid plate on the palmar region of the long protector was removed. In contrast, when on the compliant surrogate, the short protector had a higher peak force than the long protector (3,095 ± 316 vs. 2,661 ± 574 N). The difference in peak force between the protectors was smaller on the compliant surrogate, and hence, the GLM univariate analysis found that protector style had a larger effect on the stiff surrogate than the compliant surrogate (ηp^2 = 0.84 vs. 0.36). The long protector gave higher forces for a given wrist extension angle than the short protector when on both surrogates. This finding suggests that the long protector was stiffer than the short protector, in agreement with the bend test results in Chapter 4.

6.6.4   Conclusion

Surrogate design influenced the performance of snowboarding wrist protectors in a pendulum impact test. Adding a compliant outer layer to an otherwise stiff wrist surrogate reduced the peak impact force and increased the time to peak force of a short and long wrist protector. For this impact scenario (25 J impact), the peak force of both protectors on the compliant surrogate lay within the cadaver fracture range, and exceeded that range when on a comparable stiff surrogate. Protector strapping tightness affected the stiffness of the protectors, with a clear trend observed when the short protector was on the compliant surrogate (tight > moderate > loose). No clear difference of protector slippage between surrogates was observed for the long protector, but the bottom of the dorsal side of the short protector and the short protectors' strap slipped differently between surrogates.

6.7   Chapter Summary

The original surrogate for the pendulum impact rig (based on a laser scan of a human hand and forearm, as detailed in Adams (2018)) was critiqued, and a new central core (to attach the surrogate to the impact rig) was developed to facilitate attachments for either a compliant or a stiff wrist surrogate configuration. The compliant wrist surrogate from Chapter 4 was further developed, incorporating the findings from Chapter 5 of an appropriate silicone thickness for impact testing at >10 J, for the pendulum impact test. The compliant hand consisted of a 7 mm thick silicone outer layer on the palmar side and a 3 mm thick silicone layer elsewhere, with a stiff core. The compliant forearm consisted of two forearm casings, which bolted around the central core, each with a 3 mm thick silicone outer layer covering stiff plastic.

The effect of surrogate compliance on the impact performance of snowboarding wrist protectors was determined, alongside the effect of protector strapping tightness. Adding compliance to the wrist surrogate reduced the peak force and increased the time to reach this peak for both a short and a long protector, relative to a comparable stiff surrogate. Peak impact forces lay either within, or above the cadaver fracture range identified in Chapter 2 (~1,000 to 4,000 N). Protector strap tightness affected wrist angle, and thus the stiffness of the protectors. As surrogate

design (in terms of the surface material) influenced the impact test results, it is
recommended that future test reports clearly describe the surrogate used.

The novelty of this chapter was the use of the geometric geometry for a wrist
impact surrogate, the addition of a silicone outer layer to the wrist surrogate, and
the testing of snowboarding wrist protectors on the developed compliant wrist
surrogate at different strapping tightness's on the pendulum impact rig. This
chapter furthered the work of Adams *et al.* (2021) on impact testing wrist
protectors in a more representative impact scenario, and gained knowledge on the
effect of surrogate shape and biofidelity on the impact performance of
snowboarding wrist protectors. Impact testing the protectors at different strapping
tightness furthered the work on the influence of protector strapping tightness on
the protective capability of the wrist protectors, which was found to influence the
bending stiffness of the protectors. The limitations of this chapter were that only
two styles of wrist protector were tested and thus the trends found are only current
for those protectors, and furthermore, the protectors were only impacted at one
impact energy. The degradation of the silicone was not extensively tested, so the
suitability of the silicone layer on the surrogate for long term use for impact tests
was not determined.

The effect of adding silicone to an otherwise stiff wrist surrogate or anvil used to
test the performance of snowboarding wrist protectors has been established for a
bend test (Chapter 4), a basic impact test (Chapter 5) and an impact test that is
more representative of a fall (Chapter 6). The next chapter will compare the results
between these three tests, and make recommendations for testing wrist
protectors.

7. <u>Comparison of Tests for Characterising the Performance of Snowboarding Wrist Protectors</u>

7.1   Introduction

The aim of this current chapter is to compare and contrast the results, and identify trends, between the three tests that have been applied in the previous chapters to test the performance characteristics of the short and the long snowboarding wrist protectors. The trends of results between the measured bending stiffness of the protectors (Chapter 4), the impact performance of the palmar region (Chapter 5) and the impact performance of the protectors when fitted to a surrogate (Chapter 6) are noted and discussed. The tests are then compared to see how well they relate to each other, areas where they could be made to relate better, and recommendations are made to refine and improve the test procedure. As with the rest of this thesis, a key focus of this chapter is on discussing the results in relation to the design of the wrist surrogate.

7.2   How the Results Relate

In the bend test (Chapter 4), the long protector required over twice as much torque to extend the wrist to a given angle than the short protector (~3 vs. 7 Nm), suggesting that it was stiffer (Figure 7-1a). The results were similar in the pendulum impact test (Chapter 6), where the long protector required more force (about four times more at 95° on the stiff surrogate and 85° on the compliant surrogate) to extend the wrist to a given angle than the short protector (Figure 7-1c), also indicating that it was stiffer. The observed higher stiffness of the long protector over the short protector could be due to its construct having longer and wider splints. Indeed, Newton-Mann (2019) predicted with an FE model of the pendulum impact test that maximum wrist angle tended to decrease as protector splint length increased. Furthermore, within this current study adding silicone to the wrist surrogate increased the measured stiffness of both protectors in the bend test (Figure 7-1b), and increased the force required to extend the wrist to a given angle in the pendulum impact test (Figure 7-1d). Specifically, the stiffening effect from the silicone was larger for the long protector than for the short protector. Indeed,

the only surrogate-protector combination where the wrist did not fully reach the maximum reported non-injurious angle (85°) under impact, was when the long protector was on the compliant surrogate. These findings suggest that the larger splints of the long protector increased the surrogate-protector stiffness, which could prevent wrist hyperextension and reduce wrist injury risk, although this would need to be assessed specifically in future work.
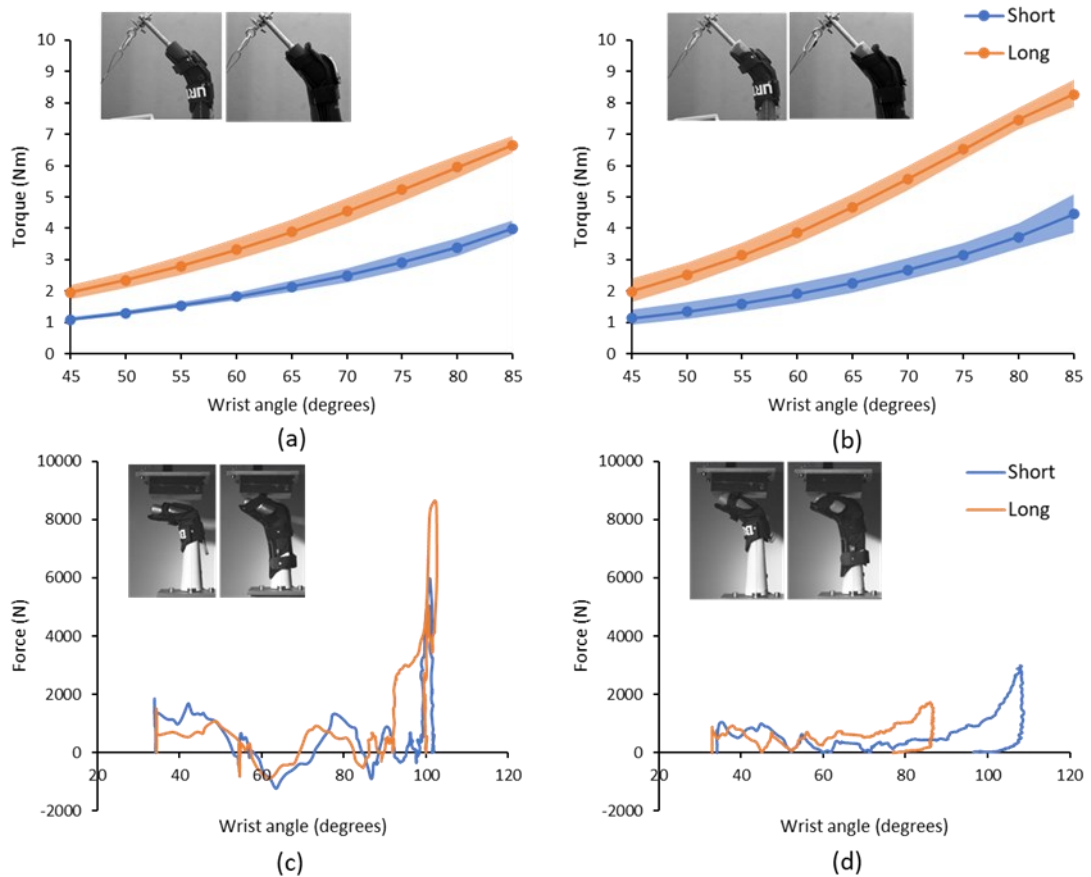
Figure 7-1 Comparison of the short and long protector in the bend test (test speed 200 mm/min) (top) on (a) the stiff surrogate and (b) the compliant surrogate, and in the pendulum impact test (impact energy 25 J) (bottom) on (c) the stiff surrogate and (d) the compliant surrogate. Both protectors strapped at moderate condition. The results for the pendulum impact test correspond to the first test on a new protector.

When silicone was added to the anvils in the linear impact test and the surrogate in the pendulum impact test, peak force decreased for both protectors (Figure 7-2). In particular, and for both tests, the decrease in force from adding silicone was larger for the long protector than for the short protector (~24 vs. 8% in the linear impact, ~68 vs. 55% in the pendulum impact). The lack of palmar padding on the long protector could mean that the silicone acted somewhat like a palmar pad, reducing the impact force, whereas the short protector already had a palmar pad, so the

silicone had less of an effect. As adding silicone to the surrogate in the pendulum impact test reduced the peak force for both protectors, the values were then closer to those obtained from the linear impact test (Figure 7-2). Specifically, with peak forces of about 3 kN, the values for the compliant surrogate in the pendulum impact test were closer to those for the hemispherical anvil than for the palm shaped anvil in the linear impact test. However, unlike with the rigid hemisphere, the linear impact test with the palm shaped anvil correctly predicted the trend of the peak force results from the pendulum impact test with the compliant surrogate (short > long).
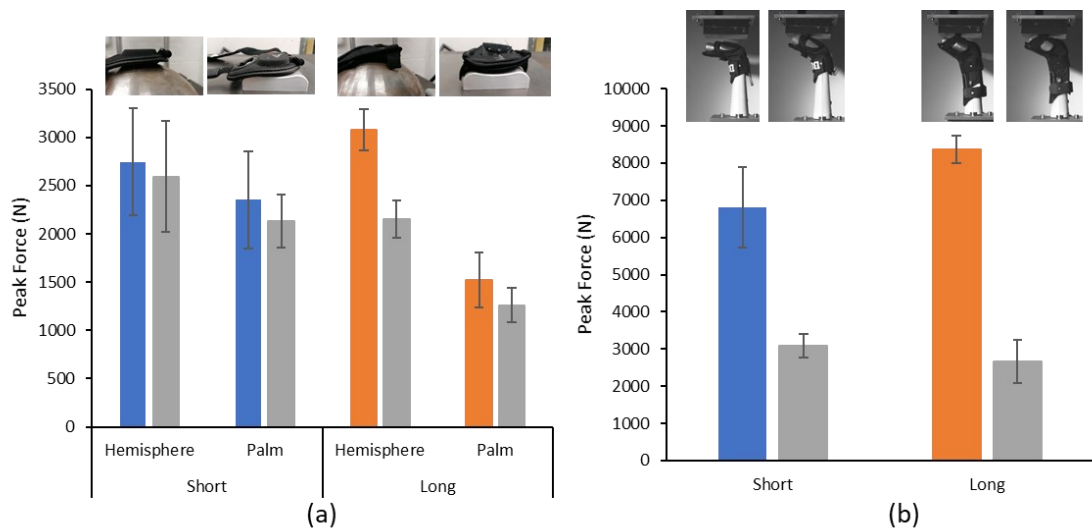
Figure 7-2 Peak force of the short and long protectors impact tested on (a) the hemispherical (as per BS EN ISO 20320:2020) and palm anvil (impact energy of 4 J) with (grey) and without silicone, and (b) on the stiff and compliant (grey) wrist surrogate (impact energy of 25 J) (5 mm silicone thickness on anvils, 7 mm silicone thickness on the palm of wrist surrogate and 3 mm silicone thickness elsewhere on wrist surrogate) (error bars showing mean ± SD).

As strapping tightness increased in the bend test, more torque was required to extend the wrist to a given angle for both protectors when on both the stiff and the compliant surrogate (Figure 7-3a, b). In the pendulum impact test, strapping tightness also affected the wrist angle of the surrogate. As strapping tightness increased, maximum wrist angle under impact tended to reduce when the protectors were on the compliant surrogate (Figure 7-3d), although the wrist did extend ~2° less when the long protector was moderately strapped. The effect of protector strapping tightness on wrist angle was less clear when impact testing with

the stiff surrogate, as the wrist always extended to its maximum possible angle of 103° (Figure 7-3c).
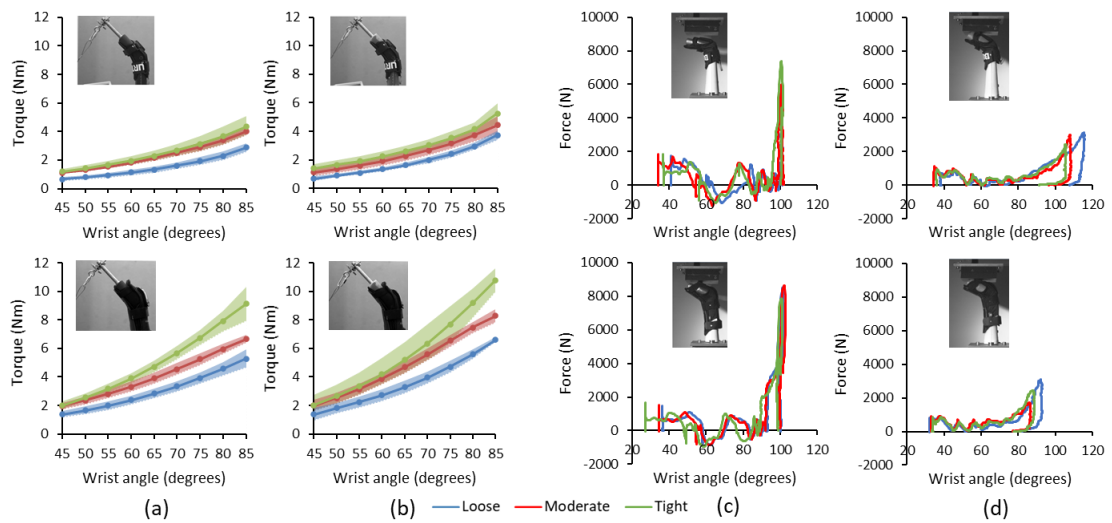
Figure 7-3 Comparison of the short (top) and long protector (bottom) at different strapping conditions in the bend test (test speed 200 mm/min) on (a) the stiff surrogate and (b) the compliant surrogate, and in the pendulum impact test (impact energy of 25 J) on (c) the stiff surrogate and (d) the compliant surrogate. The results for the pendulum impact test correspond to the first test on a new protector.

7.3 Areas Where the Tests Could Relate Better

The bend test pulled the surrogate hand backwards slowly at an angular velocity of ~1 °/s, whereas the impact test forced the wrist to extend much faster at ~2,000 to 4,000 °/s (i.e. ~two to four thousand times faster). While the bend test gives an indication of the stiffness of the protectors, the much faster loading rate in the impact test raises questions about the ecological validity of the former. It may be possible to increase the loading rate of the protector in such a bend test by mounting the surrogate differently in a uniaxial test machine (tensometer), removing the need for the "cable and pulley" arrangement. For example, perhaps the surrogate could be mounted to the device with an axis of rotation at both the top of the hand and the base of the forearm, in a "hinge style" configuration. With such a surrogate configuration, it may be possible to run the test machine faster. The maximum speed of the Hounsfield tensometer used for this project was 500 mm/min, although other devices can move faster, such as the Instron machine also used in this project for material testing, which had a maximum speed of ~1,000 mm/min. Despite the impact test being faster than the bend test, the results presented here do appear to somewhat translate between the two tests for the

177

two protectors tested here, but this finding may not transfer to all protector designs so future studies are required.

The load case for the pendulum impact test with the rigid surrogate appears to be more severe than for the linear impact test with the rigid anvils (hemisphere and palm) (Figure 7-4a, c). Indeed, the peak impact force was around three to six times higher for the pendulum impact test than for the linear impact test, suggesting that they are not fully comparable. The impact duration was also longer for the pendulum test than for the linear test, which was attributed to the ability of the surrogate wrist to extend in the pendulum test. For bare hand impacts, where the wrist was at full extension at the start of the test, the impact duration was ~0.0075 s shorter than when a protector was fitted. As such, the bare hand impact was only ~0.0025 s longer than the linear impact test. When testing the protectors on the compliant surrogate, rather than the stiff one, in the pendulum impact test, the load case was more similar to that of the linear drop test (Figure 7-4b, d), although as the contact time was longer for the pendulum impact test the loading rate was also lower. An advantage of having a compliant (i.e. with silicone) anvil or surrogate in an impact test is that results from protected and unprotected scenarios (i.e. with or without a protector) can be more meaningfully compared.

Due to clear differences between a surrogate with a wrist joint and a fully-constrained anvil, using the same energies in the linear impact test and the pendulum impact test would not be expected to load the protectors in a similar manner and give similar temporal force traces. It may, however, be possible to individually tailor the impact energies of these two tests, so they load the palmar region of the protectors in a similar manner (i.e. similar strain and strain rate). Due to the nature of the pendulum rig, with its arm contributing to the effective striking mass, there is a limited window of achievable impact energies, particularly if a minimum impact velocity is required. An alternative option could be to mount a wrist surrogate in a linear drop tower rig, with the forearm mounted at its base, like in the pendulum impact test. Such a setup would make it easier to experiment with combinations of drop masses and release heights that give a broad range of impact energies, with a view to finding the conditions that load the palmar region of the

protector in a similar manner when it is either strapped to a surrogate or mounted on an anvil. Ultimately, an impact test with a surrogate should represent the conditions that would injure an unprotected wrist, so meaningful results can be obtained when testing protectors. The impact energy of a simpler test with a fully constrained anvil could then be tuned to ensure the loading conditions on the palmar region of the protector are similar to those when testing with the surrogate. The focus should really be about the trends between tests, with a view to maintaining the ranking of protector performance between tests.
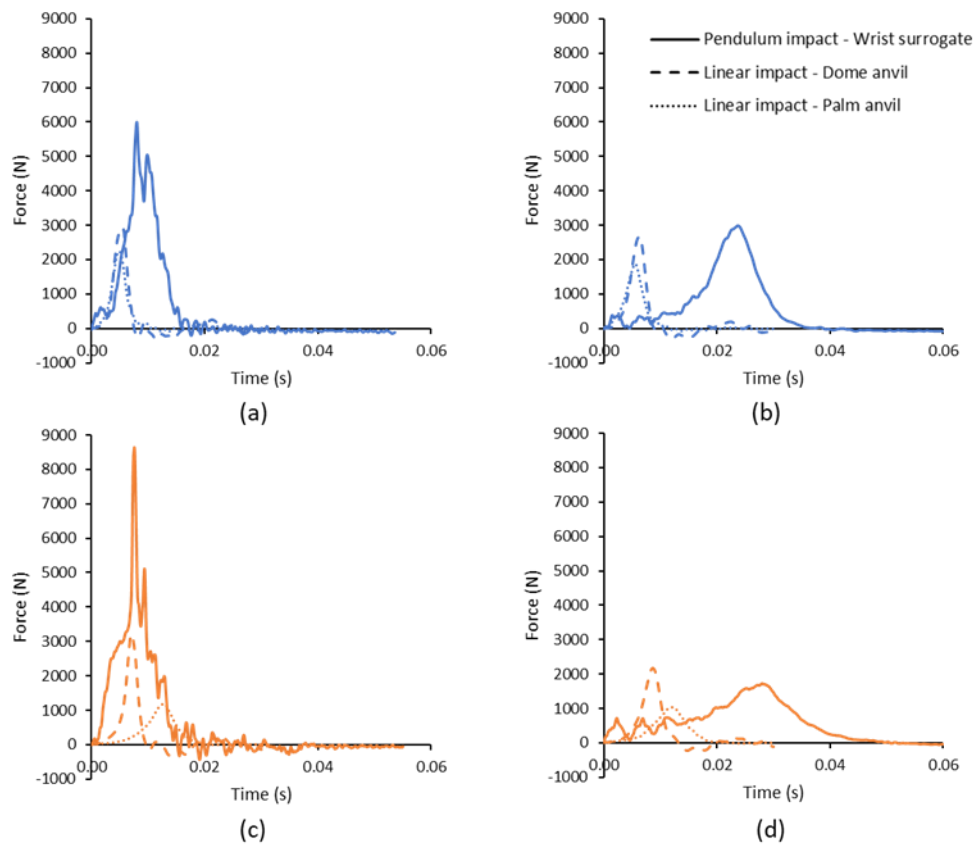
Figure 7-4 Comparison of the short (blue - (a) and (b)) and the long (orange - (c) and (d)) protector tested on the pendulum impact rig at 25 J (trimmed to the region where the force begins to clearly increase) and the linear impact rig at 4 J, without silicone (left - (a) and (c)) and with silicone (right - (b) and (d)) (5 mm silicone thickness in linear impact rig, 7 mm silicone thickness on the palm and 3 mm silicone thickness elsewhere on wrist surrogate in pendulum impact rig).

The results from the bend test (Chapter 4) observed that the protectors did not meet the pass criteria of BS EN ISO 20320:2020 (a torque of 5 Nm should cause between 50 and 75° of wrist extension, and a torque of 8 Nm should cause between 55 and 80° of wrist extension) as the surrogate-protector stiffness was low (Chapter 4 Figure 4-15). Furthermore, in the pendulum impact test (Chapter 6), the

protectors did not really limit the wrist angle, as wrist angles up to 115° were observed. As such, this indicates that the pass criteria in the standard may actually be suitable, although further testing is required to better link performance in the different tests to wrist injury risk.

7.4   Chapter Summary

The results from the bend test (Chapter 4), the linear impact test on the palm region (Chapter 5) and the pendulum impact test (Chapter 6) that were used to characterise the performance of the short and long snowboarding wrist protector were compared. The trend of surrogate-protector stiffness from the bend test translated to the pendulum impact test (long > short). Adding silicone to the pendulum impact test aligned the peak force values more closely to those from the linear impact test. Increasing the loading rate in the bend test would bring the conditions closer to those of the pendulum impact test, and this would likely require the surrogate to be reconfigured within the test device to remove the need for a cable and pulley arrangement to extend the wrist. The shape of temporal force plots differed between the linear impact test with the fully constrained anvil and the pendulum impact test with the wrist surrogate.

The novelty of this chapter was the comparison of the performance of two styles of snowboarding wrist protector when tested in the bend test, linear impact test and pendulum impact test. This work furthers the work on the testing and certification of snowboarding wrist protectors, informing revisions of BS EN ISO 20320:2020. The limitation of this chapter was that the results were only current for the two protector styles tested, and furthermore, the tests were only compared for the room temperature condition. The final chapter will highlight the novel findings from each chapter and how this work has increased the current research knowledge within testing of snowboard wrist protectors, it will also highlight limitations and suggestions for future work.

8. <u>Conclusion, Limitations and Future Research</u>

8.1 Introduction

The aim of this PhD project was to develop an enhanced novel wrist surrogate for assessing the protective capabilities of snowboarding wrist protectors further tuning previous work. The surrogate elements this current project focused on were determined through an action priority matrix. The developments of the wrist surrogate were incremental and the developed wrist surrogates were designed for use in a bend test and a pendulum impact test. Impact testing was also conducted following the newly developed BS EN ISO 20320:2020, with an aim to compare the results obtained from the three experimental tests and provide recommendations for certification tests for snowboarding wrist protectors and the future use of biofidelic surrogates.

This current chapter summarises the work carried out during this PhD thesis and presents how the objectives of the study have been met. The novelty, conclusions and limitations for each chapter are stated. The overall limitations, recommendations for future work, and recommendations for the use, and further development of biofidelic surrogates, are then presented.

8.2 Summary of Research

8.2.1 Chapter 2

Chapter 2 reviewed the existing literature and concluded that the development of a wrist surrogate should be incremental, with validation against previous work and comparison against current wrist surrogates. It was identified that the biofidelity of current wrist surrogates could be improved through the use of a skin and soft tissue simulant and instrumentation. The geometry of the geometric surrogate from Adams *et al.* (2018), which was implemented into the bending test in BS EN ISO 20320:2020, was selected as a starting point for use in this project. This chapter reviewed the literature and covered Objective 1, which was to determine the internal and external geometry, main components and articulating joint of the wrist and forearm.

8.2.2 Chapter 3

Chapter 3 investigated candidate skin and soft tissue simulants for use in a wrist surrogate. From this research it was concluded that M511 maxillofacial silicone was a suitable skin and soft tissue simulant for use in a wrist surrogate. The selection criteria was based on the stress strain relationships in comparison to organic tissue and soft tissue simulants in the literature (Payne *et al.,* 2014), repeatability of the silicone response, and the feasibility of using it within a wrist surrogate. This fulfilled Objective 2, which was to identify a suitable synthetic soft tissue simulant for a wrist surrogate to enhance the previous work within snowboard wrist protector research. The use of maxillofacial silicones within a wrist surrogate is novel as they are commonly used for prosthetics in reconstructive science due to their skin like qualities, and although they have been previously used in a biofidelic thigh surrogate (Payne *et al.,* 2016), until now they have not been incorporated into a wrist surrogate.

8.2.3 Chapter 4

Chapter 4 used the candidate silicone identified in Chapter 3 to create a compliant wrist surrogate for use in a bend test to measure the stiffness of snowboarding wrist protectors. The surrogate had a compliant hand and forearm, each consisting of a stiff core (short carbon fibre reinforced polyamide) and a 3 mm outer layer of silicone to represent skin tissue, which were connected via a hinge joint. A 2 to 3 mm thick compliant layer has been used by others to represent skin in sport surrogates (Ankrah and Mills, 2003; Payne, 2015; Maurel *et al.,* 2013). The addition of a 3 mm thick silicone outer layer to the wrist surrogate increased the surrogate-protector stiffness, relative to a comparable stiff surrogate. This chapter also investigated the effect of protector strapping tightness, which was found to increase the surrogate-protector stiffness, in agreement with previous work (Adams, 2018). The long protector was stiffer than the short protector (required over twice as much torque to extend the wrist to a given angle), as also noted before (Adams *et al.,* 2016; Adams 2018).

The bend test was found to have poor repeatability across three independent test days with the same operator, however the trend of results was repeatable. This

variation of results could be due to the use of a cable to extend the wrist, and inconsistencies in the start angle and the protector strap tightness. The repeatability of the test could potentially be improved by mounting the surrogate differently in the test device to negate the need for a cable and pulley arrangement, as noted in Chapter 7 Section 7.3, and the use of instrumentation to set protector strap tightness more reliably.

The novelty of Chapter 4 was the addition of a skin tissue simulant to the wrist surrogate during bend testing, and also the first assessment of the repeatability of such a bend test. This chapter covered Objective 3, to determine the effect of a skin simulant on the measured bending stiffness of snowboarding wrist protectors. Testing the protectors on the compliant surrogate gained knowledge on the effect of developing the biofidelity of the surrogate, in terms of soft tissue simulants, on the performance of snowboarding wrist protectors in the bend test. The results of this study can inform the use of soft tissue simulants for the testing of sports PPE. The addition of the skin simulant could be used to assess cuts and lacerations within sport, and can be applied to other sports surrogates, following the work on cuts and lacerations in rugby (Hughes et al., 2021), and lacerations due to football studs (Oudshoorn et al., 2017). Furthermore, cuts and laceration due to sports surfaces, such as recent work on skin injury risk on rugby turf (MacFarlane et al., 2022), which could translate into assessing children's playground surfaces. The bend test assessed the stiffness of the snowboarding wrist protectors, and can be used to assess the stiffness of wrist protection for other sports such as roller sports. Furthermore, such a test could be used to assess the wrist support provided by wraps and tapping techniques used to support the wrist in boxing, following the work of Gait et al. (2020). The repeatability study furthered the work of Adams *et al.* (2016) and Adams *et al.* (2018), gaining knowledge on this bend test and the implications for BS EN ISO 20320:2020. The use of pressure sensors on the wrist surrogate was trialled for measuring protector strap tightness and areas of high pressure along the surrogate during testing, although reliable results were unattainable. As such, pressure sensors were not incorporated into the wrist surrogate developed here, and they could be the subject of future studies.

The limitations of Chapter 4 were that only two styles of snowboarding wrist protector were tested, and thus the trends found are only current for those protectors. The degradation of the silicone was not extensively assessed, and thus the suitability for implementation into the standard was not determined. Therefore, future work should look into the degradation and repeatability of the silicone. Only the medium sized wrist surrogates were tested in the bend test, and thus testing of the small and large wrist protectors on the corresponding sized wrist surrogates would be required for further evaluation of BS EN ISO 20320:2020.

8.2.4 Chapter 5

Chapter 5 investigated the use of FE modelling and experimental impact tests to inform the thickness of the soft tissue simulant to be applied in the palm region of a compliant wrist surrogate intended for use in a pendulum impact test. As the silicone layer that was to be applied to the palm of the wrist surrogate was intended for impact testing and hence representing both skin and the underlying soft tissue, it needed to be thicker than that applied elsewhere on the surrogate. It was concluded that a 7 mm silicone thickness over the palm region of the surrogate, with a 3 mm silicone thickness elsewhere, would be suitable for impact energies >10 J, as typical of the pendulum impact test. Choi and Robinovitch (2011) measured a thickness of soft tissue over the palm region of 6.9 to 7.7 mm.

Impact testing against BS EN ISO 20320:2020 was conducted to determine the impact performance of the palmar region of the snowboarding wrist protectors. The effect of incorporating an anvil shaped more like a hand was also determined, alongside the effect of adding compliance to this linear impact test. The short protector was better at limiting impact force than the long protector, when impacted on the hemispherical anvil prescribed in BS EN ISO 20320:2020. In addition, both protectors were better at limiting impact force when positioned on a palm shaped anvil than the hemisphere. This finding highlights that the ability of the palmar region of the protectors to limit impact force was dependent on the shape of the anvil they were tested on. The decrease in impact force when moving from the hemispherical to the palm shaped anvil was larger for the long protector than for the short protector. Adding a 5 mm thick silicone layer to the anvils further

increased the protector's ability to limit impact force. Future work could investigate anvil shape in such a linear impact test in more detail, while testing more protector designs and sizes, with a view to finding the most suitable anvil shape for testing snowboarding wrist protectors.

The novelty of Chapter 5 was the FE modelling of different silicone thicknesses when between a snowboarding palmar pad and rigid anvil, and the impact testing of snowboarding wrist protectors against BS EN ISO 20320:2020. This chapter covered Objective 4, to determine the effect of a soft tissue simulant on the impact performance of the palmar region for snowboarding wrist protectors. The FE model utilised and furthered the work of Newton-Mann *et al.* (2018) on the palmar pad of snowboarding wrist protectors. Testing snowboarding wrist protectors against the impact test in BS EN ISO 20320:2020 was novel, as there is limited published data on the impact performance of snowboarding wrist protectors against this new standard. There is, however, some data on impact testing wrist protectors against EN 14120:2007, for which the impact test in BS EN ISO 20320:2020 was based upon (Schmitt *et al.,* 2011). The addition of the compliant layer to the anvil and incorporation of an anvil shaped more like a hand was novel, and gained knowledge on the effect of developing the biofidelity of the anvil. The results of this can inform the use of biofidelic anvils for the impact testing of sports PPE.

The limitations of Chapter 5 were than only two snowboarding wrist protectors were tested, and only the medium sizes. More snowboarding wrist protectors and more protector sizes should be impact tested to further the knowledge of the ability of the protectors to limit impact force, and implications for BS EN ISO 20320:2020.

8.2.5   Chapter 6

Building on the work of Chapters 4 and 5, Chapter 6 developed a compliant wrist surrogate to use in a pendulum impact test to determine the impact performance of snowboarding wrist protectors. Much like the one developed in Chapter 4, the wrist surrogate consisted of a compliant hand and forearm, each consisting of a stiff core and a silicone outer layer. As per Chapter 4, the silicone thickness surrounding most of the surrogate was 3 mm, and based on the findings of Chapter 5, a 7 mm

thick silicone thickness was applied over the palmar side of the hand. The wrist surrogate had a stiff central core with a similar potentiometer and timing belt mechanism (that translated the angular movement of the wrist to the potentiometer) as the surrogate from Adams (2018), which was further developed here to allow the compliant surrogate parts to be interchangeable with the stiff ones. Furthering the work of Adam *et al.* (2021), the surrogate geometry was developed to match that of the one for the bend test in BS EN ISO 20320:2020, and the compliant surrogate was compared against an otherwise equivalent stiff surrogate. Using the same surrogate geometry in both the bend test and the pendulum impact test, allowed for a direct comparison between these two tests for the first time. Adding compliance to the wrist surrogate improved the protector's ability to limit impact force, relative to a comparable stiff surrogate. The effect of protector strapping tightness was also assessed for the first time in such an impact test, and much like with the bend test in Chapter 4 it was found to affect the results. As strapping tightness increased, wrist angle under impact tended to reduce, implying the surrogate-protector combination was stiffer.

The novelty of Chapter 6 was the incorporation of the geometric wrist surrogate geometry into an impact test, the addition of compliance to the wrist surrogate, and the effect of protector strap tightness, which has not previously been examined in an impact test. This chapter covered Objective 5, to determine the effect of adding skin and soft tissue to a wrist surrogate on the impact performance of snowboarding wrist protectors in a pendulum impact test. This chapter furthered the work of Adams *et al.* (2021) on impact testing wrist protectors in a more representative impact scenario. The change of the surrogate geometry and compliance gained knowledge on the effect of surrogate shape and biofidelity on the ability of the protectors to limit impact force. This work could inform the use of biofidelic surrogates for impact testing sports PPE. The first assessment of the influence of protector strapping tightness on impact testing wrist protectors furthered the previous work on the effect of protector strapping tightness on the bend test. An impact rig, such as the one used here, could also be used to assess other forms of wrist protection, such as the Giddins Guard glove (from the authors

Giddins and Giddins (2021)), which incorporates a palmar pad into a leather glove, designed to prevent wrist injuries in the elderly population due to falls. Testing such products could gain knowledge on the effect of incorporating protective elements into regular gloves to reduce wrist injuries in the elderly population, and how that could be applied to other populations such as falls within children.

The limitations of Chapter 6 were that only two styles of wrist protector were tested and thus the trends found are only current for those protectors, and furthermore, the protectors were only impact tested at one chosen impact energy. The degradation of the silicone was not extensively tested, and thus its suitability for long term use for impact testing was not determined. Further impact testing of the wrist protectors should be conducted at different impact energies and on more wrist protectors, to gain further knowledge on the ability of snowboarding wrist protectors to limit impact force in this pendulum impact rig.

The compliant wrist surrogate could reach a higher wrist angle (115°) when the hand was forced backwards, than the stiff surrogate (103°). A wrist angle of 103° is above the non-injurious range reported in the literature (85° from Levangie and Norkin (2005); Chapter 2 Table 2-1), so there is no need to increase the maximum possible extension of the stiff surrogate to match that of the compliant surrogate. Instead, the minimum protector stiffness that prevents the wrist of the surrogate from reaching the current maximum of 103° under impact could be determined by comparing against results from the bend test. Only the long protector when on the compliant surrogate, reduced wrist extension below 103°. The results from such comparative testing could be used to set a stiffness window, or a minimum stiffness that protectors have to achieve in a bend test in a revised version of BS EN ISO 20320:2020.

The potentiometer used in the wrist surrogate for the studies in this thesis was found to be non-linear across the wrist angle range used in the test. In future work, the potentiometer should be checked before data collection and either its position adjusted so it is linear across the range of wrist angles used, or a more appropriate one could be sourced. In addition, the surrogate central core was developed to include a detachable side part, and whilst this facilitated interchanging between the

stiff and compliant surrogate configurations there were disadvantages. For example, the potentiometer was recalibrated when switching between the two surrogate configurations, as its position may have changed, and the alignment of the hand had to be checked. Going forward, a compliant surrogate could be manufactured for research purposes, and another stiff surrogate could be made specifically for developing certification tests. Such an approach would prevent uncertainties and inconsistency that may come from switching between stiff and compliant surrogate configurations.

8.2.6   Chapter 7

Chapter 7 compared the tests for characterising snowboarding wrist protectors from chapters 4 to 6. The trend of surrogate-protector stiffness from the bend test transferred to the pendulum impact test. Adding silicone further increased the measured stiffness of both protectors in the bend test, and increased the force required to extend the wrist to a given angle in the pendulum impact test. For the bend test, the surrogate could be mounted differently in the uniaxial test device, as mentioned in Chapter 7 Section 7.3. The effect of test speed could be studied, as the bend test loaded the protector much slower than the pendulum impact test. Even though the pendulum impact test was faster, the results from the best test, in terms of the ranking of surrogate-protector stiffness, do appear to transfer across to the pendulum impact test, as noted in Chapter 7 Section 7.3. More protector design would, however, need to be tested to get a better indication of the level of agreement between the bend test and the pendulum impact test.

The load case for the pendulum impact test with the rigid surrogate was more severe than for the linear impact test with the rigid anvils (hemisphere and palm). Adding silicone to the pendulum impact test aligned the peak force values more closely to those from the linear impact test. One way to bring these tests closer together could be to adjust their severity. Maintaining the ranking of the protector performance between tests should be the focus when comparing tests.

The novelty of Chapter 7 was the comparison between the results from the bend test and the pendulum impact test conducted with the same surrogate geometry, and the comparison of the basic impact test from BS EN ISO 20320:2020 to the

more specialist pendulum impact test. This chapter fulfilled Objective 6, to make recommendations on tests for snowboarding wrist protectors. This work furthered the work on the testing and certification of snowboarding wrist protectors. The recommendations for certification included increasing the loading rate of the bend test to better match the conditions of the pendulum impact test, and tailoring impact energies to load the palm in a similar manner between impact tests.

The limitations of Chapter 7 was that the results were only current for the two wrist protector styles tested and for room temperature condition. Further tests should be conducted with more styles of wrist protector and at temperatures more relevant to snowboarding conditions.

8.3   Main Limitations

This current project was limited by the lack of published data on the mechanics of snowboarding falls that cause wrist injuries, such as typical loading rates and wrist angles at impact, to inform the test setups, test parameters, and injury thresholds, for comparison of the developed surrogate to forces and fracture loads experienced in falls. Only two styles of snowboarding wrist protectors were tested in this project; a short and a long protector, and thus the trends found in this project are only current for those products. Another limitation is that the protector strap tightnesses used here were arbitrary, and simply based on those used before (Adams, 2018). Only the medium surrogate size prescribed in BS EN ISO 20320:2020 was tested in this project, and while this allowed comparison to recent research by Adams *et al.* (2018), it does not provide any information on the effect of testing different surrogate sizes. Furthermore, only one of each surrogate was manufactured, and thus the repeatability of manufacturing, and particularly silicone moulding, was not assessed. Only one impact condition (< 25 J) was tested in the pendulum impact test, and thus the effect of surrogate design on the measured protector performance at other impact energies was not assessed. All tests were performed at room temperature, and thus the performance of the protectors at cold temperatures relevant to snowboarding were not assessed. Finally, the surrogate lacked instrumentation, such as pressure sensors, which could help set

strap tightness and gain knowledge on areas of high pressure on the surrogate during testing.

8.4   Limitations and Implications for BS EN ISO 20320:2020

Testing snowboarding wrist protectors in the bend test (Chapter 4) and impact test (Chapter 5) from BS EN ISO 20320:2020 gained knowledge on the test procedures and performance of the protectors for certification. Chapter 4 concluded that the bend test lacked repeatability and protector strapping tightness influenced the bending stiffness of the protectors. Testing snowboarding wrist protectors in the pendulum impact test of Adams *et al.* (2021) (Chapter 6) provided results on the performance of snowboarding wrist protectors in a more representative impact scenario. Chapter 7 compared the results of the bend test and pendulum impact test as the wrist protectors were tested on the same surrogate geometry, and compared the linear impact test and pendulum impact test. The difference in loading rate between the bend test and pendulum impact test was identified, however, the trend of results of surrogate-protector stiffness translated from the bend test to the pendulum impact test. The loading rate for the pendulum impact test was more severe that the linear impact test, and furthermore the protector's ability to limit impact force in the linear impact test was influenced by anvil shape.

This project informed the standard that: i) the repeatability of the bend test needs to be improved, ii) the influence of protector strapping tightness needs to be reduced or accounted for, iii) the loading rate of the bend test should better match the conditions of the pendulum impact test, iv) the impact energies should be tailored to load the palm in a similar manner between impact tests, and v) anvil shape should be investigated in more detail for the linear impact test.

8.5   Future Work

Future work could focus on collecting data on snowboarding fall mechanics and wrist injury mechanisms. Such data could help inform future tests for snowboarding wrist protectors, to allow greater comparison to be made between the results obtained from surrogates and the human limb, and determine whether the

developments made to a surrogate make it a closer representation of a real life scenario.

The biofidelity of the surrogate could be developed further by incorporating more simulants to represent the different tissues within the hand and forearm, and furthermore exploring the use of a bone surrogate that fractures under load. Bone surrogates (Sawbone® femur and tibia) have been incorporated into a thigh surrogate and a shin surrogate (Payne *et al.*, 2016; Francisco *et al.,* 2000). Incorporating a frangible bone surrogate into a wrist surrogate may be costly due to the need for replacement after tests that exceed the fracture threshold. Thus such an approach would not be applicable for certifications tests undertaken in test houses, but it could be used to inform the design of a simpler surrogate and test in a revised BS EN ISO 20320:2020.. The stiffness of the wrist joint could be explored, and incorporated into the surrogate to develop the biofidelity of the joint.

Future work could quantify the strapping tightnesses people use when wearing wrist protectors, such as with the use of pressure sensors, to help inform strapping conditions during testing. The use of further instrumentation, such as pressure sensors, on the surrogate could provide a more repeatable method of setting strap tightness, and on the protectors themselves, such as strain gauges to measure the bending of splints during testing. The movements of the protectors during wrist extension when worn by people and when on the surrogate could be measured and compared, alongside further measurements of the coefficient of friction between the inner fabric of the protector and skin simulants.

Future work could examine the effect of testing the different surrogate sizes in the bend test in BS EN ISO 20320:2020, along with further determining the effect of an anvil more representative of a hand in the linear impact test, by testing more protector styles. It is important that different protector sizes are also appropriately certified with surrogates that are representative of different population groups.

Future work could investigate testing more wrist protectors to determine how they degrade with use, the repeatability of the linear impact test and the pendulum impact test, and testing more styles of wrist protector to determine whether the

trend of results found in this project are transferable across other protector designs. Furthermore, the protectors should be tested at different temperatures, i.e. temperatures which are relevant to snowsports, as BS EN ISO 20320:2020 notes that the protectors should also be tested at cold conditions (-10℃). Indeed, the effect of low temperature on the silicone response also needs to be determined.

8.6   Recommendations for Biofidelic Surrogates

Biofidelic surrogates are well suited for research purposes, as higher levels of complexity can be added, in contrast to stiff surrogates, which are better for test houses as they are simpler to make. The compliant surrogate developed here could be developed further so it is more suitable for use in test houses, such as additively manufacturing components in different materials. Flexible materials currently available for additive manufacturing tend to have a higher Shore A hardness than silicone, particularly those that are compatible with readily available printers, but they could offer an intermediate response between stiff plastic and silicone.

The addition of the skin/soft tissue simulant to the surrogate enables the assessment of cuts and laceration in sport, both from sports impact, and the interaction between sporting equipment and between sports surfaces. The addition of a bone surrogate would gain more knowledge on fractures and the injury mechanism, and would widen the field of work to health applications. A biofidelic surrogate utilising skin/soft tissue simulants and a bone surrogate could then be adapted to represent different demographics. By editing the volume of soft tissue and the density of the bone surrogate, a biofidelic surrogate representing an elderly population could be developed. This could gain knowledge on falls within the elderly, and the development of specific wrist protection to prevent wrist injuries in the elderly population. Furthermore, a child surrogate could be developed, with a suitable amount of soft tissue, and incorporation of growth plates on the bone surrogate. Senner *et al*. (2018) identified that the epiphyseal plate of the radius and ulna should be included in a wrist surrogate representing a child for assessing falls. This would improve the assessment of smaller sized wrist protectors, due to the more representative child surrogate incorporating growth plates which are not

present in adult models. This work could also be extended to other health applications such as disease related injuries.

Additional physiological data is required to develop such biofidelic surrogates, especially those which aim to represent a specific demographic. The surrogate developed in this study only consisted of a silicone outer layer representing a skin/soft tissue layer, defined from literature values, whereas data on muscle/soft tissue volume via MRI is required to ensure an appropriate amount of soft tissue simulant is incorporated into the surrogate. This would require forearm MRI scans from populations which fit within each of the different sized wrist protectors (small, medium, large). Furthermore, to develop surrogates for set demographics, scans would be required from adults over 60 (elderly population) and children ~9 years old (child population). Further physiological data on the soft tissue properties in the palm, such as the recent study by Spartacus *et al*. (2021), could further inform the biofidelity of the palmar region of the surrogate. To develop a suitable bone surrogate, MRI or CT scans of the forearm bones would be required to gain knowledge on typical bone density values for each population group. Bone density changes with age, and effects the mechanical properties of the bone (Smith and Smith, 2009), and thus it is important that the bone surrogate is representative of the specific population. Furthermore, for a child's bone surrogate, the growth plates would need to be considered as distal radial fractures can disrupt the growth plate (Whiting and Zernicke, 2008). The stiffness of the wrist joint during flexion and extension could be explored via a BIODEX or CYBEX machine, measuring the resistance torque of the wrist joint. This data could then be incorporated into the surrogate to develop the biofidelity of the joint. The novel surrogate elements developed in this project include the materials, surface friction/finish, instrumentation, and surrogate geometry enhancing previous published research within snowboarding wrist protectors. A skin and soft tissue simulant was incorporated to add compliance to the surrogate and also to improve the biofidelity of its surface friction. A potentiometer was incorporated into the impact surrogate for measuring wrist angles during testing, and pressure sensors were trialled for quantifying strap tightness and areas of high pressure during bend testing. The

geometry of the surrogate developed by Adams (2018) was improved by using a geometric surrogate geometry, with additions made to dimension a wrist joint which could achieve a suitable range of flexion / extension motion.

The action priority matrix from Chapter 2 has been updated following the developments made to the surrogate in this project (Figure 8-1). The ranking of current performance of the materials, surface finish/friction and geometry have all improved (shown by the red arrows in Figure 8-1). While pressure sensors were trailed for use on the surrogate for bend testing, providing novel findings and demonstrating potential, as these were not incorporated into the final surrogate (Appendix B Section 9.2), the ranking of the current performance of instrumentation did not change. It is envisaged that with some further work, embedding pressure sensors like those trialled in this project into a wrist surrogate could increase the ranking of the current performance of the instrumentation to about a four, while further work with pressure sensors with larger surface areas, or even the use of a bespoke pressure sensor/s, could increase the ranking above five. Further benefits could be achieved by incorporating a pressure sensor/s into the palm of the surrogate, to directly measure the loading of this region and to determine the effectiveness of any palmar padding in a wrist protector. Future surrogate developments should focus on further instrumentation, and further increasing the biofidelity of the surrogate by examining the stiffness of the wrist joint and the use of more soft tissue simulants and bone simulants.
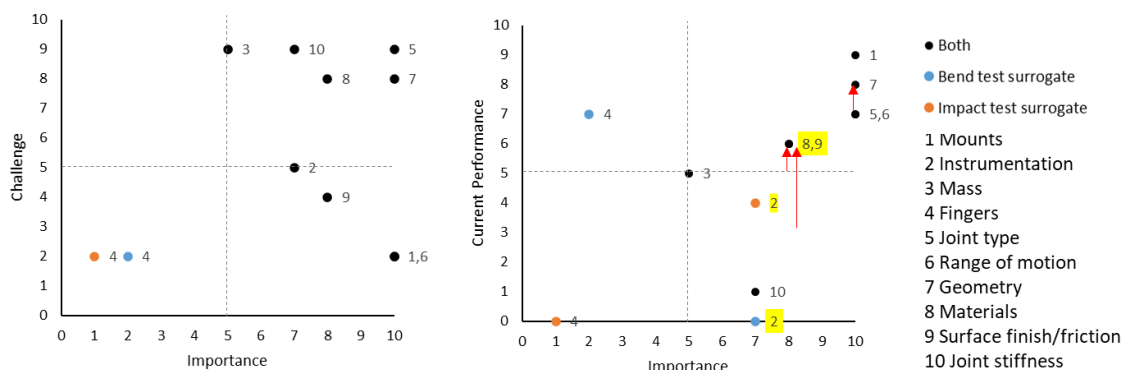
Figure 8-1 Action priority matrix of developed bend and impact test surrogate. Red arrows indicate the movement of surrogate elements 7, 8 and 9 due to the developments made in this project.

194

The surrogate developed here can easily be adapted to maintain relevance if the standard is revised. CAD was used to create the surrogate geometry, and thus dimensions can easily be edited in relation to any updates to the standard. Furthermore, CAD was used to edit the surrogate to allow for the silicone outer layer, and used to develop the hand and forearm moulds. Therefore, adaptions can be made to this outer layer, such as editing the thickness of this layer, or moulding a different material which a revised standard specifies. Other adaption to the standard may include the test procedures. The tensometer used in the bending stiffness test has a machine range of 5 to 500 mm/min, and thus if the loading rate of this test is edited within the standard, the machine speed can be adjusted accordingly, within this range. Moreover, the impact rig used for the basic linear impact test can be adjusted by setting a different drop height and mass, enabling a range of impact energies to be achieved, if the impact energy is edited within the standard.

8.7   Conclusions

This PhD thesis presented the development of a novel biofidelic wrist surrogate for assessing the performance of snowboarding wrist protectors. The biofidelic wrist surrogate was used to measure the stiffness of protectors in a bend test and the impact performance of the protectors in a pendulum impact test, relative to a comparable stiff surrogate. The novelty of this research is the incorporation of compliance to a wrist surrogate to increase its biofidelity, and the effect of compliance on the performance of snowboarding wrist protectors. Testing across the current state-of-the-art in snowboarding wrist protector tests identified trends between a quasi-static bend test and a pendulum impact test. Adjusting the loading rates and impact energies in BS EN ISO 20320:2020 could better align the conditions with more complex tests that are unsuitable for test houses. The findings of this research has provided guidance for the improvements of snowboarding wrist protector tests and certification protocols, alongside gaining knowledge on how biofidelic surrogates can be used to better assess injury risk.

References

Adams, C., James, D., Senior, T., Allen, T. and Hamilton, N., 2016. Development of a method for measuring quasi-static stiffness of snowboard wrist protectors. *Procedia engineering*, *147*, pp.378-383.

Adams, C., James, D., Senior, T., Allen, T. and Hamilton, N., 2018. Effect of surrogate design on the measured stiffness of snowboarding wrist protectors. *Sports Engineering*, *21*(3), pp.217-225.

Adams, C. (2018) *Evaluating the performance of snowboard wrist protectors. Doctor of Philosophy*. Sheffield Hallam University.

Adams, C., Allen, T., Senior, T., James, D. and Hamilton, N., 2021. Impact testing of snowboarding wrist protectors. *Proceedings of the Institution of Mechanical Engineers, Part P: Journal of Sports Engineering and Technology*, p.17543371211054752.

Alexander, H. and Miller, A.D., 1979. Determining skin thickness with pulsed ultra sound. *Journal of Investigative Dermatology*, *72*(1), pp.17-19.

Ankrah, S. and Mills, N.J., 2003. Performance of football shin guards for direct stud impacts. *Sports Engineering*, *6*(4), p.207.

Ankrah, S. and Mills, N.J., 2004. Analysis of ankle protection in Association football. *Sports Engineering*, *7*(1), pp.41-52.

Basques, B.A., Gardner, E.C., Samuel, A.M., Webb, M.L., Lukasiewicz, A.M., Bohl, D.D. and Grauer, J.N., 2018. Injury patterns and risk factors for orthopaedic trauma from snowboarding and skiing: a national perspective. *Knee surgery, sports traumatology, arthroscopy*, *26*(7), pp.1916-1926.

Bergeron, D.M., Coley, G.G., Rountree, M.S., Anderson, I.B. and Harris, R.M., 2001. *Assessment of foot protection against anti-personnel landmine blast using a frangible surrogate leg*. Canadian Centre for Mine Action Technologies.

Black, M.M., 1969. A modified radiographic method for measuring skin thickness. *British Journal of Dermatology*, *81*(9), pp.661-666.

Boone, D.C. and Azen, S.P., 1979. Normal range of motion of joints in male subjects. *JBJS*, *61*(5), pp.756-759.

Burbank, S.D. and Smith, L.V., 2012. Dynamic characterization of rigid foam used in finite element sports ball simulations. *Proceedings of the Institution of Mechanical Engineers, Part P: Journal of Sports Engineering and Technology*, *226*(2), pp.77-85.

Burkhart, T.A., Quenneville, C.E., Dunning, C.E. and Andrews, D.M., 2014. Development and validation of a distal radius finite element model to simulate impact loading indicative of a forward fall. *Proceedings of the Institution of Mechanical Engineers, Part H: Journal of engineering in medicine*, *228*(3), pp.258-271.

Chua, C.K., Yeong, W.Y. and An, J., 2017. 3D printing for biomedical engineering.

Clarys, J.P. and Marfell-Jones, M.J., 1986. Anthropometric prediction of component tissue masses in the minor limb segments of the human body. *Human Biology*, pp.761-769.

Crandall, J.R., Bose, D., Forman, J., Untaroiu, C.D., Arregui-Dalmases, C., Shaw, C.G. and Kerrigan, J.R., 2011. Human surrogates for injury biomechanics research. *Clinical anatomy*, *24*(3), pp.362-371.

Diffrient, N., Tilley, A. R. and Bardagjy, J. C. (1974) *Humanscale 1/2/3: a portfolio of information.* Vol. 1. MIT press.

Diridollou, S., Black, D., Lagarde, J.M., Gall, Y., Berson, M., Vabre, V., Patat, F. and Vaillant, L., 2000. Sex-and site-dependent variations in the thickness and mechanical properties of human skin *in vivo*. *International journal of cosmetic science*, *22*(6), pp.421-435.

Escoffier, C., de Rigal, J., Rochefort, A., Vasselet, R., Léveˆque, J.L. and Agache, P.G., 1989. Age-related mechanical properties of human skin: an *in vivo* study. *Journal of Investigative Dermatology*, *93*(3), pp.353-357.

Francisco, A.C., Nightingale, R.W., Guilak, F., Glisson, R.R. and Garrett Jr, W.E., 2000. Comparison of soccer shin guards in preventing tibia fracture. *The American journal of sports medicine*, *28*(2), pp.227-233.

Freutel, M., Schmidt, H., Dürselen, L., Ignatius, A. and Galbusera, F., 2014. Finite element modeling of soft tissues: material models, tissue interaction and challenges. *Clinical Biomechanics*, *29*(4), pp.363-372.

Frykman, G., 1967. Fracture of the distal radius including sequelae-shoulder–handfinger syndrome, disturbance in the distal radio-ulnar joint and impairment of nerve function: A clinical and experimental study. *Acta Orthopaedica Scandinavica*, *38*(sup108), pp.1-61.

Gardner, M.P., Chong, A.C., Pollock, A.G. and Wooley, P.H., 2010. Mechanical evaluation of large-size fourth-generation composite femur and tibia models. *Annals of biomedical engineering*, *38*(3), pp.613-620.

Gatt, I.T., Allen, T. and Wheat, J., 2020. Accuracy and repeatability of wrist joint angles in boxing using an electromagnetic tracking system. *Sports Engineering*, *23*(1), pp.1-10.

Giacobetti, F.B., Sharkey, P.F., Bos-Giacobetti, M.A., Hume, E.L. and Taras, J.S., 1997. Biomechanical analysis of the effectiveness of in-line skating wrist guards for preventing wrist fractures. *The American journal of sports medicine*, *25*(2), pp.223-225.

Giddins, G. and Giddins, H., 2021. Wrist and hand postures when falling and description of the upper limb falling reflex. *Injury*, *52*(4), pp.869-876.

Gislason, M.K., Nash, D.H., Nicol, A., Kanellopoulos, A., Bransby-Zachary, M., Hems, T., Condon, B. and Stansfield, B., 2009. A three-dimensional finite element model of maximal grip loading in the human wrist. *Proceedings of the Institution of Mechanical Engineers, Part H: Journal of Engineering in Medicine*, *223*(7), pp.849-861.

References

Greenwald, R.M., Janes, P.C., Swanson, S.C. and McDonald, T.R., 1998. Dynamic impact response of human cadaveric forearms using a wrist brace. *The American journal of sports medicine*, *26*(6), pp.825-830.

Greenwald, R.M., Simpson, F.H. and Michel, F.I., 2013. Wrist biomechanics during snowboard falls. *Proceedings of the Institution of Mechanical Engineers, Part P: Journal of Sports Engineering and Technology*, *227*(4), pp.244-254.

Halkon, B., Webster, J., Mitchell, S. and Mientjes, M., 2012. Development of a test methodology for the assessment of human impacts in sport. *Procedia engineering*, *34*, pp.813-818.

Halkon, B., Mitchell, S., Payne, T. and Carbo, J., 2014. Biomechanical measurements of human impacts in basketball. *Procedia engineering*, *72*, pp.214-219.

Hatamleh, M.M. and Watts, D.C., 2010. Mechanical properties and bonding of maxillofacial silicone elastomers. *Dental Materials*, *26*(2), pp.185-191.

Heiner, A.D., 2008. Structural properties of fourth-generation composite femurs and tibias. *Journal of biomechanics*, *41*(15), pp.3282-3284.

Hermann, A., Ostarhild, J., Mirabito, Y., Bauer, N. and Senner, V., 2020. Stretchable piezoresistive vs. capacitive silicon sensors integrated into ski base layer pants for measuring the knee flexion angle. *Sports Engineering*, *23*(1), pp.1-10.

Holzbaur, K.R., Murray, W.M., Gold, G.E. and Delp, S.L., 2007. Upper limb muscle volumes in adult subjects. *Journal of biomechanics*, *40*(4), pp.742-749.

Hughes, A., Driscoll, H. and Carre, M., 2021. Development of a simplified and biofidelic human shoulder surrogate for testing of padded clothing in rugby union. *European Society of Biomechanics Proceedings*

Humanetics. (2009) *Hybrid III 5th Female*. [Online] [Accessed September 2018] http://www.humaneticsatd.com/crash-test-dummies/frontal-impact/hiii-5f

Hrysomallis, C., 2009. Surrogate thigh model for assessing impact force attenuation of protective pads. *Journal of science and medicine in sport*, *12*(1), pp.35-41.

Idzikowski, J.R., Janes, P.C. and Abbott, P.J., 2000. Upper extremity snowboarding injuries: ten-year results from the Colorado snowboard injury survey. *The American journal of sports medicine*, *28*(6), pp.825-832.

Iivarinen, J.T., Korhonen, R.K., Julkunen, P. and Jurvelin, J.S., 2011. Experimental and computational analysis of soft tissue stiffness in forearm using a manual indentation device. *Medical engineering & physics*, *33*(10), pp.1245-1253.

Imam, S.A. (2021) *Analysing Efficacy of Padded Clothing in Rugby using Finite Element Analysis*. Doctor of Philosophy. Manchester Metropolitan University.

International Organization for Standardization (ISO). (2020) BS ISO EN 20320:2020 Protective Clothing for Use in Snowboarding—Wrist Protectors—Requirements and Test Methods.

International Organization for Standardization (ISO). (2003) BS EN 14120:2003+A1:2007. Protective Clothing—Wrist, Palm, Knee and Elbow Protectors for Users of Roller Sports Equipment—Requirements and Test Methods.

Jachowicz, J., McMullen, R. and Prettypaul, D., 2007. Indentometric analysis of *in vivo* skin and comparison with artificial skin models. *Skin Research and Technology*, *13*(3), pp.299-309.

Kalra, A., Lowe, A. and Al-Jumaily, A.M., 2016. Mechanical behaviour of skin: a review. *J. Mater. Sci. Eng*, *5*(4), p.1000254.

Kim, K.J., Alian, A.M., Morris, W.S. and Lee, Y.H., 2006. Shock attenuation of various protective devices for prevention of fall-related injuries of the forearm/hand complex. *The American journal of sports medicine*, *34*(4), pp.637-643.

Kim, S. and Lee, S.K., 2011. Snowboard wrist guards–use, efficacy, and design. *Bull NYU Hosp Jt Dis*, *69*(2), pp.149-57.

Kim, S., Endres, N.K., Johnson, R.J., Ettlinger, C.F. and Shealy, J.E., 2012. Snowboarding injuries: trends over time and comparisons with alpine skiing injuries. *The American journal of sports medicine*, *40*(4), pp.770-776.

Kwan, M., Cheng, C.L., Tang, W.T. and Rasmussen, J., 2010. Measurement of badminton racket deflection during a stroke. *Sports engineering*, *12*(3), pp.143-153.

Lehner, S., Geyer, T., Michel, F.I., Schmitt, K.U. and Senner, V., 2014. Wrist injuries in snowboarding–Simulation of a worst case scenario of snowboard falls. *Procedia Engineering*, 72, pp.255-260.

Leslie, G., Wang, W., Winwood, K., Liauw, C., Hamilton, N. and Allen, T., 2020. Effect of Surrogate Surface Compliance on the Measured Stiffness of Snowboarding Wrist Protectors. In *Multidisciplinary Digital Publishing Institute Proceedings* (Vol. 49, No. 1, p. 84).

Levangie, P. K. and Norkin, C. C. (2005) *Joint structure and function: a comprehensive analysis.* 4th ed., Philadelphia, PA: F.A. Davis Co.

Li, Z.M., Kuxhaus, L., Fisk, J.A. and Christophel, T.H., 2005. Coupling between wrist flexion–extension and radial–ulnar deviation. *Clinical biomechanics*, *20*(2), pp.177-183.

LSTC. (2018b) *LS-DYNA Keyword User's Manual-Volume-II Material Models.*

MacFarlane, M., Dyson, C., Douglas, M., Theobald, P. and Carre, M.J., 2022. Minimising Skin Injuries on Rugby Turf. International Sports Engineering Association – *Engineering of Sport*.

Marshall, M.M., Mozrall, J.R. and Shealy, J.E., 1999. The effects of complex wrist and forearm posture on wrist range of motion. *Human Factors*, *41*(2), pp.205-213.

Maurel, M.L., Fitzgerald, L.G., Miles, A.W. and Giddins, G.E., 2013. Biomechanical study of the efficacy of a new design of wrist guard. *Clinical biomechanics*, *28*(5), pp.509-513.

McIntosh, A.S., 2012. Biomechanical considerations in the design of equipment to prevent sports injury. *Proceedings of the Institution of Mechanical Engineers, Part P: Journal of Sports Engineering and Technology*, *226*(3-4), pp.193-199.

Mehta, S. and Nandeeshwar, D.B., 2017. A spectrophotometric analysis of extraoral aging conditions on the color stability of maxillofacial silicone. *The Journal of the Indian Prosthodontic Society*, *17*(4), p.355.

Micheau, A. and Hoa, D., 2017. MRI of the upper extremity anatomy–Atlas of the human body using cross-sectional imaging. In e-Anatomy. IMAIOS. [Online] [Accessed September 2018] https://www.imaios.com/en/e-Anatomy/Limbs/Upper-extremity-MRI

Michel, F.I., Schmitt, K.U., Greenwald, R.M., Russell, K., Simpson, F.I., Schulz, D. and Langran, M., 2013. White Paper: functionality and efficacy of wrist protectors in snowboarding—towards a harmonized international standard. *Sports Engineering*, *16*(4), pp.197-210.

Milne, R.D. and Davis, J.P., 1992. The role of the shaft in the golf swing. *Journal of biomechanics*, *25*(9), pp.975-983.

Miyatani, M., Kanehisa, H., Masuo, Y., Ito, M. and Fukunaga, T., 2001. Validity of estimating limb muscle volume by bioelectrical impedance. *Journal of Applied Physiology*, *91*(1), pp.386-394.

Mott, P.H., Dorgan, J.R. and Roland, C.M., 2008. The bulk modulus and Poisson's ratio of "incompressible" materials. *Journal of Sound and Vibration*, *312*(4-5), pp.572-575.

Myers, E.R., Sebeny, E.A., Hecker, A.T., Corcoran, T.A., Hipp, J.A., Greenspan, S.L. and Hayes, W.C., 1991. Correlations between photon absorption properties and failure load of the distal radius in vitro. *Calcified Tissue International*, *49*(4), pp.292-297.

Netter, F. H. (2014) *Atlas of human anatomy.* 25 anniversary;6th; ed., Philadelphia, PA: Saunders.

Newton-Mann, C. (2019) *Finite Element Modelling of Snowboarding Wrist Protectors*. Doctor of Physiology. Manchester Metropolitan University.

Newton-Mann, C., Winwood, K., Driscoll, H., Hamilton, N. and Allen, T., 2018. Finite element model of an impact on a palmar pad from a snowboard wrist protector. In *Multidisciplinary Digital Publishing Institute Proceedings* (Vol. 2, No. 6, p. 314).

NinjaTek. (2016) *Ninjaflex*. [Online] [Accessed September 2018] https://ninjatek.com/products/filaments/ninjaflex/

Nusser, M., Hermann, A. and Senner, V., 2016. Artificial knee joint and ski load simulator for the evaluation of knee braces and ski bindings. *Procedia engineering*, *147*, pp.220-227.

Olsen, L.O., Takiwaki, H. and Serup, J., 1995. High-frequency ultrasound characterization of normal skin. Skin thickness and echographic density of 22 anatomical sites. *Skin Research and Technology*, *1*(2), pp.74-80.

Oudshoorn, B., Driscoll, H., Dunn, M., Senior, T. and James, D., 2018. Development of a test method for assessing laceration injury risk of individual cleats during game-relevant loading conditions. *Footwear Science*, 10(1), pp.1-10.

Orsted, H.L., Keast, D.H., Forest-Lalande, L., Kuhnke, J.L., O'Sullivan-Drombolis, D., Jin, S., Haley, J. and Evans, R., 2017. Skin: anatomy, physiology and wound healing. *Foundations of Best Practice for Skin and Wound Management. A supplement of Wound Care Canada*.

Payne, T., Mitchell, S.R., Bibb, R.J. and Waters, M., 2014. Initial validation of a relaxed human soft tissue simulant for sports impact surrogates.

Payne, T. (2015) *Improved human soft tissue thigh surrogates for superior assessment of sports personal protective equipment.* Doctor of Physiology. Loughborough University.

Payne, T., Mitchell, S., Bibb, R. and Waters, M., 2015. Development of novel synthetic muscle tissues for sports impact surrogates. *Journal of the mechanical behavior of biomedical materials*, *41*, pp.357-374.

Payne, T., Mitchell, S., Bibb, R. and Waters, M., 2015. The evaluation of new multi-material human soft tissue simulants for sports impact surrogates. *Journal of the mechanical behavior of biomedical materials*, *41*, pp.336-356.

Payne, T., Mitchell, S., Halkon, B., Bibb, R. and Waters, M., 2016. Development of a synthetic human thigh impact surrogate for sports personal protective equipment testing. *Proceedings of the Institution of Mechanical Engineers, Part P: Journal of Sports Engineering and Technology*, *230*(1), pp.5-16.

PEEBLES, L., & NORRIS, B. (1998). *Adultdata: the handbook of adult anthropometric and strength measurements - data for design safety*. London, Open Ergonomics.

Petrone, N., Carraro, G., Castello, S.D., Broggio, L., Koptyug, A. and Bäckström, M., 2018. A novel instrumented human head surrogate for the impact evaluation of helmets. In *Multidisciplinary Digital Publishing Institute Proceedings* (Vol. 2, No. 6, p. 269).

Pheasant, S. and Haslegrave, C.M., 2018. *Bodyspace: Anthropometry, ergonomics and the design of work*. CRC press.

Pugh, A.W., Hamilton, R., Nash, D.H. and Otto, S.R., 2010. Characterization of the materials in golf ball construction for use in finite element analysis. *Procedia Engineering*, *2*(2), pp.3231-3236.

Qiu, K., Haghiashtiani, G. and McAlpine, M.C., 2018. 3D printed organ models for surgical applications. *Annual Review of Analytical Chemistry*.

Ranga, D. and Strangwood, M., 2010. Finite element modelling of the quasi-static and dynamic behaviour of a solid sports ball based on component material properties. *Procedia Engineering*, *2*(2), pp.3287-3292.

Richardson, J.T., 2011. Eta squared and partial eta squared as measures of effect size in educational research. *Educational research review*, *6*(2), pp.135-147.

Robinson, P.G., Duckworth, A.D. and Campbell, D.A., 2021. Acute Fractures in Sport: Wrist. In *Fractures in Sport* (pp. 155-174). Springer, Cham.

References

Roh, S., Parekh, D.P., Bharti, B., Stoyanov, S.D. and Velev, O.D., 2017. 3D printing by multiphase silicone/water capillary inks. *Advanced Materials*, *29*(30), p.1701554.

Ruznan, W.S., Laing, R.M., Lowe, B.J. and Wilson, C.A., 2018. Impact attenuation provided by shin guards for field hockey. *Sports Engineering*, *21*(3), pp.161-175.

Sawbone. (2005) *Catalog*. [Online] [Accessed September 2018] https://www.sawbones.com/products.html

Schmitt, K.U., Michel, F.I. and Staudigl, F., 2011, September. Analysing the impact behaviour of recent snowboarding wrist protectors. In *Ircobi Conference* (pp. 51-61).

Schmitt, K.U., Wider, D., Michel, F.I., Brügger, O., Gerber, H. and Denoth, J., 2012. Characterizing the mechanical parameters of forward and backward falls as experienced in snowboarding. *Sports biomechanics*, *11*(1), pp.57-72.

Senner, V., Lehner, S., Michel, F.I. and Brügger, O., 2018. Modelling and simulation to prevent overloads in snowboarding. In *Modelling and simulation in sport and exercise* (pp. 211-236). Routledge.

Shepherd, T., Winwood, K., Venkatraman, P., Alderson, A. and Allen, T., 2020. Validation of a finite element modeling process for auxetic structures under impact. *physica status solidi (b)*, *257*(10), p.1900197.

Shultz, S. J., Houglum, P. A. and Perrin, D. H. (2010) *Examination of musculoskeletal injuries.* 3rd ed., Leeds: Human Kinetics.

Slack, N., 1994. The importance-performance matrix as a determinant of improvement priority. *International Journal of Operations & Production Management*.

Smith, C.B. and Smith, D.A., 1976. Relations between age, mineral density and mechanical properties of human femoral compacta. *Acta Orthopaedica Scandinavica*, 47(5), pp.496-502.

Spadaro, J.A., Werner, F.W., Brenner, R.A., Fortino, M.D., Fay, L.A. and Edwards, W.T., 1994. Cortical and trabecular bone contribute strength to the osteopenic distal radius. *Journal of orthopaedic research*, *12*(2), pp.211-218.

Spartacus, V., Shojaeizadeh, M., Raffault, V., Shoults, J., Van Wieren, K. and Sparrey, C.J., 2021. In vivo soft tissue compressive properties of the human hand. *Plos One*, 16(12), pp 1-18.

Stahn, A., Terblanche, E. and Strobel, G., 2007. Modeling upper and lower limb muscle volume by bioelectrical impedance analysis. *Journal of applied physiology*, *103*(4), pp.1428-1435.

Stone, B., Mitchell, S., Miyazaki, Y., Peirce, N. and Harland, A., 2021. A destructible headform for the assessment of sports impacts. *Proceedings of the Institution of Mechanical Engineers, Part P: Journal of Sports Engineering and Technology*, p.17543371211055905.

Stratasys. (2017) *Our Materials*. [Online] [Accessed September 2018] http://www.stratasys.com/materials/search

Sullivan, G.M. and Feinn, R., 2012. Using effect size—or why the P value is not enough. *Journal of graduate medical education*, *4*(3), pp.279-282.

Syndaver. (2020) *Catalog.* [Online] [Accessed January 2020] https://syndaver.com/product-category/tissue-pads-plates/

Tan, C.Y., Statham, B., Marks, R. and Payne, P.A., 1982. Skin thickness measurement by pulsed ultrasound; its reproducibility, validation and variability. *British Journal of Dermatology*, *106*(6), pp.657-667.

Tekscan. (2015*) Products for Pressure Mapping and Force Measurement*. [Online] [Accessed September 2018] https://www.tekscan.com/products-solutions

Tilley, A. R. (2002) *The measure of man and woman: human factors in design.* Vol. 1. John Wiley & Sons.

Turner, J., Forrester, S.E., Mears, A.C. and Roberts, J.R., 2020. Reliability of repeat golf club testing sessions with modified club moment of inertia. *Sports Engineering*, *23*(1), pp.1-9.

Vidt, M.E., Daly, M., Miller, M.E., Davis, C.C., Marsh, A.P. and Saul, K.R., 2012. Characterizing upper limb muscle volume and strength in older adults: a comparison with young adults. *Journal of biomechanics*, *45*(2), pp.334-341.

Villwock, M.R., Meyer, E.G., Powell, J.W. and Haut, R.C., 2009. Development and evaluation of a surrogate ankle for use with a rotational traction measurement apparatus. *Proceedings of the Institution of Mechanical Engineers, Part P: Journal of Sports Engineering and Technology*, *223*(4), pp.151-158.

Vilhena, L. and Ramalho, A., 2016. Friction of human skin against different fabrics for medical use. *Lubricants*, 4(1), p.6.

Walilko, T.J., Viano, D.C. and Bir, C.A., 2005. Biomechanics of the head for Olympic boxer punches to the face. *British journal of sports medicine*, *39*(10), pp.710-719.

Weisang. (2018) *CFC Filter Analysis Object (Digital Filters Option).* FlexPro Documentation. [Online] [Accessed on 1st Nov] https://www.weisang.com/en/documentation/cfcfilteranalysis_en/

Whiting, W. C. and Zernicke, R. F. (2008) *Biomechanics of musculoskeletal injury.* 2nd ed., Leeds: Human Kinetics.

Yamauchi, K., Wakahara, K., Fukuta, M., Matsumoto, K., Sumi, H., Shimizu, K. and Miyamoto, K., 2010. Characteristics of upper extremity injuries sustained by falling during snowboarding: a study of 1918 cases. *The American Journal of Sports Medicine*, *38*(7), pp.1468-1474.

Zapata, E., Rongieras, F., Pialat, J.B., Follet, H. and Mitton, D., 2017. An *ex vivo* experiment to reproduce a forward fall leading to fractured and non-fractured radii. *Journal of biomechanics*, 63, pp.174-178.

9. <u>Appendices</u>

9.1 Appendix A: Obtaining stress vs. strain relations from impact data - Chapter 2

Impact tests were carried out on the cylindrical silicone compression samples at 1, 1.5, 2 and 2.5 J. A polynomial trend line was fitted to the raw force vs. time data (up to peak force) (Figure 9-1a), and the trendline was used to obtain smoothed temporal force. The smoothed temporal force was then converted to temporal acceleration, by dividing the force at each time increment (0.1 ms) by the mass of the dropper (2.5 kg). Multiplying acceleration by the time increment generated a value for the change in velocity at each time increment (Figure 9-1b). The velocity on impact was estimated (based on the potential energy of the dropper at the release height) and used to find the velocity of the dropper at each time increment (Figure 9-1c). Multiplying the velocity data by the time increment generated change in displacement values, which were used to calculate the total displacement of the dropper. Force vs. displacement was plotted (Figure 9-1d) and used to generate engineering stress vs. strain data (Figure 9-1e), using the measured dimensions of the sample. Strain was plotted against time and the strain rate of the sample was estimated from the gradient of the linear trend line fitted to the data (Figure 9-1f). The displacement vs. time data (Figure 9-1g) was used to estimate maximum displacement, using the time to maximum displacement from the high-speed camera footage.
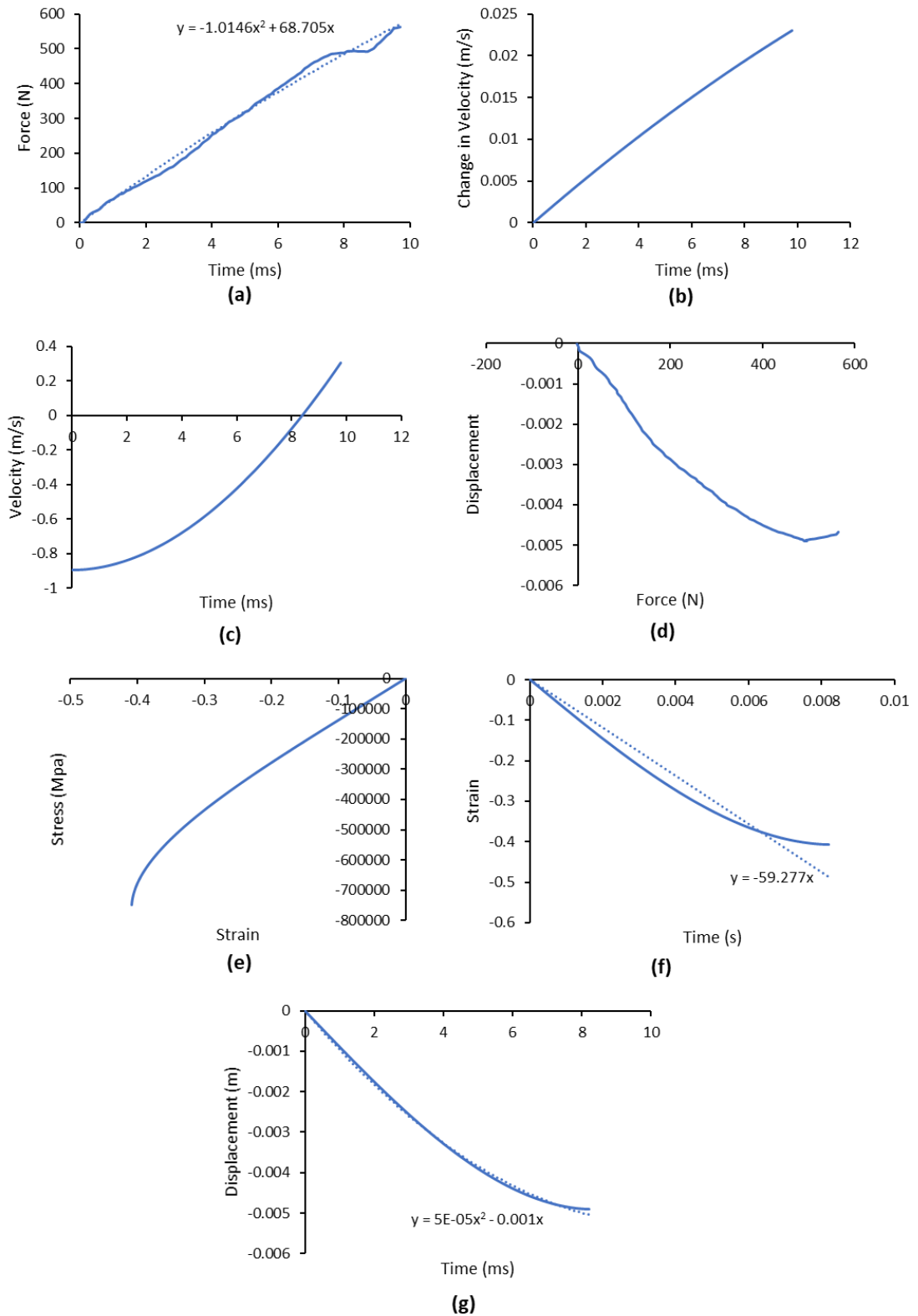
Figure 9-1 (a) force vs. time, (b) change in velocity vs. time, (c) velocity vs. time, (d) force vs. displacement, (e) stress vs. strain, (f) strain vs. time (to obtain strain rate), (g) time vs. displacement plots for the impact testing of compressive silicone samples.

9.2 Appendix B: Pressure sensor study - Chapter 3

Flexiforce pressure sensors (A201, Tekscan Inc, South Boston, USA) were trialled to measure protector strap tightness, pressure at specific points along the forearm during bend testing, and pressure on the palm during impact testing. The sensors were 191.0 × 14.0 mm and 0.2 mm thick, with a circular sensing area of 9.5 mm diameter. The thinness and flexibility of the sensors allows them to be placed on or under the silicone layer on the surrogate, and furthermore, the sensors were coupled with a quickstart board which allows a 'plug and play' approach (FlexiForce™ Quickstart Board). The sensors are available in three force ranges (4.4 N (0 - 1 lb), 111 N (0 - 25 lb), 445 N (0 - 100 lb)) and the resistance can be adjusted by a potentiometer on the quickboard. The trial studies below each use sensors with a different force range.

The pressure sensors were connected to the quickboard, and connected via BNC cable to a picoscope (picoscope, Picotech 4824). The sensors were calibrated by placing a cylindrical puck (from the supplier - 7.1 mm diameter, 0.7 mm thick) over the sensor area, and either placing a known mass on the sensor or using the tensometer to apply a set force on the sensor, and recording the voltage output. Output voltage and the applied force were plotted and a linear trendline was fitted. When analysing pressure data, the equation of the trendline was used to convert the output voltage from the sensor to force.

When trialling the sensors for use in the bend test, it was found that the uneven contact between the protector and surrogate, coupled with their low thickness, caused an issue, as they needed to be in a specific place to register force values. It was difficult to consistently achieve contact between the sensor and both the protector and the surrogate, and thus it was difficult to consistently register forces.

Placing the sensors under, rather than over, the silicone, may have meant that the silicone helped distribute the force from the protector, which could then be more easily registered by the sensor. The sensors appeared to work better underneath the silicone and thus this approach was used.

Trial study 1 involved placing three sensors (4.4 N force range) along the dorsal side of the forearm (~15 mm apart), close to the joint (Figure 9-2). The short and long wrist protectors were tested in the bend test at the three strapping conditions (loose, moderate, tight, set using the marked lines as per Chapter 4 Section 4.4.2). Images of the trialled sensor locations, alongside the temporal force obtained from the sensors and the wrist angle during these tests are presented in Figure 9-2. Higher force values were recorded on the sensors for the short protector than for the long protector. Indeed, when testing with the short protector, the sensors appear to be reaching their force limit of 4.4 N (horizontal line in force trace). As expected, force increased as the wrist extended. It was interesting to see that the sensors started to read increasing force values from about 50 to 60° wrist extension. As protector strap tightness increased, force typically increased. Higher forces were typically observed for the upper sensor (sensor 1) when testing the short protector, whereas higher forces were observed on the lower sensor (sensor 3) when testing the long protector.
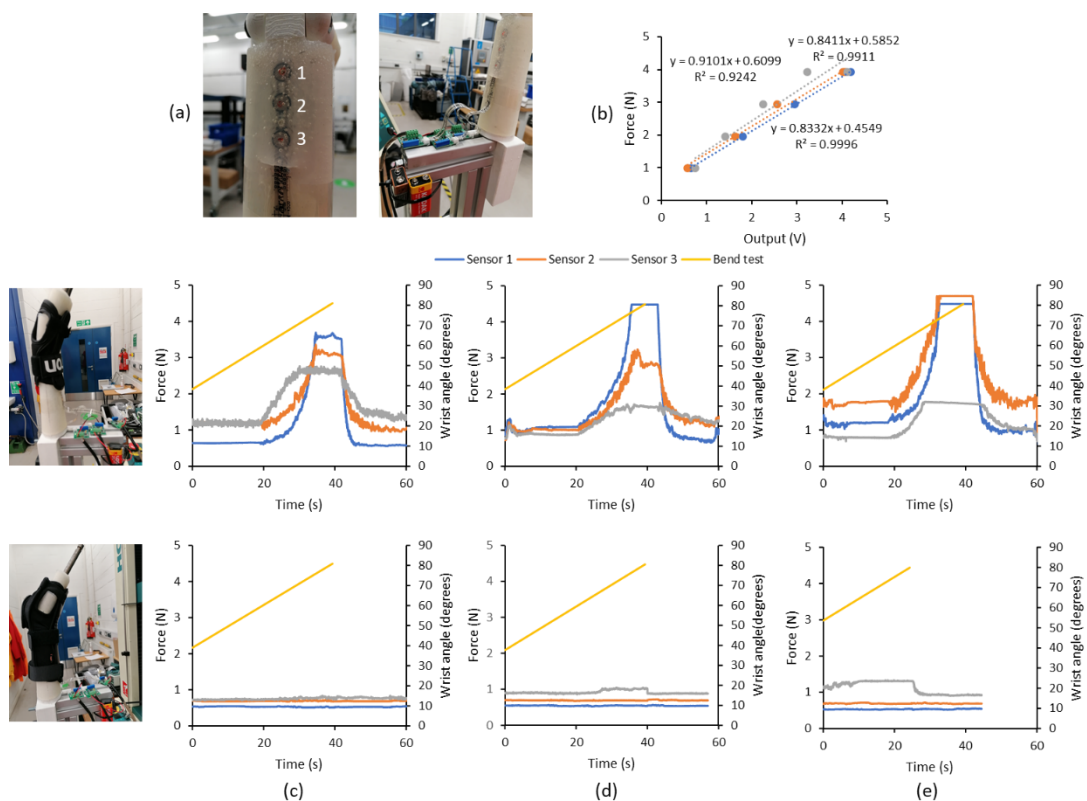
Figure 9-2 Trial study 1: using three pressure sensors to measure force at specific points along the forearm during bend testing of a short (top graphs) and long (bottom graphs) wrist protector. (a) shows the location of the sensors (~15 mm apart), (b) shows the sensor calibration plot. The temporal force for each sensor is plotted

alongside the temporal wrist angle of the surrogate during bend testing at (c) loose, (d) moderate and (e) tight strapping condition.

Trial study 2 involved reducing the number of sensors along the dorsal side of the forearm from three to two, with one close to the joint and the other towards at the lower end of the protector (~45 mm apart for the short protector and ~110 mm apart for the long protector) (i.e. sensor placement more specific to the protector tested) (Figure 9-3). The sensors in this study had a higher force range (111 N force range) as they were exceeding the maximum in the previous trial. The short and long wrist protectors were tested in the bend test at moderate strapping condition, and three repeats were conducted. Although similar force values for each sensor were obtained between repeats, no clear trends between wrist angle and force were observed. The sensor lower down the forearm (sensor 2) tended to show higher force values than the one located closer to the wrist joint (sensor 1). This result may be due to the location of the lower sensor in relation to the protector straps (i.e. the bottom sensor for the long protector was directly under the long protector's bottom strap).
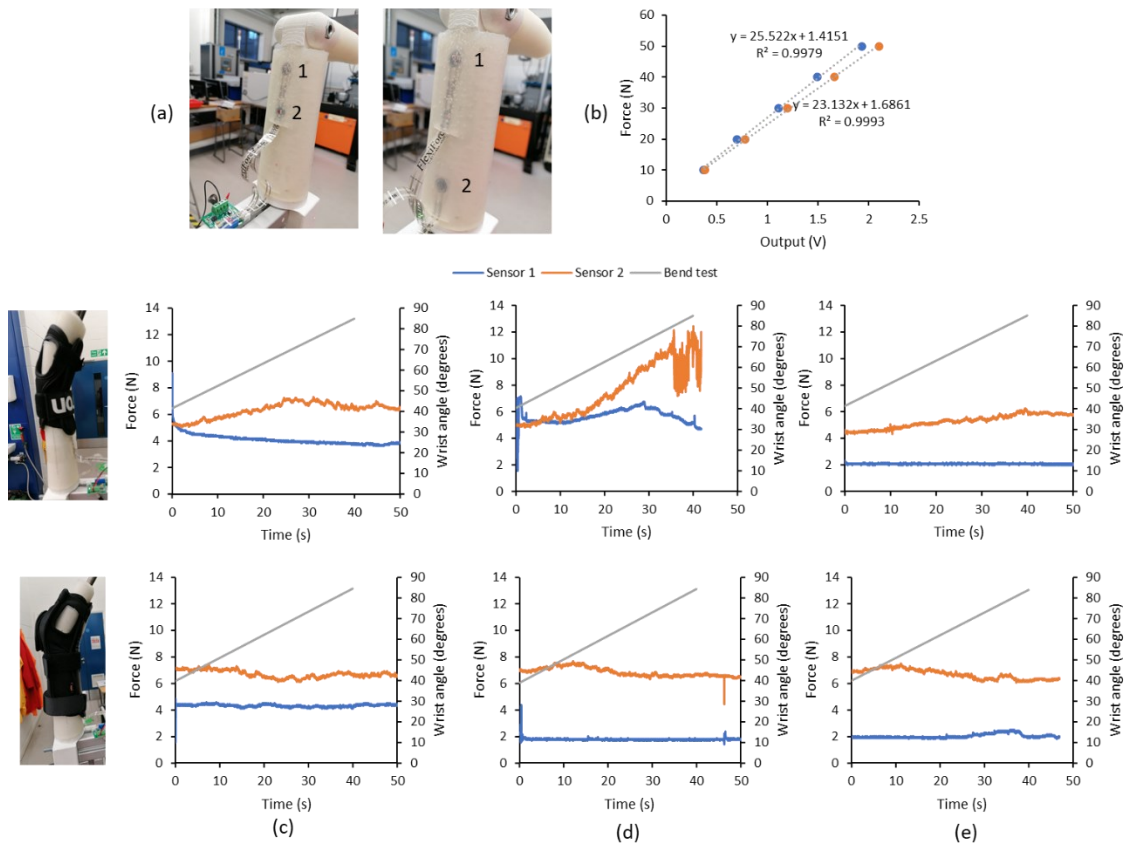
Figure 9-3 Trial study 2: using two pressure sensors to measure force at specific points on the forearm during bend testing of a short (top graphs) and long (bottom graphs) wrist protector. (a) shows the location of the sensors (~45 mm apart for the short protector and ~110 mm apart for the long protector), (b) shows the sensor calibration. The temporal force for each sensor is plotted alongside the temporal wrist angle of the surrogate during bend testing at moderate strapping condition for (c) test one, (d) repeat two and (d) repeat three.

The sensors were also trialled for use in an impact test on the palm of the surrogate (Trial study 3). A sensor (445 N force range) was placed under the silicone layer (3 mm thick) on the palm of the surrogate hand. The surrogate hand was fixed to the base plate of the impact rig (a bracket attached to the wrist joint and bolted to the base plate) and impacted with a flat dropper (at 1.6 J) and a hemispherical dropper (at 0.5 J) (Figure 9-4). An image of the impact setup, alongside the temporal force of the sensor and load cell (in the force plate) are displayed in Figure 9-4. When impacted with the flat dropper, little to no force was registered by the sensor. Due to the curvature of the palm and low impact energy, the flat dropper may have struck the sides of the hand, with little contact directly over the region of the sensor. When impacted with the hemispherical dropper, a peak force of ~150 N was registered by the sensor, which was about a third of the value from the load cells.
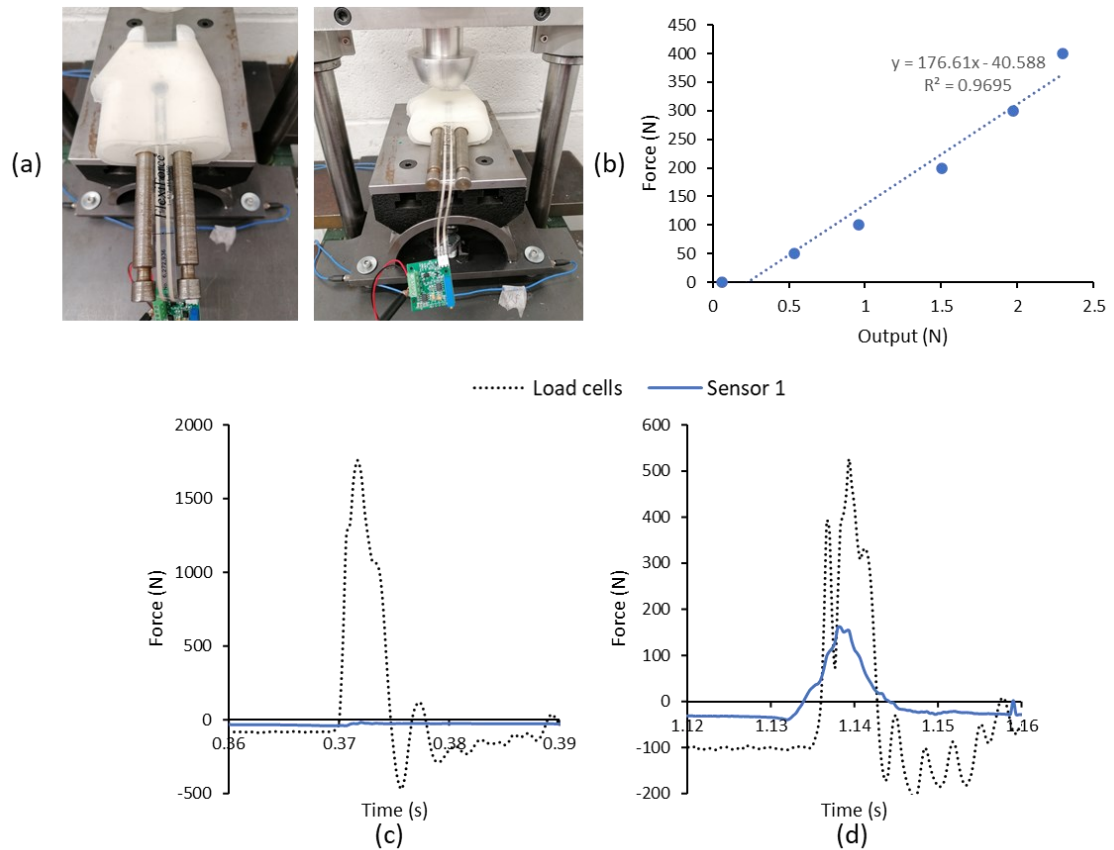
Figure 9-4 Trial study 3: impact testing one sensor located on the surrogate palm under the 3 mm thick silicone layer, at 1.6 J with a flat dropper and 0.5 J with a hemispherical dropper. (a) shows the location of the sensor and test setup with hemispherical dropper. (b) shows the sensor calibration. The temporal force for the sensor and force plate is plotted for the (c) flat dropper and (d) hemispherical dropper.

The bend test and impact test trials indicate that sensor position is important and can influence results. Placing three sensors in a row along the forearm for the bend test gave more insightful results than placing two sensors at specific positions on the surrogate forearm, however the force range of the sensors differed between studies, so further work should be conducted to confirm this. Due to the variability in force results obtained from these trial studies, it was decided that pressure sensors would not be incorporated into the wrist surrogate within this project. Further work is required to determine the suitability of these sensors in the wrist surrogate.

Future work could look at placing more sensors along the forearm of the surrogate and conducting further tests to determine the repeatability of results from them when used in the bend test. Another approach could be to use larger flexiforce sensors or a bespoke flexiforce sensor designed specifically for use on the

surrogate. Pressure mapping sensors could also be used to identify areas of high pressure on the forearm, which could then inform the location of individual flexiforce sensors or the design of a bespoke flexiforce sensor.

9.3   Appendix C: Torque values from the bend test repeatability study - Chapter 4

The torque values at 75° wrist extension for each test on test days 2 and 3, for the short and long protectors, are shown in Figure 9-5. These results are presented here to show the fluctuation of torque values between test repeats.
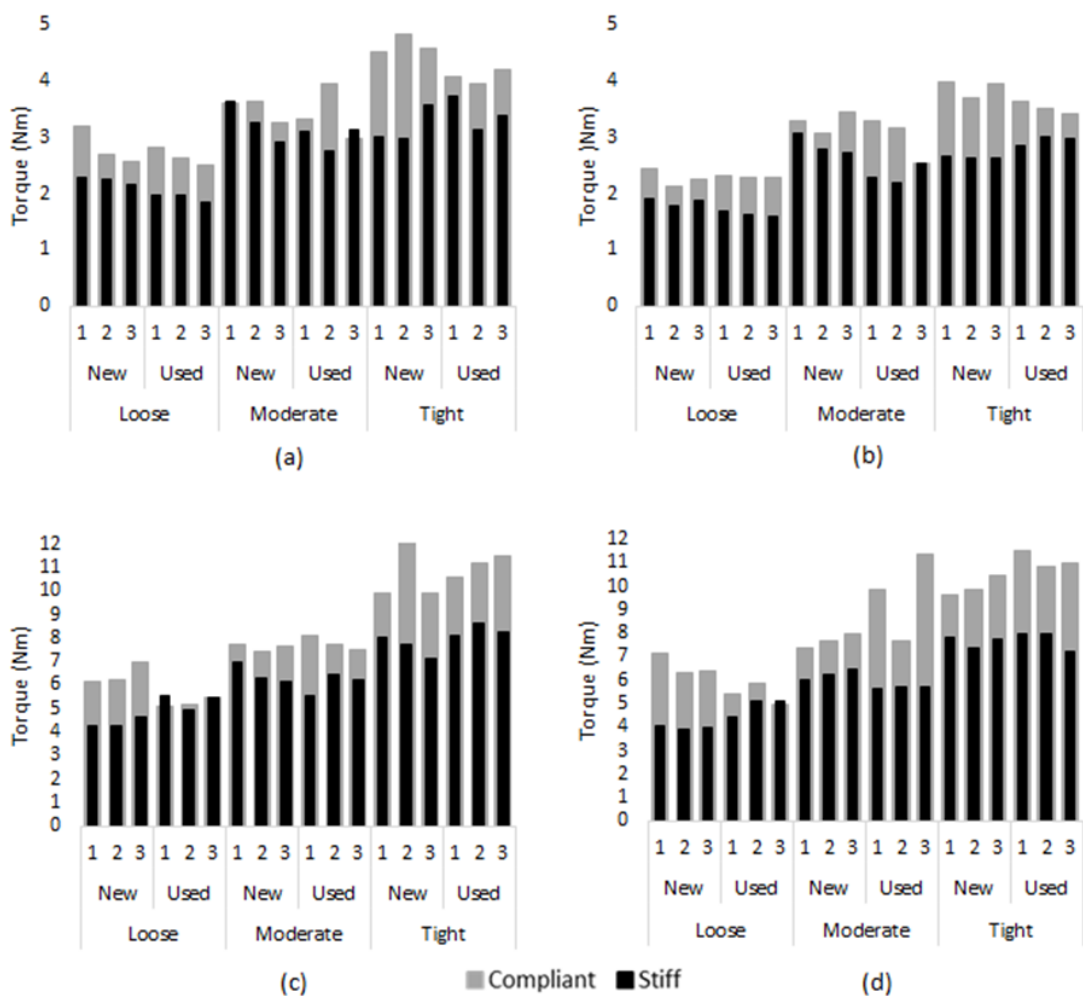
Figure 9-5 Torque at 75° wrist extension for (a) short protector test day 2, (b) short protector test day 3, (c) long protector test day 2, (d) long protector test day 3.

9.4 Appendix D: Statistical analysis

9.4.1 Protector slippage from bend test repeatability study - Chapter 4

Statistical analysis of protector slippage between the stiff and compliance surrogate was performed as per Chapter 4 Section 4.4.3. No significant differences were found between the measured slippage between surrogates at each slippage location (Table 9-1). All cases had a small to medium effect size.

Table 9-1 Statistical test results and effect sizes between surrogates for protector slippage.

Protector	Slippage location	p-value	Effect Size
		Compliant-Stiff	
Short	Dorsal top	0.091	0.008 (small)
	Dorsal bottom	0.174	-0.099 (small)
Long	Top strap	0.140	0.653 (medium)
	Bottom strap	0.152	0.728 (medium)
	Dorsal bottom	0.266	0.391 (small)

9.4.2 Shore A hardness of the silicone - Chapter 6

The Shore A hardness values across the eight points measured on the compliant surrogate were analysed at a significance level of $p < 0.05$, using Minitab. One way ANOVA was used to assess significant differences between the measurements taken after moulding, before testing and after testing. Post hoc analysis was carried out using Tukey pairwise comparison. Effect sizes were calculated as per Section 9.4.1. Significant differences were found between Shore A hardness measurements taken before testing and after moulding, and after testing and after moulding (Table 9-2). All cases had a small to medium effect size.

Table 9-2 Significance test results and effect sizes between test day for Shore A hardness measurements of the compliant surrogate.

	p-value	Effect size
Before testing - After moulding	0.000*	0.000 (small)
After testing - After moulding	0.000*	0.423 (small)
After testing - Before testing	0.934	0.786 (medium)

9.4.3 Protector slippage from pendulum impact study

The measurements of protector slippage between the stiff and compliant surrogate were compared using two-sample t-tests, at a significance level of $p < 0.05$, using Minitab. Effect sizes were calculated as per Section 9.4.1.

9.5 Appendix E: FE modelling - Chapter 5

9.5.1 Dependency and sensitivity studies

To determine a suitable coefficient of friction for use for the contacts between the surfaces in the FE model, a sensitivity study was conducted using coefficient of friction values of 0.1 to 0.6, in 0.1 increments (Figure 9-6a). With a coefficient of friction of 0.1, 0.2 and 0.3, the force vs. time plot showed some fluctuations, whereas at a coefficient of 0.4, the plots were smoother. The results plateau after a coefficient of 0.4, and therefore a coefficient of 0.4 was selected.

To determine a suitable mesh element size, a mesh sensitivity study was performed to determine its effect on total deformation (Figure 9-6b). The default mesh element size was 6.0 mm, creating a total deformation of 4.75 mm. Mesh element size was then reduced in 1.0 mm increments. The total deformation plateaued at 1.1 mm mesh element size, although the difference in total deformation was only 1.24 mm (26%) relative to 6.0 mesh size, whereas the number of elements was increased by ~12,000 (393%). Increasing the number of elements by 10,000 would drastically increase the run time, which would be unnecessary for a ~1 mm (26%) difference in total deformation. A 2 mm mesh element size was deemed sufficient as it increased the total deformation by 0.60 mm (13%) and only increased the number of mesh elements by ~3,500.

To determine the effect of the Poisson's ratio of the silicone on temporal impact force, a study was conducted with values of Poisson's ratio ranging from 0.45 to 0.49, in 0.01 increments. A mean Poisson's ratio of 0.48 was measured by DIC for the silicone sample in tension (Chapter 3 Section 3.3), however it was found that a Poisson's ratio of 0.49 (closer to incompressible 0.5) increased peak force (Figure 9-6c), bringing it closer to the experimental data.
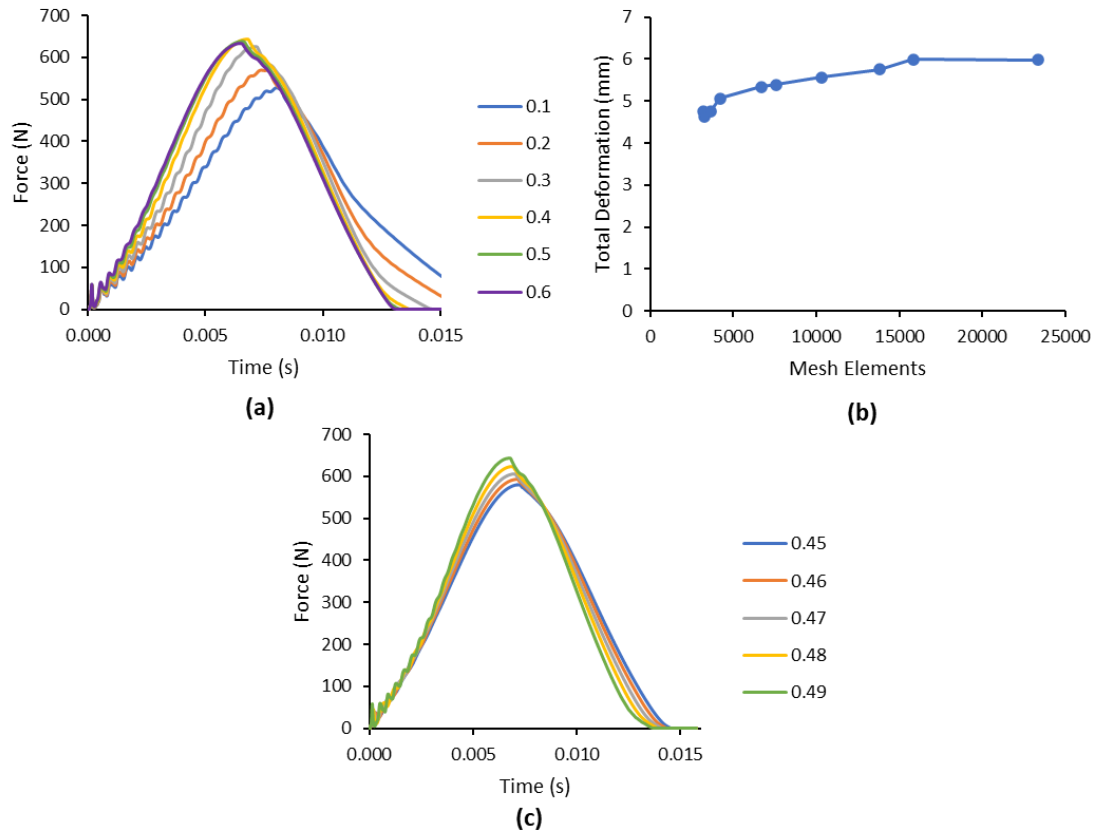
Figure 9-6 FE model sensitivity studies, (a) coefficient of friction between contacts, (b) mesh dependency, (c) Poisson's ratio.

9.5.2   Prony series

A Prony series was calculated from the stress relaxation data (Chapter 3 Section 3.3) to add time-dependent properties to the material model. When such Prony coefficients (α1 0.0478 MPa, α2 0.0375 MPa, α3 0.6976 Mpa, t1 0.3976, t2 6.7938, t3 0.0167) were added to the hyperelastic data in the material model, the force was overpredicted, compared to the experiment. Figure 9-7 shows an example for a 1 J impact. A Prony series was, therefore, not included in the final silicone material model, which only contained the hyperelastic data.
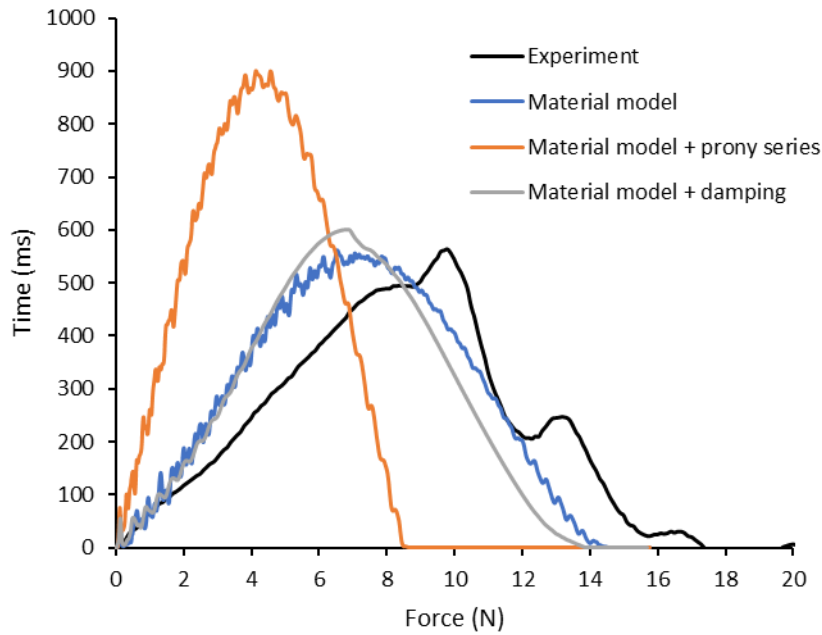
Figure 9-7 Force vs. time of a 1 J impact, comparing the experiment with the material model (containing only the hyperelastic data), the material model with a Prony series, and the material model with damping.

9.5.3 Palmar pad validation

The palmar pad model from Newton-Mann *et al*. (2018) consisted of a pad and shell. The pad was assigned a density of 64 kg/m3 and a Poisson's Ratio of 0.44. The material model for the pad consisted of an Ogden 1st order (μ_1 31512 Pa, α_1 5.319) combined with a 2 term Maxwell Prony Series (α_1 0.2075 MPa, α_2 0.1035 MPa, t1 0.2166, t2 4.6658). The shell was assigned a density of 970 kg/m3, Young's Modulus of 0.3 GPa and a Poisson's Ratio of 0.4. The palmar pad (pad and shell) material models were input into the FE model of a 2.5 J impact, and force vs. time data from the FE model was plotted alongside data from an experimental test and the model results from Newton-Mann *et al*. (2018) (Figure 9-8). FE models of the pad with a 3 and 5 mm thick silicone sample were also conducted, and compared to experimental tests.
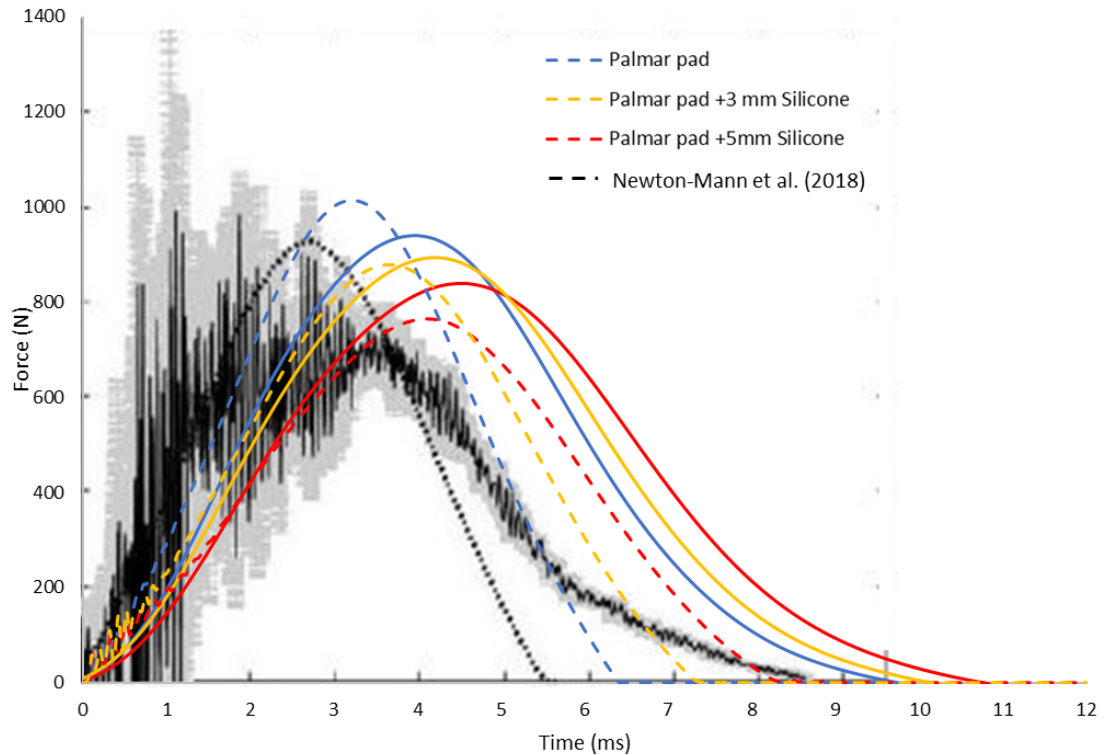
Figure 9-8 Force vs. time of the palmar pad FE model (dashed lines) compared to experiment data (solid lines), against results from Newton-Mann et al (2018), all of a 2.5 J impact. The data from Newton-Mann et al (2018) indicates the FE model and experiment (mean and standard deviation of 5 impacts).

9.5.4   Validation of the FE model

For validation of the FE model of silicone thicknesses of 1 to 10 mm impacted on a flat, hemisphere and palm anvil, experimental impacts of silicone thicknesses of 5, 8 and 10 mm on the three anvils was conducted using the bespoke drop rig (Section 3.2.2.2). Force vs. time data was compared between the FE model and experiments for 4 and 10 J impacts (Figure 9-9). Reasonable agreement was shown between the FE model and experiment across the three silicone thicknesses and anvils.
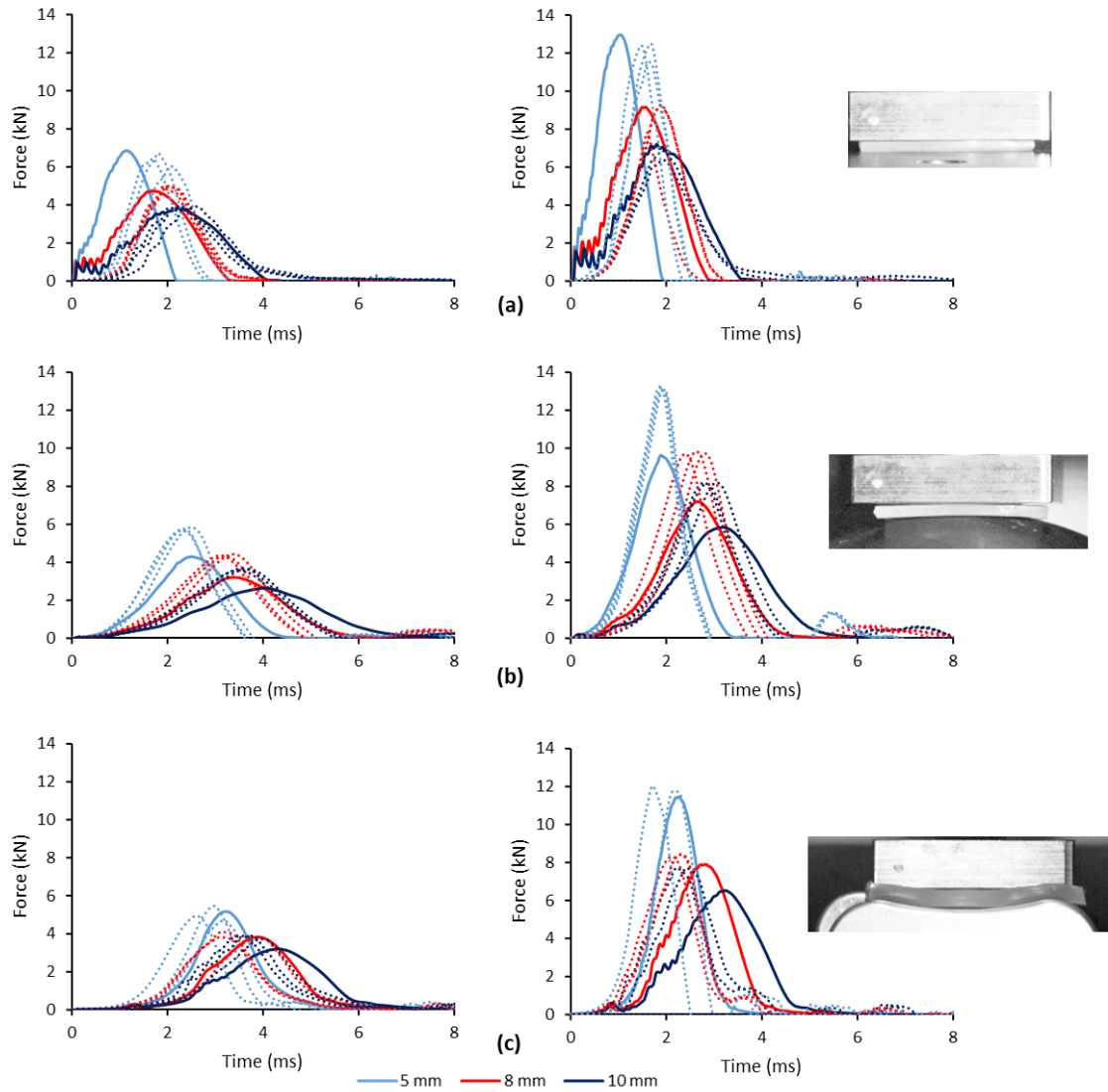
Figure 9-9 Force vs. time results for a FE model (solid lines) compared to experiment (dotted lines) for 5, 8 and 10 mm silicone sample impacted on (a) flat anvil, (b) hemisphere anvil, (c) palm anvil at 4 J (left) and 10 J (right).

9.6   Appendix F: Compliant impact surrogate - Chapter 6

9.6.1   Silicone moulding process

The silicone moulding process for the compliant impact surrogate was as per

Chapter 4 Section 4.3 (Figure 9-10).
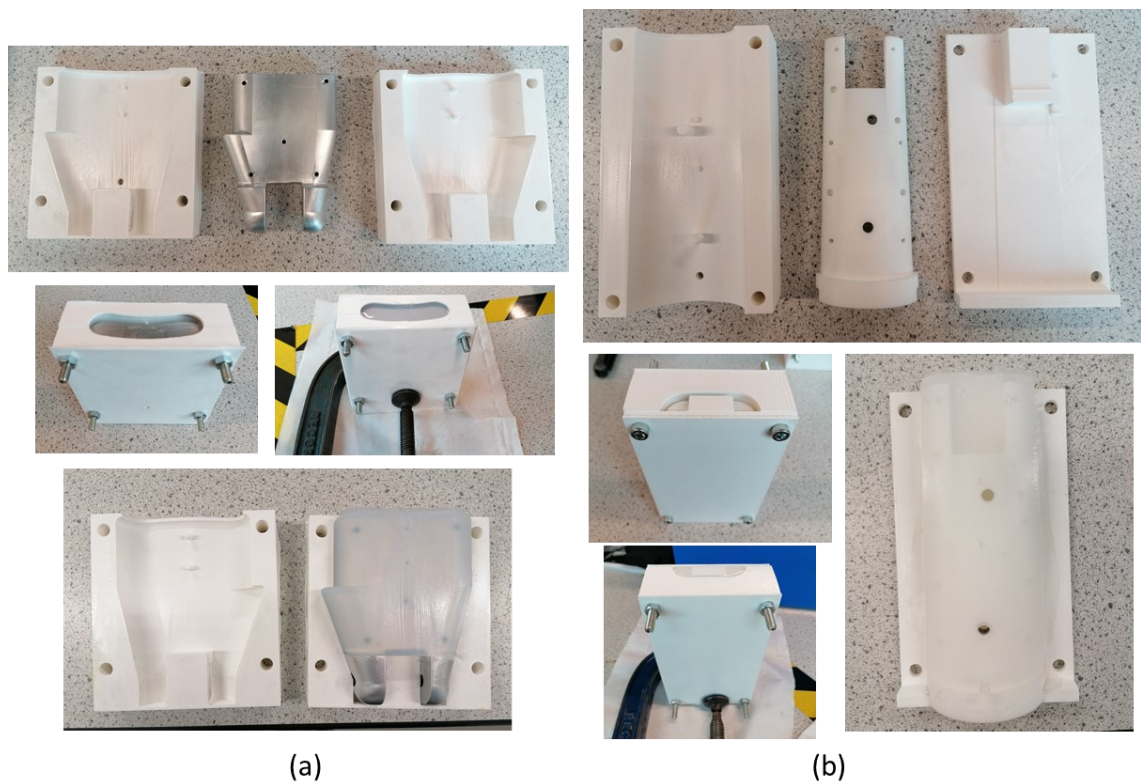
Figure 9-10 Moulding of silicone around the (a) hand core and (b) forearm casing core.

9.6.2 Assembly procedure

The assembly procedure for the compliant impact surrogate was as follows (Figure 9-11):

1. Bolt the central core to the base plate.

2. Attach the potentiometer, fit the potentiometer grub screw (to secure the potentiometer in place), attach the two timing pulleys and add the toothed timing belt (using a bar to hold the top timing pulley in place).

3. Attach the core side part, fit the three bolts (using a bar to hold the top timing pulley in place), fit the two dowels, and fit the grub screw on the bottom timing pulley. Use a screwdriver to rotate the potentiometer shaft and test the rotation of the toothed timing belt.

4. Remove the bar, put the hand in position, and refit the bar (using a screwdriver to push the top timing pulley into place).

5. Position the shaft on one end of the wrist joint and use a mallet to replace the bar with the shaft.

6. Fit and adjust the grub screw on the top timing pulley and hand to secure them to the shaft, ensuring the potentiometer shaft captures the full wrist extension.

7. Attach the forearm casings.

8. Bolt the base plate to the rig

9. Connect potentiometer wires.
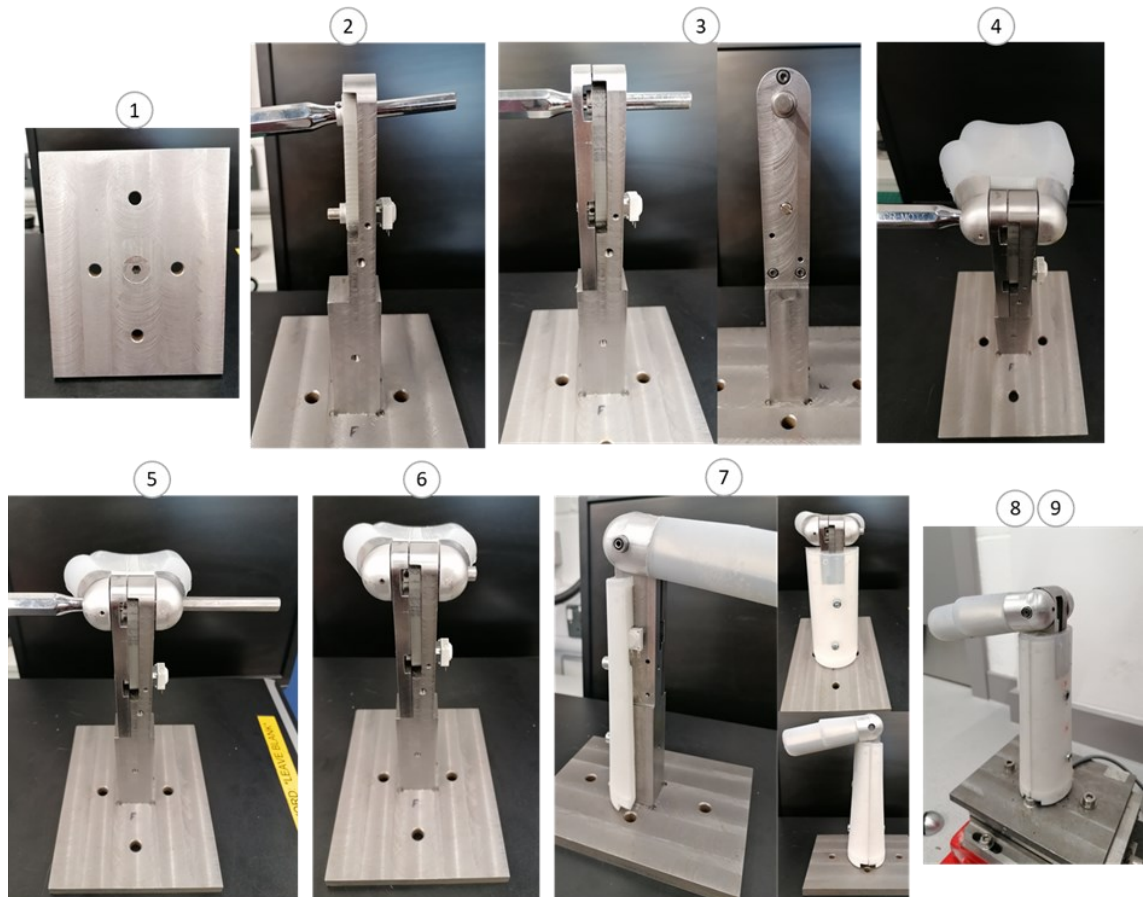
Figure 9-11 Assembly procedure for the compliant impact surrogate.

9.6.3   Interchanging between the stiff and compliant impact surrogate

The stiff and compliant surrogate can be interchanged on the central core as follows (Figure 9-12):

1. Disconnect the potentiometer wire and remove the base plate (with the surrogate attached) from the rig.

2. Remove the compliant forearm casings.

3. Undo the grub screw on the top timing pulley and hand.

4. Use a mallet to replace the shaft with a bar.

5. Remove the bar and then the compliant hand.

6. Put the stiff hand in place and refit the bar (using a screwdriver to push the top timing pulley into place).

7. Use a mallet to replace the bar with the shaft.

8. Fit and adjust the grub screw on the top timing pulley and stiff hand to ensure the potentiometer shaft captures the full wrist extension.

9. Attach the stiff forearm casings.
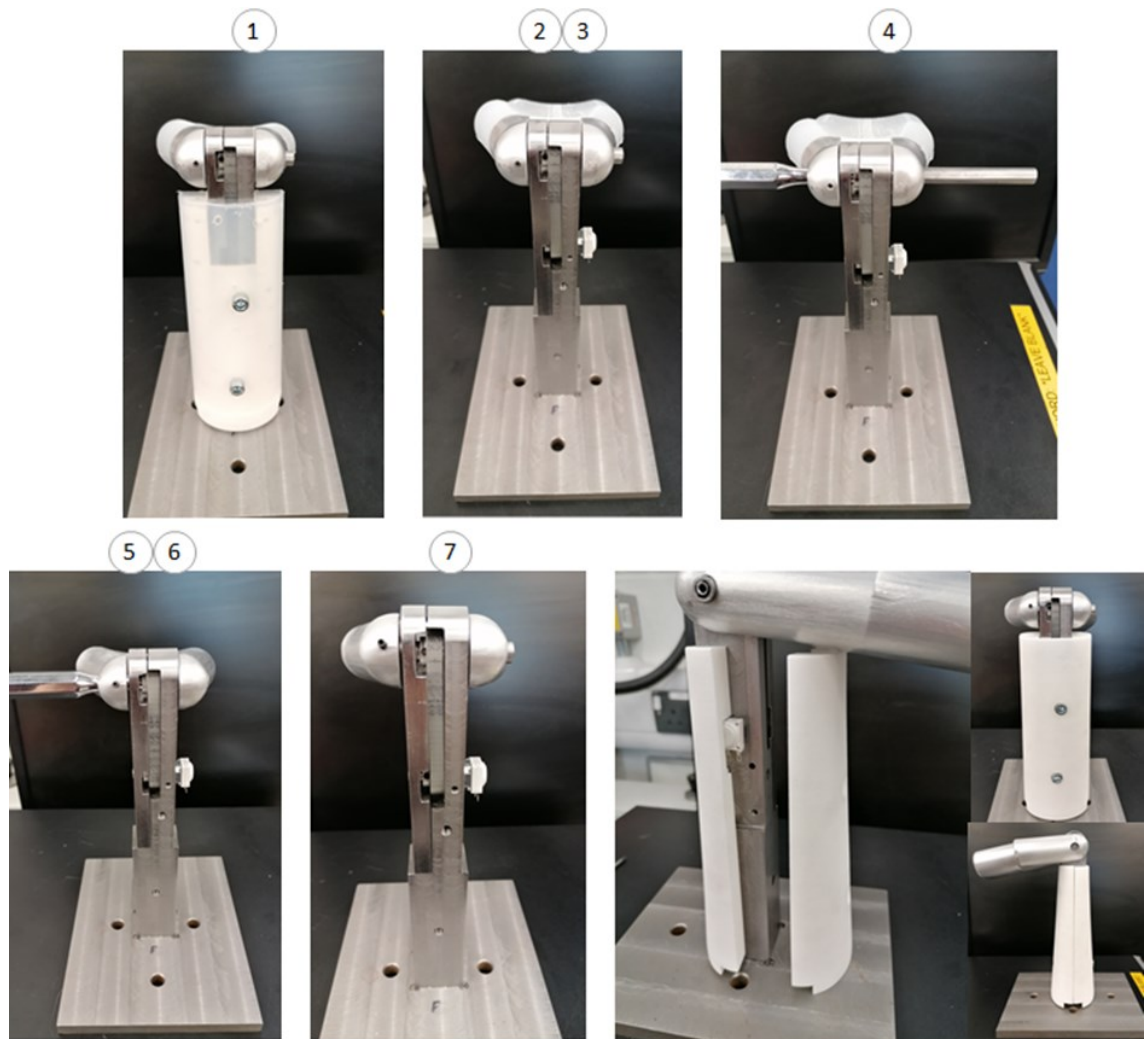
Figure 9-12 Procedure to interchange between the compliant and stiff impact surrogate on the central core.

9.7 Appendix G: Impact testing - Chapter 6

9.7.1 Static calibration

To calibrate the pendulum arm potentiometer and the wrist potentiometer, the pendulum arm and wrist were set at various angles (measured by an inclinometer) (Figure 9-13). The pendulum arm calibration procedure was undertaken at both the start of the first test day (day 1) and the start of the second test day (day 2). Voltage

vs. angular position was plotted for the pendulum arm, and a linear trendline was fitted (Figure 9-14a) (0° = pendulum arm horizontal). When analysing impact testing data, the equation of the trendline was used to convert the output voltage from the pendulum arm potentiometer to a pendulum arm angle. As the surrogate was part disassembled and reassembled to interchange between the compliant and stiff surrogate, the wrist potentiometer had to be re-calibrated. The wrist potentiometer was calibrated before testing for each surrogate. Voltage vs. angular position was plotted for the wrist potentiometer, and it was observed that once the wrist angle exceeded ~70°, the voltage vs. force gradient changed. Two linear trendlines were, therefore, fitted; one at angles <70° and one at angles >70° (Figure 9-14b and c). When analysing the wrist angle data, one calibration equation (for angles <70°) was fitted, until the resultant angle was at the crossing point of the two trendlines (~70°), and then the rest of the data was fitted with the second calibration equation.

(a)   (b)
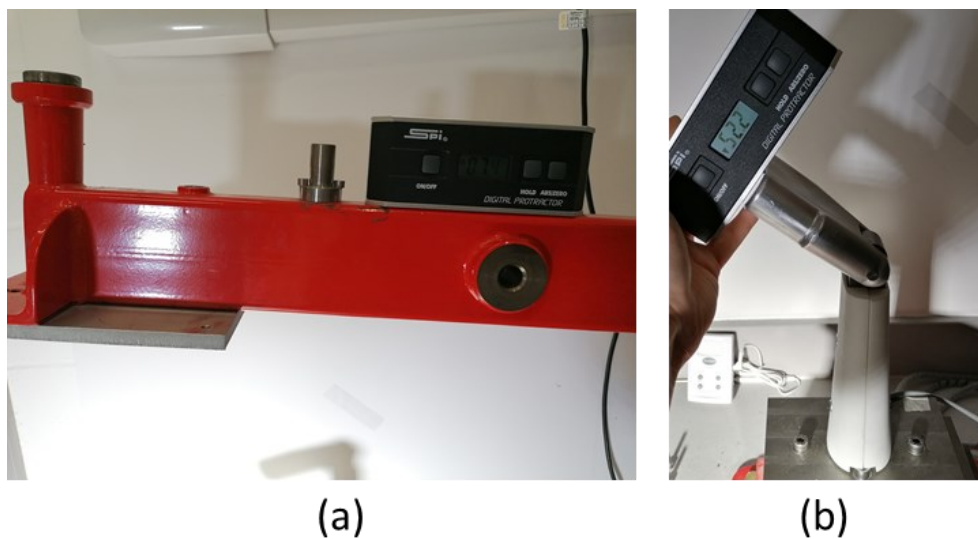
Figure 9-13 Potentiometer calibration process for (a) pendulum arm and (b) surrogate wrist.
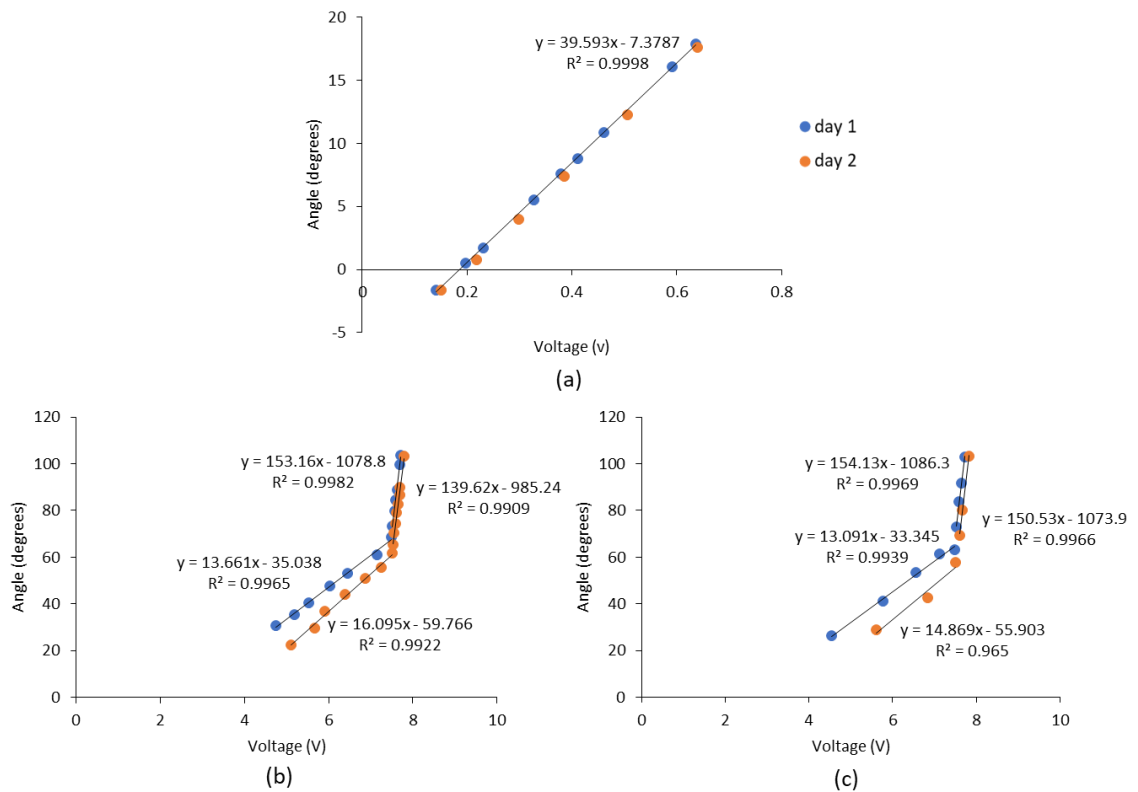
Figure 9-14 Potentiometer calibration for the (a) pendulum arm, (b) stiff surrogate, (c) compliant surrogate.

9.7.2 Dynamic calibration of the surrogate potentiometer

A dynamic calibration of the potentiometer, for both the stiff and compliant surrogate configurations, was also conducted by measuring the hand angle during impact in the video frames. The potentiometer output voltage vs. angular position data for this dynamic calibration was plotted alongside the data from the static calibration (from Figure 9-14b and c, day 1) (Figure 9-15). The measured angles from the video for the compliant surrogate were within ±1° of those obtained from the potentiometer when using the coefficients from the static calibration (Figure 9-15a). The angles measured from the video for the stiff surrogate were higher than those obtained for the potentiometer when using the coefficients from the static calibration (Figure 9-15b).
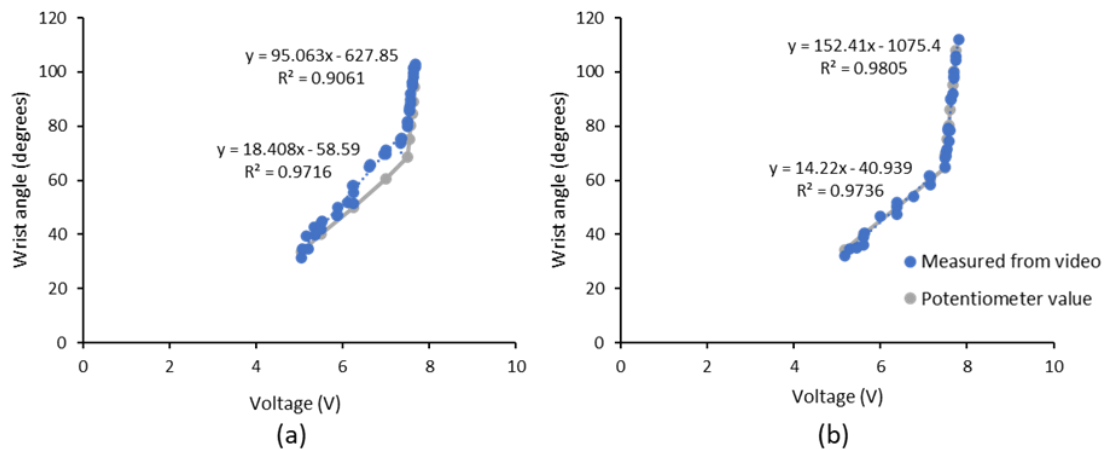
Figure 9-15 Dynamic calibration of potentiometer from video frames for the (a) stiff surrogate and (b) compliant surrogate.

Further investigation of the potentiometer was conducted by measuring the relationship between voltage and wrist angle across the full mechanical rotary range of the potentiometer. The surrogate was removed from the test rig (by unbolting the base plate), the forearm casings were removed (for access to the potentiometer), and the potentiometer was tested whilst still connected to the toothed timing belt mechanism. The potentiometer was connected to a 8.4V power supply (EL302R Bench Power Supply, AIM-TTI Instruments, UK), and the output voltage was read via a voltmeter (UT33 Series universal multimeter, Uni-Trend, China) (Figure 9-16). The relationship between wrist angle and potentiometer output voltage was measured at the potentiometers minimum, middle and maximum mechanical rotary range (by removing the grub screws, altering the potentiometer's rotary position, and refitting the grub screws). The middle range corresponded to the mechanical rotary range used in the impact testing, (i.e. 4.5V = ~30°). The hand was then removed from the surrogate, and the potentiometer's full mechanical rotary range was tested (with 0° = minimum mechanical rotary position of potentiometer, and ~288° = maximum mechanical rotary position of potentiometer) (potentiometer data sheet Appendix H Section 9.8.3).

As expected (from the nonlinearity observed in the static calibration), the angle vs. voltage 'curve' moved along the x-axis depending on the mechanical rotary range of the potentiometer, and the 'curve' moved in the y-axis depending on how the set angle of the potentiometer was defined (i.e. the angles for the original calibration,

min., mid. and max. range related to wrist extension (35 to 103°), whereas for the full range, 0° = min. rotary position and ~288° = max. rotary position) (Figure 9-17). The results here confirm that the potentiometer is non-linear across its full mechanical range. This observed nonlinearity of the potentiometer was unexpected based on the information provided in the data sheet.
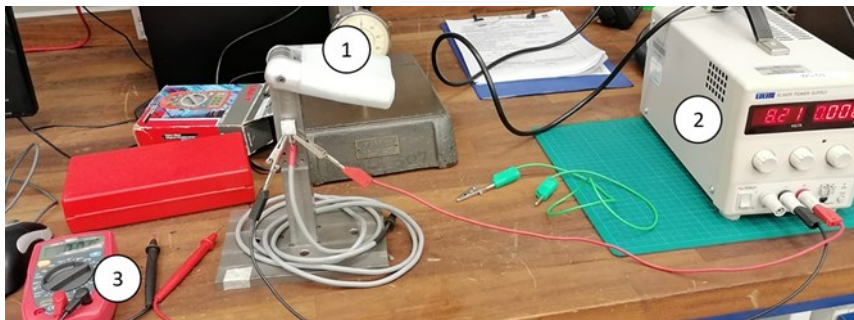
Figure 9-16 Potentiometer testing. 1- surrogate with forearm casings removed and potentiometer visible, 2 - power supply, 3 - voltmeter.
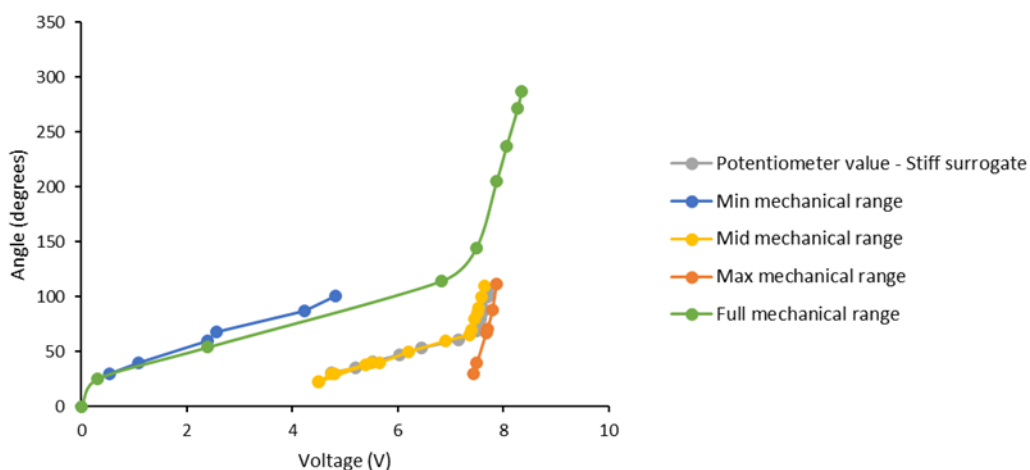
Figure 9-17 Potentiometer calibration when at its min, mid and max rotary mechanical range for wrist angles 35 to 103°, and at its full mechanical range 0 to 288° (minimum and maximum rotary position), plotted alongside the calibration of the stiff surrogate on day 1 from Figure 9-14b.

The potentiometer's rotary range used in relation to the wrist angles, determines whether the voltage vs. angle relationship was linear or not (Figure 9-17). The potentiometer was linear over the full range of wrist angles (30 to 103°) for some of the pilot testing conducted (by chance due to how it was set) (Figure 18a). To determine whether the potentiometer captured the stiff surrogate's maximum wrist angle (103°, as observed in in the video footage), when it was operating in the linear range, the temporal force, temporal wrist angle and force vs. wrist angle

from a pilot test of a used short protector on the stiff surrogate were displayed (Figure 18b and c). When the potentiometer was at its maximum rotary range and was linear over the full range of wrist angles, the potentiometer did indeed capture the maximum wrist angle of ~103° with a corresponding increase in force. This finding suggests that setting up the potentiometer differently (i.e. so that it is linear over the full range of wrist angles) could improve the corresponding wrist angle measurements.
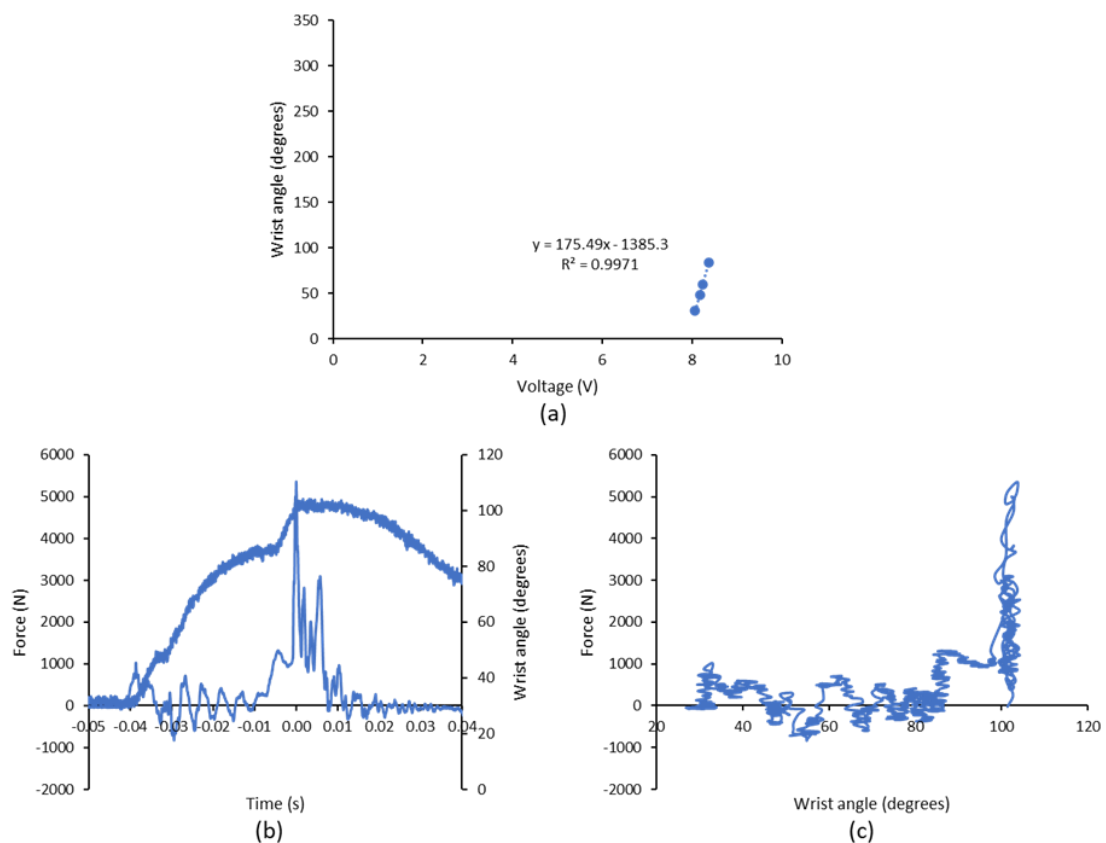
Figure 9-18 (a) Potentiometer calibration, (b) temporal force, (c) temporal wrist angle, and force vs. wrist angle (all unfiltered data) from the pilot testing of a used short protector on the stiff surrogate (drop height 0.56), where the potentiometer was linear over the full range of wrist angles.

9.7.3   Familiarisation of test rigs and cross-checking with previous work

Initial testing was undertaken to become familiar with the test rigs and to cross-check the results with previous work (Newton-Mann's 2019). A used (previously impact tested in Chapter 5) short and long protector were impact tested as per Newton-Mann's (2019) rig modifications (two neoprene blocks, drop height of 0.56 m) on Adams (2018) surrogate (scanned surrogate), and compared to previous results from Newton-Mann (2019) (Figure 9-19). Protectors were strapped to a

moderate strapping condition and the hand was set to a start angle of ~35°. A similar peak force and impact duration was observed between the testing performed here and the previous work. The wrist surrogate reached a higher wrist angle than reported in the previous work, which could be due to inherent differences between the protectors.
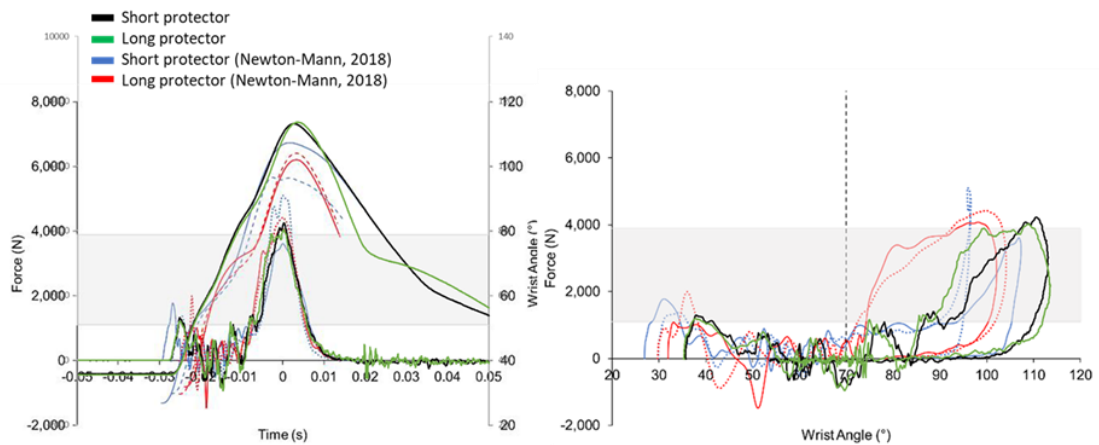
Figure 9-19 Temporal force and temporal wrist angle trace (left) and force vs. wrist angle (right) of a used short and long protector on the scanned surrogate (drop height 0.56 m), overlaid onto the results of Newton-Mann (2018).

Further testing was conducted to compare results between the original (scanned) surrogate developed by Adams (2018), and the stiff geometric surrogate developed here. A used (previously impact tested in Chapter 5) short and long protector were impact tested (drop height of 0.56 m) on both the scanned and the geometric surrogates (Figure 9-20). The peak force of both protectors tended to be higher on the geometric surrogate compared to the scanned surrogate. The impact duration was also longer on the geometric surrogate compared to the scanned surrogate. These results suggest that surrogate shape can influence the results when impact testing wrist protectors. Adams *et al*. (2018) found the scanned surrogate to be stiffer in the bend test than the geometric surrogate, which could explain these results. The wrist also extended further for protectors when on the scanned surrogate compared to the compliant surrogate. This finding was attributed to the difference in maximum wrist extension of the surrogates (110° scanned, 103° geometric).
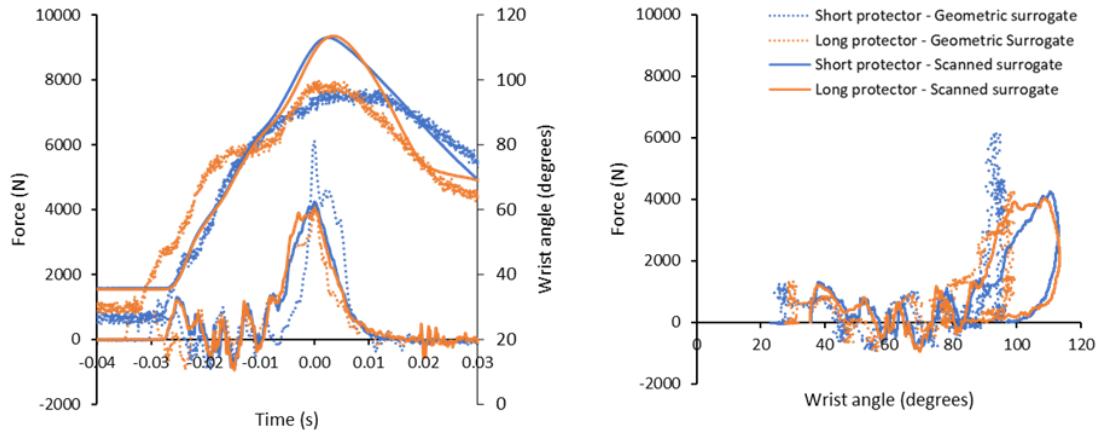
Figure 9-20 Temporal force and temporal wrist angle trace (left) and force vs. wrist angle (right) of a used short and long protector tested on the scanned surrogate (solid lines) and the geometric surrogate (dotted lines) (drop height 0.56 m).

A new and used (previously impact tested in Chapter 5) short and long protector were impact tested (drop height of 0.56 m) on the geometric surrogate (stiff surrogate) (Figure 9-21). The peak force of the new protectors was higher than for the used protectors, which was unexpected. The used protectors reached higher wrist angles than the new protectors, suggesting that the new protectors were stiffer than the used protectors. These results could be due to inherent differences between the protectors.
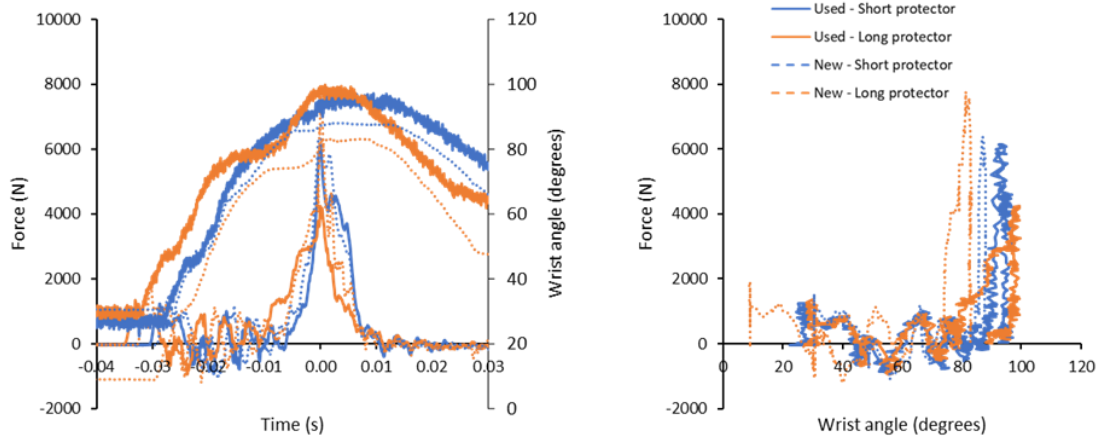
Figure 9-21 Temporal force and temporal wrist angle trace (left) and force vs. wrist angle (right) of a new (solid lines) and used (dotted lines) short and long protector tested on the geometric surrogate.

9.7.4 Effect of filtering data

A low-pass filter (4-pole phaseless Butterworth digital filter) was applied to the impact force data and wrist angle data, as per Newton-Mann (2019). A cut-off

frequency of 1,650 Hz (CFC 1000) was recommended when the sampling frequency is ≥10 kHz (Weisang, 2018). The cut-off frequency was varied here to see its effect on the temporal impact force data. An example of the unfiltered vs. filtered data (varying the cut-off frequency) for the short protector on the stiff and compliant surrogate at moderate strapping tightness is shown Figure 9-22. The impact force data from the stiff surrogate was observed to be more affected by the cut-off frequency than for the compliant surrogate. A cut-off frequency of 1,650 Hz was used for the main test, based on the recommendation from Weisang (2018).
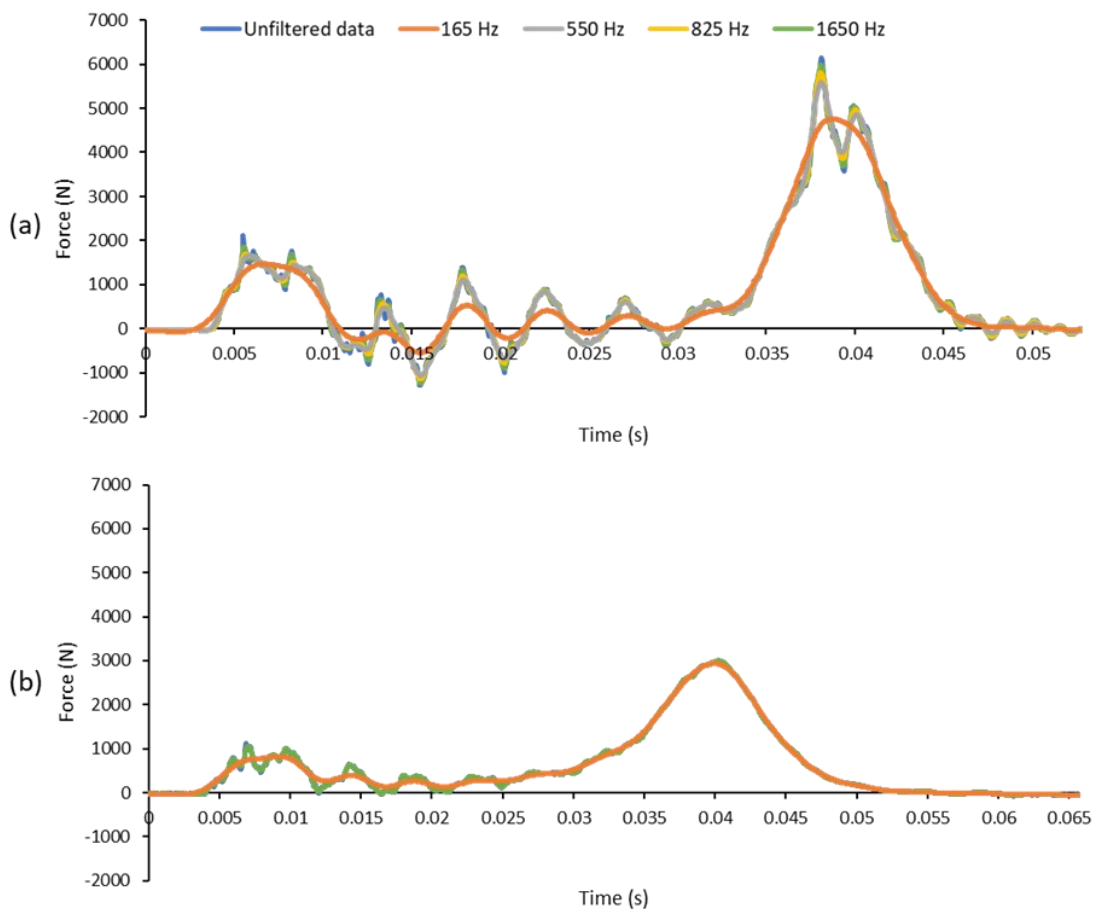
Figure 9-22 Unfiltered vs. filtered force data of the short protector (drop height 0.42 m) on the (a) stiff and (b) compliant surrogate at moderate strapping condition, with the cut-off frequency varied.

9.7.5 Loading rate

Comparison of loading case of Greenwald *et al*. (1998), Adams (2021) and Newton-Mann (2018) to the loading case of the stiff and compliant surrogate (Figure 9-23). The loading case of the stiff and compliant surrogate is between that of the 40 and 50 J impacts of Newton-Mann (2019).
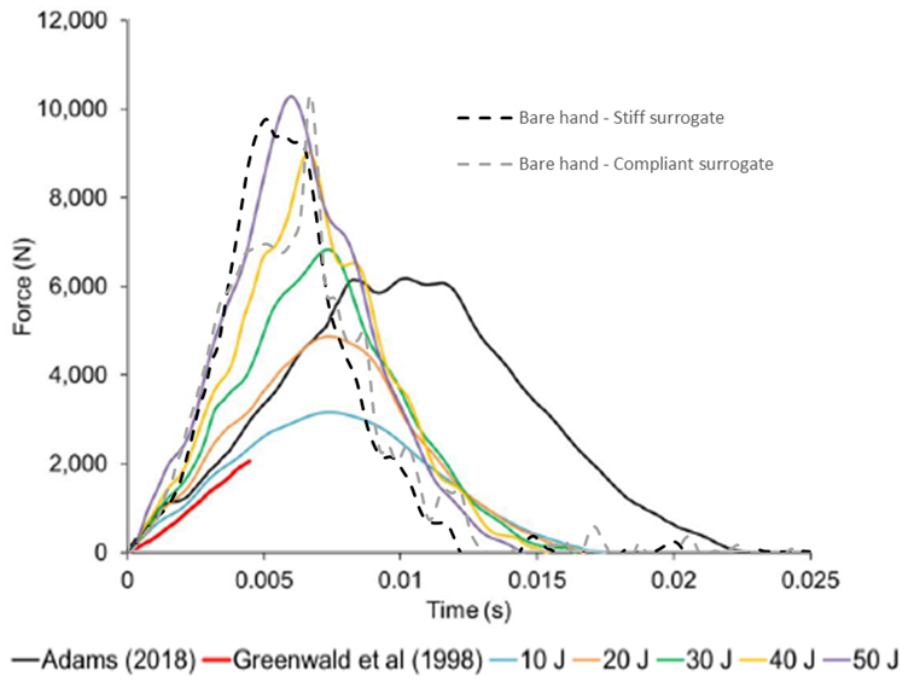
Figure 9-23 Temporal force plot showing the impact traces for the stiff and compliant surrogate from this study (drop height 0.5 m), compared to 10 to 50 J impacts by Newton-Mann (2019) using the same impact rig, an impact by Adams (2018) using a modified version of the impact rig (four neoprene blocks on the impactor), and the loading curve from the cadaveric study by Greenwald et al. (1998).

9.8 Appendix H: Datasheets

9.8.1 M511

TECHNOVENT — Technical/User Data Sheet

(M511) Maxillofacial Rubber [Page 1 of 2]

Overview

The material is a 2-part 10:1 platinum (vinyl addition) cure system and is supplied in wide necked tubs for easy removal during use.

Within the range of platinum cured materials, there is both a rubber and a gel. Each has its own catalyst.

Platinum, or vinyl addition, cure systems do not give off any vapours when curing so, consequently, there is no shrinkage of the final piece.

User Instructions

Mixing

Use 10 part A to 1 part of B

ie. 10g part A to 1g part B = 11g total

Curing

	Work Time (at room temp)	Cure time (at room temp)	Cure time (at 100 deg C)
Rubber (M511)	1hr	n/a	1hr

Please note: Work times are dependent on ambient working temperature.

Ensure that both parts are uniformly and evenly mixed.
Degassing in a vacuum chamber is recommended for bubble-free results.

N.B. Although adequate mechanical properties are achieved after the standard cure times given above the properties will improve for up to 36 hours after de-moulding.

Modifying the Standard cure

The cured properties of the maxillofacial rubber (M511) can be modified by the addition of the softener (M513) which is available separately. The maximum amount of softener added should never exceed the amount of part B added: e.g. if 10g of part A is weighed out 1g of part B should be added and a maximum of 1g of softener can also be added. Typically the addition of the maximum amount of

---

Technical/User Data Sheet

(M511) Maxillofacial Rubber [Page 2 of 2]

will reduce the hardness of the standard rubber from 15-20 Shore A to approximately 10 Shore A.

Modifying the Rheological Properties

The Anti-Slump Agent is designed to alter the rheological properties of Cosmesil platinum cure Rubber elastomers.

The purpose for this is to raise the viscosity of the elastomer base to allow for easy placing in the mould and high peaking properties to ensure it stays where it is put, while still retaining a low shear material.

This has the effect of creating a 'margarine'-like material which can still be spatulated easily.

Bonding to Acrylic

The material bonds well to acrylic baseplates (including Light-cure) with the application of Cosmesil Platinum Primer (G611) [refer to Primer tech Sheet for user instructions].

A word of warning...(applies predominantly to Platinum cured materials)

Take care when using tin catalysed silicones in conjunction with platinum catalysed systems, as the platinum systems are very easily 'poisoned' which can lead to the material not curing up as expected.

This becomes a problem when moulds previously used for curing tin (or latex, etc) systems are then used for platinum systems — it is recommended, therefore, that, where possible, different moulds are used for these two systems.

It is also recommended when using platinum catalysed systems that latex free disposable gloves are used in preference to those which contain latex, if such protection is used, to avoid poisoning the platinum catalyst.

NB — there is no such problem, however, if moulds which have previously been used for platinum systems are to be used in the future only for tin systems (the tin curing reaction is much more robust and not liable to excessive poisoning from surroundings — it is, to tempt fate, fool proof).

As with all systems, however, a degree of accuracy when weighing and mixing is essential. Good bench practices will assist in the correct, trouble free curing of these materials.

9.8.2   Z004

TECHNOVENT

Technical/User Data Sheet

Platinum Cure Rubber - Z004   [Page 1 of 2]

Overview

The material is a 2-part 1:1 platinum (vinyl addition) cure system and is supplied in wide necked tubs for easy removal during use.

Platinum, or vinyl addition, cure systems do not give off any vapours when curing so, consequently, there is no shrinkage of the final piece.

User Instructions

Mixing

Use 1 part A to 1 part of B

ie. 10g part A to 10g part B = 20g total

Curing

	Work Time (at room temp)	Cure time (at room temp)	Cure time (at 100deg C)
Rubber (Z004)	1hr	n/a	1.5 hr

Please note: Work times are dependent on ambient working temperature.

Ensure that both parts are uniformly and evenly mixed.
Degassing in a vacuum chamber is recommended for bubble-free results.

N.B. Although adequate mechanical properties are achieved after the standard cure times given above the properties will improve for up to 36 hours after de-moulding.

Z004 HAS RECENTLY BEEN RE-FORMULATED TO IMPROVE PROPERTIES. YOU WILL NOTICE THAT PART B IS SLIGHTLY MORE VISCOUS THAN PREVIOUSLY HOWEVER THE PROPERTIES WILL BE THE SAME.

9.8.3 Wrist potentiometer

ELECTRICAL SPECIFICATIONS

PARAMETER		MODEL 248	MODEL 249
Element type		Conductive plastic	Cermet
Total resistance range		500 Ω to 1 MΩ	
Standard series		1, 2, 5	
Resistance tolerance		± 20 %	± 20 % (on request ± 10 %)
Power rating	Linear	0.5 W at 70 °C	1.0 W at 70 °C
Temperature coefficient of resistance (typical)		± 500 ppm/°C	± 150 ppm/°C
Linearity (typical)		± 5 % independent	
Limiting element voltage		300 V	
Contact resistance variation (typical)		5 % of the total resistance	
Insulation resistance		1000 MΩ minimum, 500 Vdc	
Dielectric strength		750 Vrms minimum 50 Hz / 60 Hz	
End resistance		2 Ω maximum each end	
Effective electrical travel		265° ± 5°	

MECHANICAL SPECIFICATIONS

Mechanical travel	295° ± 5°
Operating torque	0.1 Ncm to 2 Ncm
End stop torque	35 Ncm (50 oz.-inch)
Max. tightening torque	150 Ncm
Weight	8.3 g (0.29 oz.) (1/4" x 7/8" F,M,F metal shaft)

ENVIRONMENTAL SPECIFICATIONS

Temperature range	-55 °C to +125 °C
Climatic category	55 / 125 / 4
Sealing	IP 50

MARKING
- Vishay model
- Vishay logo
- Variation law
- SAP code for ohmic value
- Tolerance in %
- Date code (4 digits)
- Terminal identification "3" for lead 3

PACKAGING
- In box of 25 pieces, code BO25

Note
- Hardware supplied in separate bags

PERFORMANCE

TESTS	CONDITIONS	ΔRₜ/Rₜ (%)	ΔR₁,₂/R₁,₂ (%)	OTHER
Electrical endurance	1000 h at rated power 90°/30° - ambient temp. 70 °C	± 3 %	± 5 %	Contact res. variation: < 1 %
Damp heat, steady state	4 days 40 °C 93 % HR	± 2 %	-	Dielectric strength: 1000 Vrms Insulation resistance: > 10⁴ MΩ
Change of temperature	5 cycles, -55 °C at +125 °C	± 1 %	-	ΔV₋₂/V₋₃ ≤ ± 2 %
Mechanical endurance	10 000 cycles	± 3 %	-	Contact res. variation: ≤ 2 % Rn
Shock	50 g's at 11 ms 3 successive shocks in 3 directions	± 1 %	± 2 %	ΔV₋₂/V₋₃ ≤ ± 2 %
Vibration	10 Hz to 55 Hz, 0.75 mm or 10 g's during 6 h	± 1 %	-	

TYPICAL VALUES AND DRIFTS FOR 249

VISHAY.
www.vishay.com

248, 249
Vishay Spectrol

1/2" (12.7 mm) Conductive Plastic and Cermet Potentiometers

RoHS COMPLIANT

FEATURES
- Model 248: 0.5 W at 70 °C (conductive plastic element)
- Model 249: 1 W at 70 °C (cermet element)
- Cost effective panel potentiometer
- PCB mounting
- Tests according to CECC 41000 or IEC 60393-1
- Material categorization: for definitions of compliance please see www.vishay.com/doc?99912

QUICK REFERENCE DATA

Multiple module	No
Switch module	n/a
Detent module	n/a
Special electrical laws	A: linear, L: logarithmic
Sealing level	IP 50
Lifespan	10K cycles

DIMENSIONS in millimeters (inches) ± 0.5 mm (± 0.02")

VERSION BUSHING / SHAFT	A	B		C	S
	SHAFT	SHAFT	L	BUSHING	SCREWDRIVER
	Ø			Ø	SLOT
B / BH	1/8"		3/4"	1/4"	0.8
F / GJ	1/4"		7/8"	3/8"	1.2